ISSN 1608-5043 (Print)
ISSN 1608-5078 (Online)

SCIENTIFIC AND TECHNICAL JOURNAL

# GEORESOURCES

www.geors.ru

V. 22. No. 3. 2020



GEORESURSY GEORESOURCES. SCIENTIFIC AND TECHNICAL JOURNAL

SCIENTIFIC AND TECHNICAL JOURNAL
# GEORESURSY
www.geors.ru
e-mail: mail@geors.ru

ISSN 1608-5043 (Print)
ISSN 1608-5078 (Online)
V. 22. Is. 3. 2020

**Key title: «Georesursy». Parallel title: «Georesources»**



**Publisher:** Georesursy LLC
**Editorial and Publisher's address:**
1-10, Mayakovsky st., Kazan, 420012, Russian Federation
Phone: +7 843 2390530, e-mail: mail@geors.ru

Georesursy (Georesources) is a peer-reviewed scientific and technical journal published since 1999.

**The journal is included/indexed in:**
- **Scopus;**
- **Web of Science (ESCI);**
- **Directory of Open Access Journals (DOAJ);**
- **CAS (Chemical Abstracts Service) databases;**
- **GeoRef database;**
- **EBSCOhost™ databases;**
- **Ulrich's Periodicals Directory.**

The full-text e-versions of the articles are available on: **www.geors.ru**


Registered by the Federal Service for Supervision of Communications and Mass Media No. PI FS77-38832

The Journal is issued 4 times a year. Circulation: 1000 copies
Issue date: September 30, 2020



## Table of Contents

ORIGINAL ARTICLE
**DOI**: https://doi.org/10.18599/grs.2020.3.2-11 Russian Original 2020. Vol. 22. Is. 3. Pp. 2–11

# Types of sections and oil-bearing prospects of the Bazhenov formation in the Nadym-Ob interfluve

*M.A. Fomin[1,2*], R.M. Saitov[1]*
[1]*Trofimuk Institute of Petroleum Geology and Geophysics of the Siberian Branch of the Russian Academy of Sciences, Novosibirsk, Russian Federation*
[2]*Novosibirsk State University, Novosibirsk, Russian Federation*

**Abstract**. The article presents the results of studying the geological structure of the Bazhenov formation in the Nadym-Ob interfluve of West Siberia with the aim of predicting the oil content of this black shale stratum. As a result of interpretation of a wide range of well logging represented by electric, radioactive and acoustic logging, with subsequent matching of these results with paleontological definitions of micro- and macrofauna, the distribution of the Salym, Nizhnevartovsk and Tarkosalinsky types of sections of the Bazhenov formation was clarified, transitional areas between them were identified. It has been established that the Tarkosalinsky type is more widespread in the western direction than was shown earlier and is also distinguished in the Vengayakhinskaya, Yarainerskaya and other areas. The Nizhnevartovsk type, on the contrary, has a narrower distribution and stands out directly within the same name arch and to the south by the Var'egan-Tagrinskii megauplift.

On the basis of geological, geochemical, geophysical criteria and the results of an inflow test in deep wells, a map of the oil potential prospects of the "classical" sections of the Bazhenov formation has been compiled. Regional prerequisites (high catagenesis of organic matter, significant modern concentrations of organic carbon, etc.) for the discovery of industrial accumulations of oil in the Bazhenov formation in the southern regions of the Yamalo-Nenets Autonomous District are identified. The results of the test for the inflow of the Bazhenov formation in this area in the 70–90s XX century were analyzed; repeated, interval testing of these deposits using modern methods of stimulation of the inflow is recommended. The necessity of laboratory lithological, petrophysical, geochemical study of the core of the Bazhenov formation in the southern part of the Yamalo-Nenets Autonomous District is substantiated with the aim of determining its lithological composition, identifying oil source and oil productive intervals, studying the reservoir structure and the nature of saturation of its void space, developing recommendations for calculating oil reserves and creating technology for its cost-effective production.

**Keywords**: Bazhenov formation, West Siberia, types of sections, oil content

**Recommended citation**: Fomin M.A., Saitov R.M. (2020). Types of sections and oil-bearing prospects of the Bazhenov formation in the Nadym-Ob interfluve. *Georesursy = Georesources*, 22(3), pp. 2–11. DOI: https://doi.org/10.18599/grs.2020.3.2-11

## Introduction

Black shale deposits are the main source strata throughout the world. They are common in the West Siberian, Volga-Ural, Timan-Pechora, North Caucasian oil and gas provinces of Russia, the basins of North America (Williston, Appalachian, Perm, etc.), Columbia (Middle Magdalene), the Caribbean and Middle East regions, the North Sea, etc. The main feature of these strata is that they contain rocks that are both source rocks and oil bearing reservoirs. The hydrocarbon resources in these strata are classified as difficult to recover.

The experience of studying and the success of developing hydrocarbon accumulations associated with unconventional tight reservoirs and shale complexes in the United States has provided a serious incentive for the study of similar objects around the world, including in Russia. Currently, the US shale formations play an important role in the oil and gas industry of the country, among which the largest oil formations are Bakken, Eagle Ford; gas – Marcellus, Haynesville, Fayetteville, Barnet (Prishchepa et al., 2014). Also, great prospects are currently associated with the Green River kerogen-bearing formation (Soeder et al., 2019).

In the West Siberian oil and gas province, it is more and more difficult to maintain the level of oil production from traditional granular reservoirs every year. Giant and large deposits have already been discovered, and explored reserves have been largely developed. There

*Corresponding author: Mikhail A. Fomin
*E-mail: fominma@ipgg.sbras.ru*

is a need to involve in industrial development new, as yet insufficiently studied objects, among which the most complex, perhaps, is the Bazhenov formation. Back in 1961, the outstanding Soviet geologist F.G. Gurari predicted its possible commercial oil-bearing capacity, which was confirmed in 1967 by an oil fountain at the Salym field. In recent years, new, significantly more accurate data on the geological structure, stratigraphy and paleontology, paleogeography have appeared (Kontorovich et al., 2013; Stupakova et al., 2016; Stafeev et al., 2017; Ryzhkova et al., 2018; Kontorovich et al., 2019a) of the Bazhenov formation and its age analogs in the West Siberian sedimentary basin. Based on the interpretation of a wide range of well logging, the results of which were linked to paleontological determinations of the age of micro- and macrofossils, the authors proposed significant clarifications of the boundaries of the distribution of the types of sections of the Bazhenov Formation in the Nadym-Ob interfluve.

On the first-ever diagrams and maps, the main oil-bearing prospects of the Bazhenov formation were predicted in the Salym oil and gas accumulation zone. In recent years, these forecasts have been repeatedly detailed and supplemented (Zubkov, 2016; Kolpakov et al., 2016; Baranova, 2018; Skvortsov et al., 2018a, b; Kontorovich et al., 2019b). However, even today, the main prospects for the oil-bearing capacity of the Bazhenov formation are associated with the western (Krasnoleninskaya zone of oil and gas accumulation) and central (Salym group of fields) regions of the Khanty-Mansiysk Autonomous District. To the east, commercially productive hydrocarbons have been discovered, including in anomalous sandy sections of the Bazhenov formation, which have a genesis different from the “classical shale” sections and thus are an independent object for study. They are not considered in this study.

On the territory of the the Yamal-Nenets Autonomous District, much less analytical studies of the core of the Bazhenov formation using modern techniques (Kontorovich et al., 2018a, b) have been performed; this stratum has been tested for inflow in single wells. Nevertheless, in the south of this region at the Pyakutinskoye, Malopyakutinskoye, Vengayakhinskoye and further north at the Izvestinskoye and Palnikovskoye fields, small reserves of oil in the Bazhenov formation have been discovered, which suggests higher prospects for its oil-bearing capacity in this region. Based on the interpretation of geological and geophysical materials with the involvement of data on the geochemistry of organic matter, the authors analyzed the regional prospects for the oil-bearing capacity of the Bazhenov formation in the Nadym-Ob interfluve and proposed recommendations for its further study.

## Factual material and research methodology

The study is based on data and results collected, systematized and interpreted by the authors:

1) Diagrams of electrical logging (apparent resistivity (AR – Gz3 tool), induction logging (IL), lateral logging (LL), micro-logging (MGP – microgradient tool, MPP – micropotential tool, MLL – micro-lateral logging), spontaneous polarization potential (PS), caliper logging (CL), acoustic logging (AL), radioactive logging (gamma-ray logging (GR), neutron gamma-ray logging (NGL), thermal neutron logging: long (TNLL) and short

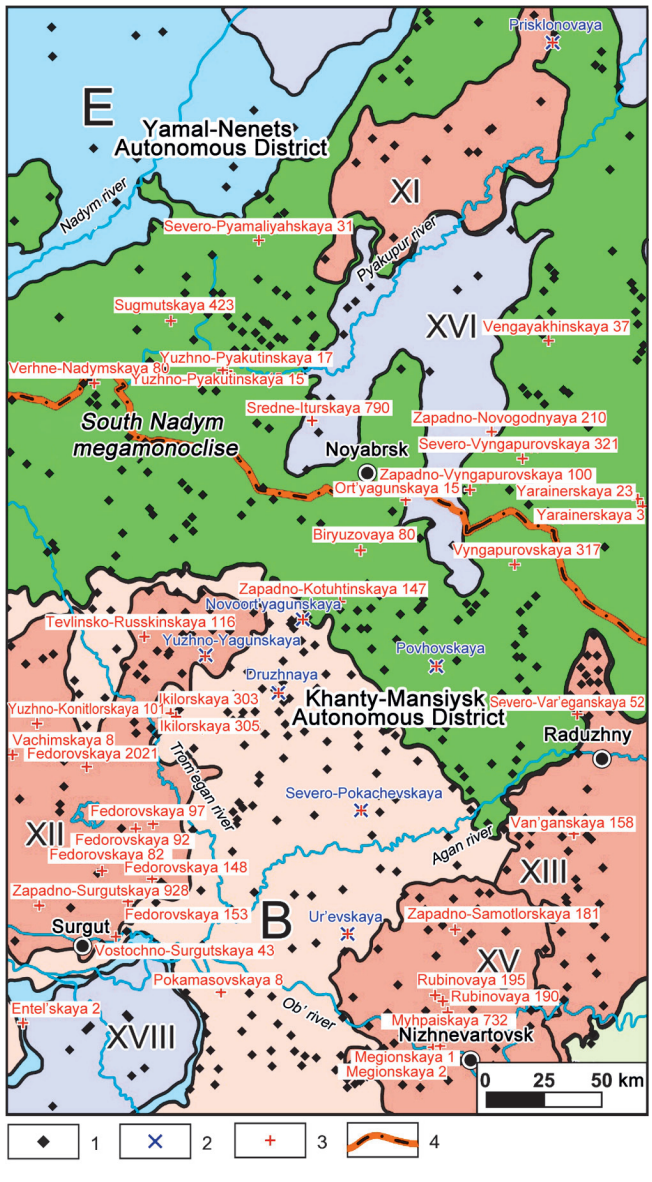


*Fig. 1. Fragment of the tectonic zoning map of the Nadym-Ob interfluve (Kontorovich et al., 2001). 1 – wells in which the authors have interpreted the logging complex data; 2 – wells with the results of analytical core studies; 3 – wells with definitions of micro- and macrofauna; 4 – administrative boundaries. Tectonic elements: B – Khentei hemianteclise, E – Nadym hemisyneclise, XI – Northern arch, XII – Surgut arch, XIII – Var'egan-Tagrinskii megauplift, XV – Nizhnevartovsk arch, XVI – Pyakupur-Amputinskii inclined trough*

(TNLS) tools, gamma -gamma density logging (DGL), for 546 deep wells (Figure 1);

2) 124 determination of the age of micro- and macrofossils of the Late Jurassic-Early Cretaceous age for 57 wells (Figure 1) from the data bank of IPGG SB RAS (definitions by A.S. Alifirov, Yu.A. Bogomolov, O.S. Dzyuba, V.A. Zakharov, L.K. Levchuk, S.V. Meledina, B.L. Nikitenko, B.N. Shurygin, O.S. Urman, O.V. Yazikova) and from published materials, including:

- Volga ammonites in wells: Zapadno-Samotlorskaya 181, Severo-Var'eganskaya 52, Yarainerskaya 3, Vengayakhinskaya 37 and 355, Zapadno-Vyngapurovskaya 100;
- Middle-Late Volga, Early Berriasian bivalves found in wells: Zap. Samotlorskaya 181, Pokamasovskaya 8, Ortyagunskaya 15, Severo-Vyngapurovskaya 321, Zapadno-Vyngapurovskaya 100, Vengayakhinskaya 37 and 355, Sugmutskaya 423.
- Foraminiferal assemblages of the upper Middle Volga – the base of the Boreal Berriasian found in well Vyngapurovskaya 317.

3) Results of inflow tests the sections of the Bazhenov formation in 19 wells.

In 2014–2016, a comprehensive study of the Bazhenov formation was carried out at the IPGG SB RAS. As part of this work, the core of deep wells in the Povkhovskaya, Druzhnaya, Yuzhno-Yagunskaya, Novoortyagunskaya, Severo-Pokachevskaya and Urievskaya areas was studied (Figure 1). As a result of analytical studies of core samples, the boundaries of the Bazhenov and Georgievka formations were precisely established (Figure 2). These wells were selected as reference wells for subsequent correlation of the Bazhenov formation sections.

In those wells where these deposits have not been studied by analytical methods, stratigraphic dissection of sections of the Upper Jurassic and Lower Cretaceous was carried out according to logging data, and a link was made with the definitions of micro- and macrofauna. After that, in each well, the arithmetic mean values of electrical resistivity, natural radioactivity and density (based on the analysis of the dependence on radioactivity with subsequent correlation by well data) of the Bazhenov rocks were calculated and maps of the distribution of these parameters presented below were constructed.

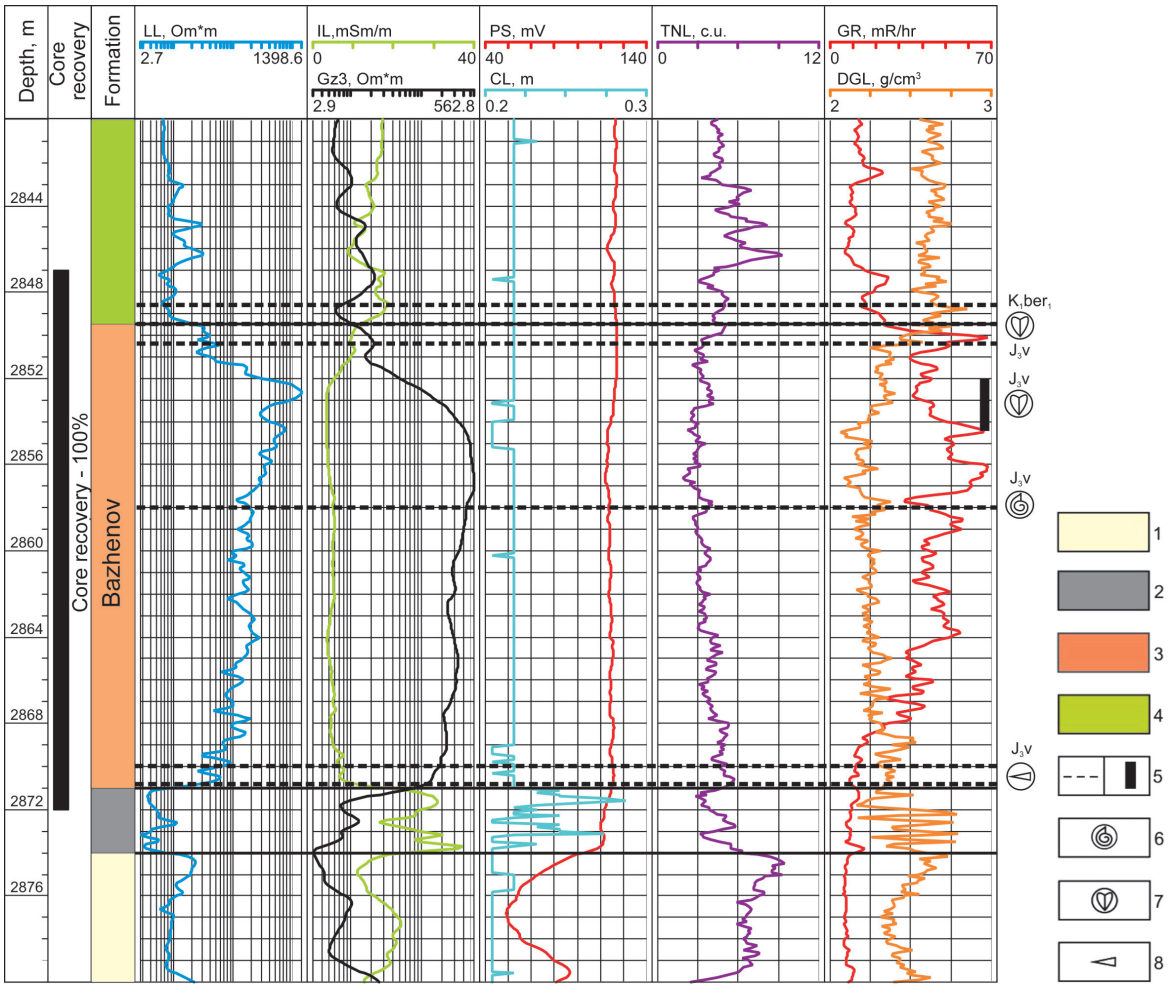


*Fig. 2. Geological and geophysical log for one of the wells of Druzhnaya area. 1 – Vasyugan formation; 2 – Georgievka formation; 3 – Bazhenov formation; 4 – Sortym formation; 5 – levels with paleontological findings; 6 – ammonites; 7 – bivalves; 8 – belemnites.*

## Types of sections of the Bazhenov formation

The systematization of the analytical material accumulated in recent years on the lithology of the Bazhenov formation and the geochemistry of the organic matter contained in it allowed different scientific teams to independently develop classifications of its rocks based on the percentage of the main rock-forming components in them (Kontorovich et al., 2016; Kalmykov et al., 2017; Makarova et al., 2017; Nemova, 2019). In the central and western parts of the study area, the Salym type of section is distinguished (Figure 3) (Braduchan et al., 1986). In the north of the Khentei hemianteclise (Figure 1), its lower part is dominated by dark brown massive silicites and kerogen silicites with interlayers of radiolarites (Eder et al., 2016). In the northern direction, a gradual decrease, up to the disappearance, of the thickness of the silicite member is observed (Eder et al., 2017). In the Povkhovskaya area, in the lower part of the formation, a radiolarite member is distinguished (Eder et al., 2016). The middle part of the section consists of dark gray kerogen-siliceous mixtites with interlayers of silicite-radiolarites with frequent interlayers of relics of bivalve shells. The upper part of the formation is represented by interbedding of kerogen-clayey and kerogen-siliceous-carbonate mixtites with relics of coccolithophorids (Eder et al., 2016). In the same part of the section, a coccolith member is distinguished, which is characterized by high values on the LL and AR, GR curves. This member is also distinguished to the north, on the Prisklonovaya area (Eder et al., 2017, 2019), in the Tarkosalinsky type of the section of the Bazhenov formation. In the north of the Nizhnevartovsk arch, the eponymous type of section of the Bazhenov formation is represented by clayey-siliceous rocks; the coccolithic member is not distinguished in the upper part of the section (Eder et al., 2015).

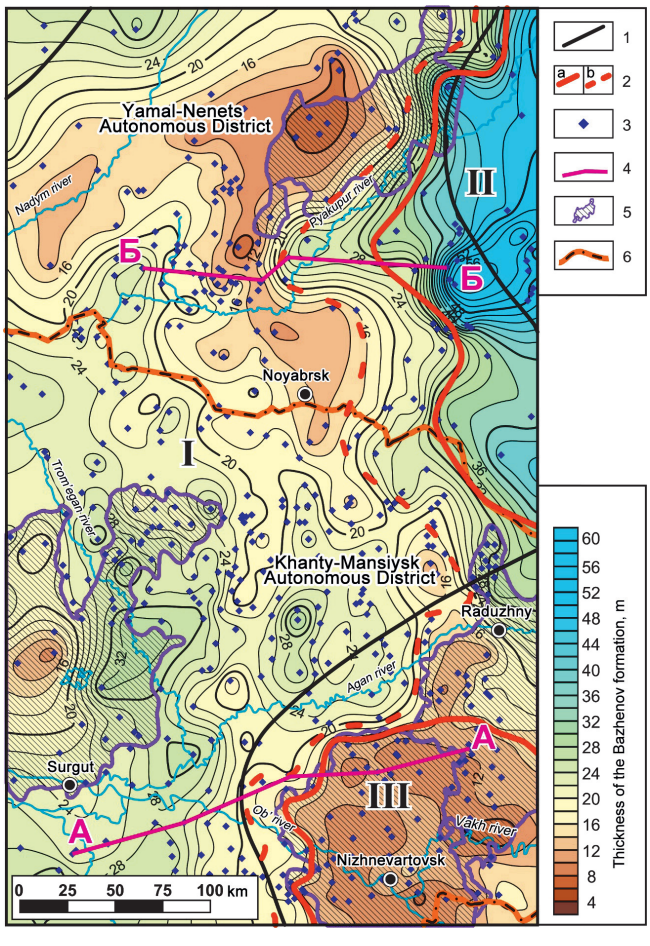


*Fig. 3. Thickness map of the Bazhenov formation. 1 – boundaries between the types of sections after (Braduchan et al., 1986): I – Salym, II – Tarkosalinsky, III – Nizhnevartovsk; 2 – author's a) boundaries of distribution of types of sections of the Bazhenov formation; b) the boundaries of the transition zones between them; 3 – wells with breakdowns by the authors, used for mapping; 4 – lines of correlation profiles; 5 – boundaries of positive tectonic elements of the 1st order; 6 – administrative boundaries.*

The largest thicknesses of the Bazhenov formation in the Salym-type sections are observed in the axial part of the Khentei hemianteclise and reach 30–32 m (Figure 3). They decrease to 10–12 m in the most elevated part of the Surgut arch. Another zone of low thickness is distinguished in the area of the Northern Arch, as well as to the south and west of it. In the north of the studied region, eastward, there is an increase in the proportion of terrigenous sediments in the section, which is accompanied by a gradual increase in the thickness of the Bazhenov formation – the Salym type of section becomes Tarkosalinsky, the thickness of which in the study area exceeds 55 m (Figure 3). In the southeast of the region, the Salym type of section is replaced by the Nizhnevartovsk type, which is accompanied by a reduction in the thickness of the Bazhenov formation at the Bazhenov arch to 12–14 m and less and, most likely, associated with its uplift in the Volgian age. The thickness of the Bazhenov formation was used by the authors as one of the main criteria for clarifying the boundaries of the distribution of sections of different types and identifying the transition areas between them.

The radioactivity of black shale rocks is closely related to the content of organic matter (OM) in them (Neruchev, 1976, 1982, etc.), which is a sorbent of uranium from seawater. Accordingly, the higher the OM concentration in the strata, the higher the radioactivity of such deposits will be. This relationship can be traced in the results obtained by the authors. The highest valuesof the average radioactivity of the Bazhenov formation are recorded within the Khentei hemianteclise (Figure 4A), where a high modern content of organic carbon (TOC) is recorded in it (Kontorovich et al., 2018c). Areas of increased radioactivity are observed in the saddle between the Surgut and Nizhnevartovsk arches, as well as to the north of the latter; values reach 60–70 μR/h (Figure 4A). Within the limits of the South Nadym

megamonoclise, the radioactivity of the rocks is much less, it varies on average from 10 to 20, in some areas up to 25 μR/h.

For the Bazhenov formation of the Salym type, increased radioactivity is characteristic of the middle and upper parts of the section and is 50–60 μR/h, reaching 75–80 μR/h in some wells, while its values decrease in the bottom part of the formation. In the Nizhnevartovsk type, high radioactivity (up to 80–90 μR/h) is noted throughout the section (Figure 5). Only in the sections of some wells of the Vatinskaya, Mykhpayskaya, Ust-Vakhskaya areas does its average values decrease to 25–30 μR/h. In the Tarkosalinsky type of section, radioactivity is distributed in the same way as in the Salym, but its maximum values are significantly lower – most often they change in the range of 20–25 μR/h (Figure 6). Such a decrease in radioactivity is apparently associated with an increase in the proportion of terrigenous sediments in the section.

The main factor affecting the current density of the Bazhenov Formation is the organic material content in it (Kontorovich et al., 2019a), which, in turn, is closely related to the radioactivity of the rocks. The lowest rock density is observed in the southern part of the study area (Figure 4B), in the zone of high average concentrations of organic carbon (Kontorovich et al., 2018c). To the north, with a decrease in TOC content, the rock density of the Bazhenov formation increases.

The electrical resistance of rocks is also closely related to radioactivity. The authors analyzed the distribution of electrical resistivity along the section (tools Gz3 and LL) of the Bazhenov formation. There are two areas of increased average values of electrical resistance. The first is located to the north of the Surgut arch (Figure 4C, D). The maximum values of both the apparent specific resistivity and true electrical resistance reach here 600–700 Ohm*m. The second zone of increased average resistance is located between the Surgut and Nizhnevartovsk arches and is most clearly distinguished by the values of the apparent resistivity, which reach here 500 Ohm*m (Figure 4G).

On the curve of apparent electrical resistivity (AR), the Salym type of section in the southern and central parts of the region is characterized by a two-term structure, the maximum values reach 500 Ohm*m (Figure 5). In the southeastern direction, the resistance of the upper part of the section gradually decreases to 30 Ohm*m, and of the bottom – to 200 Ohm*m – this is another criterion for clarifying the border between the Salym and Nizhnevartovsk types of sections. In the northern part of the region, the Salym-type Gz3 tool curve also has a two-term structure, the maximum values in the west reach 1000 Ohm*m, gradually decreasing to the east. In the Vyngapurovskaya, Zapadno-Vyngapurovskaya areas, a third peak appears on this curve, which is characteristic of the Tarkosalinsky type; such sections are transitional. To the east, the Tarkosalinsky type of section is distinguished, which is characterized by a three-member structure of the apparent resistivity curve, maximum values up to 200–250 Ohm*m in the upper part of the section. In the middle part of the section, they vary from 60 Ohm*m in the Yarainerskaya area to 200 Ohm*m in the Vyngapurovskaya and Vengayakhinskaya (Figure 6) areas.

Thus, it has been established that the Tarkosalinsky type is wider in the western direction than was shown earlier (Braduchan et al., 1986) and is also distinguished in the Vengayakhinskaya, Yarainerskaya and other areas. The Nizhnevartovsk type, according to the authors, on the contrary, has a narrower distribution and is distinguished directly within the arch of the same name and in the southern part of the Var'egan-Tagrinskii megauplift, changing to the south and east by the Vakh type of section (Braduchan et al., 1986).

## Oil-bearing prospects of the Bazhenov formation

In the Bazhenov formation, two types of reservoirs have been identified: voids (caverns) in the rock matrix and horizontal fracturing (fissility), laid down at sediment genesis. Both of these types of reservoirs are formed during catagenesis due to pseudophase transformations of kerogen (Kontorovich et al., 2018a). Thus, the concentration of organic matter and its catagenesis are the most important criteria in assessing the oil-bearing capacity of the Bazhenov formation. Comprehensive interpretation of geophysical, geological materials and data on the geochemistry of organic matter allowed the authors to predict the oil-bearing capacity of these deposits (Figure 7). Only those lands are considered as promising and highly promising lands, within which the organic matter of the Bazhenov formation is in the main phase of oil generation. On the slope of the Khentey hemianteclise, it began about 45 Ma ago (Kontorovich et al., 2019b), and later on the Surgut and Nizhnevartovsk arches (Figure 1). At these large positive structures, the thickness of the Bazhenov formation is reduced (Figure 3), and low OM catagenesis is also noted (Kontorovich et al., 2009); At the Nizhnevartovsk arch, low modern concentrations of organic carbon were recorded in the Bazhenov formation (Kontorovich et al., 2018c). All this is apparently connected with the growth of these structures in the Volgian age.

In the west and southwest of the study region, the thickness of the Bazhenov formation with a TOC concentration of 7–10% reaches 10 m or more (Kontorovich et al., 2018c). There is a high catagenesis of organic matter in these zones. In the Sorym-Iminskaya, Vat-Yoganskaya, Yuzhno-Yagunskaya,

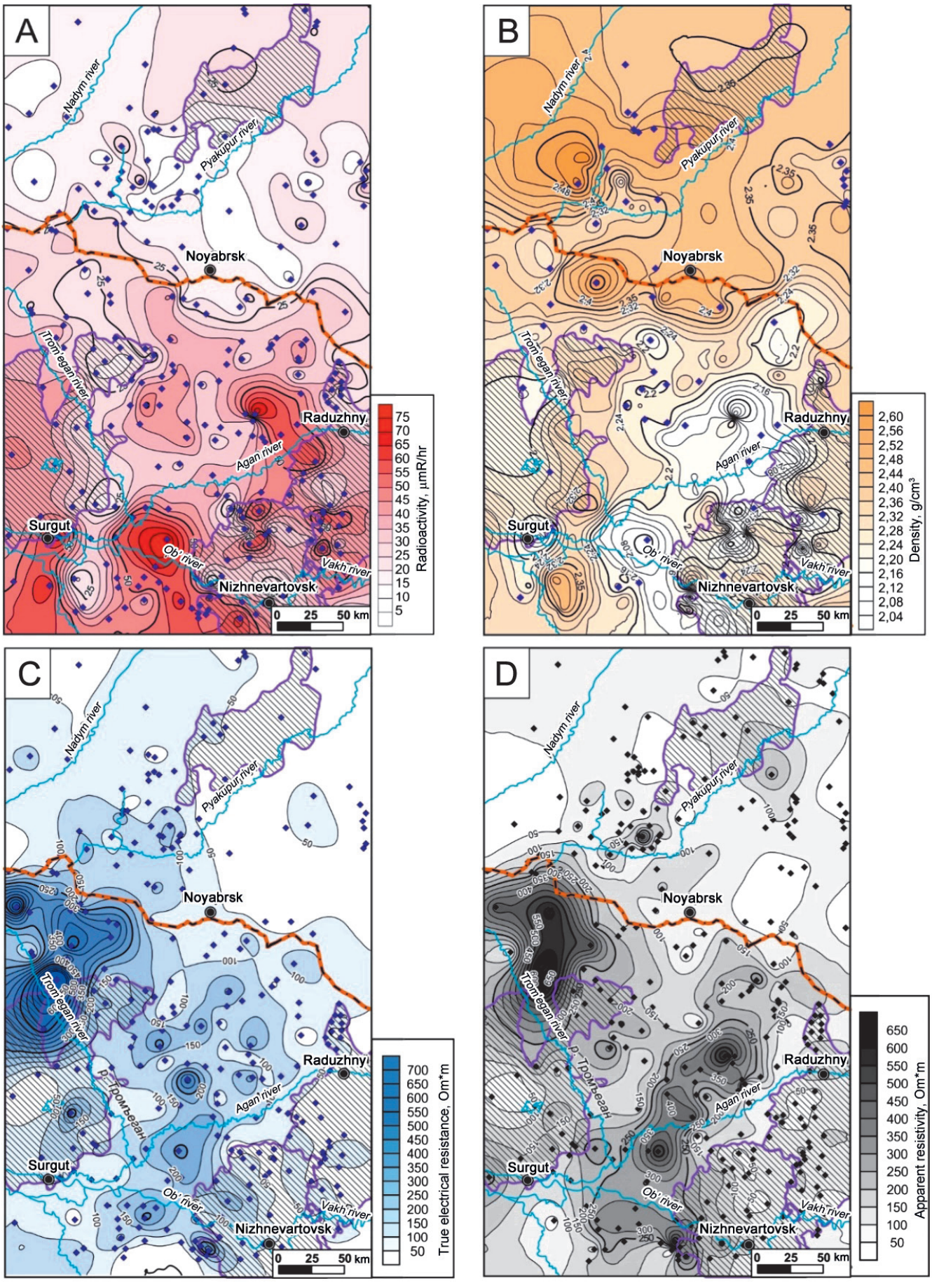


*Fig. 4. Maps of average values: A – radioactivity, B – density, C – true electrical resistance, D – apparent resistivity of the Bazhenov formation. See Figure 3 for legend.*

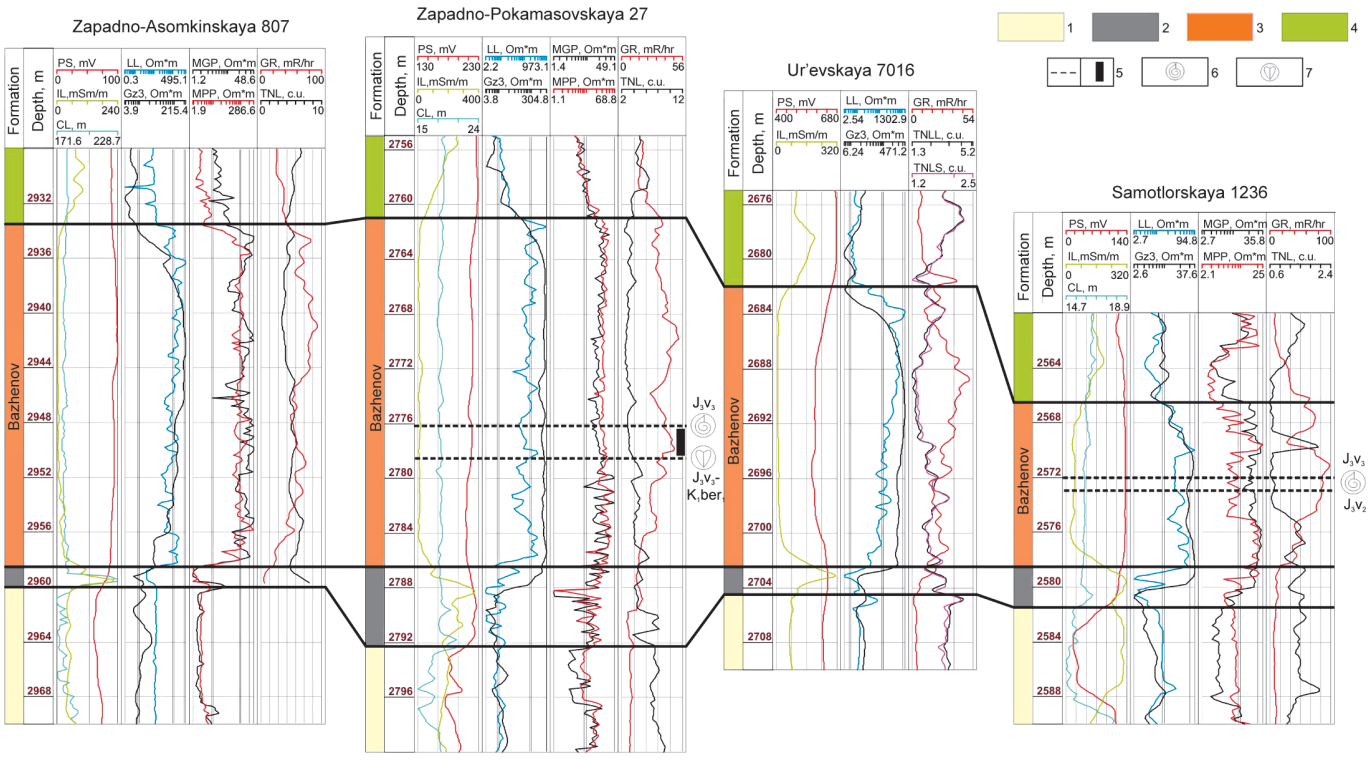


*Figure 5. Correlation profile along the A-A line. See Figure 2 for legend.*

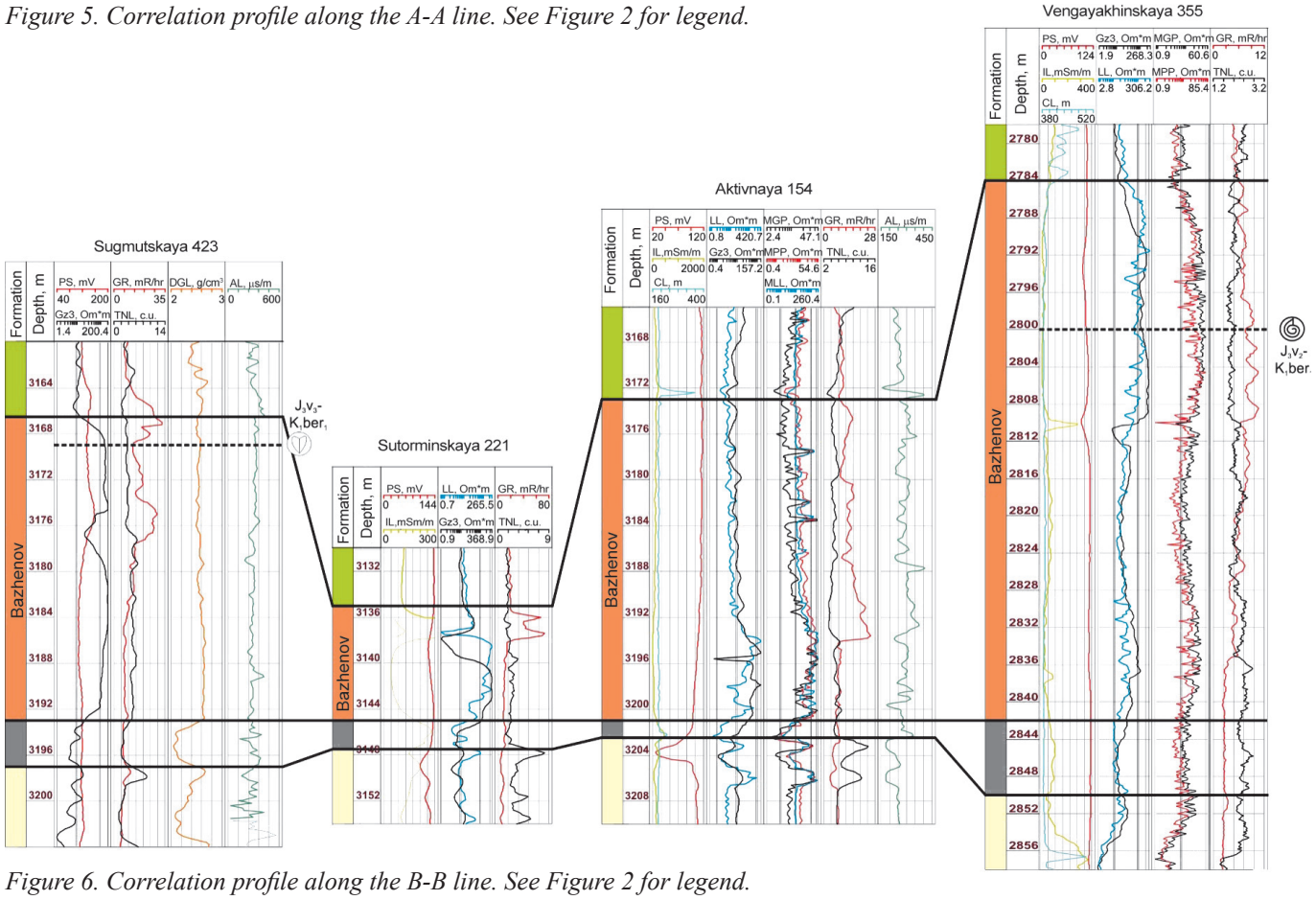


*Figure 6. Correlation profile along the B-B line. See Figure 2 for legend.*

Zapadno-Imilorskaya, Zapadno-Asomkinsky and Sogorskaya areas, the resulting flow of oil were obtained from the "classical" sections of the Bazhenov formation. All this allows us to highly assess the prospects of its oil-bearing capacity here (Figure 7).

As additional criteria for the forecast were also used:

- Modern temperatures at the top of the Jurassic complex (Zubkov, 2016; Skvortsov et al., 2018b);
- Thicknesses of the upper and lower impermeable layers, calculated by the authors on the basis of the results of the dissection of sections of the Upper Jurassic and Lower Cretaceous according to the well logging data;

• Average values of natural radioactivity and density of the Bazhenov formation (Figure 4A, B), which qualitatively characterize the modern content of kerogen in rocks;

• Average values of specific electrical resistance (Figure 4C, D), indicating oil saturation of the section.

The results of studying the lithology of the Bazhenov formation (Eder et al., 2016; Nemova, 2019, etc.) show that the interlayers, possibly with good reservoir properties, are distributed throughout its section. At the Sorym-Iminskaya and Yuzhno-Yagunskaya areas, oil inflows with a flow rate of 1 to 4.5 m$^3$/day were obtained from the middle and upper parts of the section, represented by mixtites of different composition and a "coccolith member". On the remaining areas in the southern, "Khanty-Mansiysk", half of the studied region, the entire section of the formation was tested, the inflow reaches 6 m$^3$/day.

In the Yamal-Nenets Autonomous District, at the Izvestinskoye, Vengayakhinskoye, Ety-Purovskoye fields, it was tested for oil inflow, mainly, the upper part of the section of the Bazhenov formation, which is composed of mixtites with various predominance of the main rock-forming components. On the Ety-Purovskaya area, no oil inflow was obtained in all wells, on the Vengayakhinskaya area it changes in the range of 0–1.2 m$^3$/day, on the Kraynyaya and Malo-Pyakutinskaya areas it does not exceed 1 m$^3$/day. The largest inflow of oil was obtained in the Izvestinskaya 704 well (22.8 m$^3$/day at a 6 mm choke), the Bazhenov oil reservoir in this field is on the state balance sheet. Apparently, such a large inflow is due to the significant fracturing of the formation in this area. It is important to note that tests in these areas were carried out from 1974 to 1991. The formation was stimulated by changing the clay solution to water and reducing the hydrostatic pressure. Apparently, it is the use of such an ineffective by today's standards method of testing the Bazhenov formation that explains such insignificant inflows in most wells.

In this region, in addition to Izvestinskoye, small oil deposits have been discovered at the Pyakutinskoye, Malopyakutinskoye, Vengayakhinskoye, Palnikovskoye fields. In these areas, the thickness of the Bazhenov formation with a TOC content of 7–10% reaches 4–5 m (Kontorovich et al., 2018c), it is located in the main zone of oil formation, reliably isolated by the lower and overlying seals, the current temperatures at its top exceed 90$^0$C. All this allows us to assume that there are commercial oil reserves in the Bazhenov formation. In the indicated and neighboring areas in the south of the Yamalo-Nenets Autonomous District, it is necessary

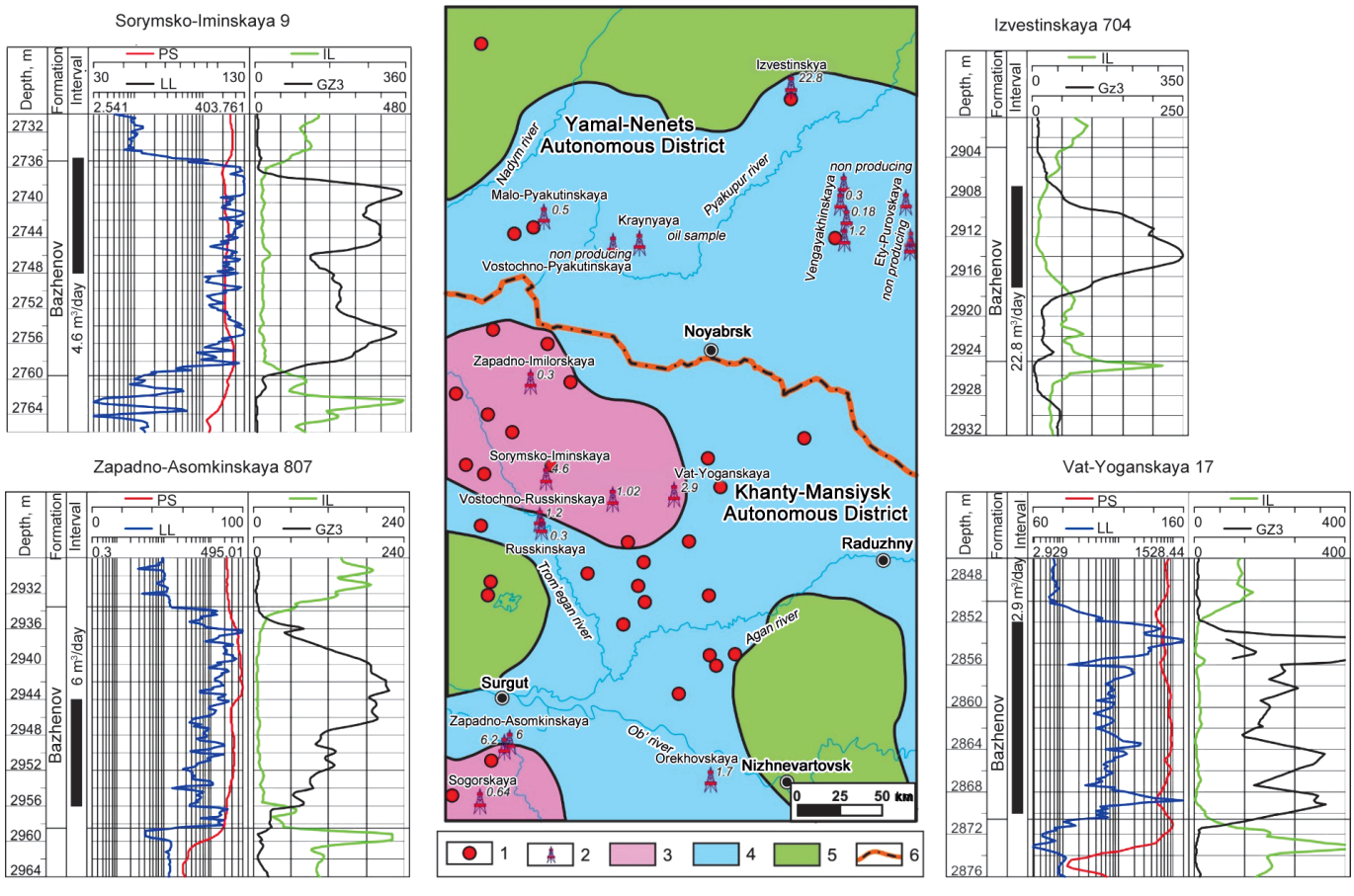


*Fig. 7. Map of oil-bearing prospects of the Bazhenov formation and logs with the intervals for testing these deposits for inflow. 1 – fields with oil deposits in the Bazhenov formation; 2 – wells with inflow testing of the Bazhenov formation; 3 – highly promising territories; 4 – promising territories; 5 – unpromising territories; 6 – administrative boundaries.*

to conduct repeated, interval testing of these deposits for inflow using modern technologies and methods of stimulation of inflow (hydraulic fracturing, catalytic reservoir stimulation, etc.). It is necessary to drill wells with full core sampling of the Bazhenov formation, as well as overlying and underlying sediments, and conduct its study using modern methods (Kontorovich et al., 2018a, b).

The study of this complex geological object using analytical methods will allow:

- To specify the lithological composition of the Bazhenov formation;
- Reliably identify oil source and oil production intervals in it;
- Study the structure of the Bazhenov reservoir and the nature of the saturation of its void space;
- Select the optimal well logging complex, with the help of which it will be possible to calculate the lithological composition and geochemical parameters of the Bazhenov formation in the wells that are not characterized by core material;
- Develop recommendations for calculating reserves in the Bazhenov formation;
- Develop recommendations for the creation of technologies for oil production from the Bazhenov formation.

## Conclusions

Based on the interpretation of a wide range of well logging data, the authors have significantly clarified the distribution boundaries of various types of sections of the Bazhenov formation in the Nadym-Ob interfluve. It was found that the Tarkosalinsky type is more widespread than it was shown earlier and is also distinguished in the Vengayakhinskaya, Yarainerskaya and other areas. The Nizhnevartovsk type, on the contrary, has a narrower distribution and is distinguished directly within the Nizhnevartovsk arch, being replaced to the south and east by the Vakh type of section.

A comprehensive analysis of the new geological, geophysical and published geochemical materials obtained by the authors showed that in the southern part of the Yamalo-Nenets Autonomous District in the interfluve of Nadym and Kharampur, it is possible to detect industrial accumulations of oil in the Bazhenov formation. At the Pyakutinskoye, Malopyakutinskoye, Vengayakhinskoye, Ety-Purovskoye, Izvestinskoye, Palnikovskoye, Extreme fields, it is necessary to retest these sediments for inflow using modern technologies and methods of inflow stimulation. In these and neighboring areas, it is necessary to drill new prospecting and exploration wells with full core sampling of the Bazhenov formation and conduct its study using modern techniques in order to study in detail the structure of the Bazhenov reservoir and the nature of saturation of its void space.

## Acknowledgments

*The study was carried out with the financial support of Project 0266-2019-0006 «Development of methods for resource assessment, exploration and calculation of reserves of hard-to-recover oil deposits in carbonaceous carbonate-clay-siliceous, carbonate and saline sand reservoirs» of the FSR Program IX.131.*

*The authors are grateful to the reviewer for a detailed analysis of the manuscript and valuable comments.*

## References

Baranova S.S. (2018). Highlighting promising zones of the Bazhenov Formation on the territory of the Yamalo-Nenets Autonomous Area. *Gornye Vedomosti*, 1, pp. 86–96. (In Russ.)

Braduchan Yu.V., Gurari F.G., Zakharov V.A. (1986). Bazhenov Horizon of Western Siberia (stratigraphy, paleogeography, ecosystem, oil content). Novosibirsk: Nauka, 216 p. (In Russ.)

Eder V.G., Kostyreva E.A., Yurchenko A.Yu., Balushkina N.S., Sotnich I.S., Kozlova E.V., Zamirailova A.G., Savchenko N.I. (2019). New data on lithology, organic geochemistry, and conditions for the formation of the Bazhenov formation of Western Siberia. *Georesursy = Georesources*, 21(2), pp. 129–142. (In Russ.) https://doi.org/10.18599/grs.2019.2.129–142

Eder V.G., Zamirailova A.G., Yan P.A. (2017) The regularities of the distribution of siliceous mudstones and "coccolith" member of the Bazhenov Formation. *Russian Geology and Geophysics*, 58(3–4), pp. 416–424. http://dx.doi.org/10.1016/j.rgg.2016.09.017

Eder V.G., Zamirailova A.G., Zhigulsky I.A. (2016). Lithology of the Bazhenov formation in the areas of the Khantey hemianteclise and Mezhovsky megamys of the West Siberian oil and gas basin. *Geologiya Nefti i Gaza = Russian Oil And Gas Geology*, 6, pp. 87–96. (In Russ.)

Eder. V.G., Zamirailova A.G., Zanin Yu.N., Zhigulsky I.A. (2015). Features of the lithological composition of the main types of sections of the Bazhenov Formation. *Geologiya Nefti i Gaza = Russian Oil And Gas Geology*, 6, pp. 96–106. (In Russ.)

Kalmykov G.A., Balushkina N.S. (2017). A model of oil saturation in the pore space of rocks of the Bazhenov formation in Western Siberia and its use for assessing the resource potential. Moscow: GEOS, 246 p. (In Russ.)

Kolpakov V.A., Spiridonov D.A., Shaykhutdinova G.Kh., Satgaleev Y.Kh., Koinova N.A., Galiev T.R. (2016). Oil content and geological structure of the normal and anomalous sections of the Bazhenov formation of the Kogalym region. *Geologiya, geofizika i razrabotka neftyanykh i gazovykh mestorozhdenii = Geology, Geophysics and Oil and Gas Field Development,* 11, pp. 5–17. (In Russ.)

Kontorovich A.E., Burshtein L.M., Livshits V.R., Ryzhkova S.V. (2019). The main directions of development of the oil complex of Russia in the first half of the XXI century. *Vestnik RAN = Bulletin of the Russian Academy of Sciences*, 89(11), pp. 1095–1104. (In Russ.)

Kontorovich A.E., Burshtein L.M., Nikitenko B.L., Ryzhkova S.V., Borisov E.V., Ershov S.V., Kostyreva E.A., Kontorovich V.A., Nekhaev A.Y., Ponomareva E.V., Fomin M.A., Yan P.A. (2019). Volgian-Early Berriasian Marginal Filter in the West Siberian Marine Basin and Its Influence on Sediment Distribution. *Lithology and Mineral Resources*, 54(3), pp. 187–199. https://doi.org/10.1134/S0024490219030039

Kontorovich A.E., Kontorovich V.A., Ryzhkova S.V., Shurygin B.N., Vakulenko L.G., Gaideburova E.A., Danilova V.P., Kazanenkov V.A., Kim N.S., Kostyreva E.A., Moskvin V.I., Yan P.A. (2013). Jurassic paleogeography of the West Siberian sedimentary basin. *Russian Geology and Geophysics*, 54(8), pp. 747–779. http://dx.doi.org/10.1016/j.rgg.2013.07.002

Kontorovich A.E., Kostyreva E.A., Rodyakin S.V., Sotnich I.S., Yan P.A. (2018b). Geochemistry of bitumoids of the Bazhenov formation. *Geologiya Nefti i Gaza = Russian Oil And Gas Geology*, 2, pp. 79–88. (In Russ.)

Kontorovich A.E., Ponomareva E.V., Burshtein L.M., Glinskikh V.N., Kim N.S., Kostyreva E.A., Pavlova M.A., Rodchenko A.P., Yan P.A. (2018). Distribution of organic matter in rocks of the Bazhenov Horizon (West Siberia). *Russian Geology and Geophysics*, 59(3), pp. 285–298. http://dx.doi.org/10.1016/j.rgg.2018.03.007

Kontorovich A.E., Rodyakin S.V., Burshtein L.M., Kostyreva E.A., Ryzhkova S.V., Yan P.A. (2018a). Porosity and oil saturation of rocks of the Bazhenov formation. *Geologiya Nefti i Gaza = Russian Oil And Gas Geology*, 5, pp. 61–73. (In Russ.)

Kontorovich A.E., Yan P.A., Zamirailova A.G., Kostyreva E.A., Eder V.G. (2016). Classification of rocks of the Bazhenov Formation. *Russian*

*Geology and Geophysics*, 57(11), pp. 1606–1612. http://dx.doi.org/10.1016/j.rgg.2016.10.006

Kontorovich V.A., Belyaev S.Yu., Kontorovich A.E., Krasavchikov V.O., Kontorovich A.A., Suprunenko O.I. (2001). The tectonic structure and history of tectonic development of the West Siberian geosyneclise in the Mesozoic and Cenozoic. *Geologiya i Geophysika = Geology and Geophysics*, 42, 11–12, pp. 1832–1845. (In Russ.)

Makarova O.M., Korobova N.I., Kalmykov A.G., Kalmykov G.A., Balushkina N.S., Belokhin V.S., Kozlova E.V., Kosorukov V.L., Manuilova E.A. (2017). The main rock types of the Bazhenov Formation on the Surgut arch and adjacent territories. *Georesursy = Georesources*, Special issue, pp. 155–164. http://doi.org/10.18599/grs.19.16

Nemova V.D. (2019). Multilevel lithological typization of rocks of the Bazhenov Formation. *Neftyanoe Khozyaystvo = Oil industry*, 8, pp. 13–17. (In Russ.)

Neruchev S.G. (1982). The relationship of the epochs of accumulation of organic matter and uranium with the boundaries of the development of the organic world. *Proc. VIII Int. Congress: Geochemistry of modern fossil sediments*, pp. 5–15. (In Russ.)

Neruchev S.G. (1976). The era of radioactivity in the history of the Earth and the development of the biosphere. *Geologiya i Geophysika = Geology and Geophysics,* 5, pp. 3–13. (In Russ.)

Prischepa O.M., Averyanova O.Yu., Ilyinsky A.A., Morariu D. (2014). Oil and gas of low-permeability shale strata – the reserve of the raw material base of hydrocarbons in Russia. St.Petersburg: VNIGRI, 323 p. (In Russ.)

Ryzhkova S.V., Burshtein L.M., Ershov S.V., Kazanenkov V.A., Kontorovich A.E., Kontorovich V.A., Nekhaev A.Y., Nikitenko B.L., Fomin M.A., Shurygin B.N., Beizel A.L., Borisov E.V., Zolotova O.V., Kalinina L.M., Ponomareva E.V. (2018). The Bazhenov Horizon of West Siberia: structure, correlation, and thickness. *Russian Geology and Geophysics*, 59(7), pp. 846–863. http://dx.doi.org/10.1016/j.rgg.2018.07.009

Skvortsov M.B., Kuznetsov G.V., Surova N.D., Kopilevich E.A. (2018b). New data on the location of oil and gas productive zones of Bazhenov deposits in Western Siberia. *Geologiya Nefti i Gaza = Russian Oil And Gas Geology*, 2018b, 2, pp. 89–96. (In Russ.)

Skvortsov M.B., Nemova V.D., Panchenko I.V., Kirsanov A.M. (2018a) Oil-bearing criteria for sediments of the Bazhenov Formation. *Geologiya Nefti i Gaza = Russian Oil And Gas Geology*, 1, pp. 109–114. (In Russ.)

Soeder J. Daniel, Borglum J. Scyller (2019). The fossil fuel revolution. Shale gas and tight oil. Elsevier, 336 p.

Stafeev A.N., Stoupakova A.V., Suslova A.A., Gilaev R.M. (2017). Conditions of sedimentation and paleogeographic zoning of the Bazhenov Horizon (Tithon-Lower Berrias) in West Siberia. *Georesursy = Georesources*. Special issue, pp. 134–143. http://doi.org/10.18599/grs.19.14

Stupakova A.V., Stafeev A.N., Suslova A.A., Gilaev R.M. (2016). Paleogeographic conditions in the West Siberian Basin during the Tithonian–Early Berriasian. Moscow University Geology Bulletin, 72, pp. 8–17. https://doi.org/10.3103/S0145875217010112

Zubkov M.Yu. (2016). Regional and local forecasts of the oil content of the Bazhenov and Abalak Formations (Western Siberia). *Gornye Vedomosti,* 3–4, pp. 46–68. (In Russ.)

## About the Authors

*Mikhail A. Fomin* – Cand. Sci. (Geology and Mineralogy), Head of the Laboratory for Problems of Geology, Exploration and Development of Hard-to-Recover Oil Fields, Trofimuk Institute of Petroleum Geology and Geophysics of the Siberian Branch of the Russian Academy of Sciences; Senior Lecturer, Novosibirsk State University

3, Ak.Koptyug ave., Novosibirsk, 630090, Russian Federation. E-mail: FominMA@ipgg.sbras.ru

*Rashid M. Saitov* – Junior Researcher, Laboratory for Problems of Geology, Exploration and Development of Hard-to-Recover Oil Fields, Trofimuk Institute of Petroleum Geology and Geophysics of the Siberian Branch of the Russian Academy of Sciences

3, Ak.Koptyug ave., Novosibirsk, 630090, Russian Federation

*Manuscript received 8 April 2020;*
*Accepted 16 June 2020; Published 30 September 2020*

ORIGINAL ARTICLE

**DOI**: https://doi.org/10.18599/grs.2020.3.12-20 Russian Original 2020. Vol. 22. Is. 3. Pp. 12–20

# Petroleum source rocks of the Silurian deposits on the Chernov swell (Timan-Pechora basin)

*I.S. Kotik[1*], T.V. Maydl[1], O.S. Kotik[1], N.V. Pronina[2]*

[1]*Institute of Geology of Komi Science Centre of the Ural Branch of the Russian Academy of Sciences, Syktyvkar, Russian Federation*

[2]*Lomonosov Moscow State University, Moscow, Russian Federation*

**Abstract**. Silurian source rocks are among the least studied in the Timan-Pechora basin. This is mainly due to their occurrence at great depths (3.0–4.5 km) and the limited penetration of this stratigraphic interval by wells. Another source of information is the outcrops of the Silurian, which are known in the eastern and northeastern parts of the Timan-Pechora basin. The studied section of the Silurian deposits is exposed on the Padimeityvis River, located on the Chernov swell in the northeastern part of the basin. This article is devoted to the study of Silurian source rocks based on the results of lithological, coal petrographic studies and geochemistry of organic matter. The studied section is composed of carbonate and clay-carbonate deposits formed in shallow-water shelf conditions. Most of the section, composed of microcrystalline and microcrystalline with bioclasts limestones, is characterized by low concentrations of organic matter (TOC is generally less than 0.3 %). Elevated TOC contents (up to 1.16 %) are characteristic of clay-carbonate rock varieties, which make up about 20 % of the section. Sediments with increased concentrations of organic matter were formed in isolated and deepened areas of the bottom of the shallow-water basin as a whole. Assessment of the catagenetic transformation based on Rock-Eval pyrolysis data, coal petrographic studies, and conodont color indices showed that organic matter reached the conditions of the middle-end of the main oil generation zone (gradation $MC_2$-$MC_3$). The obtained geochemical characteristics (TOC, $S_2$, HI), taking into account a certain level of organic matter maturity, indicate that the Silurian source rocks had an average hydrocarbon potential.

**Keywords**: Chernov swell, Silurian deposits, source rocks, organic matter, catagenesis, hydrocarbons

**Recommended citation**: Kotik I.S., Maydl T.V., Kotik O.S., Pronina N.V. (2020). Petroleum source rocks of the Silurian deposits on the Chernov swell (Timan-Pechora basin). *Georesursy = Georesources,* 22(3), pp. 12–20. DOI: https://doi.org/10.18599/grs.2020.3.12-20

## Introduction

Silurian deposits in the Middle Ordovician-Lower Devonian oil and gas bearing complex in the Timan-Pechora basin are considered as one of the sources for the generation of hydrocarbons (HC) (Bazhenova et al., 2008; Klimenko, Anischenko, 2010; Danilevskiy et al., 2003). Oil deposits in Silurian sediments have been established in the territories adjacent to the Chernov swell – the Chernyshev Ridge and the Varandey-Adzva structural zone. The presence of petroleum source rocks with geochemical parameters necessary for generation processes indicates the generation of hydrocarbons in the Silurian deposits. The assessment of the oil source properties in the Silurian deposits in the studied area of the Timan-Pechora basin is given in a few publications and on limited core material (Bazhenova et al., 2008, Danilov et al., 2011, Kotik et al., 2016, Pesetskaya, Pavlova, 1997). This is mainly due to their occurrence at great depths (3.0–4.5 km) and the limited penetration by wells of this stratigraphic interval. The lack of factual material can be compensated for by studying the Silurian deposits in outcrops, which are known at the Chernov swell. The study of the structure of the Silurian sedimentary section in outcrops, the identification of potential oil and gas-generating strata and the characteristics of organic matter (OM) are the goals of the lithological, organic geochemical and coal-petrographic studies, the results of which are discussed in this article.

## Area and object of research

The study area is located in the northeast of the Timan-Pechora oil and gas bearing basin within the Chernov swell. The Chernov swell is a linear structure that separates the Korotaikha depression from the Varandey-Adzva structural zone and the Kosyu-Rogov depression (Timonin, Yudin, Belyaev, 2004) (Figure 1). The northwestern half of the swell (Vashutkino-Talota

[*]*Corresponding author: Ivan S. Kotik*
*E-mail: iskotik@geo.komisc.ru*

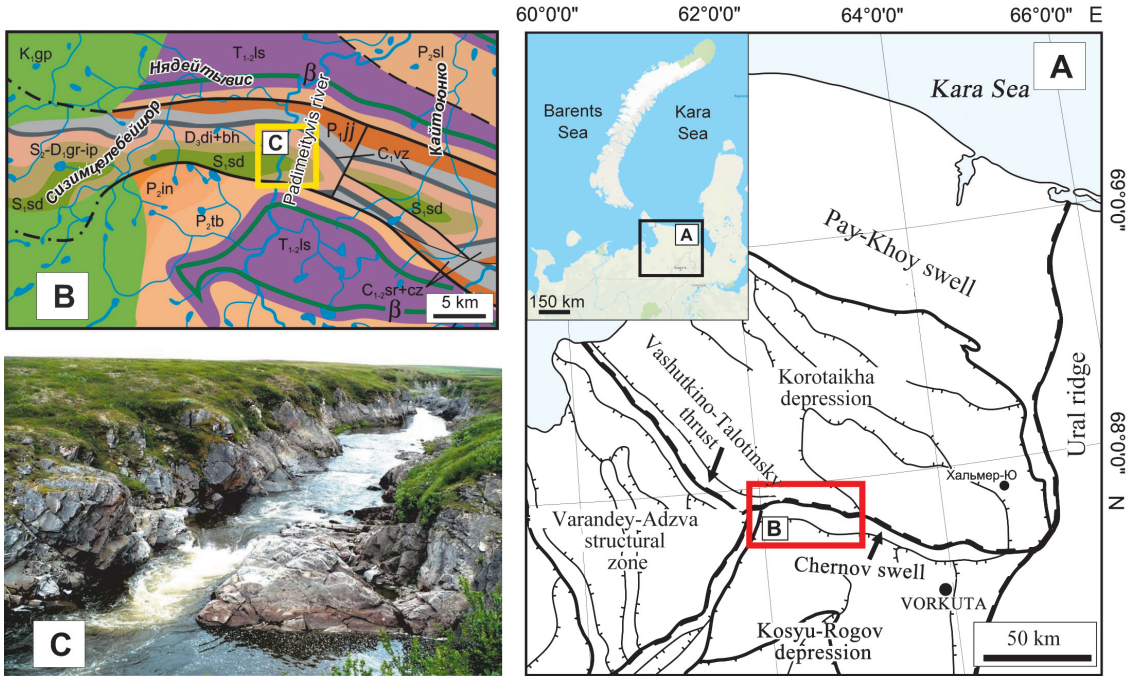


*Fig. 1. Overview map of the studied area and the location of the studied section of the Silurian deposits. A – tectonic zoning map (Belonin et al., 2004), B – geological map (State Geological Map ..., 2007), C – photo of outcrops of Silurian deposits in the canyon of the Padimeityvis river.*

thrust) in the form of monoclinal subsiding deposits has a simpler structure, and the southeastern half is complicated by back-thrasts, forming a wedge shape in the section.

The section of the Silurian deposits studied by us for about 500 meters is exposed in the canyon of the river Padimeityvis of the left tributary of the river Korotaikha. The bedding of the rocks is fairly consistent, with a general dip to the north at an angle of 60–65°. The exposed thickness of the section is about 460 m. In the age range, the Silurian deposits are represented here by the Wenlock, Ludlow, Pridoli stages (Chernov, 1972; Beznosova, 2008).

## Methods

The complex of studies included petrographic and chemical studies of the lithological composition of rocks, as well as coal petrographic and geochemical studies of dispersed OM.

Microscopic study of the OM of rocks was carried out in polished sections under simple reflected and ultraviolet light on a Leica DM-2500 microscope (Lomonosov Moscow State University, Moscow), as well as in thin sections in transmitted light on a MeF-2 microscope.

The content of organic carbon (TOC, %) in the rock was determined on an AN-7529 express analyzer by combustion in an oxygen stream of samples pretreated with 10% hydrochloric acid. The yield of bitumen in the rocks was determined by hot extraction with chloroform in Soxhlet apparatus. Gas chromatographic analysis of hydrocarbons in the composition of the saturated fraction (n-alkanes and isoprenoids) of chloroform extracts was carried out on a Kristall 2000M device. This set of studies was carried out at the Geoscience Center (Syktyvkar).

The pyrolytic characteristics of OM $S_1$, $S_2$, $T_{max}$ were obtained on a Source Rock Analyzer (SR Analyzer, Humble Instruments) (IPGG SB RAS, Novosibirsk). To determine the influence of free hydrocarbons on the magnitude of the $S_2$ peak and obtain more correct values of the parameter $T_{max}$, repeated pyrolysis of rock samples after extraction with chloroform was performed on a Rock-Eval 6 Standard (Vinci Technologies) device (VNIGNI, Moscow).

## Results and discussion

### *Lithological characteristics of the section*

In the Silurian period, the area under consideration was a marine epicontinental basin with settings of a typical shallow-water carbonate platform (Antoshkina et al., 2011, 2015). The facies conditions in the sedimentary basin changed repeatedly, which led to the accumulation of carbonate and clay-carbonate sediments of different material composition and structural-textural features. In the studied section of the Silurian deposits, according to the peculiarities of the lithological composition, 4 members are distinguished from bottom to top: clay-limestone, limestone, clay-dolomite-limestone and limestone (Figure 2).

The first clay-limestone pack (160 m) is composed of limestones, dolomitic limestones with interlayers of clay limestones and marls (Figure 3, a-e). Limestones are represented by wavy-layered microbial-clotted,

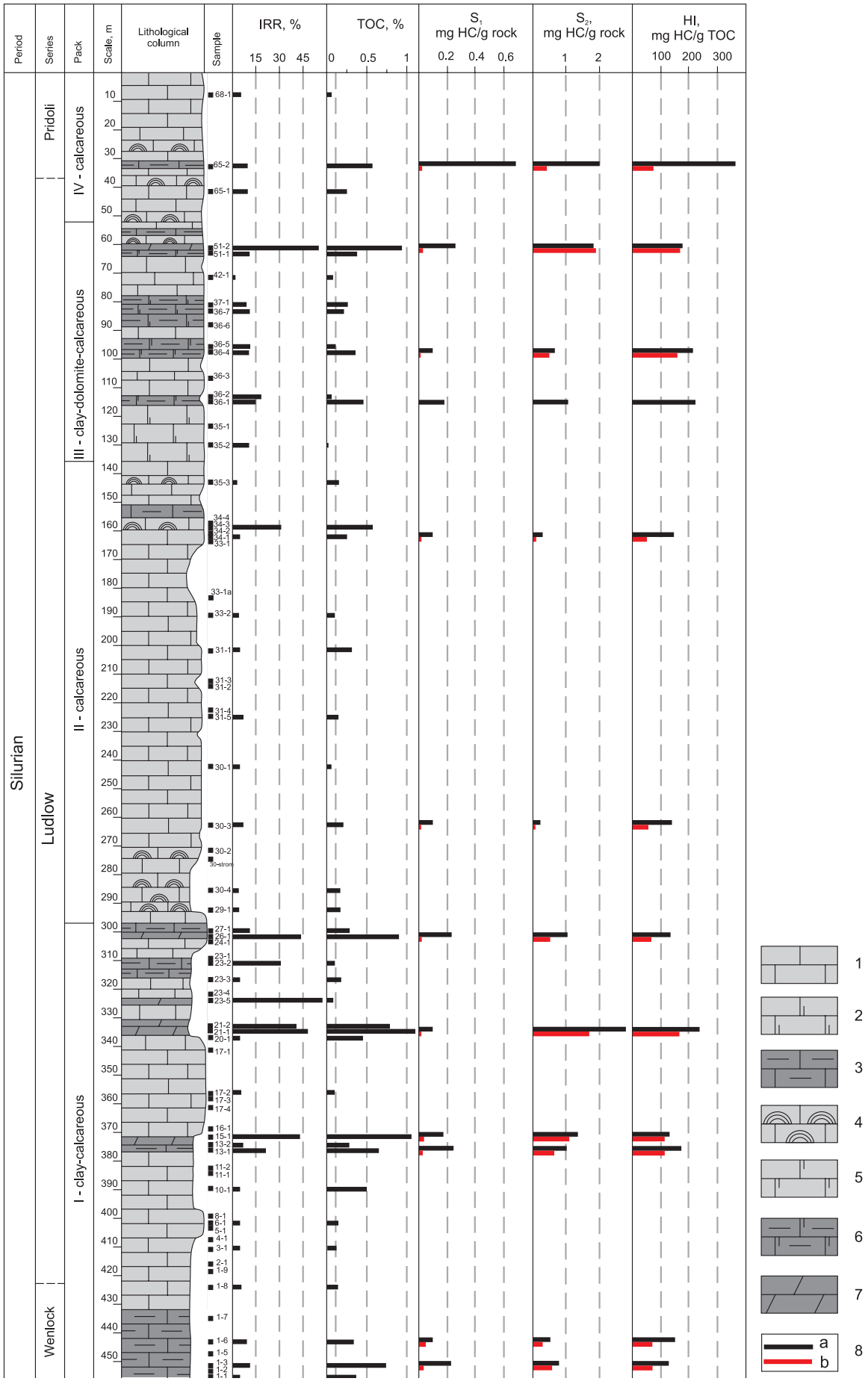


*Fig. 2. Lithological composition and distribution of geochemical parameters along the section. 1 – limestone, 2 – dolomitic limestone, 3 – clay limestone, 4 – stromatolitic limestone, 5 – limestone dolomite, 6 – clay limestone dolomite, 7 – marl, 8 – Rock-Eval pyrolysis data: a – before extraction, b – after extraction.*

microcrystalline and microcrystalline with bioclasts varieties with spotty-banded and spotty textures. Limestones with the structure of mudstones and wackstones prevail, less often pack-wackstones (Figure 3, a, b). In the upper part, the proportion of clay-carbonate layers increases. The limestones are dominated by microcrystalline mudstones and peloid-ostracodic wackstones with small lithoclasts (Figure 3, c). The second limestone pack (161 m) is composed mainly of bioclastic and microcrystalline with bioclasts limestones, in structure by pack-wackstones, less often by mudstones (Figure 3, f, e). The lower and upper parts of the pack contain limestones with stromatolite biostromes. The third member (84 m) has a clay-dolomite-limestone composition. It is composed of limestones, dolomitic peloid-bioclastic limestones, and limestone clay dolomites (Figure 3, h-j). The structure is dominated by mudstones and wackstones. The section is completed by a limestone member (52 m), composed of limestone mudstones with rare bioclasts (Figure 3, k) and stromatolite limestones. The top of the pack contains bioclastic limestones with a packstone structure (Figure 3, l).

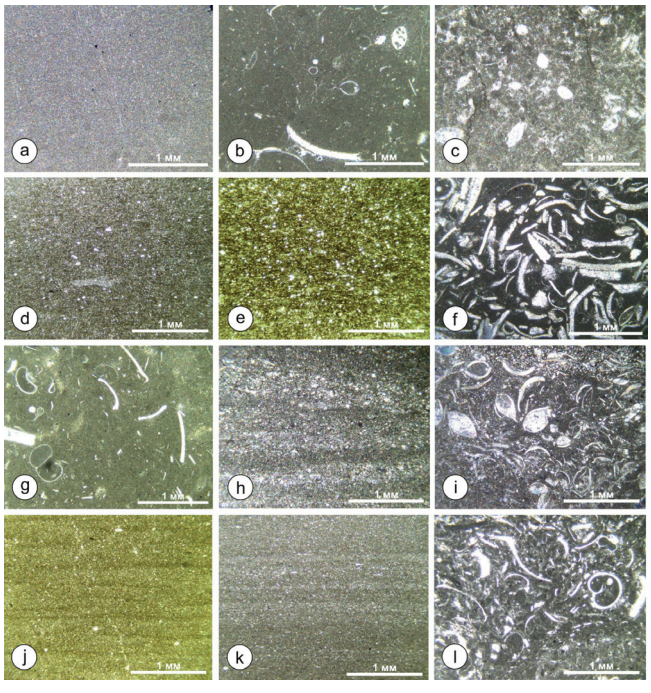


*Fig. 3. The main lithological types of rocks of the Silurian deposits composing the identified units. Pack I: a – microcrystalline limestone, mudstone, sample 6-1, b – microcrystalline limestone with bioclasts, wackstone, sample 17-2, c – peloid-ostracod limestone, wackstone, sample 23-3, d – clay limestone, mudstone, sample 13-1, e – marl, sample 26-1; Pack II: f – bioclastic limestone, packstone, sample 30-2, g – microcrystalline limestone with bioclasts, wackstone, sample 31-5, pack III: h – limestone dolomite, mudstone, sample 36-5, i – peloid-bioclastic dolomitic limestone, packstone, sample 36-6, j – clay dolomite, mudstone, sample 51-1; pack IV: k – microcrystalline limestone, mudstone, sample 65-1, l – bioclastic limestone, packstone, sample 68-5.*

## Facial conditions of OM accumulation

Consideration of the lithological composition in the studied section shows that the formation of Silurian deposits in the conditions of a shallow shelf did not contribute to the accumulation of petroleum source deposits with a consistent thickness and enriched OM (Figure 2). The accumulation of clay-carbonate deposits with increased TOC contents in the studied section is associated with individual deepened areas of the bottom of the shallow-water basin as a whole.

OM-enriched clay limestones and dolomites, which mainly compose packs I and III, were formed under sublittoral conditions. Microcrystalline structure, bedding character, rare traces of bioturbation, poor faunal remains indicate the relative isolation of the sedimentation basin (Figure 4, a). In the deeper areas of the sublittoral, during the periods of maximum sea level, the most OM enriched marls were formed (Figure 4b). In both cases, the sedimentation environment favored the relative accumulation of organic material and its conservation. This is due to the fact that the limited circulation of water prevents free oxygen exchange and decomposition of OM by aerobic heterotrophic organisms. The presence of terrigenous admixtures in the sediments also favors the accumulation of OM. The adsorption of dissolved OM on the surface of mineral particles promotes faster deposition through the water column and increases its protection from destruction by bacteria (Bazhenova et al., 2000).

The OM poverty in bioclastic and peloid-bioclastic limestones characteristic of packs II and IV is due to their accumulation in the littoral-sublittoral zone with active hydrodynamics of the aquatic environment and the vital activity of benthic organisms that did not contribute to the retention and concentration of OM (Figure 4b). Active circulation in the water column provided constant oxygen replenishment, which was spent on the decomposition of OM. Bioturbation of sediments by benthic organisms provided additional aeration of sediments and degradation of OM (Demaison, Moore, 1980).

### *Content, HC potential and catagenesis of OM*

The TOC concentrations in the studied rocks vary from 0.02 to 1.16% and depend on their lithological composition (Figure 2). Bioclastic, peloid-bioclastic, microcrystalline and microcrystalline with bioclasts limestones are characterized by low TOC contents, generally not exceeding 0.30%. In clay limestones and dolomites (IRR – insoluble rock residue – 9–21%), the TOC concentration rises to 0.74%. The maximum contents up to 0.83–1.16% are found in carbonate-argillaceous rocks with an increased clay component

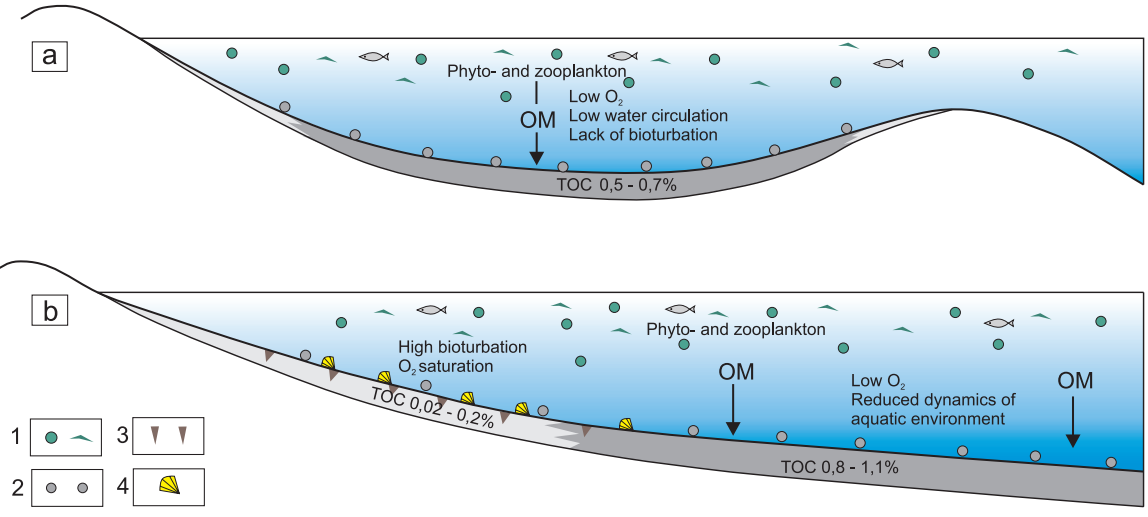


*Fig. 4. Model of accumulation of OM-enriched Silurian sediments in isolated (lagoon) (a) and open sea (sublittoral) (b) conditions. 1 – phyto- and zooplactone; 2 – organic matter; 3 – bioturbation; 4 – benthic fauna.*

(IRR – 43–55%). In general, clay-carbonate deposits with an increased OM content are mainly distributed in members I and III, with a total thickness of about 110 m, which is about 20% of the section (Figure 2).

The values of the parameters $S_1$ and $S_2$ obtained during the Rock-Eval pyrolysis for the studied samples are 0.10–0.68 mg HC/g rock and 0.21–2.76 mg HC/g rock, respectively (Table 1, Figure 2). The hydrogen index (HI) varies within the range of 122–363 mg HC/g TOC. The generation potential ($S_1 + S_2$), like the TOC content, depends on the lithology of the rocks. The highest values are found in clay limestones and dolomites – 1.06–2.86 mg HC/g rock. For bioclastic limestones, the $S_1 + S_2$ value is the lowest – 0.31–0.37 mg HC/g rock.

Pyrolysis studies of samples after hot extraction, partially freed from HC and resinous-asphaltene components, show a reduction in peaks $S_1$ and $S_2$. Parameter $S_1$ significantly decreases and levels out, amounting to 0.01–0.05 mg HC/g rock (Figure 2, Table 1). $S_2$ is reduced by 15–79%. A decrease in the $S_2$ peak leads, respectively, to a decrease in the HI

| Samp. | Rock | IRR % | TOC, % | $TOC^{ex}$, % | $S_1$, mg HC/g rock | $S_2$, mg HC/g rock | $S_1^{ex}$, mg HC/g rock | $S_2^{ex}$, mg HC/g rock | HI, mg HC/g TOC | $HI^{ex}$, mg HC/g TOC | $T_{max}^{ex}$, ºC | $PI^{ex}$ |
|---|---|---|---|---|---|---|---|---|---|---|---|---|
| 1-3 | clay limestone | 12 | 0.70 | 0.66 | 0.21 | 0.85 | 0.03 | 0.62 | 122 | 73 | 441 | 0.05 |
| 1-6 | limestone | 9 | 0.34 | 0.30 | 0.10 | 0.51 | 0.05 | 0.30 | 148 | 71 | 438 | 0.14 |
| 13-1 | clay limestone | 21 | 0.62 | 0.57 | 0.24 | 1.06 | 0.02 | 0.68 | 170 | 110 | 452 | 0.02 |
| 15-1 | marl | 43 | 1.10 | 1.06 | 0.18 | 1.35 | 0.03 | 1.15 | 123 | 111 | 448 | 0.02 |
| 21-1 | marl | 48 | 1.16 | 1.13 | 0.10 | 2.76 | 0.01 | 1.70 | 238 | 168 | 440 | 0.01 |
| 26-1 | marl | 44 | 0.83 | 0.77 | 0.23 | 1.03 | 0.02 | 0.49 | 124 | 67 | 438 | 0.03 |
| 30-3 | bioclasts limestone | 7 | 0.15 | 0.12 | 0.10 | 0.21 | 0.02 | 0.05 | 144 | 56 | 421 | 0.30 |
| 34-1 | bioclasts limestone | 5 | 0.19 | 0.16 | 0.10 | 0.27 | 0.02 | 0.11 | 140 | 52 | 429 | 0.18 |
| 36-1 | clay dolomite | 15 | 0.44 | | 0.19 | 0.95 | | | 217 | | | |
| 36-4 | limestone dolomite | 11 | 0.31 | 0.28 | 0.10 | 0.67 | 0.01 | 0.52 | 215 | 162 | 446 | 0.02 |
| 51-2 | marl | 55 | 0.98 | 0.91 | 0.25 | 1.81 | 0.03 | 1.89 | 184 | 172 | 440 | 0.02 |
| 65-2 | clay limestone | 10 | 0.55 | 0.48 | 0.68 | 1.98 | 0.02 | 0.41 | 363 | 76 | 435 | 0.05 |

*Table 1. Data from pyrolysis studies (Rock-Eval). IRR – insoluble rock residue; TOC – organic carbon content; $TOC^{ex}$, – organic carbon content after extraction; HI – 100*$S_2$ /TOC; $S_1^{ex}$, $S_2^{ex}$, $HI^{ex}$, $T_{max}^{ex}$, $PI^{ex}$ – $S_1^{ex}$ / $S_1^{ex}$ + $S_2^{ex}$, – results of pyrolysis of samples after extraction*

values (Figure 2). For a number of clay limestones and dolomites, HI after extraction decreased by 10–30%, and a significant decrease in the index to 60% is typical for bioclastic limestones (Table 1, Figure 2).

The degree of catagenetic transformation of OM was determined on the basis of pyrolysis data, coal petrographic studies, and conodont color alteration index (CAI).

The level of catagenetic transformation of OM according to the results of pyrolysis was assessed by two parameters – the $T_{max}$ value and the values of the productivity index (PI). The $T_{max}$ value varies in the range 421–452 °C. The PI index values for most of the samples vary in the range of 0.02–0.14 (Table 1, Figure 5). The high PI values of 0.18–0.30 observed for samples 30-3 and 34-1 at low values of $T_{max}$ 421–429 reflect the effect of the presence of migratory bitumen in the rocks (Lopatin, Emets, 1987) (Figure 5). In general, the obtained $T_{max}$ and PI data indicate the OM maturity level corresponding to the middle-end of the main oil generation zone ($MC_2$ – $MC_3$).

The results of determining the OM maturity from the pyrolysis data are consistent with the earlier assessment of catagenesis based on the CAI data (Kotik et al., 2017). The color change of conodont elements is used as an approximate estimate of the degree of thermal transformation of the host rocks and, accordingly, the OM contained in them. The obtained CAI values for the Silurian deposits are 1.5–2 (Figure 6), which indicates the intensity of heating of the enclosing strata up to 140 °C (Epstein, Epstein, Harris, 1977). This level of thermal impact corresponds to the conditions of catagenesis at the $MC_2$ gradation of the main zone of oil generation (Handbook…, 1998).

Coal petrographic studies did not allow assessing the catagenetic transformation of OM due to the lack of macerals suitable for measuring the reflection index. However, the presence of qualitative features such as a weak glow in ultraviolet light or its complete absence, as well as the absence of aureole bituminous structures may indicate a significant transformation of OM at the level of the end of the oil generation zone.

Earlier studies by D.A. Bushnev, N.S. Burdel'naya (2012) for samples of Silurian deposits of the Padimeityvis river and its tributary Bezymanny, a higher catagenetic maturity of OM was established. According to the distribution of polycyclic HCs of the sterane and hopane series, OM catagenesis reaches the $MC_2$ – $MC_3$ gradations and possibly higher values (Bushnev, Burdel'naya, 2012).

Thus, the totality of the available data indicates the level of OM catagenetic transformation corresponding to the middle-end of the main oil generation zone. The obtained geochemical characteristics (TOC, $S_2$, HI), taking into account a certain level of OM maturity, indicate that the studied petroleum source rocks of the Silurian deposits had an average HC potential.

### *Composition and type of OM*

The study of samples of clay-carbonate rocks (samples 21-1, 26-1, 51-2), the most enriched in OM by coal-petrographic methods, did not reveal the content of such macerals as bituminite (pre-mature, mature) and "hard bitumen" (post-mature) (Taylor, Liu, Teichmüller, 1991). All organic components are bitumen, which are the end products of the transformation of algogenic OM. In rocks, bitumen is present in the form of films between mineral grains and deposits, which gives it a brownish tint in simple reflected light (Figure 7, a-c). The most distinct distribution of bitumen in the rock is observed in ultraviolet light, where they form extended layers and separate isolated inclusions (Figure 7, d-f).

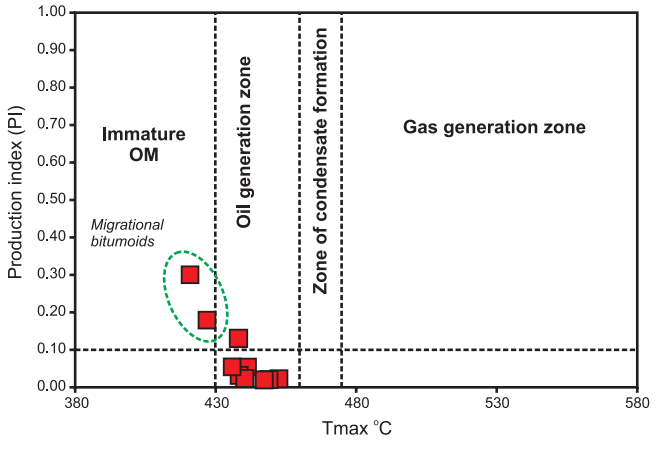


*Fig. 5. Catagenesis of OM according to the values of pyrolysis parameters $T_{max}$ and productivity index (PI)*

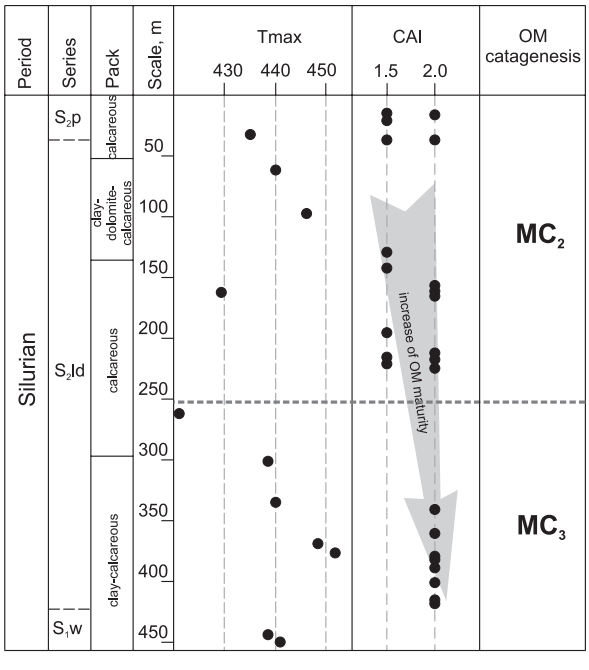


*Fig. 6. Changes in the catagenetic transformation of OM along the section*

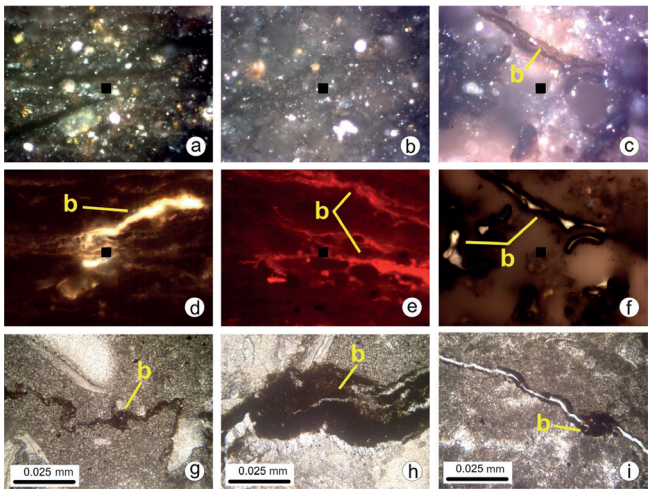


*Fig. 7. Micrographs of bitumen in reflected (a-f) and transmitted (g-i) light. a-c – reflected white light, oil immersion, x 50: a – sample 21-1, b – sample 26-1, c – sample 51-2; d-f – ultraviolet light, oil immersion, x 50: d – sample 21-1, e – sample 21-1, f – sample 51-2. b – bitumen. Black mark in the center of the frame 5x5 μm. g – i – transmitted light: g – sample 35-3, h – sample 29-1, i – sample 23-3.*

In carbonate rocks, which are a kind of reservoirs for hydrocarbons, bituminous content is manifested in a different way. Bitumen fill in the rock stylolite seams, cracks and voids, which indicates their partial or significant movement relative to the source rock (Figure 7, g-i). The carbonate rocks are also characterized by an increased content of bitumen against a background of low concentrations of TOC, the bitumen coefficient ($\beta_{CB}$) is 14–34% (Table 2). High $\beta_{CB}$ values also indicate the allochthonous nature of bitumen in the host rocks.

The study of HC composition of the saturated fraction of bitumen extracted from rocks was carried out according to the data of gas chromatography analysis. The previously studied features of the hydrocarbon composition of bitumen in the Silurian deposits of the Chernov swell showed differences in the nature of the molecular weight distribution of n-alkanes and isoprenoids (Kotik et al., 2017). Studies have shown that the nature of HC distribution depends on the lithological composition of the sediments (carbonate/clay content).

In the petroleum source rocks of clay-carbonate composition, bitumen of heavier hydrocarbon composition with an increased content of medium and high molecular weight n-alkanes are almost everywhere (Figure 8, a, b). Two types of distribution of normal and isoalkanes have been established. Bitumens of the first group (samples 15-1, 21-1, 26-1, 51-2) are characterized by the maximum distribution of n-alkanes in the n-$C_{13}$–$C_{20}$ range and the highest n-$C_{17}$/n-$C_{27}$ ratio – 1.26–2.84 (Table 2, Figure 8, a). The lighter composition of the HC fraction is confirmed by the presence of light HC accumulations in the rocks (Figure 7, f). For the second group of samples (1-3, 1-6, 10-1), the maximum of the distribution of n-alkanes is shifted to the high-molecular range > n-$C_{20}$, the values of the n-$C_{17}$/n-$C_{27}$ ratio for them are the lowest – 0.36–1.42 (Table 2, Figure 8, b). In such rocks, there is a greater amount of clay-bituminous interlayers and streaks of bitumen with an increased content of resinous-asphaltene components, without visible luminescence. The ratio of isoprenoid and n-alkanes such as Pr/n-$C_{17}$, Ph/n-$C_{18}$, Pr+Ph/$C_{17}$+$C_{18}$ (isoprenoid coefficient, Ki) and Pr/Ph for the studied samples is also determined by the type

| No. | Samp. | TOC,% | TOC$^{ex}$, % | CEB,% | $\beta_{CB}$, % | $\beta_{CB}^{ex}$, % | *н*-$C_{17}$ / *н*-$C_{27}$ | Pr / *н*-$C_{17}$ | Ph / *н*-$C_{18}$ | Pr+Ph/ *н*-$C_{17}$+*н*-$C_{18}$ | Pr / Ph | CPI |
|---|---|---|---|---|---|---|---|---|---|---|---|---|
| 1 | 1-3 | 0.70 | 0.66 | 0.0527 | 8 | 8 | 0.81 | 0.51 | 0.83 | 0.66 | 0.71 | 1.02 |
| 2 | 1-6 | 0.34 | 0.30 | 0.0468 | 14 | 15 | 0.67 | 0.45 | 0.69 | 0.57 | 0.68 | 0.97 |
| 3 | 10-1 | 0.50 | 0.45 | 0.0593 | 12 | 13 | 0.91 | 0.26 | 0.45 | 0.34 | 0.80 | 0.99 |
| 4 | 13-2 | 0.28 | 0.22 | 0.0414 | 15 | 17 | 1.17 | 0.22 | 0.31 | 0.27 | 0.78 | 0.95 |
| 5 | 15-1 | 1.10 | 1.06 | 0.0551 | 5 | 5 | 3.43 | 0.16 | 0.18 | 0.17 | 1.39 | 0.96 |
| 6 | 20-1 | 0.46 | 0.37 | 0.1079 | 23 | 29 | 0.64 | 0.20 | 0.28 | 0.24 | 0.76 | 0.97 |
| 7 | 21-1 | 1.16 | 1.13 | 0.0386 | 3 | 3 | 1.26 | 0.08 | 0.08 | 0.08 | 1.15 | 0.97 |
| 8 | 23-3 | 0.18 | 0.15 | 0.0383 | 21 | 26 | 1.06 | 0.10 | 0.12 | 0.11 | 0.85 | 0.99 |
| 9 | 26-1 | 0.83 | 0.77 | 0.0748 | 9 | 10 | 2.49 | 0.15 | 0.18 | 0.16 | 1.26 | 0.97 |
| 10 | 29-1 | 0.18 | 0.16 | 0.0298 | 17 | 19 | 1.13 | 0.12 | 0.13 | 0.12 | 1.08 | 0.98 |
| 11 | 30-3 | 0.15 | 0.12 | 0.0375 | 25 | 31 | 2.84 | 0.06 | 0.09 | 0.08 | 1.04 | 0.95 |
| 12 | 34-1 | 0.19 | 0.16 | 0.0420 | 22 | 27 | 1.74 | 0.12 | 0.25 | 0.17 | 0.87 | 0.95 |
| 13 | 35-3 | 0.15 | 0.11 | 0.0504 | 34 | 46 | 0.36 | 0.15 | 0.16 | 0.15 | 1.02 | 0.99 |
| 14 | 36-4 | 0.31 | 0.28 | 0.0415 | 13 | 15 | 0.97 | 0.10 | 0.25 | 0.16 | 0.67 | 0.97 |
| 15 | 42-1 | 0.08 | 0.06 | 0.0272 | 34 | 47 | 1.42 | 0.18 | 0.37 | 0.25 | 0.87 | 0.98 |
| 16 | 51-2 | 0.98 | 0.91 | 0.0891 | 9 | 10 | 1.81 | 0.26 | 0.40 | 0.31 | 1.03 | 1.01 |
| 17 | 65-1 | 0.25 | 0.21 | 0.0440 | 18 | 20 | 2.63 | 0.14 | 0.35 | 0.20 | 0.98 | 0.96 |

*Table 2. Geochemical parameters of bitumen of the Silurian deposits. CEB – chloroform extracted bitumen. $\beta_{CB}$ – CEB/TOC*100; $\beta_{CB}^{ex}$ – CEB/TOC$^{ex}$*100; CPI – ½*($C_{25}$+$C_{27}$+$C_{29}$+$C_{31}$+$C_{33}$)/($C_{26}$+$C_{28}$+$C_{30}$+$C_{32}$+$C_{34}$)+ ($C_{25}$+$C_{27}$+$C_{29}$+$C_{31}$)/($C_{24}$+$C_{26}$+$C_{28}$+$C_{30}$+$C_{32}$)*

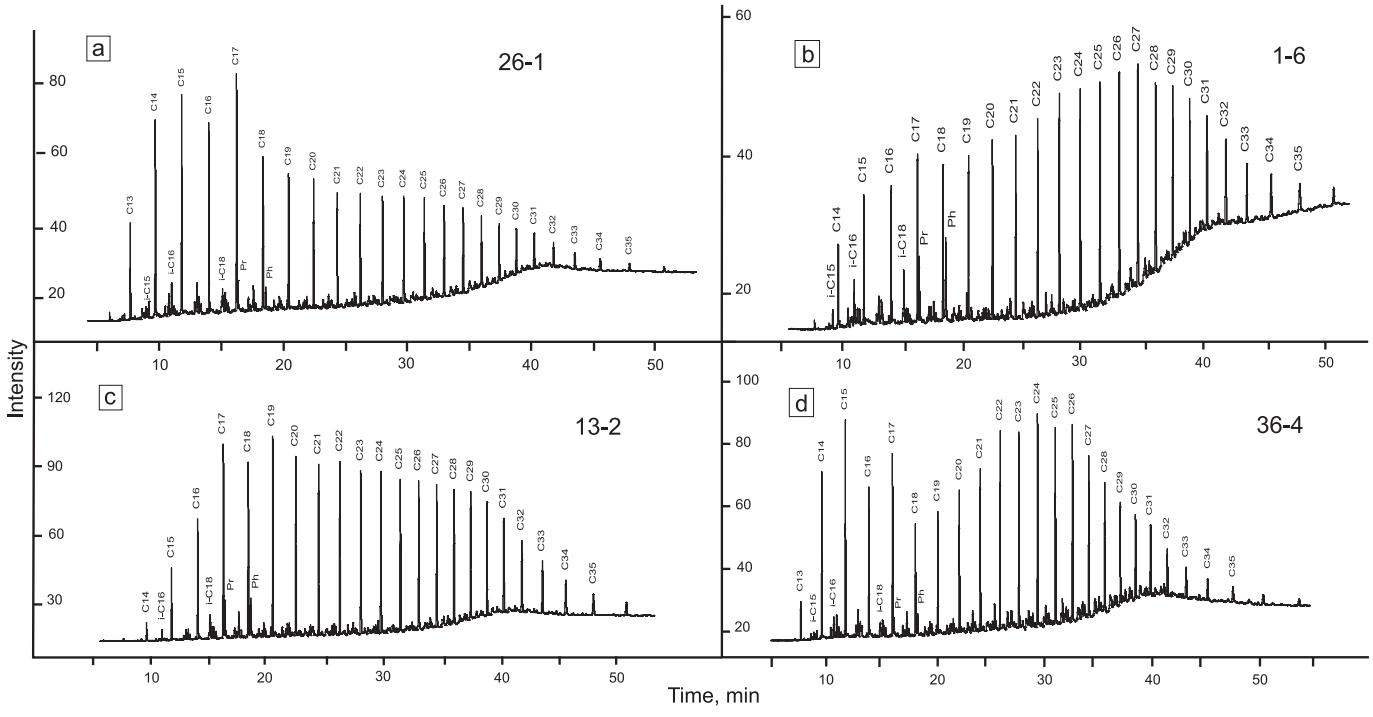


*Fig. 8. Chromatograms of the distribution of n-alkanes and isoprenoids in the saturated fraction of bitumen*

of molecular weight distribution of hydrocarbons (Table 2). For bitumens with increased concentrations of high molecular weight n-alkanes (Figure 8, b), the values of Pr/n-$C_{17}$, Ph/n-$C_{18}$, Ki are higher and phytane predominates (Pr/Ph – 0.67–1.08) (Table 2).

In carbonate rocks containing a fraction of displaced bitumen, two types of distribution of n-alkanes are mainly observed. In the first type, the HC maximum is in a wide molecular range $C_{17}$–$C_{30}$ (Fig. 8, c). The second type is characterized by a bimodal distribution of n-alkanes with maxima at $C_{15}$–$C_{17}$ and $C_{24}$–$C_{27}$ (Figure 8, d). For rocks containing bitumen with a bimodal distribution, stylolite seams with bitumen are almost everywhere (Figure 7, g-i). In carbonate rocks, all bitumen are similar to the first group of bitumen of clay-carbonate rocks in terms of variations in the values of the geochemical parameters Pr/n-$C_{17}$, Ph/n-$C_{18}$, Ki (Table 2). This allows us to classify them as parautochthonous bitumoids.

Despite the differences in hydrocarbon distribution, common to all studied bitumen is the predominance of odd n-alkanes of the composition $C_{15}$, $C_{17}$, $C_{19}$ in the middle molecular part, which is a characteristic biomarker of marine OM (Petrov, 1984).

## Conclusion

1. Studies have shown that the Silurian deposits contain petroleum source rocks that had an average HC potential. Clay-carbonate packs with increased generation potential make up about 20% of the sedimentary section.

2. The initial organic material was marine planktonic OM. The accumulation of sediments enriched in organic matter took place in low energy and deep areas of the bottom of the shallow-water basin as a whole.

3. Evaluation of the degree of catagenetic transformation according to pyrolysis data, conodont color indices and coal petrography indicates that the OM of rocks has reached the conditions of the middle-end of the main oil generation zone.

4. Correspondence of hydrocarbons to the composition of bitumen of carbonate and clay-carbonate sediments indicates the emigration and redistribution of hydrocarbons from petroleum source rocks into more permeable carbonate rocks.

## Acknowledgments

*The authors are grateful to M.V. Dakhnova (VNIGNI, Moscow) and A.N. Fomin (IPGG SB RAS, Novosibirsk) for the possibility of performing Rock-Eval pyrolysis. The authors thank T.K. Bazhenova (VNIGRI, St.Petersburg) for the discussion of the article materials and the comments made.*

## References

Antoshkina A.I., Saldin V.A., Sandula A.N., Nikulova N.Yu., Ponomarenko E.S., Shadrin A.N., Shebolkin D.N., Kaneva N.A. (2011). Paleozoic sedimentation on the outer shelf zone of the passive margin in the North-East of European platform. Syktyvkar: Geoprint, 200 p. (In Russ.)

Antoshkina A.I., Saldin V.A., Nikulova N.Yu., Yurieva Z.P., Ponomarenko E.S., Sandula A.N, Kaneva N.A., Shmeleva L.A., Shebolkin D.N., Shadrin A.N, Inkina N.A. (2015). Reconstruction of sedimentary environments in the Paleozoic Timan-Northern Ural region: research trends, results, problems and challenges. *Izvestiya Komi nauchnogo tsentra UrO RAN = Proceedings of the Komi Science Centre of the Ural Division of the RAS,* 1(21), pp. 55–72. (In Russ.)

Bazhenova O.K., Burlin Yu.K., Sokolov B.A., Khain V.E. (2004). Petroleum geology and geochemistry. Moscow: MSU, 415 p. (In Russ.)

Bazhenova T.K., Shimanskiy V.K., Vasil'eva V.F., Shapiro A.I., Yakovleva (Gembitskaya) L.A., Klimova L.I. (2008). Organic geochemistry

of the Timan-Pechora basin. St.Petersburg: VNIGRI, 164 p. (In Russ.)

Belonin M.D., Prischepa O.M., Teplov E.L., Budanov G.F., Danilevskiy S.A. (2004). The Timan-Pechora province: geological structure, petroleum potential and prospects of development. St.Petersburg: Nedra, 396 p. (In Russ.)

Beznosova T.M. (2008). Brachiopod communities and biostratigraphy Upper Ordovican, Silurian and Lower Devonian deposits of the northeastern margin of the BaltiaPaleocontinent. Ekaterinburg: UB RAS, 217 p. (In Russ.)

Bushnev D.A., Burdel'naya N.S. (2012). Organic matter in Silurian rocks from the Chernov uplift. *Geokhimiya = Geochemistry International*, 7, pp. 683-691. (In Russ.) https://doi.org/10.1134/S0016702912050023

Chernov G.A. (1972). Paleozoic of the Bolshezemelskaya tundra and prospects of its oil and gas potential. Moscow: Nauka, 318 p. (In Russ.)

Danilevskiy S.A., Sklyarova Z.P., Trifachev Yu.M. (2003). Geofluid systems of the Timan-Pechora province. Ukhta, 298 p. (In Russ.)

Danilov V.N., Ogdanets L.V., Makarova I.R, Gudel'man A.A., Sukhanov A.A., Zhuravlov A.V. (2011). Adak area – main results of organic matter and hydrocarbon fluids study. *Neftegazovaya geologiya. Teoriya i praktika = Petroleum Geology.Theoretical and Applied Studies*, 6(2). (In Russ.) http://www.ngtp.ru/rub/1/ 22_2011.pdf

Demaison G., Moore G. (1980). Anoxic environments and oil source bed genesis. *Org. Geochem*., 2, pp. 9–31. https://doi.org/10.1016/0146-6380(80)90017-0

Epstein A.G., Epstein J.B., Harris L.D. (1977). Conodont color alteration – an index organic metamorphism. *U.S. Geological Survey Professional Paper,* 995, 27 p. https://doi.org/10.3133/pp995

Handbook of petroleum geochemistry. St.Petersburg: Nedra, 576 p. (In Russ.)

Klimenko S.S., Anischenko L.A. (2010). Features of evolution of naphthide genesis of Timan-Pechora basin. *Izvestiya Komi nauchnogo tsentra UrO RAN = Proceedings of the Komi Science Centre of the Ural Division of the RAS,* 2, pp. 61–69. (In Russ.)

Kotik I.S., Danshchikova I.I., Kotik O.S., Valyaeva O.V., Mozhegova S.V., Sokolova L.V. (2016). Lithological and geochemical characterization of Silurian deposits in the Talbeysky block of Chernyshev ridge. *Vestnik Instituta geologii Komi NTs UrO RAN = Vestnik of the Institute of Geology of the Komi Science Centre UB RAS*, 11, pp. 15–22. (In Russ.) DOI: 10.19110/2221-1381-2016-11-15-22

Kotik I.S., Kotik O.S., Valyaeva O.V., Sokolova L.V. (2017). Silurian and Lower Devonian petroleum source rocks of the Chernov ridge (Timan-Pechora basin). *Neftegazovaya geologiya. Teoriya i praktika = Petroleum Geology.Theoretical and Applied Studies*, 12(4). (In Russ.) http://www.ngtp.ru/rub/1/41_2017.pdf

Lopatin N.V., Emets T.P. (1987). Pyrolysis in petroleum geochemistry. Moscow: Nauka, 143 p. (In Russ.)

Pesetskaya V.A., Pavlova S.N. (1997). Organic matter geochemical characteristics of the Ordovician-Lower Devonian rocks of the Pechora basin. *Geology of the European North of Russia: Proceedings of the Institute of Geology of the Komi SC, UB RAS*, 92, pp. 63-68. (In Russ.)

Petrov Al. (1984). Petroleum hydrocarbons. Moscow: Nauka, 264 p. (In Russ.)

State geological map of Russian Federation. (2007). Scale 1:1 000 000 (third generation). Ural Series. Sheet Q-41 – Vorkuta. M.A. Shishkin, Ya.E. Faybusovich, A.P. Astapov, A.S. Voronin, E.V. Molchanova. St.Petersburg: VSEGEI, ZapSibGeoNATs. (In Russ.)

Taylor G.H., Liu S.Y., Teichmüller M. (1991). Bituminite – a TEM view. *International Journal of Coal Geology*, 18, pp. 71–85. https://doi.org/10.1016/0166-5162(91)90044-J

Timonin N.I., Yudin V.V., Belyaev A.A. (2004). Paleogeodynamics of Pai-Khoi. Yekaterinburg: UB RAS, 226 p. (In Russ.)

## About the Authors

*Ivan S. Kotik* – Cand. Sci. (Geology and Mineralogy), Senior Researcher, Laboratory of Petroleum Basins Geology, Institute of Geology of Komi Science Centre of the Ural Branch of the Russian Academy of Sciences

54, Pervomayskaya st., Syktyvkar, 167982, Russian Federation

E-mail: ivkotik@gmail.com

*Tatyana V. Maidl* – Associate Professor, Cand. Sci. (Geology and Mineralogy), Senior Researcher, Laboratory of Petroleum Basins Geology, Institute of Geology of Komi Science Centre of the Ural Branch of the Russian Academy of Sciences

54, Pervomayskaya st., Syktyvkar, 167982, Russian Federation

*Olga S. Kotik* – Cand. Sci. (Geology and Mineralogy), Senior Researcher, Laboratory of Petroleum Basins Geology, Institute of Geology of Komi Science Centre of the Ural Branch of the Russian Academy of Sciences

54, Pervomayskaya st., Syktyvkar, 167982, Russian Federation

*Natalia V. Pronina* – Associate Professor, Cand. Sci. (Geology and Mineralogy), Petroleum Geology Department, Lomonosov Moscow State University

1, Leninskie gory, Moscow, 119234, Russian Federation

*Manuscript received 29 March 2019;*
*Accepted 3 June 2020; Published 30 September 2020*

ORIGINAL ARTICLE

**DOI**: https://doi.org/10.18599/grs.2020.3.21-27

Russian Original 2020. Vol. 22. Is. 3. Pp. 21–27

# Geochemistry of the insoluble organic matter (kerogen) components in Jurassic deposits in northern regions of the Latitudinal Ob area

*L.S. Borisova[1,2*], A.N. Fomin[1,2], E.S. Yaroslavtseva[1]*

[1]*Trofimuk Institute of Petroleum Geology and Geophysics of the Siberian Branch of the Russian Academy of Sciences, Novosibirsk, Russian Federation*

[2]*Novosibirsk State University, Novosibirsk, Russian Federation*

**Abstract**. The paper addresses the issues of evaluation of the oil-generating potential of deep buried Jurassic sediments of the Nadym-Taz interfluve area within West Siberian basin (WSB) on the basis of geochemical data. Rock samples from superdeep (SD) and deep boreholes that tapped the Mesozoic-Cenozoic sedimentary cover in the north of the central part of WSB (Yen-Yakhinskaya, Yevo-Yakhinskaya, Yarudeiskaya, Tyumenskaya and other wells) were used as the study materials. A portion of the organic matter (OM) that is insoluble in organic solvents (i.e. kerogen) sampled from Upper, Middle and Lower Jurassic deposits (54 samples) was chosen to be object of the study. The methods used for the comprehensive study of the kerogen involved elemental and isotope analyses and Rock-Eval pyrolysis, which allowed to obtain important information about the genetic type of OM, its maturity, and residual oil-generation potential.

Application of the Surfer and Corel Draw software enabled construction of schematic maps and diagrams reflecting changes in the most informative geochemical parameters of kerogen (as well as their analysis) in the study area and down the section (from Upper to Lower Jurassic). The geochemical data obtained indicate that the highest generation potential of OM of the Jurassic interval of the Nadym-Taz interfluve is attributed to the Bazhenov horizon, as well as to individual reservoirs of the Malyshevka, Leontievskiy, Sharapovo, and Kiterbyut horizons. The level of maturity of OM in Upper and Middle Jurassic sediments allowed to infer that these may contain preserved accumulations primarily of oils and wet gases, while Lower Jurassic deposits may host wet and dry gases.

**Keywords**: insoluble organic matter, oil-generating potential of Jurassic deposits, Western Siberia

**Recommended citation**: Borisova L.S., Fomin A.N., Yaroslavtseva E.S. (2020). Geochemistry of the insoluble organic matter (kerogen) components in Jurassic deposits in northern regions of the Latitudinal Ob area. *Georesursy = Georesources*, 22(3), pp. 21–27. DOI: https://doi.org/10.18599/grs.2020.3.21-27

## Introduction

A series of superdeep (SD) wells (Yen-Yakhinskaya, Yevo-Yakhinskaya, Yarudeiskaya, etc.) drilled in the northern part of the West Siberian megabasin (WASB) over the last decade, have penetrated the Mesozoic-Cenozoic sedimentary cover, thereby providing a unique opportunity for geochemists to study transformations of the organic matter (OM) during meso- and apo-catagenesis.

Since the beginning of the 1990s, there have been conducted numerous studies addressing different aspects of the organic geochemistry of petroleum reservoirs in the northern West Siberian basin, among them those guided by academician Alexey E. Kontorovich at the Trofimuk Institute of Petroleum Geology and Geophysics, Siberian Branch of the Russian Academy of Sciences (IPGG SB RAS) (Oil and gas basins and regions of Siberia..., 1994; Kontorovich et al., 2002; Kontorovich, 2004; Kontorovich et al., 2019). Analysis of the source rock generating potential from the Tyumenskaya SD-well data showed that Upper Jurassic deposits, whose OM is characterized by a moderate maturity level ($R^0_{vt}$ – 0.8–0.9%), are localized in the oil window, and could be producing liquid hydrocarbons thereat. The Lower-Middle Jurassic sequences are located in the gas generation window, with the level of maturity interpreted to be high ($R^0_{vt}$ – 1.15–2.1%) for these sediments (Kontorovich et al., 2002). While the petroleum generating potential of Lower Jurassic deposits in the Nadym-Taz interfluve is also estimated as medium to low (Nekhaev et al., 2009), however taking into account thicknesses of oil-prone source rocks and density of hydrocarbon generation, the authors managed to identify lands fairly promising for gas in the area of these deposits distribution.

*Corresponding author: Lyubov S. Borisova
E-mail: BorisovaLS@ipgg.sbras.ru

Accordingly, the present study objectives are aimed to identify the geochemical signatures of the kerogen composition and residual oil-generating potential of the deep-buried sequences in the Nadym-Taz interfluve area.

## Materials and object of the study

This research is largely based on results of the study of OM of Jurassic deposits from the drilled wells data (Yen-Yakhinskaya, Urengoyskaya, Yevo-Yakhinskaya, Tyumenskaya, Zapadno-Tarkosalinskaya, Tarkosalinskaya, Vostochno-Tarkosalinskaya, Geologicheskaya, Medvezh'ya, Stakhanovskaya, Gubkinskaya, Chernichnaya, Yubileinaya, Zapadno-Novogodnyaya, Yutyrmalskaya, and Yuzhno-Russkaya). An overview map of the study area is shown in Figure 1.

Kerogen, which was made the object this study, is defined as the portion of organic matter in sedimentary rocks that is insoluble in organic solvents and alkaline aqueous solutions (IOM). Ever since the 1960s, when V.A. Uspenskii and co-authors published first classification of the OM types based on results of the kerogen studies (Uspenskii et al., 1958), much of the emphasis began to be placed particularly on the chemical and micro-component composition of the insoluble part of OM (Bogorodskaya, 1973; Parparova, Neruchev, 1977; Bogorodskaya, Kontorovich, 1982; Kontorovich et al., 1985, etc.). Among the fundamental contributions of Russian scientists to this research area, the most complete and detailed study of kerogens was made by L.I. Bogorodskaya. In cumulative efforts with A.E. Kontorovich and A.I. Larichev (2005), they provided most informative summary of the available materials and data on kerogen parameters which enabled identification of major genetic types of OM and the degree of its catagenetic transformation (i.e. maturity level). The kerogen types classification offered by foreign scientists was largely based on the structural and chemical characteristics (Tissot, Welte, 1981), which anyway shows a good correlation with the Kontorovich-Bogorodskaya classification.

In the classical scheme for kerogen analysis (Bogorodskaya, Kontorovich, Larichev, 2005), the study of insoluble organic matter which involves a number of chemical and physical methods, is applied upon removing the bitumen component of the OM, dissolving the mineral sediment with hydrofluoric and hydrochloric acids, and the removal of elemental sulfur. The most informative methods and parameters chosen to be exploited in this work are: elemental analysis ($H/C_{at}$), stable carbon isotope analysis ($\delta^{13}C$), Rock-Eval pyrolysis (HI, $T_{max}$).

## Research results

A total of 54 kerogen samples recovered from Upper, Middle and Lower Jurassic deposits occurring

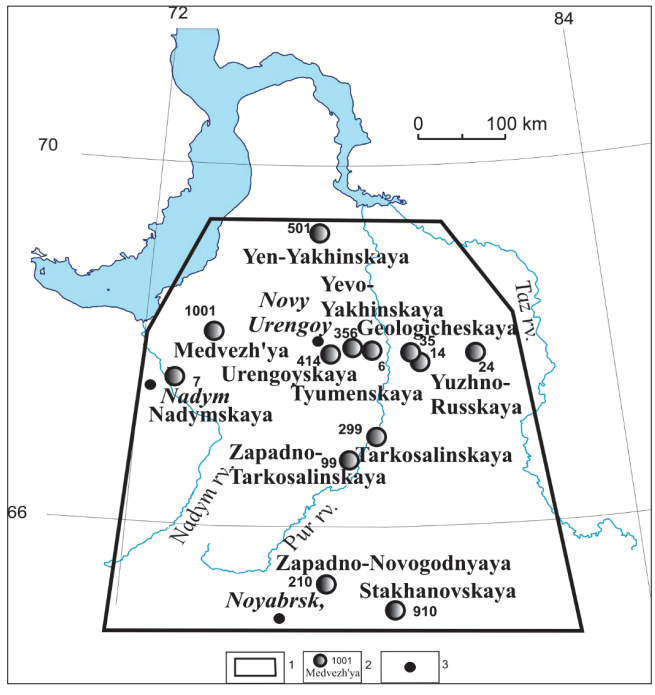


*Fig. 1. Overview map showing location of the study area. 1 – study area; 2 – wells that penetrated Jurassic deposits; 3 – cities.*

in the Nadym-Taz interfluve were studied with respect to their elemental and stable isotope compositions and pyrolytic characteristics. The integrated data listed in Table 1 include average values and spread of the most informative parameters which allow to infer basic characteristics of OM such as genetic type, its maturity level (catagenetic transformations), as well as oil-generating potential of the studied kerogen samples from the studied horizons.

Results of the elemental analysis (Tissot, Welte, 1981; Kontorovich et al., 2019) demonstrated that kerogen of Upper Jurassic deposits (represented by the Bazhenov Formation) is composed of predominantly hydrogen-rich (up to 7.4%) OM and has high H/C atomic ratio up to 1.05 (Table 1) and therefore can be generally assigned to type II OM, while kerogen of Lower and Middle Jurassic deposits whose organic matter is interpreted to be type III OM which is hydrogen-poor (on average 4.7%) and is characterized by the $H/C_{at}$ ratio averaging 0.66 (which is higher than $O/C_{at}$ ratio for type II OM).

For a more detailed analysis, the data obtained from the study of 54 samples of insoluble organic matter from Jurassic sediments were integrated in the overall model of chemical evolution and elemental composition of kerogens with their major genetic types during catagenesis developed by A.E. Kontorovich and L.I. Bogorodskaya (1985–1990) (C-H-NSO trigonograms) (Bogorodskaya, Kontorovich, Larichev, 2005).

The research results have shown that the kerogen samples from Lower-Middle Jurassic deposits are localized primarily in the region of high maturity OM

| Productive horizon | TOC | C, % | H, % | S, % | $(H/C)_{at}$ | $\delta^{13}C$, ‰ | HI, mg HC/ g TOC |
|---|---|---|---|---|---|---|---|
| Upper Jurassic deposits | | | | | | | |
| Bazhenov | 4.3-10.5<br>6.5 | 80.3-88.4<br>84.5 | 6.7-7.4<br>7.0 | 2.1-2.4<br>2.2 | 0.96-1.05<br>1.00 | (-31.5)-(-30.4)<br>-30.9 | 167-326<br>235 |
| Georgievka | 1.5-3.3<br>2.4 | 84.8-85.4<br>85.1 | 6.4-6.5<br>6.5 | 0.1-5.0<br>2.5 | 0.90-0.91<br>0.91 | (-30.7)-(-25.0)<br>-27.9 | 80-96<br>85 |
| Vasyugan | 2.5-6.6<br>3.4 | 81.9-86.0<br>83.3 | 4.2-5.4<br>5.0 | 1.0-6.3<br>2.6 | 0.61-0.78<br>0.71 | (-23.7)-(-22.5)<br>-23.0 | 51-90<br>68 |
| Middle Jurassic deposits | | | | | | | |
| Malyshevka | 1.1-7.9<br>3.6 | 80.2-85.9<br>82.8 | 4.4-6.5<br>5.5 | 0.2-0.7<br>0.4 | 0.70-1.00<br>0.80 | (-29.4)-(-23.2)<br>-23.5 | 64-175<br>152 |
| Leontievskiy | 0.7-10.6<br>4.0 | 81.7-86.3<br>83.9 | 4.6-5.4<br>5.1 | 0.3-0.9<br>0.6 | 0.65-0.80<br>0.72 | (-29.8)-(-27.6)<br>-28.5 | 90-160<br>146 |
| Vym | 0.9-8.6<br>4.9 | 79.5-86.7<br>84.5 | 4.3-5.7<br>4.9 | 0.3-6.1<br>1.4 | 0.65-0.70<br>0.70 | (-28.0)-(-21.8)<br>-24.9 | 40-170<br>93 |
| Lower Jurassic deposits | | | | | | | |
| Nadoyakha | 2.2-5.3<br>4.0 | 86.9-89.2<br>88.2 | 4.0-4.7<br>4.3 | 0.2-04<br>0.3 | 0.55-0.64<br>0.61 | (-28.6)-(-24.2)<br>-25.9 | 18-45<br>32 |
| Kiterbyut | 0.2-1.9<br>1.1 | 84.7-87.1<br>85.7 | 4.2-4.9<br>4.5 | 0.3-0.7<br>0.4 | 0.59-0.68<br>0.63 | (-29.9)-(-24.9)<br>-25.4 | 37-92<br>56 |
| Sharapovo | 1.5-4.4<br>3.0 | 86.0-89.2<br>87.2 | 3.9-5.3<br>4.8 | 0.0-0.4<br>0.3 | 0.54-0.73<br>0.65 | (-29.5)-(-23.4)<br>-24.4 | 27-94<br>52 |
| Levinskiy | 0.4-2.5<br>1.3 | 82.4-87.4<br>85.4 | 3.3-4.9<br>4.0 | 0.0-0.5<br>0.3 | 0.46-0.68<br>0.56 | (-28.6)-(-24.7)<br>-24.6 | 16-64<br>33 |
| Zimnyaya | 0.4-2.3<br>1.9 | 81.3-90.2<br>87.0 | 3.5-4.7<br>4.2 | 0.0-0.4<br>0.2 | 0.55-0.69<br>0.58 | (-27.7)-(-26.4)<br>-26.9 | 14-28<br>25 |

*Table 1. Distribution of major kerogen parameters across the horizons. Numerator = range of values, denominator = mean value.*

(Figure 2). Kerogens of these deposits have a high carbon content against low concentrations of hydrogen and heteroatoms. However, the hydrogen contents allow to interpret OM of some Middle Jurassic samples as occupying an intermediate position between aquagenic and terragenous types (Malyshevka and Leontievskiy horizons).

Results of the analysis of kerogens from Upper Jurassic deposits represented by the Bazhenov, Georgievka, and Vasyugan horizons revealed that a low-hydrogen (hydrogen content: on average, 5.0) organic matter of the Vasyugan horizon is dominantly terragenous, while kerogens of the Georgievka and Bazhenov horizons are subsumed into the domain of aquagenic OM (hydrogen content: from 6.4 to 7.4%) (Figure 2). The IOM elemental analysis data enabled determination of the genetic type of organic matter, and in addition, provided insights into OM alterations. It follows from the C-H-NSO trigonograms that while the organic matter of Lower-Middle Jurassic deposits is generally strongly altered ($MC_1^2$–$MC_2$), it is only the Malyshevka, Levinsky, and Sharapovo horizons that have entered the oil window ($MC_1^2$–$MC_2$). Besides, Upper Jurassic deposits are also recognized to be presently passing the oil window ($MC_1^{1-2}$–$MC_2$). The interplay of catagenesis factors has resulted in gradually increasing organic carbon in the bulk composition of IOM and dehydrogenation, while Upper Jurassic deposits became depleted of heteroelements (primarily oxygen and sulfur) down the section. The hydrogen content reduction in the process of OM conversion clearly demonstrates a decrease in the H/C ratio: from 1.1 to 0.70 during mesocatagenesis (MC) (in Upper and partially Middle Jurassic deposits), and down to 0.46 during apocatagenesis (AC) in individual samples.

The genetic type of OM can be primarily inferred from the carbon isotope analysis data obtained for kerogen samples, along with indicators of elemental analysis (Table 1). Kerogen sampled from Lower-Middle Jurassic deposits belong to terragenous type (Kontorovich et al., 1985). However, some of the samples have light carbon isotope composition, suggesting a partial contribution of aquagenic OM. As such, the mixed type OM is inherent in kerogens sampled from rocks of the Sharapovo, Kiterbyut ($J_1$), Leontievskiy, and Malyshevka horizons ($J_2$). Kerogen samples from the Vasyugan horizon have heavy carbon isotope composition (–23.7)–(–22.5) ‰. The OM from the Bazhenov and locally from Georgievka horizons is characterized by light carbon isotope composition (–31.5)–(–30.4) ‰, thereby bearing evidence of its aquagenic origin (Table 1).

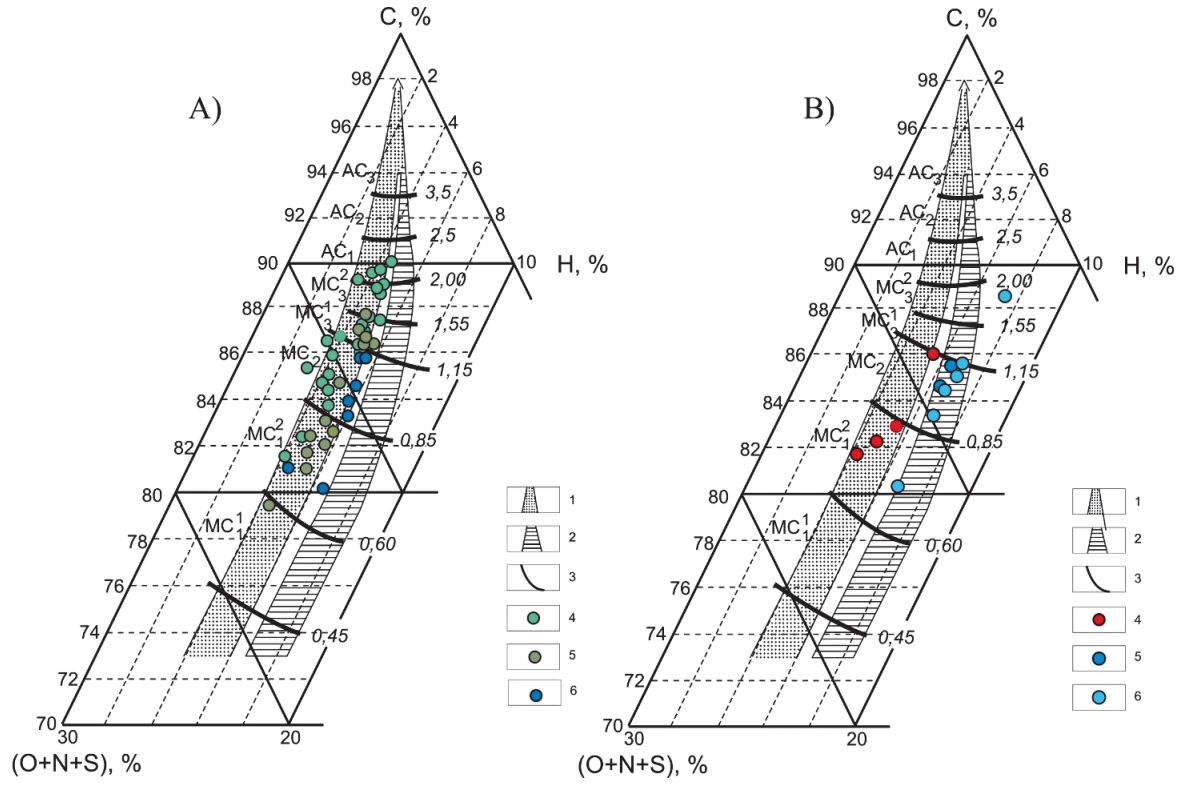


*Fig. 2. Trigonograms of the composition of kerogens sampled from Jurassic deposits in the Nadym-Taz interfluve area within the WSB. OM maturation-induced changes in the elemental composition of 1 – coals and kerogen (terragenous type); 2 – kerogen (aquagenic type); 3 – boundaries of the catagenesis zones, with the numbers indicating $R_oVt$ values. Age of deposits: A) $J_1$: 4 – $J_1$ (Zimnyaya, Levinskiy, Sharapovo, Kiterbyut, Nadoyakha horizons); $J_2$: 5 – Leontievskiy, Layda horizons; 6 – Malyshevka horizon; B) $J_3$: 4 – Vasyugan Fm, Sigovoye Fm, Tochino Fm; 5 – Georgievka Fm; 6 – Bazhenov Fm.*

Results of the study based on Rock-Eval pyrolysis of kerogen samples from Lower, Middle and Upper Jurassic deposits in the Nadym-Taz interfluve have provided insights about their residual hydrocarbon-generating potential (Figure 3). Hydrocarbon potential of the IOM is known to be strongly depleted with progressively increasing burial depth of the sediment and because of the generated liquid and gaseous hydrocarbons (Espitalie, 1988), while the OM type plays nonetheless important role. Samples from the Bazhenov Formation recovered in the study area are characterized by a relatively high hydrocarbon generating potential (up to 326 mgHC/g TOC), while passing the oil window ($T_{max}$ 440–450°C). Despite a relatively low oil-generative potential (51–90 mgHC/g TOC) of the kerogens sampled from the Upper Jurassic interval (the Vasyugan formation), their position in the HI-$T_{max}$ diagram also corresponds to the oil window, which is corroborated by the paleogeographic data for the period of the Vasyugam Fm accumulation within the study area (Kontorovich et al., 2013), and by the continental type of their OM.

The IOM samples from Lower and Middle Jurassic deposits in the Nadym-Taz interfluve have predominantly low oil-generating potential averaging 25–56 mgHC/g TOC and 93–152 mgHC/g TOC, respectively, and are attributed to the gas generation window ($T_{max}$ 470–520°C) (Figure 3), except some kerogen samples from Middle Jurassic (Malyshevka, Leontievskiy, Vym horizons) in the north-western and southern regions of the study area (wells: Medvezh'ya-1001; Yevo-Yakhinskaya-356; Stakhanovskaya-910), which are characterized by relatively high HI values (175, 160 and 170 mgHC/g TOC, respectively).

## Discussions

A detailed study of a total of 54 IOM samples from Lower-Middle Jurassic and Upper Jurassic deposits allowed to infer their basic characteristics.

Lower Jurassic deposits have generally low TOC values (on average, 1.8, except few samples from the Sharapovo horizon with TOC reaching 4.4%).

The element concentrations in the studied kerogens are described as minor for pyrite sulfur (on average 4.0) and essentially high for carbon (up to 90.2%), at this hydrogen and sulfur are at the levels of 3.3–5.3%, and 0.0–0.7%, respectively. The H/C atomic ratio is low (0.46–0.73), and carbon isotope composition is heavy (on average, –25.4‰) (Figure 2, Table 1). Kerogens sampled from Lower Jurassic sediments are dominated by terragenous OM. However, sporadic samples from the Kiterbyut and Sharapovo horizons are differentiated by light carbon isotope compositions (–29.9‰) and (–29.4‰, respectively).

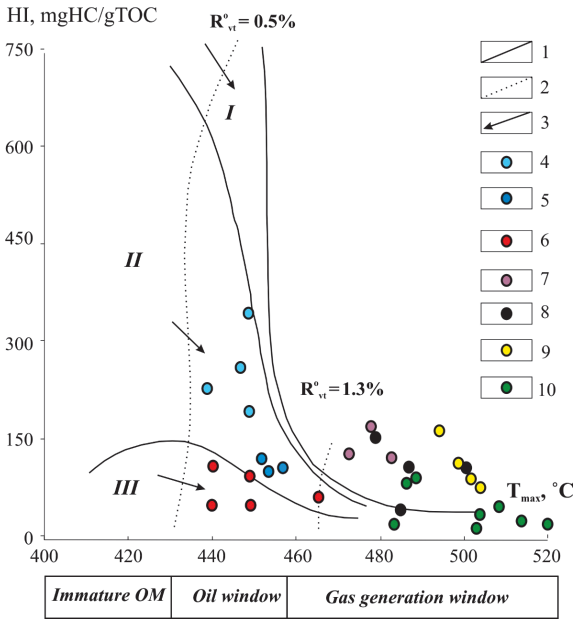


*Fig. 3. Pyrolytic characteristics of kerogens sampled from Jurassic deposits. In the Nadym-Taz interfluve area. Age of the deposits: $J_3$: 4 – Bazhenov, 5 – Georgievka, 6 – Vasyugan horizons; $J_{1-2}$: 7 – Malyshevka, 8 – Leontievskiy, 9 – Vym horizons; 10 – Lower Jurassic deposits.*

The OM of Lower Jurassic deposits was subjected to a material transformation up to AC catagenesis stage. Whereas OM in Middle Jurassic deposits altered to a lesser extent ($MC_1^2$–$MC_3^1$). Middle Jurassic deposits are also characterized by higher TOC values (on average, 4.1%) and pyrite sulfur contents in the kerogen (on average, 7.3%). Results of the elemental analysis data showed that IOM samples have rather high carbon content (79.5–89.2%) at relatively low contents of hydrogen (4.5–5.6%) and sulfur (0.8% on average). The H/C atomic ratio is higher than in Lower Jurassic deposits (0.65–1.00). The highest H/C atomic ratios are reported from kerogens of Middle Jurassic deposits (Malyshevka and Leontievskiy horizons), which may suggest an admixture of aquagenic OM. Some samples from these horizons display high TOC contents (up to 7.9% and 10.6%, respectively). In addition, some kerogen samples are characterized by a lighter carbon isotope composition (–29.4‰ and –29.8‰, respectively). However, kerogen sampled from Middle Jurassic deposits are represented by terragenous OM and have a heavy carbon isotope composition averaging (–25.6‰) (Figure 2, Table 1). In the Lower-Middle Jurassic interval, hydrocarbon potential changes from 14-64 mgHC/g TOC (for terragenous OM type) and to 92–175 mgHC/g TOC (for OM admixed with aquagenic OM).

The Bazhenov Fm samples from Upper Jurassic deposits next to their having high TOC values (4.3–10.5%) are characterized by high levels of pyrite sulfur in kerogen (in the range from 13.9 to 36.1%). Carbon concentrations in IOM vary between 80.3 and 88.4%, while hydrogen content is relatively high (from 6.7 to 7.4%). The samples are characterized by higher sulfur contents. Their H/C atomic ratio is elevated (from 0.96 to 1.05), while the $\delta^{13}C$ carbon isotope compositions vary within the interval (–31.5)–(–30.4)‰. Unlike typically aquagenic IOM in the Bazhenov Fm and Georgievka Fm, IOM in the Vasyugan Fm and Sigovoye Fm is attributed to terragenous type OM (Figure 2, Table). Catagenetic alteration of OM (according to the elemental analysis (Bogorodskaya, Kontorovich, Larichev, 2005) corresponds to $MC_{1-2}$ meso-catagenesis stages.

The constructed schematic maps of changes in the most informative geochemical parameters (using the Surfer software) represent the kerogen properties distribution within the study area. Other maps reflecting changes in the atomic H/C ratio and residual oil-generating potential (HI) in the Nadym-Taz interfluve area were constructed separately for Lower, Middle and Upper Jurassic (dominantly Bazhenov) deposits. In most of the study area, the $H/C_{at}$ values which are high for Upper Jurassic deposits (Figure 4), and tend to decrease only in the east and south-east (primarily in boreholes where the kerogen is sampled from the Vasyugan Fm). The residual oil-generating potential in the Upper Jurassic interval varies from 107 mgHC/g TOC in the east and northeast to 244-326 mgHC/g TOC in the central parts of the study area (Figure 5).

Kerogens of Middle Jurassic deposits occurring in the study area (Figures 4, 5) is featured by minor values of $H/C_{at}$ and HI, which show an increasing trend (to 0.8 and 175 mgHC/g TOC, respectively) only in the south (Stakhanovskaya-910 well) and in the north-west (Medvezh'ya-1001 well). While these parameters are generally lower for the kerogen of Lower Jurassic deposits (Figure 4), as compared to Middle Jurassic deposits, with the lowest values reported from the basin's central parts where Jurassic horizons have the greatest burial depth. However, the kerogen parameters are locally characterized by relatively high $H/C_{at}$ values (around 0.70). Should the residual oil-generating potential of Lower Jurassic deposits be taken into consideration as well, specifically such areas (along the meridian running from Zapadno-Novogodnaya-210 well to Medvezh'ya-1001 well) will accommodate a zone of essintially high HI values in the Kiterbyut (Togur rock unit) and Sharapovo horizons (up to 80 mgHC/g TOC) (Figure 5).

Comparison of the schematic maps of changes in kerogen parameters for Lower, Upper, and Middle Jurassic sediments revealed a decline in oil-generating potential and H/C atomic ratio as progressive burial of the sedimentary cover takes place in the subsurface (Figures 4, 5). The level of OM maturity is critical in evaluation of the oil and gas potential of sedimentary sequences. This paper draws a comparison between the data inferred from the study of residual oil-generating

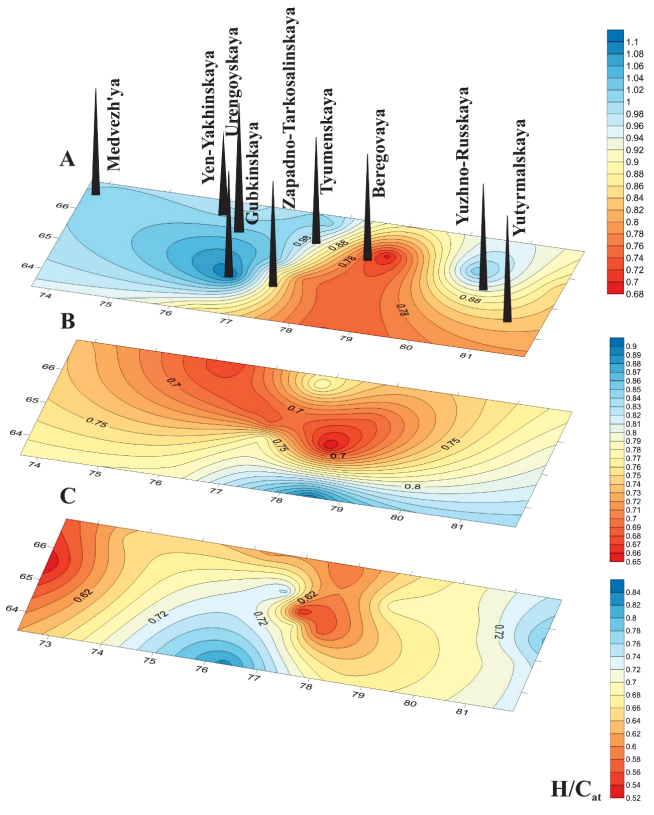


*Fig. 4. Schematic maps showing variations in the H/C ratio for the kerogen of the OM from Jurassic deposits in the Nadym-Taz interfluve area. Age of deposits: A – Upper Jurassic; B – Middle Jurassic; C – Lower Jurassic. Notations represent isolines of equal values.*

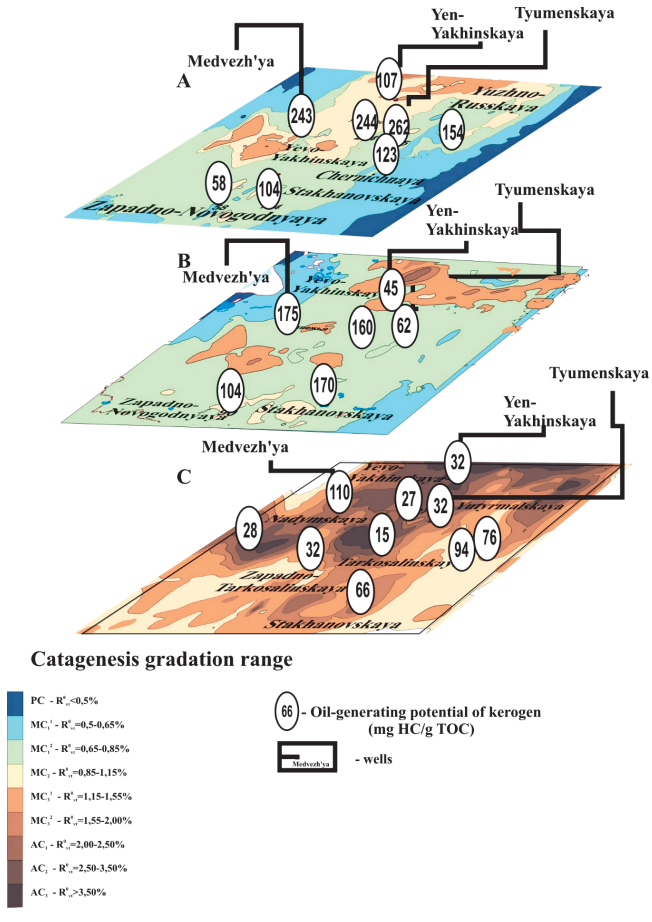


*Fig. 5. Compared levels of catagenetic transformations of Jurassic deposits (Fomin et al., 2001) and petroleum-generating potential of IOM in some exploration wells drilled in the Nadym-Taz interfluve area. Age of deposits: A – Upper Jurassic; B – Middle Jurassic; C – Lower Jurassic.*

potential and vitrinite reflectance measurements performed by A.N. Fomin and colleagues for Jurassic rocks of Western Siberia (Fomin et al., 2001).

In the Upper Jurassic interval (Bazhenov formation and its equivalents), the level of maturity of organic matter corresponds to $PC_3$–$MC_1^1$–$MC_2$ (from low maturity to mature OM (oil window). The OM is least altered ($PC_3$–$MC_1^1$) within the oil window in marginal parts of the megabasin and the study area. Approaching the basin's center, catagenesis gradually increases ($MC_1^2$–$MC_2$) and reaches maximum (oil window) ($MC_3^{1-2}$) in the north. The HI values for the Bazhenov Fm part of totally agree with the OM maturity derived from vitrinite reflectance, showing the lowest values for residual oil-generating potential in the north of the area's central part (Figure 5).

Maturity level of the OM in the samples from Middle Jurassic sequences is moderate within some horizons (Malyshevka, Vym), i.e. moderate catagenesis; kerogen samples in a number of boreholes drilled in western and southern regions of the study area is characterized by relatively high values of the residual oil-generating potential (up to 175 mgHC/g TOC). Given that sediments in the basal Jurassic horizons were exposed to complex temperature and pressure (T-P) conditions, in most of Western Siberia and the study area, the OM underwent significant alterations (became over-mature) and reached the $MC_3^1$–$AC_3$ (apo-catagenesis stage).

The HI values for Lower Jurassic deposits in the north of central Nadym-Taz interfluve area are also indicative of a high level of OM maturity and low residual oil-generating potential (<20 mgHC/g TOC) (Figure 5), except some of the regions in western and north-western regions (Medvezhya-1001 well) of the Nadym-Taz interfluve area, where the Kiterbyut and Sharapovo horizons are located in the moderate catagenesis zone ($MC_2$), with residual oil-generating potential estimated as relatively high (up to 90 mgHC/g TOC).

Thus, the level of maturity of OM (hence, the degree of its transformation) progressively increases from marginal to central parts and reaches maximum (oil window) in the north, as the burial depth of the sedimentary cover increases.

## Conclusions

Jurassic deposits within the Nadym-Taz interfluve are characterized by relatively high TOC content throughout the cross-section, which allows considering them as potential petroleum source rocks. The highest

TOC concentrations are documented in the Bazhenov mudstones (shales), as well as in rock units of the Malyshevka, Leontievskiy, and Vym horizons.

2. While Upper Jurassic deposits in most of the study area have not yet passed oil window, they may generate liquid hydrocarbons. The study of the insoluble organic matter in these sedimentary sequences confirmed high hydrocarbon generating potential of the Bazhenov formation, whose organic matter is the primary source of oil accumulations both in $Yu_0$ horizon and in the over- and underlying reservoir rocks, which is emphasized by A.E. Kontorovich and co-authors (2019). The organic matter of the Vasyugan and Georgievskaya formations has a significantly lower hydrocarbon potential. The Lower Jurassic sequences are generally characterized by a terragenous type of OM and are inferred to be in the gas generation window. Kerogen in these deposits has a lower generation potential as compared to Upper Jurassic sequences (Bazhenov horizon). In Middle Jurassic sequences, maturity level of the organic matter in interpreted as moderate (hence, moderate hydrocarbon potential) in some intervals of the section, which is consistent with results of the elemental and isotope analyses of the kerogen.

It is shown that the hydrogen content decreases significantly with depth, while the kerogen having very low values of hydrogen (HI) and the hydrogen and carbon (H/C) atomic ratios became over-mature (apocatagenesis stage). However, in Middle Jurassic (Malyshevka and Leontievskiy horizons) and Lower Jurassic deposits (Kiterbyut, Sharapovo horizons), rock units characterized by a relatively high residual oil-generating potential are widespread in some regions of the study area.

The constructed schematic maps allow to identify zones of high hydrocarbon potential in the Nadym-Taz interfluve whose paleogeothermal conditions allow for preservation of hydrocarbon accumulations contained therein. The level of maturity of OM sampled from Upper and Middle Jurassic sediments suggests the presence of preserved oil and oil- and gas acumulations, and in lower Jurassic – wet and dry gas accumulations.

## Acknowledgments

*The work was financially supported by the Russian Science Foundation project No. 0331-2019-0022.*

*The authors thank V.N. Melenevsky, senior researcher at the IPGG SB RAS, for performing Rock-Eval analyses.*

## References

Bogorodskaya L.I. (1973). Method for determination of oxygen-containing functional groups in debituminized dispersed organic matter] *Modern methods of analysis in organic geochemistry*. Novosibirsk: SNIIGGiMS, p. 14. (In Russ.)

Bogorodskaya L.I., Kontorovich A.E. (1982). Chemical composition of organic matter dispersed in rocks and ways of its classification. *Sedikachites at different stages of lithogenesis.* Moscow: Nauka, p. 49. (In Russ.)

Bogorodskaya L.I., Kontorovich A.E., Larichev A.I. (2005). Kerogen. Study methods, geochemical interpretation. Novosibirsk: Geo, 255 p. (In Russ.)

Espitalie J. (1988). Use of Tmax as a maturation in dexin petroleum exploration. Petroleum Geochmistry and exploration in the Afro-Asian Region. Rotterdam, BROOKFIELD, pp. 67-73.

Fomin A.N., Kontorovich A.E., Krasavchikov V.O. (2001). Catagenesis of organic matter and petroleum potential of the jurassic, triassic, and paleozoic deposits in the northern areas of the west siberian megabasin. *Geologiya i geofizika*, 42(11), pp. 1875-1887. (In Russ.)

Kontorovich A.E. (2004). Essays on the theory of naphthydogenesis. Novosibirsk: SO RAN, 548 p. (In Russ.)

Kontorovich A.E., Bogorodskaya L.I., Borisova L.S., Burshtein L.M., Ismagilov Z.R., Efimova O.S., Kostyreva E.A., Lemina N.M., Ryzhkova S.V., Sozinov S.A., Fomin A.N. (2019). Geochemistry and catagenetic transformations of kerogen from the Bazhenov horizon. *Geochemistry International*, 57, pp. 621–634. https://doi.org/10.1134/S0016702919060028

Kontorovich A.E., Bogorodskaya L.I., Golyshev S.I. (1985). Distribution of stable carbon isotopes in sedicachites of various regions. *Geologiya i geofizika*, 7, pp. 3–11. (In Russ.)

Kontorovich A.E., Danilova V.P., Fomin A.N., Kostyreva E.A., Borisova L.S., Melenevskii V.N. (2002). Distribution of stable carbon isotopes in sedicachites of various regions. *Izvestiya TPU. Geologiya i razrabotka neftyanykh i gazovykh mestorozhdenii = Bulletin of the Tomsk Polytechnic University. Geo Assets Engineering*, 305(8), p. 45. (In Russ.)

Kontorovich A.E., Kontorovich V.A., Ryzhkova S.V., Shurygin B.N., Vakulenko L.G., Gaideburova E.A., Danilova V.P., Kazanenkov V.A., Kim N.S., Kostyreva E.A., Moskvin V.I., Yan P.A. (2013). Jurassic paleogeography of the West Siberian sedimentary basin. *Russian Geology and Geophysics*, 54(8), pp. 747–779. (In Russ.) https://doi.org/10.1016/j.rgg.2013.07.002

Methodical recommendations for the application of the pyrolytic method in organic geochemistry. (1985). Ed. A.E. Kontorovich. Novosibirsk: SNIIGiMS, 42 p. (In Russ.)

Oil and gas basins and regions of Siberia. West Siberian Basin. (1994). Ed. A.E. Kontorovich. Novosibirsk: OIGGM SO RAN, SNIIGGiMS, 201 p. (In Russ.)

Nekhaev A.Yu., Moskvin V.I., Melenevskii V.N. (2009). Estimation of the scale of hydrocarbon generation in the Lower Jurassic deposits of the Nadym-Taz interfluve. Novosibirsk: GeoSibir, p. 51. (In Russ.)

Parparova G.M., Neruchev S.G. (1977). Fundamentals of the genetic classification of organic matter. *Geologiya i geofizika*, 5, pp. 45–51. (In Russ.)

Tissot B., Velte D. (1981). Petroleum Formation and Occurrence. Moscow: Mir, 499 p. (In Russ.)

Uspenskii V.A., Indenbom F.B., Chernysheva A.S., Sennikova V.N. (1958). To the development of a genetic classification of dispersed organic matter. *Issues of oil formation*. Leningrad: Gostoptekhizdat, p. 221. (In Russ.)

## About the Authors

*Lyubov S. Borisova* – Dr. Sci. (Geology and Mineralogy), Senior Researcher, Trofimuk Institute of Petroleum Geology and Geophysics of the Siberian Branch of the Russian Academy of Sciences; Associate Professor, Novosibirsk State University

3, Ak.Koptyug ave., Novosibirsk, 630090, Russian Federation. E-mail: BorisovaLS @ ipgg.sbras.ru

*Alexander N. Fomin* – Dr. Sci. (Geology and Mineralogy), Chief Researcher, Trofimuk Institute of Petroleum Geology and Geophysics of the Siberian Branch of the Russian Academy of Sciences; Head of the Department of Oil and Gas Fields Geology, Novosibirsk State University

3, Ak.Koptyug ave., Novosibirsk, 630090, Russian Federation

*Ekaterina S. Yaroslavtseva* – Junior Researcher, Trofimuk Institute of Petroleum Geology and Geophysics of the Siberian Branch of the Russian Academy of Sciences

3, Ak.Koptyug ave., Novosibirsk, 630090, Russian Federation

*Manuscript received 12 November 2020;*
*Accepted 4 April 2020; Published 30 September 2020*

ORIGINAL ARTICLE

**DOI**: https://doi.org/10.18599/grs.2020.3.28-37 Russian Original 2020. Vol. 22. Is. 3. Pp. 28–37

# A new method of «geochemical logging» for studying Domanic deposits

*S.B. Ostroukhov[1], N.V. Pronin[1], I.N. Plotnikova[1,2*], R.K. Khairtdinov[3]*

[1]*Academy of Sciences of the Republic of Tatarstan, Kazan, Russian Federation*

[2] *Kazan National Research Technological University, Kazan, Russian Federation*

[3]*CJSC «Predpriyatie Kara Altyn», Almetyevsk, Russian Federation*

**Abstract**. Based on the study of the rocks of the Semiluksky horizon from the northwestern slope of the South Tatar arch (Tatarstan Republic), new data on the ratio of scattered organic matter, carbonate and siliceous components in domanicite rocks were obtained. Based on the results of geochemical studies of the bitumoids of these rocks, new information was obtained on the distribution patterns of aromatic biomarkers in rocks of various lithological composition. Peculiarities of distribution of paleorenieratane and isorenieratane in such rocks are revealed. Due to the use of aromatic biomarkers, a number of new geochemical coefficients have been developed, which make it possible to characterize not only Domanic strata along the sediment section, but also the processes of their transformation, starting from the stage of biota formation. The substantiation of the use of these geochemical coefficients when carrying out geochemical logging along the well column to establish the boundaries of the Domanic strata formation and productive intervals in them, as well as to assess the facies conditions of their formation, is given. At the same time, the patterns established by these coefficients correlate well with other geochemical and geological parameters. The studies performed have shown that at least two types of organic matter are present in the domanicite sequence: migrational, more mature and thermocatalytically transformed, and syngenetic, less mature with a low degree of thermocatalytic transformation. The application of the developed geochemical coefficients determines a new approach to the use of «geochemical logging» in the complex of express logging while drilling. When studying cuttings, these coefficients make it possible to identify reservoir intervals, zones of fracturing and decompression, containing traces of migrational hydrocarbon fluids, moved hydrocarbons, which may indicate the presence of oil deposits. The integration of geochemical studies of cuttings with its rapid study by pyrolysis and X-ray analysis methods can significantly increase the accuracy of identifying interlayers with a high content of organic matter in the section of domanicite rocks, as well as potential reservoirs with moved migrational hydrocarbons.

**Keywords**: Domanic, domanikites, aromatic hydrocarbons, geochemical coefficients, geochemical logging, migrational bitumoids

**Recommended citation**: Ostroukhov S.B., Pronin N.V., Plotnikova I.N., Khairtdinov R.K. (2020). A new method of «geochemical logging» for studying Domanic deposits. *Georesursy = Georesources*, 22(3), pp. 28–37. DOI: https://doi.org/10.18599/grs.2020.3.28-37

## Introduction

At present, much attention is paid to the study of Domanik deposits. Evaluation of the prospects for the production of shale oil from high-carbon strata of the Semiluksko-Rechitsky complex initiated the beginning of more detailed work on their study, including geochemical studies. A new stage in the study of the Semiluksko-Rechitsky high-carbon rocks (Ostroukhov et al., 2015; Plotnikova et al., 2017a, b) clearly showed that at the present stage more detailed knowledge is needed about the conditions of their formation and distribution in the depths. To do this, it is necessary to expand the previously created and used today complex of geochemical studies, since the isolation of high-carbon strata in the section only by the amount of organic matter (OM) content in the rocks with an assessment of its catagenetic maturity is insufficient and does not fully characterize the geological history of OM formation and its distribution along the section of the sedimentary cover.In addition, the problem of identifying promising oil-saturated intervals in the section of Domanik deposits by well logging methods has not been fully resolved, and the complex of geological and technical studies used needs to be supplemented with mobile express methods of pyrolysis, X-ray studies of the rock matrix and geochemical study of dispersed organic matter and mobile hydrocarbons. The use of new geochemical coefficients will make it possible to differentiate the section of Domanik deposits by the nature of the saturating fluid and to identify areas with

*Corresponding author: Irina N. Plotnikova
*E-mail: irena-2005@rambler.ru*

the predominant development of immobile syngenetic organic matter in dense carbonate-siliceous rocks and mobile migratory bitumoids, which are responsible for the formation of commercial accumulations.

Deposits of the Semiluksko-Rechitsky age on the territory of the Republic of Tatarstan are referred to the so-called "Domanik type" deposits. They stand out among the higher and lower bedding rocks with a certain mineralogical composition and a high content of scattered organic matter (total organic carbon, Total Organic Carbon, TOC, varies from 5 to 20% and above), which gives grounds to class them as oil shale. The standard set of geochemical studies used at the present stage does not always allow a full assessment of their features, the nature of distribution and the conditions of formation. This necessitates the creation and application of new approaches to geochemical studies of organic matter, which will expand their practical significance both at the stage of prospecting and exploration, and during the development of identified deposits.

## Materials and research methods

In this work, the object of study was the rocks of the Semiluksky horizon of the Frasnian stage of the Upper Devonian, exposed in the interval 1775–1800 m by well No. 5055 at the Tavelskoye oil field in the Republic of Tatarstan. It should be noted that these deposits are lithologically heterogeneous and are represented by alternation of limestones, dolomitized limestones, siliceous-carbonate, carbonate-siliceous and predominantly siliceous rocks. To study them, studies were carried out by the method of X-ray phase analysis (12 samples), pyrolytic studies (16 samples), geochemical studies of bitumoids (25 samples) extracted from rocks that most fully characterize the specified interval of the section. Due to the high lithological heterogeneity of the studied interval of the section, work was carried out to identify and study interlayers of various lithological types, which contributed to obtaining more complete information for these deposits.

The studies carried out are mainly focused on the geochemical study at the molecular level of the bitumoids of rocks of the Domanik facies, the characteristic compounds of these bitumoids in rocks of various lithological composition. For these purposes, new geochemical coefficients were used, which make it possible to differentiate bitumoids according to the conditions of formation, according to the degree of thermocatalytic transformation, as well as according to their confinement to certain types of rocks of the studied section.

To study the OM of the sedimentary rocks, at the first stage, a standard complex of geochemical studies was used, including sample preparation using hot chloroform extraction, determination of the bitumen content, followed by its division into groups by liquid column chromatography.

Oil fractions of OM of rocks were analyzed on a gas chromatography-mass spectrometer "Thermo Fisher Scientific" (USA), using computer data processing in the SCAN mode. Separation of hydrocarbons (HC) was carried out on a capillary column 30 m long, 0.32 mm in diameter with a PE-XLB phase. Chromatography was carried out in the linear programming mode from 100°C to 300°C, in the temperature range from 100°C to 150°C, the rate of temperature rise was 12.5°C per minute and 3°C per minute in the range from 150°C to 300°C. The isothermal regime at the initial temperature lasted 2 minutes, at the final (300°C) – 14 minutes. Evaporator temperature is 300°C. The carrier gas is helium, the flow rate is 2 ml/min. Under these chromatographic conditions, special attention was paid to the analysis of isorenieratane, a high-molecular aromatic compound of the composition C40.Oil fractions of OM of rocks were analyzed on a gas chromatography-mass spectrometer «Thermo Fisher Scientific» (USA), using computer data processing in the SCAN mode. Separation of hydrocarbons (HC) was carried out on a capillary column 30 m long, 0.32 mm in diameter with a PE-XLB phase.

To compare the data of gas chromatography-mass spectrometry (CMS), pyrolysis of rock samples was carried out using a HAWK Resource Workstation (Wildcat Technologies, USA) in the BulkRock mode before and after extraction, as well as X-ray studies of rock samples.

## Results

The studied area of the geological section of the well in the depth interval of 1775–1800 m is characterized by high lithological heterogeneity and is represented by alternating layers of gray or light gray limestones, dark gray siliceous limestones, as well as carbonate-siliceous, carbonate-siliceous-carbonaceous and mainly siliceous-carbonaceous rocks of black color. The thickness of the alternating layers varies from the first millimeters to 10-15 centimeters.

In the series limestone → siliceous limestone → carbonate – siliceous rock → carbonate – siliceous – carbonaceous rock → siliceous – carbonaceous rock (Figure 1), there is a decrease in the content of the carbonate component (from 100 to 11%, hereinafter, wt% is used), an increase silica content (from 0 to 80%) and an increase in TOC content (from 0.7 to 23.6%).

The content of TOC and a wide range of its values are associated with the lithotype of rocks (Figure 2). The lowest OM content, not exceeding 0.7%, is typical for limestones (Figure 3, A). An abnormally high TOC value of 23.6% was recorded in one sample of siliceous rock without carbonate interlayers (Figure 3, D). The main OM content, ranging from 3.5 to 6.5%, is associated

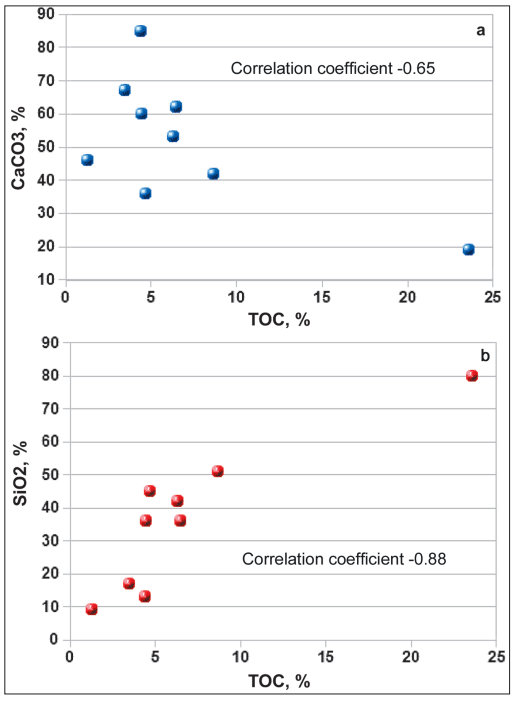


*Fig. 1. Dependence of the content of total organic carbon (TOC) on the content of carbonate (a) and siliceous (b) components in the rock*

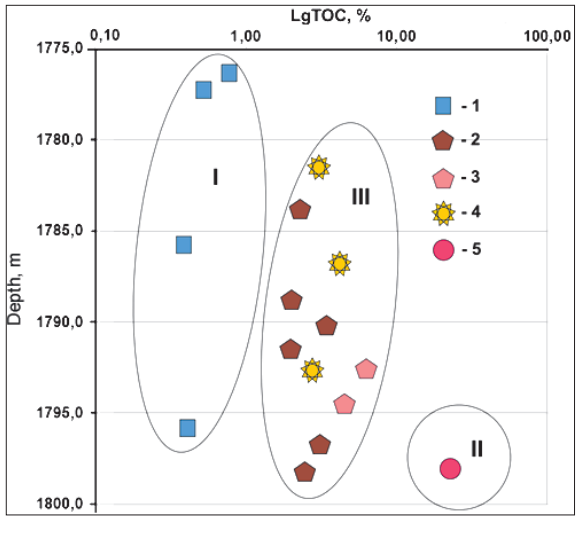


*Fig. 2. TOC values in rock samples from the interval 1775–1800 m. 1 – limestones, 2 – siliceous-carbonate rocks, 3 – carbonate-siliceous rocks, 4 – fine alternation of siliceous-carbonate, carbonate-siliceous, siliceous rocks and limestone interlayers, 5 – siliceous rock (silicite).*

with siliceous-carbonate and carbonate-siliceous rocks with limestone interlayers (Figure 3, B, C).

Figure 4 shows the dependence of the content of free mobile hydrocarbons S1 on the TOC of the rocks of the considered interval of the studied section. The main part of the values on it is grouped in a rather narrow range, which evenly increases with increasing TOC (blue dots), which is quite natural. However, some of the samples (red dots) indicate the presence of an increased content of mobile (allochthonous) HC in a number of samples,

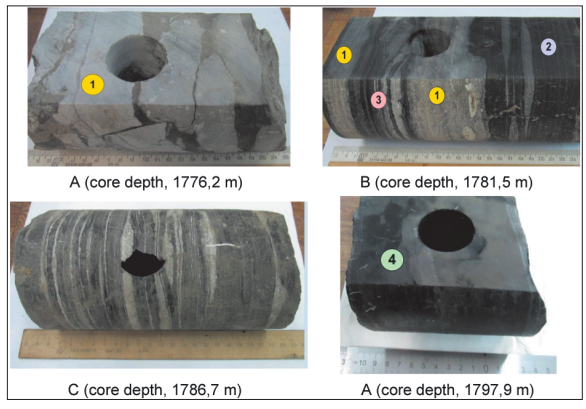


*Fig. 3. Examples of rock samples from the Semiluksky horizon. A – limestone; B, C – alternation of interlayers of carbonate-siliceous and siliceous-carbonate rocks with interlayers of light limestone; D – carbonate-siliceous rock without limestone interlayers; 1 – limestone, 2 – thin interbedding of carbonate-siliceous and siliceous-carbonate rocks, 3 – thin layering of limestones and carbonate-siliceous rocks, 4 – siliceous rock (SiO2 – 80%).*

which may indicate different types of HC in the samples under study.

According to the results of group analysis, the composition of chloroform bitumen A (CBA) of rocks is dominated by resins with a content – from 24.31% to 64.47%, and asphaltenes – from 14.08% to 72.62%. This is mainly typical for limestone interlayers. The content of oils varies from 5 to 34% and is directly related to the OM content in the rock.

The complexity of the geological section of the Semiluksky horizon and the need to create new solutions in the search and exploration of industrial oil deposits confined to it determines the relevance of creating new geochemical approaches to the development of an effective complex of methods for finding oil in domanikites based on previously created and actively used criteria and geochemical coefficients (Petrov, 1984; Peters et al., 2005).

Expanded geochemical studies of the hydrocarbon composition of OM in the rocks of the Semiluksky horizon made it possible to identify a group of compounds characteristic of these deposits. They are monocyclic aromatic compounds of the C10-C30 composition with an isoprenoid alkyl chain of irregular structure (Ostroukhov et al., 1982), which are derivatives of the natural aromatic carotenoid (AC) of the C40 composition (isorenieratane). Isorenieratane (ISR) is widely represented in wildlife since the age of the Earth of 1.6 billion years (Paleoproterozoic) (Brocks et al., 2005, 2008) to the present. Moreover, its content in the natural environment has not been constant over the entire geological time. At certain periods, the content of isorenieratane (a diagenetic product of ISR) in wildlife, and then in sediments, either increased significantly or practically disappeared (French et al., 2015). One of

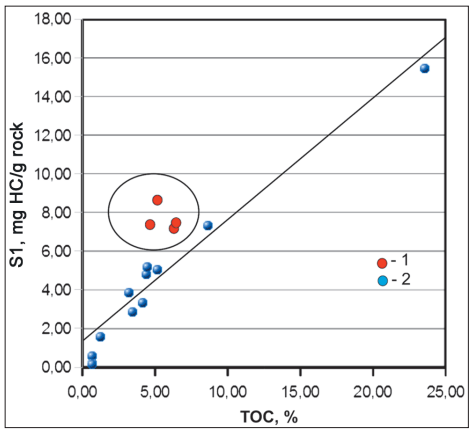


*Fig. 4. The nature of the dependence of S1 (according to pyrolysis data) on TOC. 1 – S1 values indicating the presence of HC migration; 2 – S1 values, presumably not associated with migratory HC.*

the periods with an increased content of isorenieratane includes the Frasco-Famennian deposits of the Late Devonian.

ISR refers to isoprenoid pigments produced by photosynthesized brown and green sulfur bacteria (Chlorobiaceae) (Maresca et al., 2008a). Since the metabolism of bacteria requires simultaneous access to both light and $H_2S$ in their aquatic habitat, the discovery of their diagenetic and catagenetic products in the OM of rocks or oils is considered as evidence of the existence of the sulfide euxinic zone of the paleobasin (Summons, Powell, 1987; Rocks et al., 2005; Connock et al., 2018). This allows, when conducting geochemical logging, to identify similar areas in the studied sediments with the determination of their boundary values.

For the first time on the territory of the Republic of Tatarstan, isorenieratane, its diagenetic and catalytic products were found in the sediments of the Semiluki age in 2013–2014. and are described in (Ostroukhov et al., 2015). Similar compounds are observed in the rocks of the Domanik facies and in the adjacent territories of Tatarstan, which indicates the scale of the manifestation of common geological and facies conditions of sedimentation, which contribute to the periodic active development of the biota.

The mass fragmentogram scanned for ions m/z 133+134 (Figure 5A) shows a group of aromatic carotenoids of the composition C14-C22 (hydrocarbons of this series are denoted by the symbol Δ) with methyl substitution of the benzene ring at position 2,3,6- ratio of the alkyl chain and individual compound II (isorenieratane) with methyl substitution of two benzene rings at position 2,3,6-/2,3,6- (Koopmans et al., 1996b), which are derivatives of the natural ISR of composition C40 (Figure 6).

Mass fragmentograms (Figure 5) also show the presence of a second homologous series (on the mass fragmentograms, hydrocarbons of this series are indicated by ∇) and individual compound I (paleorenieratane) in composition and distribution in a series similar to compounds of the Δ series and compound II. The structure of the compounds of this series was adopted on the basis of the studies described in the works (Hartgers et al., 1993, 1994; Clifford et al., 1998), according to which the compounds designated by ∇, have a methyl substitution of the benzene ring at position 3,4,5- and compound I (paleorenieratane ) with methyl substitution of benzene rings at position 3,4,5-/2,3,6- (Fig. 7).

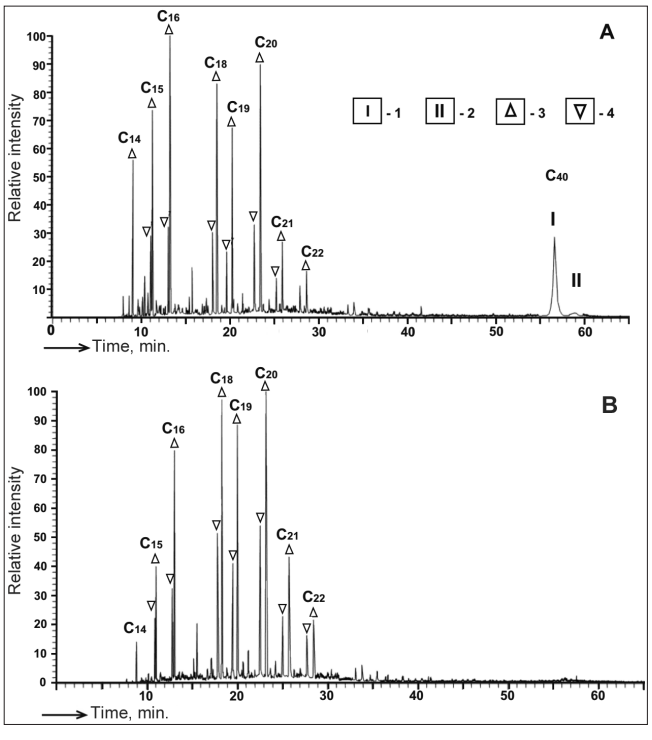


*Fig. 5. Composition of aromatic carotenoids in the OM of rocks of the Semiluksky horizon, borehole 5055. A – depth 1781.0 m; B – depth 1790.5 m. 1 – 3.4.5-/2.3.6-paleorenieratane; 2 – 2,3,6-/2,3,6-isorenieratane; 3 – 2,3,6-trimethyl-1-isoalkylbenzenes; 4 – 3,4,5-trimethyl-1-isoalkylbenzenes (m/z 133+134).*

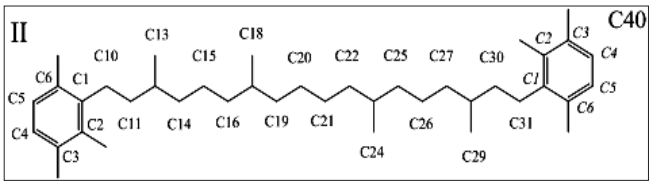


*Fig. 6. The structure of isorenieratane with methyl substitution of two benzene rings at position 2,3,6-/2,3,6-, which are derived from the natural ISR of the composition C40*

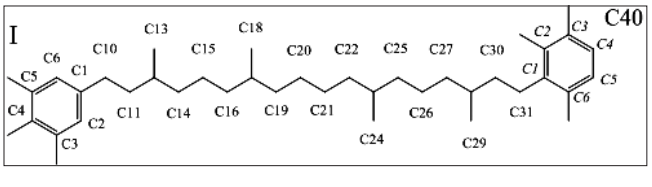


*Fig. 7. The structure of paleorenieratane with methyl substitution of benzene rings at position 3,4,5-/2,3,6-*

The presence of paleorenieratane (I) is noted in the OM of all rocks along the section of the Semiluksky horizon. It should be noted that its content is always higher than that of isorenieratane (II). The high representativeness of compound I implies its widespread use in the complex of geochemical studies of Domanik deposits. But this requires an understanding of the conditions for its formation and transformation in the natural environment. However, at present, there is a problem associated with the impossibility of establishing its natural analogue. In the composition of more than 700 identified natural compounds, no carotenoid compounds with methyl substitution 3,4,5-/2,3,6- in the ring have been identified (Maresca et al., 2008a). At the same time, a significant amount of compound I is present in the Late Devonian sediments (French et al., 2015). This arouses a certain interest both in its origin and in its association with Domanik type deposits.

In the natural environment, the end product of the biochemical process of transformation of carotenoids in the structure of green sulfur bacteria Chlorobiaceae under the conditions of a euxinic environment is isorenieratene (ISR) (Koopmans et al., 1996a, b). This occurs as a result of the action of the crtU genome, leading to the destruction of the geminal methyl groups of cyclohexene rings during their aromatization with the preservation of the number of methyl substituents in it with 2,3,6-/2,3,6- substitution with respect to the alkyl chain (Maresca et al., 2008b). In paleorenieratane, in contrast to isorenieratane, the methyl substitution of one of the rings is 3,4,5-.

Thermocatalytic effect on cyclic compounds with dimethyl geminal substitution in the process of aromatization leads to the destruction of the methyl group. As a result, one of the methyl groups is displaced to form two possible compounds with methyl substitution 2,3,6- and 2,4,6- (Ostroukhov et al., 1982). The formation of compounds with methyl substitution 3,4,5- was not established. Of the reaction products, only one compound with 2,3,6- substitution corresponded to oil, while compounds with 2,4,6- substitution were not found in the OM of rocks and oil. It should be added that the main product of thermocatalysis is trisubstituted alkylbenzenes with methyl substitution 2,6-, also not found in the composition of oil and OM of rocks.

The isomerization of one of the benzene rings of renieratane can be considered as one of the options for the formation of paleorenieratane (Figure 8).

Renieratane is a derivative of the naturally occurring compound renieratene (RNR) classified as a carotenoid (Schaechaee et al., 1977, 1997). Renieratane is present in the OM of rocks and oils (Connock et al., 2018; Wanglu et al., 2007) of a certain age and conditions of formation of the oil source material. Isomerization of high-molecular-weight alkylbenzenes occurs mainly due to a change in the position of the alkyl chain in the benzene ring. In this embodiment, the migration of the alkyl chain along the ring from position 1 to position 2 is assumed to form the most stable isomer with methyl substitution 3,4,5-. But there is some discrepancy in this, due to the fact that the methyl substitution of the isoprenoid chain, in contrast to its regular structure, blocks the migration process during thermocatalysis. In this regard, the possibility of isomerization of the benzene ring of natural RNR as a result of a biological process occurring at an early stage of the transformation of dispersed organic matter is not excluded.

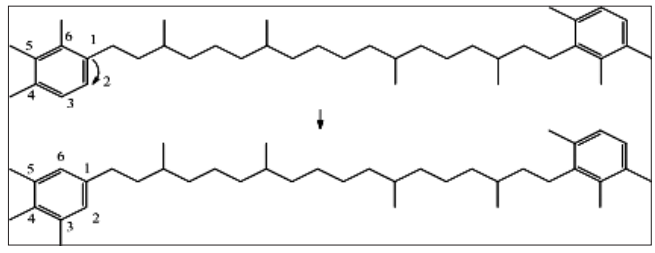

*Fig. 8. Scheme of the formation of paleorenieratane as a result of isomerization of one of the benzene rings of renieratane*

At present, due to the absence of an established initial natural compound for paleorenieratane, pseudo paleorenieratane (PAR) can be taken as its precursor, by analogy with the compounds isorenieratane and renieratane. This makes it possible to fully use it for solving geochemical problems with the participation of paleorenieratane.

The representativeness and informational content of the oil series AC makes it possible to use them in a complex of geochemical studies. First of all, this concerns the features of the molecular weight distribution (MWD) of members of their homologous series. Earlier in the work (Schwark, Frimmel, 2004), the AIR coefficient (aryl isoprenoid ratio) was proposed, which reflects the ratio between the compositions C13-C17 and C18-C22 of AC in order to assess the variability and stability of the photic zone of the paleobasin under conditions of an anoxidic environment. This coefficient has a narrow focus and is not capable of solving other geochemical problems. In this regard, in this work, a number of geochemical coefficients have been proposed that make it possible, through the composition of the AC, to characterize some of the processes associated with the formation and transformation of the initial OM in the composition of Domanik rocks.

One of the main indicators in the complex of geochemical studies is the thermocatalytic transformation of organic matter. This characteristic can be obtained based on the transformation of a number of AC compounds, expressed by the coefficient:

$$Kac1 = [\sum C10/(\sum C10+CI+CII)],$$

where ∑C10 is the sum of prenitol and isodurol; CI – content of paleorenieratane (I); CII is the content of isorenieratane (II).

The coefficient is based on the ratio of the contents of compounds I and II and alkylbenzenes of composition C10 with methyl substitution of the benzene ring at positions 1,2,3,4- (prenitol) and 1,2,3,5- (isodurol), shown in Figure 9. The choice of these compounds is based on the fact that alkylbenzenes of composition C10 are the main products of thermal destruction of individual compounds I and II. This process has been confirmed by laboratory studies on rock samples with a high content of compounds I and II. In all products of flash pyrolysis up to 650°C of the studied rocks, a high content of two newly formed target compounds of composition C10 and a complete absence of starting compounds I and II were observed (Figure 10A, B). In this case, the preservation of the initial compounds of AC with the composition C16-C22 was also observed, which indicates a high thermocatalytic stability of these compounds and the absence of their effect on the formation of C10. This is also indicated by their dominance in the composition of pyrolysis products, in contrast to extracts.

It should be especially noted that the pyrolysis products do not contain low-molecular AC compounds with the composition C11-C15. It is known that the composition of the OM pyrolysis products is mainly represented by low-molecular aliphatic and cyclic compounds formed due to the destruction of high-molecular compounds. The absence of low molecular weight AC indicates the impossibility of high molecular weight analogs under these conditions to form compounds other than C10. At the same time, their presence in the composition of oils arouses interest in the process that contributes to their formation. Most likely, it is realized at an early stage of transformation of the initial oil source material.

The value of the coefficient Kac1 reflects the degree of transformation (destruction) of compounds I and

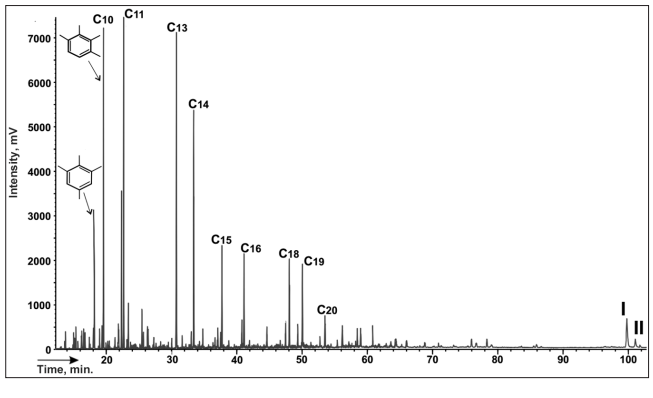


*Fig. 9. Composition of aromatic carotenoids in oil (mz 133+134). C10-C20 is the number of carbon atoms in the molecule; I – 3,4,5-/2,3,6-paleorenieratane; II – 2,3,6-/2,3,6-isorenieratane.*

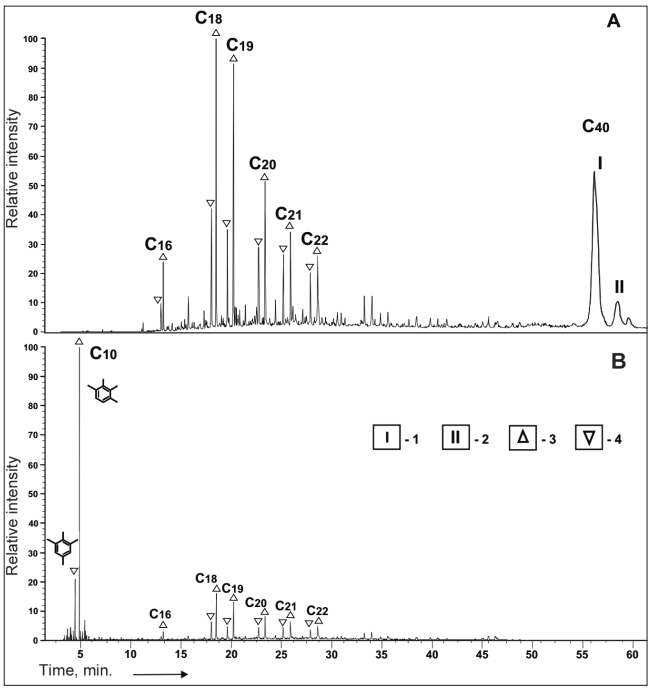


*Fig. 10. Composition of aromatic carotenoids in the extract of the original sample (A), and in the product of its flash pyrolysis (B). 1 – 3,4,5-/2,3,6-paleorenieratane; 2 – 2,3,6-/2,3,6-isorenieratane; 3 – 2,3,6-trimethyl-1-isoalkylbenzenes; 4– 3,4,5-trimethyl-1-isoalkylbenzenes (m/z 133+134).*

II. The maximum value of Kac1 is associated with the complete absence of compounds I and II in the oil composition. The Kac1 values for oils from the Semiluksky horizon in Tatarstan range from 0.7 to 1.0. That is, in a number of the studied oils, compounds I and II are practically absent.

The use of this coefficient to estimate the OM of rocks in most cases is difficult due to the absence in the homologous series of compounds with a composition up to C14, including alkylbenzenes C10 (Figure 5A, B). Despite this, rock samples that do not contain compounds I and II (Figure 6B) can be classified as highly transformed. These, in the considered depth interval, include all OM samples from limestone deposits that do not contain or contain compounds I and II at the background level (Figure 5B).

The organic matter of all carbonate-siliceous-carbonaceous rocks contains a sufficiently large amount of compound I with an insignificant content of compound II (Figure 5A). Unfortunately, the absence of C10 alkylbenzene in the composition of the samples does not allow us to determine the degree of their transformation, but the presence of compounds I and II indicates that it is much lower than for limestone deposits.

The composition of homologous series ∇ and ΔAC of organic matter of rocks of the Domanik facies is represented by compounds C14-C22 of different intensities, in contrast to unfractionated oils, in which the composition of the homologous series starts from

C10. But the fact that low-molecular-weight C10-C13 compounds could be in their composition is beyond doubt, since they are an integral part of homologous series in the composition of oils in Domanik deposits, representing full-fledged products of a single process of destruction of the initial natural compounds ISR and PAR.

When considering the composition of homologous series, the absence of members of the series above C23-C30 is observed. In the presence of a high content of C10-C19 compounds formed as a result of chain destruction of ISR and PAR compounds of C40 composition, it is logical to expect the presence, respectively, of fragments of the C21-C30 composition with the same content. Nevertheless, they are practically absent or present in small quantities in the OM of rocks. This fact requires additional research. But such a distribution is possible due to the destruction of natural C40 compounds Chlorobactene (Maresca et al., 2008b), which have one benzene ring in their structure.

Despite the above-mentioned features of AC formation, the molecular weight distribution of members of their homologous series is highly informative and can be successfully used in the study of OM in Domanik deposits. Compounds of homologous series ∇ and Δ have their own regularities, reflecting a wide range of natural processes associated with the formation of hydrocarbon deposits. This should include the genetic relationship between the compounds of the series Δ and I, since they, presumably, are products of the natural compound PAR containing one of two benzene rings with methyl substitution 3,4,5-. In turn, the members of the Δ series are represented by the sum of the degradation products of the initial natural compounds PAR and ISR containing benzene rings with methyl substitution 2,3,6-.

Since in the composition of oils and organic matter of rocks there is a significant dominance of compound I over II, it is interesting to follow this pattern for low-molecular compounds of the same composition. The predominance of one or another natural compound (PAR or ISR) in the formation of the composition of the Δ and ∇ series can be estimated based on the following coefficient:

$$Kac2 = PAR / (PAR + ISR) = 2\sum C\nabla / (2\sum C\nabla + \sum C\Delta),$$

where – $2\sum C\nabla$ characterizes the contribution of PAR to the formation of members of the homologous series ∇, $\sum C\nabla$ is the sum of the heights H or the area S of chromatographic peaks C15-C22.

The $\sum C\Delta$ value characterizes the share of ISR in the composition of the Δ series members. Their number is determined as a result of deducting from the total content of the member of the series the share of C∇.

Due to the fact that in most cases the ratio between the peaks of the same composition in the series Δ and ∇ remains practically unchanged, then in the calculation of this coefficient, the values of AC C18 can be used.

In the OM of carbonate-siliceous-carbonaceous rocks, the Kac2 coefficient is 0.40, which indicates the predominance of ISR over PAR during the formation of compounds of the ∇ and Δ series. In the OM of limestones, the prevalence of ISR is also observed, as indicated by the value of the considered coefficient, which is 0.45. The difference between them sufficiently indicates the absence of a direct genetic link. The OM values of rocks with interlayers fall into the intermediate region with an interval of 0.41–0.44. Moreover, depending on the predominance and nature of the interlayer, they tend to one or another area of its location.

Comparison of the results obtained in order to establish the effect of natural compounds ISR and PAR on the composition of members of the homologous series ∇ and Δ and compounds I and II revealed a certain pattern. One might expect that during the formation of the composition of oil or OM of rocks, both for low-molecular hydrocarbons and for high-molecular compounds I and II of composition C40 one type of initial substance should prevail, but this is not the case. In practice, it is revealed that for the Domanik deposits of Tatarstan, in the composition of the homologous series AC∇ and Δ, there is a predominance of ISR products over PAR, as indicated by the values of K = 0.35–0.49. At the same time, for the same deposits among compounds I and II, the PAR product always prevails over ISR in a ratio of 2 to 10 times. From this it follows that ISR is almost completely converted into low molecular weight compounds, while PAR is more preserved and is represented in high molecular weight compound I. This indicates a rather complex nature of the transformation of the initial natural substances of the carotenoid type in the interior.

For the complex characterization of OM of Domanik deposits, the coefficient $Kac3 = (C\Delta+C\nabla)/(C\Delta+C\nabla+C_I+C_{II})$ was also used, developed on the basis of compounds I and II and members of the series ∇ and Δ of composition C20. The members of the indicated series are accepted on the basis of their location in the representative area of the sample composition. This is especially true for the OM of rocks subject to the greatest changes. The Kac3 coefficient supplements the information obtained by using the Kac1 and Kac2 coefficients on the processes associated with the formation and change in the composition of this group of compounds. Kac3 is based on the ratio of compounds I and II to the degradation products of the initial biological substance. The main changes in the values of the coefficient in a single geological object are associated with the content of $C_I$ and $C_{II}$, which is significantly influenced by both thermal impact and migration through porous media. Clarification of the dominance of one of these processes, if necessary, is carried out according to the results of comparison with other specialized methods of analysis.

For the considered Domanik sediments, opened within the Republic of Tatarstan, due to the absence or extremely low content of compound II ($C_{II}$) in the OM of rocks, a coefficient with a simplified set of parameters was used:

$Kac3 = 2C\nabla/(2C\nabla + C_I)$.

Figure 11 shows the change in the value of this coefficient (Kac3) with the depth of the rocks in the section of the interval under consideration. Its values vary in a fairly wide range from 0.3 to 1.0. At the same time, low Kac3 values are associated with a high content of compound I in the composition of the OM of rocks, while high values are associated with its decrease.

Comparison of the Kac3 values with the lithological type of rocks reveals a certain relationship between them. For example, it was found that its lowest values (up to 0.55) are characteristic of the OM composition of carbonate-siliceous-carbonaceous rocks, which is associated with the high content of compound I. Its highest values (over 0.8) are characteristic of OM in interlayers light gray limestone. It is necessary to pay attention to the range of values of the coefficient Kac3 in the range of 0.55–0.8. These values are typical for rock samples from the transitional region between carbonate-siliceous-carbonaceous varieties containing paleorenieratane and light gray limestones not containing paleorenieratane. The lithology of these rocks has a more complex composition and is represented by thin interlayers that are difficult to separate during sample preparation. This affects the values of the coefficient characterizing the total OM composition of these interlayers.

For a comparative assessment of the transformation of the OM composition in the rocks, the C27 hopane isomers with the Ts and Tm configurations, traditionally used in the complex of geochemical studies, were used. The use of hopanes is associated with a high bacterial activity (Kannenberg et al., 1999) in the anaerobic sulfide euxinic environment of the considered paleobasin.

Thermocatalytic action on saturated polycyclic compounds leads to their isomerization with the accumulation of more thermodynamically stable isomers in the mixture. The required thermal energy in the interior increases with the depth of OM, thus activating isomerization in the composition of hopane of the composition C27 with the Tm configuration in Ts. To assess this process in practice, the coefficient Kg = Ts/(Ts+Tm) is widely used, the values of which are in the range 0–1. The maximum Kg value indicates the complete transformation of hopane with the Tm configuration into Ts and, accordingly, a high degree of the thermocatalytic process.

The values of the coefficient Kg for the investigated samples vary in the range from 0.1 to 0.4 and indicate a low degree of thermocatalytic conversion. Figure 11 shows the distribution of values with the depth of the

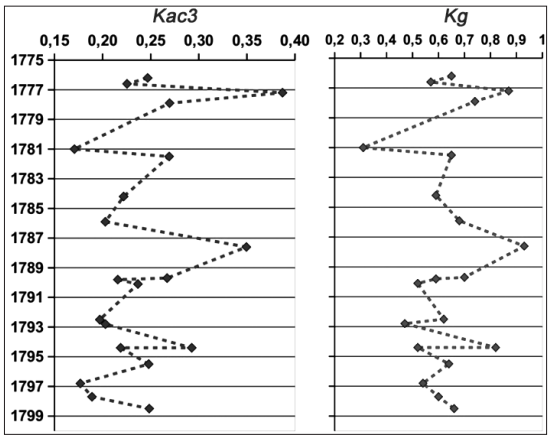


*Fig. 11. Distribution of the values of the coefficients Kac3 and Kg in the depth interval 1775–1800 m.*

samples. It is quite natural that due to the small thickness of the studied interval, this distribution does not reveal any definite relationship with the depth of the samples. However, there is a dependence of the values of the coefficient Kg on the lithology of rocks. The lowest Kg values (up to 0.15) are characteristic of OM-enriched carbonate-siliceous-carbonaceous rocks with the highest content of compound I. Kg values above 0.27 are characteristic of the OM of limestones or siliceous-carbonate rocks with a low silica content, which are depleted of OM. Paleorenieratane is absent or is at the background level.

The Kg values equal to 0.15 and 0.27 characterize the transition region associated with the heterogeneity of the rock due to the presence in it of thin interbedding of limestones and carbonate-siliceous-carbonaceous varieties. The dominance of one or another interlayer in the sample brings its value closer either to the group of limestones or to the group of carbonate-siliceous rocks enriched in OM.

In a small interval of depths, the wide scatter of the values of the coefficient Kr, which reflects the activity of the isomerization process, requires a special explanation, which cannot be linked with the difference in the catalytic activity of rocks with practically the same thermal effect on the formation. The catagenic transformation of OM in pure limestones, based on the values of the coefficient, is 2 times higher than that for carbonate-siliceous and siliceous rocks. At the same time, attention is drawn to the clear separation of OM according to the values of transformation at the boundaries of the interlayers. This indicates the absence of a genetic relationship between the OM of limestones and the OM of carbonate-siliceous interlayers.

Comparative analysis of the values of the coefficients Kac2 and Kg from the depths of occurrence showed a certain relationship between them. The following basic patterns are noted:

- in sediments with low isomerization of hopane C27, a high content of paleorenieratane is observed;

- in sediments with high isomerization of hopane C27, the absence of paleorenieratane is observed;

- in layered rocks, the transformation of hopan and paleorenieratane changes synchronously depending on the composition of the rock.

The correlation relationship between the values of Kac3 and Kg is well illustrated in Figure 11. A decrease and an increase in the values of these coefficients is observed synchronously in a narrow interval of depths, which indicates that hydrocarbons with a high degree of catagenetic transformation are mainly associated with interlayers filled with pure limestone (in which, according to according to pyrolysis data, the presence of syngenetic OM is minimal). Thus, in a narrow interval with a thickness of 15 m, hydrocarbons formed under different catagenetic conditions are simultaneously present. Considering that the temperature difference during the entire geological evolution of the studied section interval (15 m) did not exceed 2°C, the presence of hydrocarbons formed at higher temperatures in this interval unambiguously indicates the presence of at least two HC-systems in the studied part of the section – syngenetic scattered OM, the catagenetic degree of transformation of which is small, and migratory hydrocarbons that migrated into fractured limestone layers from another source and have a different genesis. The issue of the presence of migratory bitumoids in the Domanik strata and in other overlying horizons of the sedimentary cover was considered earlier (Plotnikova et al., 2017a, b).

Consequently, the observed regularities in the change in the composition of the OM of rocks indicate the influence on it of the migration process of hydrocarbons that entered the studied rocks from another source of their formation.

In our case, the higher isomerization of hopane and the absence of compounds I and II in the bitumoids from the interlayers of pure limestone indicate a higher thermocatalytic transformation of these hydrocarbons in comparison with the original syngenetic matter of the siliceous-carbonaceous-carbonate interlayers of the Semiluksky horizon.

Taking into account the practical absence of syngenetic organic matter in limestone interlayers and their low catalytic activity, as well as the conditions of their formation, which do not contribute to a high transformation of syngenetic organic matter, the following can be assumed. One of the reasons for the presence of hydrocarbons in a narrow interval of the geological section, significantly differing in the degree of catagenetic transformation, is that hydrocarbons characterized by high thermocatalytic transformation are migratory, that is, they migrated into the studied rocks of the Semiluksky horizon from another source of generation associated with high-temperature formation conditions hydrocarbons. At the same time, carbonate interlayers, which have increased porosity and permeability in comparison with dense siliceous-carbonaceous ones, have more favorable conditions for the migration of mobile hydrocarbons along them. It was also established that the source of the formation of these migratory bitumoids is not related to the syngenetic OM of the siliceous-carbonaceous rocks of the Semiluksky horizon in the study area, but is probably of a deep nature.

## Conclusions

The studies carried out have shown that at least two types of bitumoids are present in the Domanikite sequence – migratory, more mature and thermocatalytically transformed, and syngenetic, less mature with a low degree of thermocatalytic transformation (autochthonous and allochthonous bitumoids, as it was commonly called earlier). This conclusion fully confirms the previously obtained results (Ostroukhov et al., 2017; Plotnikova et al., 2017a, b), which indicate the presence of migratory bitumoids in the rocks of the sedimentary cover and in the Semiluksky horizon, which are not related by their genesis to the scattered organic matter of the Domanik complex rocks within the study area. The use of new geochemical coefficients based on aromatic carotenoids characteristic of Domanik deposits allows, at a new level, in the "geochemical logging" mode, to assess the presence of "mobile" migratory and "stationary" syngenetic hydrocarbons in the rocks. This will make it possible to differentiate the section of the Semiluksky horizon and reveal dense interlayers with a high content of syngenetic OM, reservoir intervals and fracture zones.

It is logical to assume that migratory hydrocarbons are mainly associated with more permeable and fractured rocks, which include interlayers of limestones and siliceous-carbonate rocks. Carbonate-siliceous-carbonaceous and siliceous rocks enriched with OM, due to their lower permeability, seem to accept less "mobile" migratory hydrocarbons, while maintaining the composition of syngenetic organic matter and indicators of a low degree of its transformation.

The developed geochemical coefficients are the basis for a new approach to the use of "geochemical logging" in the general complex of express geological and technological research in the process of drilling wells. This approach can be very effective in determining OM concentrations in high-carbon strata, complementing gamma ray data, since there is a positive correlation between OM and uranium content. These new coefficients can be successfully applied in the study of cuttings to determine the reservoir intervals, fracture and decompaction zones, in which there are traces of hydrocarbon fluid migration, mobile HC, which may indicate the presence of oil deposits.

The integration of geochemical studies of cuttings with its rapid study by pyrolysis and X-ray analysis methods will significantly increase the accuracy of identifying interlayers with a high OM content in the Semilukski horizon, as well as potential reservoirs with mobile hydrocarbons.

## References


Brocks J.J. Love G.D., Summons R.E. et al. (2005). Biomarker evidence for green and purple sulphur bacteria in a stratified Palaeoproterozoic sea. *Nature,* 437, pp. 866–870. https://doi.org/10.1038/nature04068

Brocks J.J., Schaeffer P. (2008). Okenane, a biomarker for purple sulfur bacteria (Chromatiaceae), and other new carotenoid derivatives from the 1640 Ma Barney Creek Formation. *Geochimica et Cosmochimica Acta*, 72(5), pp. 1396–1414. https://doi.org/10.1016/j.gca.2007.12.006

Clifford D.J., Clayton J.L., Sinninghe Damste J.S. (1998). 2,3,6–/3,4,5–Trimethyl substituted diaryl carotenoid derivatives (Chlorobiaceae) in petroleums of the Belarussian Pripyat River Basin Org. *Geochem*, 29(5–7), pp. 1253–1267. https://doi.org/10.1016/S0146-6380(98)00086-2

Connock G.T., Nguyen T.X., Philp.R.P. (2018). The development and extent of photic-zone euxinic concomitant with Woodford Shale deposition. *AAPG Bulletin*, 102(6), pp. 959–986. https://doi.org/10.1306/0726171602017224

French, K.L., Rocher, D., Zumberge, J.E., Summons, R.E. (2015). Assessing the distribution of sedimentary C40 carotenoids through time. *Geobiology*, 13, pp.139–151. https://doi.org/10.1111/gbi.12126

Hartgers W.A., Sinninghe Damste J.S., Koopmans M.P. and de Leeuw J.W. (1993). Sedimentary evidence for a diaromatic carotenoid with an unprecedented aromatic substitution pattern. Journal of the Chemical Society, *Chem. Commun.*, pp. 1715–1716. https://doi.org/10.1039/C39930001715

Hartgers W.A., Sinninghe Damste J.S., Requejo A.G., Allan J., Hayes J.M., Ling Y., Xie T.-M., Primack J., de Leeuw J.W. (1994). A molecular and carbon isotopic study toward the origin and diagenetic fate of diaromatic carotenoids. *Org. Geochem*., 22(3–5), pp. 703–725. https://doi.org/10.1016/0146-6380(94)90134-1

Kannenberg E.L., Poralla K. (1999). Hopanoid biosynthesis and function in bakteria. *Naturwissenschaften*, 86, pp. 168–176. https://doi.org/10.1007/s001140050592

Koopmans M.P., Koster J., Van Kaam-Peters H.M.E., Kenig F., Schouten S., Hartgers W.A., Dc Leeuw J.W. and Sinninghe Damste J.S. (1996a). Diagenetic and catagenetic products of isorenieratene: molecular indicators for photic zone anoxia. *Geochimica et Cosmochimica Acta*, 60, pp. 4467–4496. https://doi.org/10.1016/S0016-7037(96)00238-4

Koopmans M.P., Schouten S., Kohnen M.E.L. and Sinninghe Damste J.S. (1996b). Restricted utility of aryl isoprenoids for photic zone anoxia. *Geochimica et Cosmochimica Acta,* 60, pp. 4873– 4876. https://doi.org/10.1016/S0016-7037(96)00303-1

Maresca, J.A., Graham, J.E., Bryant, D.A. (2008a). The biochemical basis for structural diversity in the carotenoids of chlorophototrophic bacteria. *Photosynth. Res*., 97, pp. 121–140. https://doi.org/10.1007/s11120-008-9312-3

Maresca, J.A., Romberger S.P., Bryant D.A. (2008b). Isorenieratene biosynthesis in green sulfur bacteria requires the cooperative actions of two carotenoid cyclases. *J.Bacteriol*., 190(19), pp. 6384–6391. https://doi.org/10.1128/JB.00758-08

Ostroukhov S.B., Arefyev O.A., Makusina V.M., Zabrodrina M.N., Petrov A.A. (1982). Monocyclic aromatic hydrocarbons with isoprenoid side chains. *Neftehimia,* 22, pp. 723–788.

Ostroukhov S.B., Plotnikova I.N., Nosova F.F., Pronin N.V. (2015). Geochemical Criteria for Facies Conditions in the Formation of Shale Deposits. *Georesursy = Georesources*, 3(62), pp. 42-47. http://dx.doi.org/10.18599/grs.62.3.8

Ostroukhov S.B., Plotnikova I.N., Nosova F.F., Salakhidinova G.T., Pronin N.V. (2015). Characteristic features of the composition and structure of crude oil from the Pervomai and Romashkino fields in Tatarstan. *Chem Technol Fuels Oils*, 50, pp. 561–568. https://doi.org/10.1007/s10553-015-0564-2

Peters K.E., Walters C.C., Moldowan J.M. (2005). The Biomarker Guide. 2nd Ed. Cambridge: Cambridge University Press. https://doi.org/10.1017/CBO9780511524868

Petrov A.A. (1984). Hydrocarbons of oil. Moscow: Nauka, 260 p. (In Russ.)

Plotnikova I.N., Ostroukhov S.B., Laptev A.A., Gazizov I.G., Emelyanov V.V., Pronin N.V., Nosova F.F., Salikhov A.D. (2017). Migration aspect in the oil-Bearing capacity of the Domanic formation in Tatarstan.*Georesursy = Georesources*, 4(19), pp. 348–355. https://doi.org/10.18599/grs.19.4.7

Plotnikova I.N., Ostroukhov S.B., Pronin N.V. (2017b). Facies features and conditions for the formation of high-carbon rocks of the Semiluk horizon (on the example of the territory of Tatarstan). *New directions of oil and gas geology and geochemistry. Development of geological exploration works: Coll. papers*. Moscow: MSU, pp. 316–325. (In Russ.)

Schaefle J., Ludwig B. (1977). Ourisson G. Hydrocarbures aromatiques d'origine geologique. II: *Tetrahedron Letters,*18, pp. 3673–3676. https://doi.org/10.1016/S0040-4039(01)83324-4

Schaefle J., Adam P., Wehrung P., Albrecht P. (1997). Novel aromatic carotenoid derevaties from sulfur photosynthetic bacterial in sediments. *Tetrahedron Letters,* 38(48), pp. 8413–8416. https://doi.org/10.1016/S0040-4039(97)10235-0

Schwark L., Frimmel A. (2004). Chemostratigraphy of the Posidonia Black Shale, SWGermany: II. Assessment of extent and persistence of photic-zone anoxia using aryl isoprenoid distributions. *Chem. Geol*., 206, pp. 231–248. https://doi.org/10.1016/j.chemgeo.2003.12.008

Summons R.E., Powell T.G. (1987). Identification of aryl isoprenoids in source rocks and crude oils: biological markers for the green sulpfur bacteria, *Geochimica et Cosmochimica Acta,* 51, pp. 557–566. https://doi.org/10.1016/0016-7037(87)90069-X

Wanglu J., Ping'an P., Chiling Y., Zhongyao X. (2007). Source of 1,2,3,4-tetramethylbenzene in asphaltenes from the tarim basin. *Journal of Asian earth sciences*, 30, pp. 591–598. *https://doi.org/10.1016/j.jseaes.2006.09.003*


## About the Authors


*Sergey B. Ostroukhov* – Cand. Sci. (Chemistry), Researcher, Academy of Sciences of the Republic of Tatarstan

20 Bauman st., Kazan, 420111, Russian Federation

*Nikita V. Pronin* – Engineer, Academy of Sciences of the Republic of Tatarstan

20 Bauman st., Kazan, 420111, Russian Federation

*Irina N. Plotnikova* – Leading Researcher, Academy of Sciences of the Republic of Tatarstan; Professor, Kazan National Research Technological University

20 Bauman st., Kazan, 420111, Russian Federation

*Ruslan K. Khairtdinov* – Deputy General Director – Chief Geologist, CJSC «Predpriyatie Kara Altyn»

48 Shevchenko st., Almetyevsk, 423450, Russian Federation


*Manuscript received 3 February 2020;*
*Accepted 10 August 2020; Published 30 September 2020*

ORIGINAL ARTICLE

**DOI**: https://doi.org/10.18599/grs.2020.3.38-47 Russian Original 2020. Vol. 22. Is. 3. Pp. 38–47

# Quantitative methods for quantification of montmorillonite content in bentonite clays

*P.E. Belousov[1*], B.V. Pokidko[2], S.V. Zakusin[1,3], V.V. Krupskaya[1,3,4]*

[1]*Institute of Ore Geology, Petrography, Mineralogy and Geochemistry of the Russian Academy of Science, Moscow, Russian Federation*

[2]*MIREA – Russian Technological University, Moscow, Russian Federation*

[3]*Lomonosov Moscow State University, Moscow, Russian Federation*

[4]*Nuclear Safety Institute of the Russian Academy of Sciences, Moscow, Russian Federation*

**Abstract**. This article is devoted to the comparison of various methods for the quantitative determination of montmorillonite content in bentonite clays based on the adsorption of organic molecules and cations. The studies were conducted on samples of natural bentonite clays of the main Russian industrial deposits and the CIS: 10th Khutor (Republic of Khakassia), Zyryanskoe (Kurgan region), Dash-Salakhlinskoe (Republic of Azerbaijan), Dinozavrovoe (Republic of Kazakhstan). All samples selected for the study are characterized by relatively high content of montmorillonite (more than 70 %). As reference values for the contents of montmorillonite, we used the data of X-ray diffraction analysis according to the Rietveld method. As the tested methods, the most common approaches were used both in the research and industrial sectors of Russia, based on the adsorption of a mixture of rhodamine 6zh and chrysoidine dyes (GOST 28177-89), adsorption of methylene blue dye and adsorption of copper (II) complex with triethylenetetramine (Cu-trien), as well as thermal characteristics after saturation with organic compounds.

The best convergence of the montmorillonite content values was shown by modified techniques based on the adsorption of methylene blue dye and the adsorption of the Cu-trien complex. Other methods are characterized by a large measurement error. A common problem with these methods is overs equivalent adsorption on highly charged alkaline bentonites and reduced adsorption on alkaline earth bentonites, as well as the presence of impurity minerals and amorphous phases capable of sorption in the composition of bentonite. The research results can be used to compare the results of the content of montmorillonite, cited by various authors in scientific publications and used in production.

**Keywords**: bentonite, montmorillonite, X-ray diffraction, adsorption, organic dyes

**Recommended citation**: Belousov P.E., Pokidko B.V., Zakusin S.V., Krupskaya V.V. (2020). Quantitative methods for quantification of montmorillonite content in bentonite clays. *Georesursy = Georesources*, 22(3), pp. 38–47. DOI: https://doi.org/10.18599/grs.2020.3.38-47

## Introduction

Bentonite clays are valuable mineral raw materials. Due to its binding sorption and swelling properties and high thermal stability, bentonite has become an indispensable raw material in various industries. The most important areas of application for bentonite clay in Russia are (in order of consumption): metallurgy, where bentonite is used as a binder for pelletizing iron ore concentrate; in drilling, for the production of drilling fluids; in foundry, in the manufacture of sandy-clay molds for iron casting; in agriculture and medicine. In total, there are more than 200 areas of use for bentonite (Belousov, Krupskaya, 2019). The main rock-forming components in bentonite clay are smectite-group minerals, in particular, montmorillonite (MMT). Commonly, it is the content of mintmorillonite which is the determining factor when choosing raw materials for industrial needs.

Montmorillonite belongs to the class of layered aluminosilicates of the dioctahedral smectite group and is a 2:1 layer, consisting of Si-O tetrahedral networks joined in the middle with an Al-OH octahedral network (Drits, Kossovskaya, 1990; Guggenheim et al., 2006). Due to the isomorphic substitutions of $Al^{3+}$ for $Mg^{2+}$ and $Fe^{2+}$ in the octahedral networks (predominantly) and a small fraction of isomorphic substitutions of $Si^{4+}$ for $Al^{3+}$ in the tetrahedral networks, the montmorillonite layer has a negative charge of about 0.33-0.66 f.u., which is neutralized by exchange interlayer hydrated cations of $Ca^{2+}$ $Na^{+}$, $Mg^{2+}$, etc. Such a structure leads to the lability of the montmorillonite structure, makes the external and internal surfaces in crystallites available for adsorption

[*]*Corresponding author: Petr E. Belousov*
*E-mail: e-mail: pitbl@mail.ru*

and provides high swelling and high sorption capacity in relation to heavy metals, radionuclides and other anthropogenic components hazardous to human health. Currently, the most correct methodological approach for calculating the quantitative content of crystalline mineral phases in a mixture (rock, soil, material) is X-ray diffraction using the Rietveld method (Krupskaya, Zakusin, 2019; Zhou et al., 2018; Motoso et al., 2006; Srodon et al., 2001).

Analyzing the content of clay minerals is not a trivial task, it requires specialized equipment and the work of experienced analysts. The micron and submicron sizes of aggregates of clay particles, the complex structure of crystallites, the presence of mixed-layer formations and numerous impurities together make it difficult to diagnose clays. With the development of the instrumental and analytical base, the methods for monitoring the content of montmorillonite in bentonite clay have also improved. It should be understood, however, that most mining and processing plants and foundries date back to the middle of the twentieth century, and they often use old techniques that require neither expensive equipment nor highly qualified specialists in the diagnosis of clay minerals.

The main methods for determining the content of montmorillonite are associated with the calculation of the adsorption value of organic dyes. Despite the fact that these methods are outdated, have a large error and, in fact, determine the sorption capacity of montmorillonite, but not its actual content, they are still used at most Russian enterprises. These include the method for determining montmorillonite, described in GOST 28177-89 «Forming bentonite clays». In addition to industry standards, generally accepted methods include the assessment of the montmorillonite content by the value of the cation exchange capacity (CEC) of bentonite clay. The most common methods for determining CEC include methods for the adsorption of the methylene dye (MB) and triethylene tetramine complex of copper (Cu-trien) (Kahr, 1998; Kaufhold et al., 2002). In the literature, there are also more rare methods for the quantitative determination of montmorillonite that require specialized equipment, for example, thermogravimetric analysis of samples pre-saturated with ethylene glycol (Holtzer et al., 2009, 2011; Nieto et al., 2008).

The results of determining MMT using the above listed and similar methods depend on the structural features of a particular montmorillonite and the composition of impurities in bentonite clay, which, in turn, are associated with the geological conditions of formation and transformation, structural features and characteristics of the mineral composition in general. The presence in the rock of minerals such as zeolite, amorphous silica, cristobalite, calcite, as well as other clay minerals (vermiculite, kaolinite, halloysite, palygorskite, etc.) significantly affects the adsorption rates and amount of organic dyes and, as a consequence, the results of measurements of the montmorillonite content. The main factors influencing the results of quantitative determination of montmorillonite by such methods are its (Kaufhold et al., 2002; Dormann, Kaufhold, 2009): cation exchange capacity; composition of exchangeable cations (ratio of alkaline and alkaline earth cations); total layer charge; layer charge density; mineral composition (the presence of impurities of other mineral phases which are able to adsorb organic dyes); the volume of micro and mesopores; the size of the clay particles; the presence of a pH-dependent charge, and as a consequence, the pH value of the clay suspension; and the presence of water-soluble salts.

The purpose of this article is to compare the main methods for determining the content of montmorillonite based on the adsorption of organic substances with the results of quantitative mineral analysis using the X-ray diffraction method, which is referenced as the most reliable and generally accepted method, as mentioned above. The paper presents the results of measuring the MMT content in bentonite clays and draws conclusions about the peculiarities of the identified differences.

## Materials and methods

Natural samples of bentonite from large deposits of Russia and the CIS countries, varying in their genesis, structural features and the composition of their interlayer complex, were selected as objects of research: 10th Khutor (Republic of Khakassia), Zyryanskoe (Kurgan region), Dash-Salahlinskoe (Republic of Azerbaijan), Dinozavrovoe (Republic of Kazakhstan). The bentonites of the Dinozavrovoe deposit are similar in composition and properties to the well-known bentonites of the Tagansky deposit (Krupskaya et al., 2017) and represent one bentonite-bearing province. The samples were selected in such a way that the content of montmorillonite (according to the data of X-ray diffraction analysis, as will be shown below) was sufficiently high and similar in all samples (Krupskaya et al., 2020).

*Quantitative determination of mineral content by X-ray diffraction*

X-ray diffraction analysis (XRD) was carried out using an Ultima-IV X-ray diffractometer (Rigaku, Japan). The operating mode used was: 40 kV, 40 mA, copper anode, nickel filter, scan range 3–65°2θ, scan speed 3°2θ/min and step 0.02°2θ, fixed system of focusing slits. To speed up the survey and improve the quality of the experimental data, a new generation semiconductor detector, DTex/Ultra, was used: the scanning speed is 5°2θ/minute. The study of the composition of the sample was carried out using non-oriented preparations, which provides the maximum misorientation of particles. This

is necessary to obtain high-quality diffraction patterns for calculating the quantitative mineral composition (Krupskaya, Zakusin, 2019).

Diagnostics of the mineral composition were carried out by comparing the experimental and reference (from database PDF-2) diffraction patterns in the software package Jade 6.5 (MDI company). The quantitative determination of the mineral composition was carried out by the method of full-profile processing of X-ray pictures from non-oriented preparations (modified Rietveld method). The error in calculating quantitative grades by the Rietveld method is usually estimated at 2–3%. The determination error consists of the sum of the calculation errors for each phase and is given in mass percent. Meanwhile, for individual phases the determination error will differ and may range from 0.5 to 2–3%. The presence or absence of kaolinite was checked for by the presence of diagnostic absorption bands in the IR spectra of bentonites.

The method for calculating the content of clay and non-clay minerals in a mixture by the XRD method is generally recognized in global scientific community, as evidenced by the results of the international competition for quantitative analysis Reynolds Cup (www.clays.org; Omotoso et al., 2006) and was chosen as a reference, with the results of which all other calculations are compared.

*Quantitative determination of MMT content by thermogravimetric analysis (TG*)

The quantitative determination of the montmorillonite content was carried out in accordance with the method of F. Nieto (Nieto et al., 2008), based on the determination of the weight loss of bentonite samples saturated with ethylene glycol vapor. According to this technique, the most stable weight loss values are demonstrated by clay samples converted to the monocationic magnesium form. For this, natural samples are saturated twice with 1M $MgCl_2$ solution, followed by repeated washing to remove excess salts. The saturation with ethylene glycol (EG) is carried out at a temperature of 60°C for 3 days.

According to the authors of this technique (Nieto et al., 2008), the proposed method is inexpensive and easy to use. It can be used in addition to X-ray diffraction, including in the diagnosis of dioctahedral Al-smectite (montmorillonite) in soils. To obtain a quantitative relationship between weight loss and MMT content, the authors of the method prepared 8 artificial mixtures. By plotting the graphs of the dependence of weight loss in different temperature intervals, on the known value of the montmorillonite content, a conversion equation was derived for the interval of 100–450°C:

$$y = 3{,}96x - 4{,}05 \ (R2 = 0{,}96) \quad (1)$$

where, x is the weight loss of the sample (in mass %) in the temperature range from 100 to 450°C, and y is the montmorillonite content, in %.

The largest weight loss due to the desorption of $H_2O$, $CO_2$ and $CH_3$-CHO occurs up to a temperature of 300°C, after which the loss sharply decreases and practically ends at 450°C. For this reason, a limit of 450°C was chosen as the upper temperature limit. At this temperature, the desorption of $CO_2$ is almost completed, but the octahedral networks of aluminosilicates are still stable, since the loss of hydroxyls from the octahedral networks of most clay minerals lies in the temperature range of 500-700°C. Below 100°C, the weight loss corresponds to the loss of surface (atmospheric) moisture.

To stabilize the moisture values (Paterson, Swaffield, 1987) and standardize the experiment, the authors of this method proposed converting the MMT sample into a magnesium form and saturating it with EG vapor as much as possible.

TG analysis of the samples was performed on an EXSTAR TG/DTA 7300 (SII) instrument. The samples were heated in corundum crucibles at a constant rate of 10°C/min. To remove gases released during heating, the furnace space was purged with air dried by passing it through a column with silica gel at a volumetric air circulation rate of 100 ml/min. The weighed portion of the sample was 10–20 mg (accuracy up to 0.01 mg). During the analysis, the weight loss of the sample (TG curve) was determined simultaneously with the enthalpy change accompanying thermal reactions (DTG curve).

*Quantitative determination of MMT content by adsorption of rhodamine 6G and chrysoidine*

Determination of montmorillonite content by rhodamine adsorption method was carried out in accordance with GOST 28177-89 «Forming bentonite clays». The method is based on ion-exchange adsorption of fluorescent organic dyes, which causes coagulation of the clay particles. This technique is used at Russian iron-ore processing plants and foundries and does not require a preliminary conversion of MMT into a monocationic form.

This method is based on the adsorption of dye molecules on charged MMT surfaces. The cation of the dye chrysoidine has a higher molecular weight compared to the cation of rhodamine 6G and is more readily sorbed on the surface of montmorillonite, causing coagulation and coloring the resulting precipitate in red color. While the amount of chrysoidine cations is insufficient to fill all charged surfaces, the adsorption of rhodamine 6g cations occurs, in which case the tendency to adsorption is significantly lower. After the surface is completely filled with organic cations, the addition of a new portion of the dye mixture leads to an increase in the adsorption of chrysoidine and the displacement of rhodamine 6g cations, causing luminescence in the solution over the precipitate. Thus, the presence of weak luminescence of

the solution, simultaneously with the formation of the maximum volume of the precipitate, corresponds to the end point of the titration.

*Quantitative determination of MMT content by adsorption of methylene blue*

This technique is based on the determination of CEC in lumpy (natural, without additional processing) clay ($CEC_{raw}$) and a fine (<0.5 μm) fraction ($CEC_{100\%}$), the content of montmorillonite of which is close to 100%. The montmorillonite content in the rock is defined as the proportion of $CEC_{raw}$ over $CEC_{100\%}$.

Purification of bentonites and the preparation of a fine fraction (<0.5 μm) were carried out by centrifugation (Sigma 3-18K centrifuge, 18000g). The montmorillonite content in the fine fraction was controlled by XRD and was found to be >96% in all studied samples.

The method for determining CEC by the adsorption of the methylene blue (MB) dye is described both in Russian standards (GOST 21283-93) and in foreign literature (Kaufhold et al., 2002; Dormann, Kaufhold, 2009).

Due to the fact that the monovalent cationic dye is not able to completely displace the divalent cations of the exchange complex of montmorillonite under experimental conditions, in order to obtain adequate information, it is first necessary to convert the natural bentonite (and the fine fraction) into the monocationic sodium form, which is characterized by a greater lability of cations. This procedure also allows for a better selection of the clay fraction and increases its yield, which is a problem for calcium-magnesium varieties prone to aggregation of clay particles in suspension. Conversion to the monocationic form is carried out by repeated treatment of samples with 1M NaCl solution, followed by washing, to remove excess salt, in dialysis tubes. In order to minimize the contribution to CEC from the pH-dependent active centers located on the lateral hydroxylated surface of clay particles, MB adsorption is carried out in an acidic medium.

*Quantitative determination of MMT content by adsorption of triethylenetetramine copper (II) complex*

This technique is similar to the above described method for MB adsorption, except that copper (II) triethylenetetramine complex (Cu-trien) is used instead of methylene blue dye. Currently, this method is most popular in world practice, which is associated with the high accuracy of determining the CEC values due to the more complete replacement of bivalent exchangeable cations of montmorillonite (Lorenz et al., 1999, Dohrmann et al., 2012). The main advantages of this method include its simplicity and low time consumption, which is an important factor for use in production. As in the previous case, to estimate the MMT content, a finely dispersed fraction (<0.5 μm) was isolated from the preliminarily obtained monocationic $Na^+$ form of bentonite.

## Research results

*Mineral and chemical composition of studied bentonites*

Studies of the samples by X-ray diffraction showed that all the presented samples contain more than 70% montmorillonite (Table 1). Quartz and calcite are present in all samples as impurities. In addition, chlorite, feldspar and pyrite are present in the bentonite form 10th Khutor (10Kh) deposit and illite, kaolinite, feldspar in the sample from the Zyryanskoe (ZR) deposit. Bentonite from the Dash-Salahlinskoe (DS) deposit contains cristobalite and feldspar, and from the Dinozavrovoe (DIN) deposit – illite and pyrite. The obtained X-ray diffraction patterns of bulk samples are shown in Figure 1, the results of quantitative X-ray diffraction

| Deposit | Sample | MMT | Il | Chl | Kaol | Q | Cr | PSh | Kts | P |
|---|---|---|---|---|---|---|---|---|---|---|
| Dinozavrovoe | DIN | 73 | 1 | - | - | 22.5 | | - | 2.3 | 1.2 |
| Dash-Salahlinskoe | DS | 73.9 | - | - | - | 3.7 | 5 | 13.8 | 3.6 | - |
| Zyryanskoe | ZR | 74.4 | 0.9 | - | 2.6 | 19.4 | - | 0.6 | 2.1 | - |
| 10th Khutor | 10Kh | 73.0 | - | 1.2 | - | 14.2 | - | 8.6 | 3 | - |

*Table 1. Mineral composition of bentonite clay samples, wt.%. Note: MMT – montmorillonite, Il – illite, Chl – chlorite, Kaol – kaolinite, Q – quartz, Cr – cristobalite, PSh – feldspars (potassium feldspars and plagioclase), Kts – calcite, P – pyrite.*

| Sample | LOI | $Na_2O$ | MgO | $Al_2O_3$ | $SiO_2$ | $K_2O$ | CaO | $TiO_2$ | MnO | $Fe_2O_3$ | $P_2O_5$ | S |
|---|---|---|---|---|---|---|---|---|---|---|---|---|
| DIN | 8.00 | 1.50 | 3.81 | 16.71 | 61.15 | 0.14 | 1.43 | 0.70 | 0.16 | 6.35 | 0.02 | 0.04 |
| DS | 13.20 | 2.79 | 2.82 | 14.36 | 56.16 | 0.35 | 2.66 | 0.94 | 0.7 | 5.45 | 0.17 | 0.4 |
| ZR | 9.04 | 0.46 | 1.79 | 19.38 | 57.42 | 0.77 | 2.20 | 1.01 | 0.04 | 7.78 | 0.05 | 0.07 |
| 10Kh | 7.64 | 1.04 | 2.96 | 18.10 | 61.71 | 1.01 | 2.24 | 0.74 | 0.09 | 4.23 | 0.14 | 0.11 |

*Table 2. Chemical composition of rock-forming oxides, %. Note: LOI – loss on ignition.*

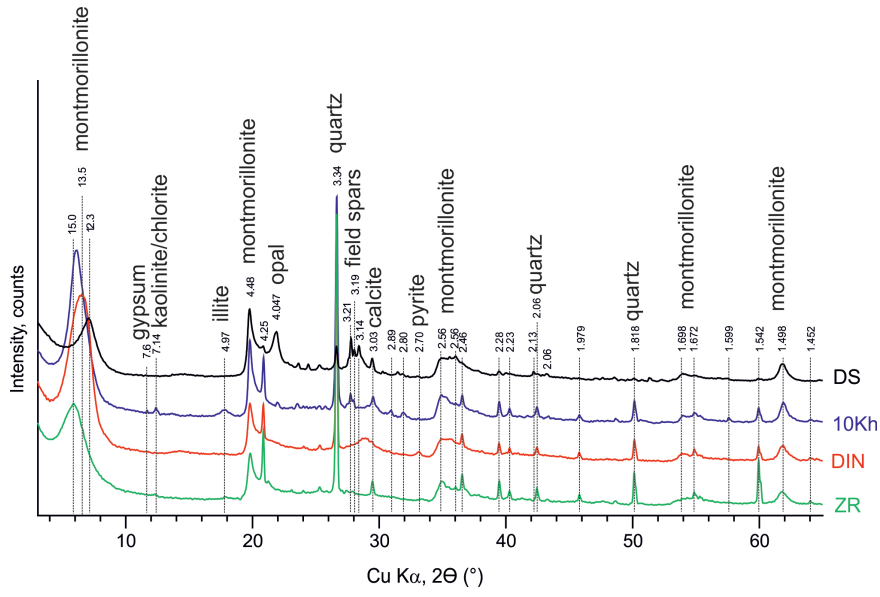


*Figure 1. X-ray diffraction patterns of non-oriented preparations of the studied samples of bentonite clays. Deposit names: DIN – Dinozavrovoe; DS – Dash-Salahlinskoe; ZR – Zyryanskoe; 10Kh – 10th Khutor. Interplanar spacings are given in angstroms.*

and chemical analyzes are presented in Tables 1 and 2, respectively. Montmorillonite was identified by a series of main diagnostic reflections corresponding to the following interplanar spacings (hkl): 12.3–15.0 Å (001), 4.97–5 Å (003), 4.48 Å (100), 2.56 Å (110), 1.69–1.7 Å (210), 1.492–1.504 Å (060).

In addition to calculating the montmorillonite content in bulk samples, this method was used to control the quality of the separated fractions <0.5 μm and monocationic forms.

*Determination of MMT content from thermal data*

Figure 2 shows the results of thermal analysis of clays prepared according to the above procedure. For all samples, the DTG curve shows two peaks in the temperature ranges 159–186 and 273–294°C. The first peak is due to the destruction of ethylene glycol (EG) molecules, the boiling point of which is 197°C. The second maximum is associated with the desorption of more tightly bound EG molecules fixed in the interlayer space.

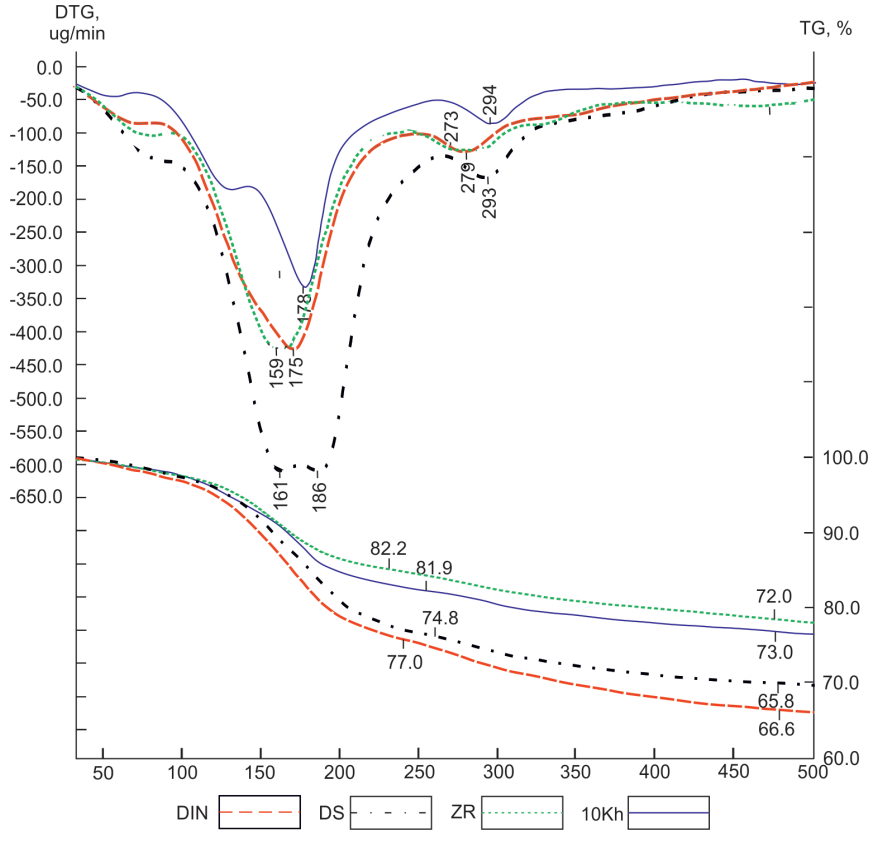


*Figure 2. Results of thermal analysis*

Calculated according to equation (1), the MMT content turned out to be overestimated for all studied samples (Table 3). The largest overestimation of the MMT content was obtained for DS and DIN samples, which is most likely associated with the peculiarities of the charge density distribution on the surface of montmorillonite particles in these samples, as well as with the possible presence of indistinguishable XRD of amorphous Fe, Si, and Al oxides, which can make contribution to a maximum at 250–300°C. The values of the montmorillonite content of more than 100% obtained for these samples indicate the unsuitability of this formula for calculating the MMT content in bentonite clays of other deposits.

It can be assumed that this technique could indeed be used to calculate the content of montmorillonite with the condition that the samples must have the same origin and structural features (layer charge, CEC, etc.). For example, if they are sampled from the same deposit or formed in specific facies settings. In that event, in each specific case, it is necessary to select the working temperature range and estimate the calculation formula anew.

The high convergence of the results of X-ray diffraction analysis and thermal analysis for 8 samples presented in the work of F. Nieto (Nieto et al., 2008) is due to the fact that the studied samples are artificially prepared mixtures based on the same smectite, for which the calculation formula really turned out to be true.

Thus, the main disadvantage of the method for determining the content of montmorillonite from the data of thermal analysis is the impossibility of using the same calculation formula for bentonite from different deposits. In addition, the use of the method requires a rather large amount of time.

It should be noted that in order to verify the correctness of the results obtained by different methods, it is necessary to compare them with XRD data in order to assess the presence of other minerals with high sorption properties, the purity of fine fractions, and to identify the structural features of montmorillonite that can affect the calculation results.

*Method for determination of MMT content by adsorption of rhodamine 6g and chrysoidine*

Based on the detailed description of the procedure given above, it follows that this method gives no distinction between the montmorillonite content and the CEC value. This situation, in fact, means that the intrinsic cation exchange capacity of the monomineral phase of montmorillonite is equal to 100 meq/100 g, which is not true in the overwhelming majority of cases. The second source of error is associated with the specifics of sample preparation. To disperse particles in an aqueous environment, a polyanionic inorganic polymer, sodium tripolyphosphate, is used as a peptizing agent, which itself can chemically interact with organic cations and also partially change their composition. In addition, the technique involves the use of $Na_2$-EDTA, which partially binds divalent cations, increasing the degree of ion exchange of organic dyes. Along with this, the technique involves the use of potassium hydroxide, which further complicates the interpretation of the results, since potassium is the strongest known coagulant of clay particles and has a very high adsorption capacity, which can compete with organic cations. All of these factors can make the interpretation of the results very difficult.

| Sample | **Method 1** | | **Method 2** | | **Method 3** | | **Method 4** | | | **Method 5** | | |
|---|---|---|---|---|---|---|---|---|---|---|---|---|
| | In lump sample, % | Faction, % | Weight loss in the range of 100-450, % | MMT content, % | Dye volume, ml | MMT content, % | CEC, mg-eq /100g | $CEC_{(100\%)}$, mg-eq/100g | MMT content, % | CEC, mg-eq/100g | $CEC_{(100\%)}$, mg-eq/100g | MMT content, % |
| DIN | **73.0** | 96 | 28.8 | **110.0** | 3.6 | **89.7** | 93.8 | 110.5 | **84.9** | 88.1 | 106.3 | **82.9** |
| DS | **73.9** | 96 | 28.9 | **110.0** | 3.8 | **90.9** | 87.7 | 110.0 | **79.7** | 80.4 | 99.3 | **81.0** |
| ZR | **74.4** | 96 | 23.0 | **87.0** | 2.2 | **52.3** | 64.1 | 87.5 | **73.3** | 55.1 | 89.9 | **61.3** |
| 10Kh | **73.0** | 96 | 21.1 | **79.6** | 3.0 | **72.5** | 63.1 | 89.0 | **70.9** | 73.5 | 101.9 | **72.1** |

*Table 3. The results of comparing the determination of the content of montmorillonite in bentonite clays by different methods. Methods: 1 – Measurement of the montmorillonite content according to the results of the XRD by the Rietveld method; 2 – Determination of MMT content based on the results of thermal analysis of samples after saturation with ethylene glycol (Nieto et al., 2008); 3 – Determination of MMT content by adsorption of rhodamine 6G and chrysoidine dye – GOST 28177-89; 4 – Determination of MMT content by adsorption of MB (Kaufhold et al., 2002; Dormann, Kaufhold, 2009). 5 – Determination of the MMT content by adsorption of Cu-trien (Lorenz et al., 1999., Dohrmann et al., 2012);*

The experiments carried out showed an overestimated content of montmorillonite in the DIN and DS samples, namely 89 and 90%, respectively, compared with 73 and 73.9% (Table 1). The higher the particle charge and the proportion of sodium cations in the exchange complex, the stronger the super-equivalent adsorption of organic dyes. On the other hand, the ZR sample showed underestimated results in comparison with XRD, which is apparently associated with a significant content of calcium and magnesium cations in the MMT exchange complex, a low CEC value, and also with the presence of films of iron oxides and hydroxides on the particle surface. The outer surfaces of particles containing ferrous films can act as active sorption centers and reduce the access of large organic cations to the interlayer space and the surface of MMT crystallites. The best agreement between the results of determining the MMT content by this method and the XRD data is observed for sample 10Kh (Table 3).

In addition to the above disadvantages, it is worth noting the difficulty of determining the equivalence point when titrating samples, which, as practice shows, has a rather strong effect on the measurement results.

*Determination of MMT content by adsorption of methylene blue*

The methylene blue cation is easily sorbed on the surface and in the interlayer of smectite minerals. At the initial stage, MB cations are adsorbed on the outer surfaces of the clay particles, and then these organic dye molecules begin to replace the cations in the interlayer space of montmorillonite. The end of the substitution reaction for interlayer cations and the appearance of free MB cations in the solution are considered to be the equivalence point in the titration. In addition to the exchange reaction, MB cations can be adsorbed on the surface of particles in a super-equivalent manner, due to polar and hydrophobic interactions, and also due to the high tendency of dye molecules to aggregate.

It was found that in the presence of divalent cations existing in the interlayer space, the adsorption of the MB dye decreases. The amount of adsorption of MB will depend on certain experimental conditions, such as the concentration of the dye and the duration of adsorption. On the other hand, for alkaline varieties of bentonites and finely dispersed fractions, the CEC values can be significantly overestimated, which is more typical for minerals with a high charge density. Studies of the mechanism of adsorption of MG showed that for a correct diagnosis of smectite, it is necessary to know the dependence of the CEC value on pH to take into account the so-called 'variable charge' associated with the adsorption of cations on hydroxyl groups (Bujda'k, Komadel, 1997; Lagaly, 1993).

The conducted experiments showed a high convergence of the results with the XRD data for alkaline earth bentonites (ZR, 10Kh), with an average error of 2-3%. However, for the samples of alkaline bentonites (DIN, DS) the values turned out to be overestimated.

Among the negative factors, it's worth mentionning the need for preliminary conversion of lumpy clay and fine fraction into sodium form, which significantly complicates the process of sample preparation.

*Determination of MMT content by adsorption of triethylenetetramine copper complex*

As noted above, the method for determining CEC by adsorption of Cu-trien differs from other methods by a high ability to replace divalent metal cations in the interlayer space of montmorillonite due to the fact that the copper complex has a high selectivity with respect to negatively charged adsorption sites on the basal surfaces of MMT. This method does not imply the need to convert the samples into the monocationic sodium form; however, the inaccuracy in assessing the MMT content may be associated with incorrect fractionation of the samples. As in the case of the adsorption technique using the MB dye, the MMT content is estimated by comparing the CEC values of the bulk sample and the fine dispersed fraction. It is necessary that the fraction be representative, and consist of practically pure montmorillonite. Therefore, for the preparation of the fraction, just as in the case with MB, it is necessary to convert the sample into the monocationic form. Other disadvantages of the method are associated with obtaining inaccurate CEC values for initial samples that contain water-soluble salts, gypsum, and carbonates. These inaccuracies can be associated both with the reactions of copper cations with carbonates and specific adsorption of amine, and with a change in the pH of the samples in the presence of carbonates and hydroxides.

These problems can be eliminated using fairly simple techniques described in (Dormann, Kaufhold, 2009) and avoiding the influence of calcite and other carbonates on the determined CEC value. These laboratory techniques include the method of using a fivefold increase in the concentration of Cu-trien complex, which makes it possible to reduce the solubility of calcium carbonate by reducing the amount of water, as well as the method for determining the CEC of bentonites after saturation of the titrated dispersion with calcite. As shown in (Kaufhold et al., 2013), these approaches are most convenient to use when used in combination.

The results of determining the CEC and calculating the MMT content are presented in Table 3. As in the case with the determination of the MMT content by the adsorption of MB, the results of measurements on the sample from the 10th Khutor deposit showed a high convergence with the results of quantitative XRD, while the values of measurements on alkaline bentonites are higher. In the case of the Zyryanskoe

deposit sample, the MMT content determined by copper adsorption is somewhat underestimated. One of the reasons for this discrepancy may be specific reactions of tritylenetetramine with with iron-containing active centers on the surfaces. Indeed, this sample is characterized by a high iron content (up to 10–11% in terms of iron (III) oxide), and iron cations in the form of hydroxo complexes and oxide nanoparticles are present on the surface of montmorillonite and are capable of specific reactions with triethylenetetramine, which changes the equilibrium in the system. In addition, the presence of oxide/hydroxide shells can hinder the penetration of large complex copper cations to certain surface areas in the interlayer space of montmorillonite.

**Discussion**

The studies carried out make it possible to assess the capabilities of various adsorption methods in assessing the content of montmorillonite and to identify certain difficulties in their use.

The general problem of methods using cationic dyes is associated with the super-equivalent adsorption of the dyes on areas of the surface with a high charge due to the high tendency of dyes to aggregate, as well as to complication of the ion exchange reaction for montmorillonites containing polyvalent cations in the interlayer space and on the surface of crystallites (magnesium, calcium, iron, etc.). In most cases, this problem can be solved by preliminary converting the samples into sodium form, which is a rather laborious task.

However, as shown by the results of the present study, even after transferring the samples to the sodium monocationic form, alkaline bentonites demonstrate overestimated results in comparison with the XRD data. The Cu-trien adsorption techniques used in this work have good theoretical validity and are widely used in the scientific community. It can be assumed that such a significant difference in the results may be associated with the size of montmorillonite particles and texture features (the number and volume of micro/mesopores). As shown in previous works (Krupskaya et al., 2017), alkaline bentonite of the Tagansky deposit is characterized by the presence of natural nanosized particles of montmorillonite, which have low values of coherent scattering regions (1–2 nm versus 3–4 nm for ordinary montmorillonites). Such nano-sized phases can practically not contribute to the intensity of diffraction maxima, as a result of which somewhat underestimated values of the MMT content can be obtained when using XRD. At the same time, the presence of such nanosized particles will lead to the over-adsorption of MB and Cu-trien and, as a consequence, to an overestimation of the MMT content.

In addition to the capacity and composition of the exchange complex, an important role is played by the presence of mineral impurities with a high sorption capacity, for example, zeolites, carbonates, amorphous phases and other clay minerals (vermiculite, kaolinite, halloysite, palygorskite, mixed-layer minerals, etc.), which can distort the results.

Thus, despite the apparent self-sufficiency of the considered methods, there is a need for additional studies and manipulations with samples, for example, the use of XRD, infrared, Mössbauer, atomic adsorption spectroscopy, etc. to analyze the composition and structure of montmorillonite, the presence of impurity phases, and control the quality of the fine fraction.

In view of the need to complicate traditional adsorption techniques in order to obtain adequate results on the MMT content, in some cases, there should be a clear understanding of the required accuracy of determining the MMT content and the expediency of such calculations. Thus, the chosen method for the determination of the content of montmorillonite is of great importance in carrying out research work, in geological exploration, as well as in some innovative applied areas of using bentonite clay, where the properties of the product and the amount of added chemical reagents depend on the content of montmorillonite.

When using bentonite in classical industrial areas such as metallurgy, foundry, drilling, etc., in most cases, the determining factor is the properties of the clay, and not the content of montmorillonite, because there is often no direct correlation between them (provided that the content is sufficiently high, over 50–60%). These properties are understood as specific physical indicators, the value of which determines the quality of the final product in certain technological processes and prescribed in the standards of this industry. For example, for pelleting iron ore the main properties of clay that affect the quality of the pellets are its swelling index, moisture content, and thermal stability. In the production of sandy-clay molds in the foundry industry, the main factors are the strength properties and the thermal stability of bentonite. In drilling it is rheological properties.

The presence of restrictions on the content of montmorillonite in industry standards does not always give a real idea of the quality of the clay, which is associated with the peculiarities of the composition and properties of a particular bentonite, which in turn are primarily determined by the structural and textural characteristics of montmorillonite, and to a lesser extent – by its content. An example is the international standard of the American Petroleum Institute (API, Specification 13A), which specifies the properties of the raw material, and does not specify content of montmorillonite.

As a result, the indicator of the content of montmorillonite is a reason for speculation, both on the part of the consumer and the manufacturer of bentonite

products. On the other hand, in a number of applications for bentonite, the content of montmorillonite is one of the key indicators, for example, as in the case of the development and creation of engineering safety barriers for the disposal of radioactive waste, where the content of montmorillonite is a limiting criterion for the use of clays in various disposal sites (Krupskaya et al., 2018; 2020; Kaufhold, Dohrmann, 2016; Ahonen et al, 2008).

**Conclusion**

The studies carried out illustrate the possibilities and limitations of various methods for determining the content of MMT, used in both research and industrial sectors. Comparative analysis of the results showed good agreement between the results of X-ray diffraction analysis with the data on the adsorption of methylene blue dye in determining the content of montmorillonite in alkaline earth varieties of bentonite. The error was less than 3%. The difference in the results of the analysis of alkaline bentonites, apparently, is associated with the presence of nanosized particles of montmorillonite, which leads to the over-adsorption of dyes in the case of MB and, at the same time, can underestimate the values according to the quantitative XRD data. A similar situation is observed when using the method based on the adsorption of the triethylenetetramine complex of copper (Cu-trien); however, in this case, the measurement results were influenced by the presence of films of iron oxides and hydroxides on the surface of montmorillonite particles in the Zyryanskoe bentonite sample, which led to a decrease in the MMT content in that specified bentonite. It was also revealed that in order to more completely replace the exchangeable cations in the montmorillonite interlayer, it is necessary to carry out a preliminary conversion of both lumpy clay and fine fractions into a sodium form, which significantly complicates and lengthens the study process.

The measured montmorillonite content according to the industry standard by the method of adsorption of the rhodamine 6G and chrysoidine dyes showed the greatest variations relative to the reference values according to the XRD data. At the same time, it was noted that for alkaline bentonites, there is a significant over-adsorption of the dye, leading to overestimated results (by 8–10%). On the other hand, the alkaline-earth sample of the Zyryanskoe bentonite showed underestimated results, which is probably due to an increase of the tetrahedral charge and other structural features that would require a separate study. Measurements of the montmorillonite content in the bentonites of the 10$^{th}$ Khutor deposit by all methods showed the most comparable results with the XRD data.

The content of montmorillonite, determined by the method of thermal analysis, turned out to be overestimated in comparison with the reference values for all samples of bentonite, which is primarily due to the impossibility of using the same calculation formula for bentonites of different genesis and with different structural features. The measurement error by this method was 17–30%. In addition, this method requires a significant amount of time spent on sample preparation and sampling and can hardly be recommended for mass use.

In general, when using the considered methods for the determination of montmorillonite associated with the adsorption of organic substances and complex cations, the sorption properties of a particular montmorillonite, the magnitude and distribution of the layer charge, the composition of the absorbed complex, micro- and mesoporosity parameters, and other structural and textural features of montmorillonite play an important role, and are directly related to the geological conditions of formation. Also, the results are significantly influenced by impurities of other minerals with a high sorption capacity, such as, zeolite, carbonates, other clay minerals (vermiculite, kaolinite, halloysite, palygorskite, etc.), as well as amorphous phases.

Thus, it can be concluded that determining the content of montmorillonite is not a trivial task. Each method has its own characteristics and limitations, which indicates the need for a clear understanding of the goals and objectives of each specific study. Of all the methods available to researchers for determining the content of montmorillonite, the most accurate is the X-ray diffraction method based on information on the individual crystal-chemical structure of mineral phases.

**Acknowledgments**

*Studies on the quantitative content of montmorillonite in bentonite clays were supported by the Russian Science Foundation (grant 16-17-10270), experiments on the adsorption of organic dyes were supported by the Russian Foundation for Basic Research (grant no. 18-29-12115).*

*The authors are grateful to S.A. Garanina (Lomonosov Moscow State University), I.S. Morozov (IGEM RAS) for their help at various stages of preparation and writing of this work.*

**References**

Ahonen L., Korkeakoski P., Tiljander M., Kivikoski H., Laaksonen R. (2008). Quality Assurance of the Bentonite Material. Posiva Working Report 2008-33. Eurajoki, Finland, 126 p.

Belousov P.E., Krupskaya V.V. (2019). Bentonite clays of Russia and neighboring countries. *Georesources*, 21(3), pp. 79-90. https://doi.org/10.18599/grs.2019.3.79-90

Bujda´k, J., Komadel, P. (1997). Interaction of Methylene-blue with reduced charge montmorillonite. *J. Phys. Chem.*, B 101, pp. 9065–9068. https://doi.org/10.1021/jp9718515

Dormann R., Kaufhold S. (2009). Three new, quick CEC methods for determining the amounts of exchangeable cations in calcareous clays. *Clays and Clay Minerals*, 57, pp. 338–352. https://doi.org/10.1346/CCMN.2009.0570306

Dohrmann R., Genske D., Karnland O., Kaufhold S.at al. (2012). Interlaboratory CEC and exchangeable cation study of bentonite buffer

materials: I. Cu(II)-triethylenetetramine mthod. *Clays and Clay Minerals*, 60(2), pp. 162–175. https://doi.org/10.1346/CCMN.2012.0600206

Drits V.A., Kossovskaya A.G. (1990). Clay minerals: smectites, mixed-layer formations. Moscow: Nauka, 214 p. (In Russ.)

Guggenheim S., Adams J.M., Bain D.C., Bergaya F., Brigatti M.F., Drits V.A., Formoso M.L.L., Galan E., Kogure T. and Stanjek H. (2006). Summary of recommendations of Nomenclature Committees relevant to clay mineralogy: Report of the Association Internationale Pour L'etude des Argiles (AIPEA) nomenclature committee for 2006. *Clays and Clay Minerals*, 54(6), pp. 761–772. https://doi.org/10.1346/CCMN.2006.0540610

Holtzer M., Grabowska B., Bobrowski A., Żymankowska-Kumon S. (2009). Methods of the montmorillonite content determination in foundry bentonites. *Archives of foundry engineering*, 9(4), pp. 69-72.

Holtzer M., Bobrowski A, Grabowska B. (2011). Montmorillonite: a comparison of methods for its determination in foundry bentonites. *Metalurgija*, 50(2), pp. 119-122.

Kahr G. (1998). Methoden zur Bestimmung des Smektitgehaltesvon Bentoniten. In: Henning, K.-H., Kasbohm, J. (Eds.), Be-richte der Deutschen Ton- und Tonmineralgruppe (DTTG), Greifswald, 6, pp. 163–172.

Kaufhold S., Dohrmann R., Ufer K., Meyer F.M. (2002). Comparison of methods for the quantification of montmorillonite in bentonites. *Applied Clay Science*, 22, pp. 145–151. https://doi.org/10.1016/S0169-1317(02)00131-X

Kaufhold S., Emmerich K., Dormann R., Steudel A., Ufer K. (2013). Comparison of methods for distinguishing sodium carbonate activated from natural sodium bentonites. *Applied Clay Sci*., 86, pp. 23–37. https://doi.org/10.1016/j.clay.2013.09.014

Kaufhold S., Dohrmann R. (2016). Distinguishing between more and less suitable bentonites for storage of high-level radioactive waste. *eClay Minerals*, 51, 289–302. https://doi.org/10.1180/claymin.2016.051.2.14

Krupskaya V.V., Biryukov D.V., Belousov P.E., Lekhov V.A., Romanchuk A.Yu., Kalmykov S.N. (2018). The use of natural clay materials to increase the nuclear and radiation safety level of nuclear legacy facilities. *Radioaktivnye otkhody = Radioactive Waste*, 2(3), pp. 30–43. (In Russ.)

Krupskaya V.V., Zakusin S.V. (2019). Determination of the mineral composition of soils by x-ray diffractometry. In a book: *Laboratory Workshop on Soil Science*: A Training Manual. Ed. V.A. Koroleva, V.N. Shirokova and V.V. Shanina. Moscow: KDU, Dobrosvet, pp. 14–46.

Krupskaya V.V., Zakusin S.V., Dorzhieva O.V., Zhukhlistov A.P., Belousov P.E., Tyupina E.A., Timofeeva M.cN. (2017). Experimental study of montmorillonite structure and transformation of its properties under treatment with inorganic acid solutions. *Minerals*, 7(4), 49. https://doi.org/10.3390/min7040049

Krupskaya V.V., Zakusin S.V., Lekhov V.A., Dorzhieva O.V., Belousov P.E., Tyupina E.A. (2020). Buffer properties of bentonite barrier systems for radioactive waste isolation in geological repository in the Nizhnekansky massif. *Radioaktivnye otkhody = Radioactive Waste*, 1, pp. 35–55. DOI: 10.25283/2587-9707-2020-1-35-55

Lagaly G. (1993). Layer charge determination by alkylammonium ions. In: Mermut, A.R. (Ed.), CMS Workshop Lectures. Layer Charge Characteristics of 2:1 Silicate Clay Minerals, vol. 6. The Clay Mineral Society, Boulder, CO. https://doi.org/10.1346/CMS-WLS-6.1

Lorenz P., Meier L. and Kahr G. (1999). Determination of the cation exchange capacity (CEC) of clays minerals using the complexes of copper (II) ion with triethylenetetramine and tetraethylenepentamine. *Clays and Clay Minerals*, 47(3), pp. 386–388. https://doi.org/10.1346/CCMN.1999.0470315

Motoso Oladipo & McCarty, Douglas & Hillier, Stephen & Kleeberg, Reinhard. (2006). Some successful approaches to quantitative mineral analysis as revealed by the 3rd Reynolds Cup contest. *Clays and Clay Minerals*, 54. http://dx.doi.org/10.1346/CCMN.2006.0540609

Nieto F., Abad I., Azañón J.M. (2008). Smectite quantification in sediments and soils by thermogravimetric analyses. *Applied Clay Science*, 38(3–4), pp. 288–296. https://doi.org/10.1016/j.clay.2007.04.001

Omotoso O., McCarty D.K., Kleeberg R. and Hillier S. (2006). Some successful approaches to quantitative mineral analysis as revealed by the 3rd Reynolds cup contest. *Clays and Clay Minerals,* 54(6), 748–760. https://doi.org/10.1346/CCMN.2006.0540609

Paterson, E., Swaffield, R. (1987). Thermal analysis. In: Wilson, M.J. (Ed.), A Handbook of Determinative Methods in Clay Mineralogy. Blackie and Sons, Ltd., Glasgow, pp. 99–132.

Srodon J., Drits V., Mccarty D., Hsieh J., Eberl D. (2001). Quantitative X-ray diffraction analysis of clay-bearing rocks from random preparations. *Clays and Clay Minerals*, 49, pp. 514–528. https://doi.org/10.1346/CCMN.2001.0490604

Zhou X., Liu D. Bu H, Deng L., Liu H., Yuan P., Du P., Song H. (2018). XRD-based quantitative analysis of clay minerals using reference intensity ratios, mineral intensity factors, Rietveld, and full pattern summation methods: A critical review. *Solid Earth Sciences*, 3(1), pp. 16–29. https://doi.org/10.1016/j.sesci.2017.12.002

## About the Authors

*Petr E. Belousov* – Cand. Sci. (Geology and Mineralogy), Senior Researcher, Institute of Ore Geology, Petrography, Mineralogy and Geochemistry of the Russian Academy of Science

35 Staromonetny Lane, Moscow, 119017, Russian Federation

*Boris V. Pokidko* – Cand. Sci. (Chemistry), Associate Professor, Institute of Fine Chemical Technologies, MIREA – Russian Technological University

86 Vernadsky Ave., Moscow, 119571, Russian Federation

*Sergey V. Zakusin* – Junior Researcher, Institute of Ore Geology, Petrography, Mineralogy and Geochemistry of the Russian Academy of Science; Leading Engineer, Lomonosov Moscow State University

35 Staromonetny Lane, Moscow, 119017, Russian Federation

*Victoria V. Krupskaya* – Cand. Sci. (Geology and Mineralogy), Senior Researcher, Institute of Ore Geology, Petrography, Mineralogy and Geochemistry of the Russian Academy of Science; Senior Researcher, Lomonosov Moscow State University

35 Staromonetny Lane, Moscow, 119017, Russian Federation

*Manuscript received 20 February 2020;*
*Accepted 18 July 2020; Published 30 September 2020*

ORIGINAL ARTICLE

**DOI**: https://doi.org/10.18599/grs.2020.3.48-54

Russian Original 2020. Vol. 22. Is. 3. Pp. 48–54

# Vosnesensky Cu-porphyry deposit (Southern Urals): formation conditions, trace elements, sulfur isotopes and fluid sources

*S.E. Znamensky[1*], N.N. Ankusheva[2], D.A. Artemiev[2]*

[1]*Institute of Geology of the Ufa Federal Research Centre of the Russian Academy of Sciences, Ufa, Russian Federation*

[2]*Institute of Mineralogy of the South Urals Federal Research Center of Mineralogy and Geoecology of the Urals Branch of the Russian Academy of Sciences, Miass, Russian Federation*

**Abstract**. The paper shows new fluid inclusion and isotopic-geochemical data for minerals from sulphide-carbonate-quartz veins of Vosnesensky Cu-porphyry deposit. Fluid inclusions were analyzed by means Linkam TMS-600 cryostage equipped with Olympus BX 51 optical microscope; trace element amounts were performed used Agilent 7700x and ELAN 9000 mass-spectrometers; sulphur isotopic composition was analyzed on DeltaPLUS Advantage mass-spectrometer. We determined that fluid inclusions in quartz were homogenized between 215 and 315ºC, and in latest calcite, they are 230–280ºC. Fluids are K-Na water chloride with salinity of 3–12 wt % NaCl-eq. Quartz contain high amounts of Al (184–5180 ppm), K (20.1–1040 ppm), Na (30.2–1570 ppm) and Ti (38.4–193 ppm). The REE distribution spectra of pyrite are characterized by light lanthanides accumulation (LaN/YbN = 3.6–6.44), and negative of Ce anomalies (0.7–0.92) and Eu (0.78–0.99). The Y/Ho ratio in pyrite varies from 27.6 up to 36.8. The $\delta^{34}S$ values in pyrite were –1.01…0.8 ‰, in chalcopyrite – 0.9 ‰. The data testify the Cu-porphyry mineralization of Vosnesensky deposit was formed due to magmatic acid high-aluminous K-Na chloride fluid enriched with light REE in mesothermal environment. We identified the geochemical markers of interaction between fluid and host rocks.

**Keywords**: Southern Urals, Cu-porphyry deposit, fluid inclusions, trace elements, LA-ICP-MS, sulphur isotopic composition

**Recommended citation**: Znamensky S.E., Ankusheva N.N., Artemiev D.A. (2020). Vosnesensky Cu-porphyry deposit (Southern Urals): formation conditions, trace elements, sulfur isotopes and fluid sources. *Georesursy = Georesources*, 22(3), pp. 48–54. DOI: https://doi.org/10.18599/grs.2020.3.48-54

## Introduction

The Vosnesensky Cu-porphyry deposit is located in the Main Ural Fault zone in the Southern Urals. Cu-porphyry mineralization, which until recently was considered atypical for the Urals, is beginning to acquire more and more economic importance. In recent years, several large Cu-porphyry deposits have been discovered only in the Southern Urals, some of which are already being mined or prepared for exploitation (Mikheevsky, Severo-Tominsky, etc.). At the same time, the degree of knowledge of the formation conditions and genetic characteristics of the porphyry family in the Urals remains insufficient. This also applies to the Vosnesensky deposit, which by many researchers belongs to the reference Cu-porphyry objects associated with island arc diorite magmatism (Grabezhev, 2009; Seravkin et al., 2011). Thanks to the works of V.B. Shishakov et al. (Shishakov et al., 1988), A.I. Grabezhev and E.A. Belgorodsky (Grabezhev, Belgorodsky, 1992), A.M. Kosarev et al. (Kosarev et al., 2014), S.E. Znamensky et al. (Znamensky et al., 2019), the structure, petrological and geochemical characteristics of the ore-hosting rocks, the structure and composition of the near-ore aureole of the deposit were studied. In order to clarify the conditions for the Cu-porphyry mineralization formation and the nature of the mineral-forming fluid, for the first time we carried out thermobarogeochemical studies, determined the concentrations of trace elements and isotopic ratios of S in ore minerals.

## Geological background

The Vosnesensky deposit is located at the northern end of the massif of the same name, in the structure of which hornblende gabbro-diorites, diorites and, in some places, granodiorites (Figure 1). The U-Pb age of zircons from the diorites of the massif is 412±3 Ma (Kosarev et al., 2014). The massif occurs in serpentinite melange containing blocks of serpentinite-clastic breccias, pyroxenites, diabases, basalts and silica of unknown age, as well as Lower Devonian organogenic limestones.

Stringer sulfide-carbonate-quartz mineralization (Figure 2) is spatially closely related to dikes of quartz-

*Corresponding author: Sergey E. Znamensky
*E-mail: Znamensky_Sergey@mail.ru*

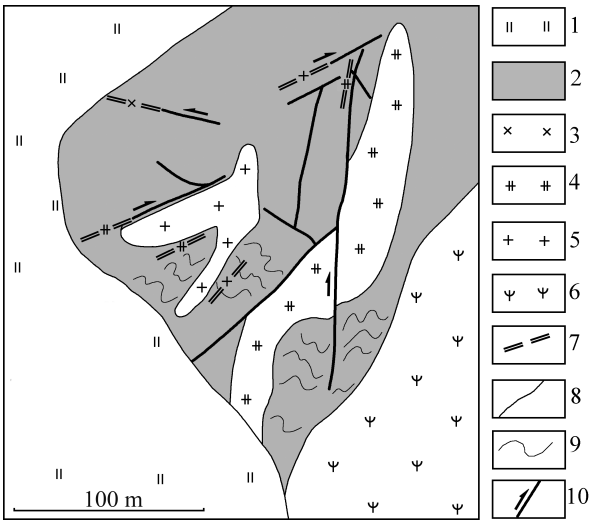


*Fig. 1. Geological and structural scheme of the Vosnesensky deposit (Znamensky et al., 2019). 1 – Quaternary sediments; 2 – hornblende gabbro-diorites, diorites and granodiorites of the Vosnesensky massif; 3–5 – dike series: 3 – diorite-porphyrites, 4 – granodiorite-porphyry, 5 – plagiogranite-porphyry, 6 – serpentinite, 7 – dikes (shown outside the scale); 8 – geological boundaries; 9 – banding in the dioritoids of the Vosnesensky massif; 10 – magma-ore-controlling faults (arrows indicate the direction of displacement of the wings).*


*Fig. 2. Stringer pyrite-chalcopyrite-carbonate-quartz ore mineral*

bearing diorite-porphyrites, granodiorite-porphyry, and plagiogranite-porphyry (Znamensky et al., 2019). All types of granitoids are characterized by porphyry precipitates of plagioclase and hornblende. In the host rocks of the Vosnesensky massif, the intensity of mineralization decreases. The placement of dikes is controlled by faults of near-meridional, northwestern and northeastern striking, forming a zone of right strike slip within the massif. Ore-hosting granitoids belong to the island arc calc-alkaline magmatites of normal alkalinity. Geochemically, they are close to the rocks of the Vosnesensky massif and, apparently, represent its late "porphyry" phase (Znamensky et al., 2019).

Pyrite and chalcopyrite are the main ore minerals in stringer sulfide-carbonate-quartz ores. Sphalerite, pyrrhotite, and molybdenite are found sporadically. According to V.B. Shishakov et al. (Shishakov et al., 1988), molybdenite is present in the form of scattered dusty in rare quartz veins and only in some cases forms single radial-radiant aggregates 0.3–1.0 mm in size in these veinlets. Molybdenite mineralization has no practical value. The total content of sulfides in the total mass of ore usually does not exceed 2–3%. According to its optical properties and thermal analysis data, carbonate in ores is represented by calcite. Near-ore metasomatites have sericite-quartz or sericite-quartz-chlorite composition, often with an admixture of carbonate. The metasomatites of individual dikes contain biotite and potassium feldspar in association with magnetite. At a distance from the ore halo, the rocks of the Vosnesensky massif underwent propylite alteration of the chlorite-epidote and actinolite-epidote facies.

## Analytical methods and results

### Fluid inclusions

Fluid inclusions in quartz and later calcite of stockwork ores were studied. The studies were carried out in the laboratory of thermobarogeochemistry of the South Ural State University (Miass, analyst N.N. Ankusheva). Thermometric measurements were carried out in a TMS-600 cryostage (Linkam) with LinkSystem 32 DV-NC software and an Olympus BX51 optical microscope. The interpretation of the eutectic temperatures of fluids in inclusions was carried out using the work (Davis et al., 1990). The salinities of fluids in inclusions were determined from the final melting temperatures of ice in inclusions according to (Bodnar, Vityk 1994). The homogenization temperatures of the inclusions are taken as the minimum temperatures of mineral formation (Roedder, 1984). The processing of the results was performed using the Statistica 12 program. The results are shown for 140 inclusions.

Quartz in ore veins forms large grains. The mineral is translucent to milky white, medium-grained. It contains syngenetic two-phase inclusions 10–15 μm in size (Figure 3a, 2). Gas vacuoles occupy up to 15–20% of their volume. The inclusions have an oval, angular shape, sometimes with small processes and/or with elements of crystallographic facets and are evenly distributed, occur both singly and in groups of 2–3 inclusions.

For inclusions, eutectic temperatures equal to –21 ... –24°C and temperatures of the end of ice melting – –8.3 ... –3.7°C were obtained. These data correspond to a chloride fluid containing K and Na ions with a concentration of 4.8–12 wt. % NaCl-eq. with a mode of 8–9 wt. % (Figure 3b). Homogenization temperatures (into liquid) were 215–315°C with a polymodal distribution of values (Figure 3c).

Calcite forms semitransparent grains with weak birefringence and cryptocrystalline aggregates and veinlets cutting through quartz. It also analyzed

syngenetic two-phase inclusions (Figure 3a, 1). They are 8–15 μm in size, isometric or sinuous in shape, are located singly, gas vacuoles in them are medium-sized, occupy about 15% of the inclusion volume.

The eutectic temperatures of solutions in inclusions, varying from –21 to –23°C, indicate the content of Na and K chlorides in the fluid. Salt concentrations, according to ice melting points ($T_{m.}$ = –4 ... –2°C), are 3–10 wt. % NaCl-eq. with a bimodal distribution of values and unexpressed modes of 3–4 and 7–8 wt. % (Figure 3b). The temperatures of homogenization into the liquid phase were 230–280°C with peaks at 240–250 and 260–270°C (Figure 3c).

The values of the homogenization temperatures and fluid salinity in inclusions in both quartz and calcite are characterized by a weak positive correlation (Figure 3d). Most inclusions in quartz and calcite are characterized by similar parameters and salinity, but more highly concentrated inclusions in quartz and low-salinity inclusions in calcite are distinguished. This may indicate the deposition of both minerals as a result of the evolution (cooling) of a fluid of the same composition and genesis.

In calcite and quartz, secondary two-phase inclusions with sizes of the first micrometers, tracing cracks in minerals, were also studied (Figure 3a). Salt concentrations of 1.5–1.9 wt.% were obtained for them. % NaCl-eq. ($T_{m.}$ = –0.9 ... –1.1°C) and homogenization temperatures (into liquid) equal to 110–120°C (Figure 3a). In addition, a large number of single-phase inclusions with the size of the first micrometers, located around two-phase syngenetic inclusions, are recorded.

## Trace elements in quartz

The concentrations of trace elements in quartz were determined by the method of laser ablation with inductively coupled plasma on an Agilent 7700x mass spectrometer with the MassHunter software package and a New Wave Research UP-213 laser sampler at the Institute of Mineralogy of the SU FRC MG UB RAS (Miass, analyst D.A. Artemiev).

The main trace elements in quartz are: Al (184–5180 ppm), K (20.1–1040 ppm), Na (30.2–1570 ppm), and Ti (38.4–193 ppm) (Table 1), which are most often included in its structure and depend on the conditions of formation. Li, Mg, P, Ca, Sc, and Fe are also found in high concentrations. The Al content in the quartz lattice, which depends on the pH of the fluid, varies within the range 184–750 ppm (on average, 440 ppm). In some cases, an increase in its content to 5180 ppm is noted, which, along with increased concentrations of Na, K, and Ca, indicates that feldspar microinclusions (points B-9-10 and B-9-11) have entered the ablation area. The Ti content is in the range 38.4–193 ppm (121 ppm on average) and depends on the temperatures of quartz formation. Lithium (1.2–7 ppm), K (20.1–212 ppm), Mg (4.4–49 ppm), and Na (30.2–174 ppm) can enter in small amounts in the crystal lattice of quartz, but usually, their increased concentrations are associated with fluid inclusions containing chlorides in the liquid phase. So, at point B-9-7, the sodium content differs sharply from the neighboring points, due to inclusions in the ablation zone. The Ca content varies within the range of 47.7–108 ppm; higher concentrations may be associated with microinclusions of calcite and feldspars in quartz veins (points B-9-10 and B-9-11). Normal Fe concentrations for the Vosnesensky quartz deposit are in the range of 3.3–10.9 ppm (on average, 5.4 ppm). Higher grades, up to 67 ppm, are likely associated with microinclusions of carbonates (point B-9-8) and feldspars (points B-9-10 and B-9-11). The contents of P and Sc are homogeneous, but can only serve as informative values, since in silicon-

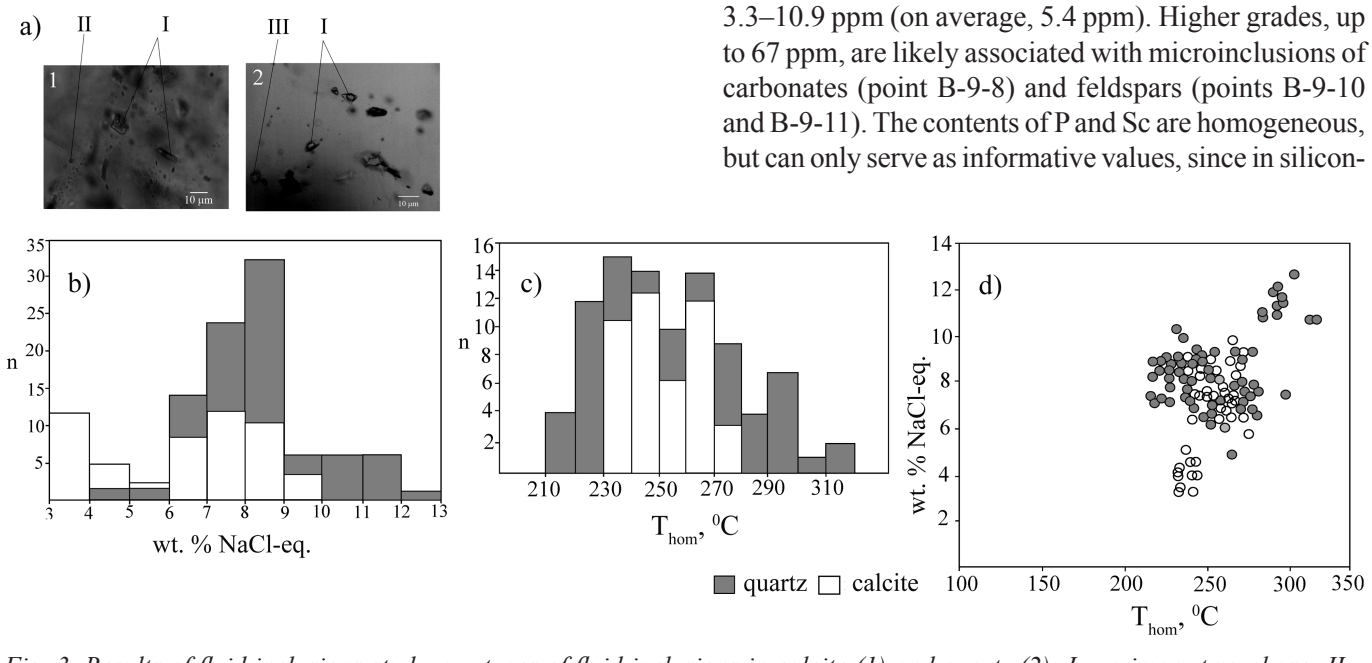


*Fig. 3. Results of fluid inclusions study. a – types of fluid inclusions in calcite (1) and quartz (2): I – primary two-phase; II – secondary two-phase; III – single phase. b, c – distribution of salinity (b) and homogenization temperatures (d); n is the number of measurements; d – ratio of salinity and homogenization temperatures of inclusions.*

| Element/ sample | Li | Na | Mg | Al | P | K | Ca | Sc | Ti | Fe |
|---|---|---|---|---|---|---|---|---|---|---|
| B-6-1 | 6.09 | 71 | 21.5 | 184 | 40 | 20.1 | 108 | 14.23 | 166 | 6.7 |
| B-6-2 | 5.3 | 30.2 | 23.19 | 527 | 29.2 | 160.4 | 47.7 | 12.89 | 193 | 5.37 |
| B-6-3 | 4.79 | 44.8 | 16.28 | 384 | 30.5 | 109.2 | 61.8 | 12.37 | 117 | 3.49 |
| B-6-4 | 4.47 | 35 | 21.6 | 471 | 31.4 | 174.1 | 55 | 12.03 | 167 | 5.65 |
| B-6-5 | 5.59 | 59.5 | 23.05 | 557 | 38.8 | 141.7 | 60.8 | 11.43 | 164 | 5.29 |
| B-6-6 | 7 | 33.1 | 21.4 | 450 | 33 | 186 | 74 | 11.3 | 168 | 6.8 |
| B-6-7 | 5.15 | 47.41 | 23 | 516 | 42.7 | 162.9 | 75.9 | 10.43 | 159 | 5.69 |
| B-6-8 | 4.25 | 45 | 9.23 | 259 | 40.7 | 56.9 | 84.6 | 10.12 | 146 | 3.28 |
| B-6-9 | 5.01 | 36.3 | 25.25 | 539 | 37.6 | 186.6 | 60 | 9.94 | 177 | 6.65 |
| B-9-1 | 3.99 | 66.7 | 6.66 | 202 | 29.1 | 52.5 | 94 | 9.59 | 146 | 2.46 |
| B-9-2 | 2.92 | 53.7 | 4.38 | 245 | 34.1 | 70.8 | 79 | 8.65 | 58.9 | 1.09 |
| B-9-3 | 2.75 | 76.6 | 19.69 | 400 | 31.9 | 132 | 67.5 | 8.46 | 76.3 | 10.88 |
| B-9-4 | 4.78 | 42.8 | 17.8 | 522 | 40.2 | 186.5 | 85 | 8.09 | 78.4 | 6.54 |
| B-9-5 | 1.23 | 44.5 | 4.87 | 261 | 40 | 84.5 | 101 | 8.16 | 38.4 | 1.5 |
| B-9-6 | 2.74 | 48 | 10.64 | 426 | 44.5 | 132.8 | 77 | 8.06 | 62.3 | 7.61 |
| B-9-7 | 4.02 | 174 | 17.1 | 620 | 44 | 134.6 | 56.7 | 7.77 | 134 | 6.18 |
| B-9-8 | 1.23 | 47.73 | 49 | 750 | 49.8 | 158 | 123 | 7.85 | 59 | 36 |
| B-9-9 | 3.07 | 57.9 | 11.7 | 588 | 46.6 | 212 | 145 | 7.63 | 76.6 | 6.3 |
| B-9-10 | 3.57 | 72 | 35 | 1370 | 46.4 | 532 | 131 | 7.58 | 86.4 | 20.7 |
| B-9-11 | 1.94 | 1570 | 124 | 5180 | 55.3 | 1040 | 350 | 7.34 | 88 | 66.7 |

*Table 1. Content of trace elements in quartz, ppm*

oxygen compounds in mass spectrometry, interference overlaps of $^{31}P$ with $^{30}Si+H$ or $^{14}N+^{16}O+H$ and others are observed, and $^{45}Sc$ – with $^{29}Si+^{16}O$ or $^{28}Si+^{17}O$.

## Distribution of rare earth elements and yttrium in ore pyrite

The contents of rare earth elements and yttrium in pyrite were determined by inductively coupled plasma mass spectrometry (ICP-MS) on a PerkinElmer ELAN 9000 instrument at the Institute of Geology and Geochemistry of the Ural Branch of the Russian Academy of Sciences (Yekaterinburg, analyst D.V. Kiseleva). The standardization was carried out for CI chondrite (McDonough, Sun, 1995). The Eu and Ce anomalies were calculated using the formulas:

$Eu/Eu^* = Eu_N/(Sm_N/(Tb_N \times Eu_N)^{0,5})^{0,5}$,

$Ce/Ce^* = Ce_N/((2La_N + Sm_N)/3)$.

The results of the determinations are shown in Table 2.

### Sulfur isotopic composition of sulfides

Stable sulfur isotopes have been studied in pyrite and chalcopyrite ores (Table 3). The sulfur isotopic composition was determined on a DeltaPLUS Advantage mass spectrometer coupled with an EA Flash 1112 elementary analyzer and a ConFlo IIII interface at the Institute of Mineralogy of the SU FRC MG UB RAS (Miass, analyst S.A. Sadykov). The error in determining δ34S was 0.27 ‰. The measurement results are given in relation to the international CDT standard. According to the data obtained, the δ34S values in pyrite are – 1.01… 0.8 ‰, in chalcopyrite – 0.9 ‰.

| Element/ sample | B3-7 | B3-9 | B3-12 | B3-11 | B3-14 | B3-13 |
|---|---|---|---|---|---|---|
| La | 1.1 | 0.5 | 1.7 | 0.7 | 1.3 | 0.6 |
| Ce | 1.9 | 1 | 2.45 | 1.35 | 2.1 | 0.9 |
| Pr | 0.16 | 0.11 | 0.23 | 0.14 | 0.21 | 0.12 |
| Nd | 0.65 | 0.47 | 0.76 | 0.52 | 0.63 | 0.43 |
| Sm | 0.17 | 0.1 | 0.19 | 0.14 | 0.16 | 0.1 |
| Eu | 0.056 | 0.025 | 0.062 | 0.04 | 0.05 | 0.03 |
| Gd | 0.2 | 0.12 | 0.25 | 0.17 | 0.21 | 0.13 |
| Tb | 0.03 | 0.03 | 0.04 | 0.023 | 0.03 | 0.02 |
| Dy | 0.24 | 0.14 | 0.28 | 0.18 | 0.24 | 0.16 |
| Ho | 0.05 | 0.029 | 0.06 | 0.04 | 0.05 | 0.031 |
| Er | 0.16 | 0.09 | 0.18 | 0.12 | 0.15 | 0.08 |
| Tm | 0.024 | 0.013 | 0.029 | 0.02 | 0.024 | 0.011 |
| Yb | 0.17 | 0.1 | 0.19 | 0.14 | 0.16 | 0.08 |
| Lu | 0.027 | 0.015 | 0.031 | 0.021 | 0.023 | 0.012 |
| Y | 1.6 | 0.8 | 2.21 | 1.33 | 1.45 | 1.13 |
| ∑REE | 4.94 | 2.73 | 6.45 | 3.6 | 5.34 | 2.7 |
| $La_N/Yb_N$ | 4.66 | 3.6 | 6.44 | 3.6 | 5.85 | 5.39 |
| $La_N/Sm_N$ | 4.18 | 3.23 | 5.78 | 3.23 | 5.25 | 3.87 |
| $Gd_N/Yb_N$ | 0.97 | 0.99 | 1.09 | 1.0 | 1.09 | 1.34 |
| Eu/Eu* | 0.99 | 0.78 | 0.95 | 0.9 | 0.93 | 0.9 |
| Ce/Ce* | 0.82 | 0.92 | 0.7 | 0.9 | 0.78 | 0.71 |
| Y/Ho | 32 | 27.6 | 36.8 | 33.3 | 29.2 | 36.5 |

*Table 2. Content of rare earth elements and yttrium in pyrite, ppm*

## Discussion and conclusion

According to the data of fluid inclusion study, ore quartz of the Vosnesensky deposit was formed at temperatures not less than 215–315ºC, and calcite was deposited later at 230–280ºC. The mineral-forming fluid is characterized by salinity, which in inclusions of quartz varies from 4.8 to 12 wt. % NaCl-eq., in calcite – from 3 to 10 wt. % NaCl-eq. Crystallization of quartz and

| No. | Sample | Isotopic composition of sulfur $\delta^{34}S$ ‰, CDT | Comment |
|---|---|---|---|
| 1 | В3-7п | 0.72 | pyrite |
| 2 | В3-8п | -1.01 | pyrite |
| 3 | В3-9п | -0.07 | pyrite |
| 4 | В3-11п | -0.08 | pyrite |
| 5 | В3-12п | -0.06 | pyrite |
| 6 | В3-14п | 0.80 | pyrite |
| 7 | В3-17х | 0.90 | chalcopyrite |
| 8 | В3-19п | 0.04 | pyrite |

*Table 3. Isotopic composition of sulfur in sulfides*

calcite occurred from K-Na aqueous chloride fluid. The obtained temperature values correspond to the conditions of mesothermal sericite-quartz metasomatism, which ore-bearing granitoids underwent. In general, they are comparable with the results of studying the temperature regime of the formation of Cu-porphyry mineralization in sericite-quartz metasomatites of many other porphyry deposits of the Southern Urals associated with island arc diorites magmatism (Grabezhev, 2009). For example, at the Mikheevsky deposit, the Cu-Mo porphyry mineralization was formed at temperatures of 250–300ºC (Abramova et al., 2016).

The coexistence of single-phase gas, liquid and more concentrated two-phase inclusions indicates fluid heterogenization (Prokofiev et al., 1994 and references therein), considered the homogenization temperatures of inclusions as real fluid temperatures during mineral formation. In turn, the presence of a heterogeneous fluid consisting of a concentrated water fluid in equilibrium with the gas phase indicates the boiling in the environment of pressure reduction.

Using the highly sensitive LA-ICP-MS method, which was first used in the study of quartz from porphyry copper deposits in the Southern Urals, it was found that the Vosnesensky quartz deposit is characterized by high contents of Al (184–5180 ppm) and Ti (38.4–193 g/t). The Al concentration in quartz reflects the solubility of this element in the mineral-forming fluid, which largely depends on the pH of the fluid (Rusk et al., 2008). At relatively low temperatures (<500ºC), the Al concentration in quartz is related to the pH of the fluid by an inverse correlation dependence. The results indicate that the quartz of the Vosnesensky deposit crystallized from a high-alumina acidic fluid.

In terms of the quantitative ratio of Al and Ti in quartz, the Vosnesensky deposit is comparable to other Cu-porphyry deposits in the world. The Al-Ti diagram proposed by B.G. Rusk (Rusk, 2012) to separate epithermal, mesothermal orogenic and porphyry deposits according to this indicator, the points of quartz composition of the Vosnesensky deposit fall into the quartz deposit of porphyry deposits or are grouped around this deposit (Figure 4). We also determined the contents of REE and Y, close to them in chemical properties, in the ore pyrite of the deposit. Studies in recent years have shown (Znamensky, 2017; Rimskaya-Korsakova, Dubinin, 2003; Guangzhou et al., 2009; etc.) that the compositions of REE and Y in sulfides inherit the composition of the fluid from which they crystallize and can serve as an indicator of its physical and chemical parameters and source. Lanthanides and yttrium are concentrated in sulfides in crystal lattice defects and in fluid inclusions. In addition, heavy REEs can enter the crystal lattice of sulfides, while light lanthanides can be sorbed on their surface in the form of free ions and, possibly, in the form of hydroxo complexes (Rimskaya-Korsakova, Dubinin, 2003).

The ore pyrite of the Vosnesensky deposit has low REE (∑REE = 2.7–6.45 ppm) and Y (0.8–2.21 ppm) contents. The REE distribution spectra are enriched in light lanthanides (LaN/YbN = 3.6–6.44), which is typical of minerals crystallizing from acidic fluids with a low content of complexing ligands (Schwim, Markl, 2005), as well as small negative anomalies Eu (Eu/Eu* = 0.78–0.99) and Ce (Ce/Ce* = 0.7–0.92) (Figure 5). Differentiation within heavy lanthanides is not pronounced (GdN/YbN = 0.97–1.34).

The redox potential of Eu in aqueous solutions depends on a number of factors and mainly on temperature (Sverjensky, 1984). Negative Eu anomalies

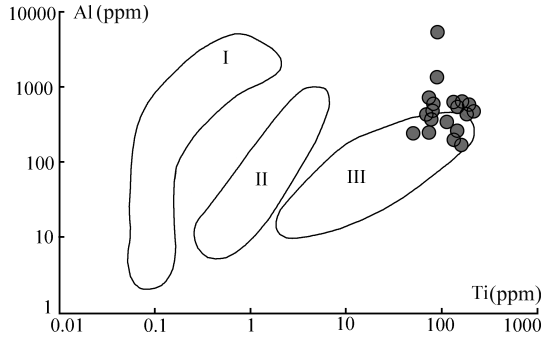


*Fig. 4. Al-Ti diagram for quartz on the Vosnesensky deposit. Roman numerals denote the compositional deposits of ore quartz of epithermal (I), mesothermal orogenic gold ore (II) and porphyry (III) deposits (Rusk, 2012). Data for the Vosnesensky deposit are shown with gray circles.*

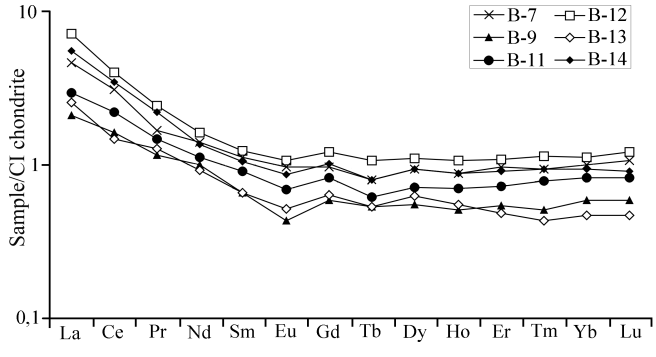


*Fig. 5. Graphs of REE distribution in pyrite*

indicate the crystallization of pyrite from a relatively oxidized fluid at low temperatures, apparently below 250°C (Bau, Möller, 1992).

Negative Ce anomalies could arise as a result of the interaction of fluid with marine limestones, which are present in the exocontact zones of the Vosnesensky massif. For marine limestones, negative Ce anomalies are characteristic, which persist during fluid/limestone interaction (Castorina, Masi, 2008). In addition, oxidized meteoric waters could have been involved in the ore-forming system of the deposit, which is indirectly indicated by a weak positive trend in the relationship between the homogenization temperatures of inclusions and the salinity of fluids (Wilkinson, 2001). The dilution of fluids with meteoric waters led to a drop in fluid temperatures and salinity.

The sources of ore-forming fluids can be judged by the value of the Y/Ho ratio in ore minerals (Bau, 1996). The Y/Ho values in the pyrite of the Vosnesensky deposit vary in the range 27.6–36.8. Some of these values fall within the range of Y/Ho values characteristic of ore-hosting granitoids (29.4–35.7), while others – for marine carbonates (Figure 6).

The results of the studies made it possible to assume the participation of a magmatic fluid in the ore-forming processes of the deposit and, like negative Ce anomalies, indicate its interaction with the host limestones. It should be noted that the distribution spectra of REE in pyrite are very close to the trends in the distribution of lanthanides in ore-bearing granitoids. Chondrite-normalized REE distribution spectra in granitoids of the deposit are also characterized by enrichment in light lanthanides (LaN/YbN = 1.5–6.0) and lack of differentiation among heavy rare earths (GdN/YbN = 0.83–1.07) (Znamensky et al., 2019). In our opinion, this can serve as an additional argument in favor of the magmatogenic nature of the ore-forming fluid. The participation of magmatogenic fluids in ore formation is confirmed by the results of S isotope analysis in sulfides. The $\delta^{34}S$ values, which are –1.01 ... 0.8 ‰ in pyrite and 0.9 ‰ in chalcopyrite, are close to the meteorite standard. The obtained $\delta^{34}S$ values correspond to the isotopic ratios of sulfur in sulfides of most porphyry deposits in the Southern Urals, as well as in North and South America (0 ± 5 ‰) (Grabezhev, 2009; Ohmoto, Rye, 1979; Ohmoto, Goldhaber, 1997).

Thus, the porphyry Cu mineralization of the Vosnesensky deposit was formed under mesothermal conditions with the participation of acidic K-Na aqueous chloride fluids of magmatic nature, enriched in aluminum and light rare earth elements. The reduction in temperature and salinity of the fluid is due to its dilution by meteoric waters. Geochemical signs of the interaction of the fluid with the host limestones, expressed in negative Ce anomalies and increased values of the Y/Ho coefficient in ore pyrite, have been established.

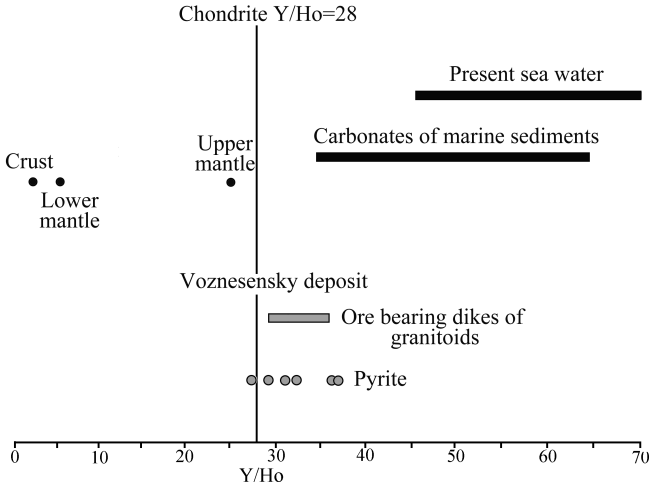


*Fig. 6. The magnitude of the Y/Ho ratio in pyrite. Y/Ho values in chondrite, crust, upper and lower mantle, sea water, and carbonates of marine sediments according to (Bau, 1996; Bau, Dulski, 1995), in ore bearing dikes of the Vosnesensky deposit granitoids according to (Znamensky et al., 2019).*

## Acknowledgements

*Field works were carried out under the Government Order of the Institute of Geology of the UFRC RAS No. 0246-2019-0078. Isotope and geochemical studies were supported by the RFBR (No. 17-45-020717). Fluid inclusion and LA-ICP-MS studies were supported by the State Contract of the Institute of Mineralogy SU FRC MG UB RAS (2019-21).*

## References

Abramov S.S.,Plotinskaya O.YU. Groznova Ye.O. (2016). History of hydrothermal processes at the Mikheevsky Mo-Cu field according to the study of secondary changes and fluid inclusions. Proc. XVII All-Russ. Conf. on Thermobaric geochemistry. Ulan-Ude: BNTS SO RAN, pp. 11–12. (In Russ.).

Bau M. (1996). Controls on the fractionation of isovalent trace elements in magmatic and agueous systems: evidence from Y/Ho, Zr/Hf and lanthanide tetrad effect. *Contrib. Mineral. Petrol*., 123, pp. 323–333. https://doi.org/10.1007/s004100050159

Bau M., Dulski, P. (1995). Comparative study of yttrium and rare-earth element behaviours in fluorine-rich hydrothermal fluids. *Contrib. Mineral. Petrol*, 119, pp. 213–223. https://doi.org/10.1007/BF00307282

Bau M., Möller P. (1992). Rare Earth Element Fractionation in Metamorphogenic Hydrothermal Calcite, Magnesite and Siderite. *Mineralogy and Petrology*, 45, pp. 231–246. https://doi.org/10.1007/BF01163114

Bodnar R.J., Vityk M.O. (1994). Interpretation of microthermometric data for $H_2O$-NaCl fluid inclusions. Fluid inclusions in minerals: methods and applications (Eds. De Vivo B. and Frezzotti M.L). Pontignana-Siena, Virginia Polytechnic Institute and State University, 1994, pp. 117–130.

Castorina F., Masi U. (2008). REE and Nd-isotope evidence for the origin siderite from the Jebel Awam deposit (Central Morocco). *Ore Geology Reviews*, 34, pp. 337–342. https://doi.org/10.1016/j.oregeorev.2008.03.001

Davis D.W., Lowenstein T.K., Spenser R.J. (1990). Melting behavior of fluid inclusions in laboratory-grown halite crystals in the systems NaCl-$H_2O$, NaCl-KCl-$H_2O$, NaCl-$MgCl_2$-$H_2O$ and $CaCl_2$-NaCl-$H_2O$. *Geochim. Et Cosmochim. Acta*, 54, pp. 591–601. https://doi.org/10.1016/0016-7037(90)90355-O

Grabezhev A.I. (2009). Sr-Nd-C-O-H-S isotope-geochemical description of South Urals porphyry-copper fluid-magmatic systems: probable sources of matter. *Litosfera*, 6, pp. 66–89. (In Russ.)

Grabezhev A.I., Belgorodsky E.A. (1992). Productive granites and metasomatites of copper-porphyry deposits. Ekaterinburg: Nauka, 199 p. (In Russ.)

Guangzhou M., Renmin H., Jianfeng G., Weiqiang L., Kuidong Z., Guangming L.(2009). Existing forms of REE in gold-bearing pyrite of the Jinshan gold deposit, Jiangxi Province, China. *Journal of rare earths*, 27(6), pp. 1079–1087. https://doi.org/10.1016/S1002-0721(08)60392-0

Kosarev A.M., Puchkov V.N., Seravkin I.B., Kholodnov V.V., Grabezhtv A.I., Ronkin Y.L. (2014). New data on the age and geodynamic position of copper-porphyry mineralization in the Main Uralian Fault zone (Southern Urals). *Doklady Earth Sciences,* 495(1), pp. 1317–1321. https://doi.org/10.1134/S1028334X1411004X

McDonough W. F., Sun S. (1995). The composition of the Earth. *Chemical Geology*, 120, pp. 223–253. https://doi.org/10.1016/0009-2541(94)00140-4

Ohmoto H., Rye R. O. (1979). Isotopes of sulfur and carbon. *Geochemistry of hydrothermal ore deposits*. N.-Y.: John Wiley and Sons, pp. 509–567.

Ohmoto H., Goldhaber M. B. (1997). Sulfur and carbon isotopes. *Geochemistry of hydrothermal ore deposits*. N.-Y.: Wiley, pp. 517–611.

Prokofev V.Y., Afanaseva Z.B., Ivanova G.F., Boiron M.C., Marignac C. (1994). Study of fluid inclusions in minerals of the Olimpiadinskoe Au (Sb-W) deposit (Enisey Mountain-Ridge). *Geokhimiya,* pp. 1012-1029. (In Russ.)

Rimskaya-Korsakova M.N., Dubinin A.V. (2003). Rare earth elements in sulfides of submarine hydrothermal vents of the Atlantic ocean. *Doklady Earth Sciences,* 389(3), pp. 432–436.

Roedder E. (1984). Fluid inclusions. *Reviews in mineralogy,* 12, 646 p.

Rusk B.G. (2012). Cathodoluminescent textures and trace elements in hydrothermal quartz. Quartz: Deposits, Mineralogy and Analytics. New-York: Springer, 360 p. https://doi.org/10.1007/978-3-642-22161-3_14

Rusk B.G., Lowers H.A., Reed M.H. (2008). Trace elements in hydrothermal quartz: Relationships to cathodoluminescent textures and insights into vein formation. *Geology*, 36(7), pp. 547–550. https://doi.org/10.1130/G24580A.1

Schwim G., Markl G. (2005). REE systimatics in hydrothermal fluorite. *Chemical Geology*, 216, pp. 225–248. https://doi.org/10.1016/j.chemgeo.2004.11.012

Shishakov V.B., Sergeeva N.E., Surin S.V. (1988). The Voznesenskoe porphyry copper deposit at South Urals. *Geologiya rudnykh mestorozhdeniy,* 2, pp. 85–90. (In Russ.)

Sverjensky D.A. (1984). Europium redox equilibria in aqueous solution. *Earth Planet Science Letters*, 67, pp. 70–78.

Wilkinson J.J. (2001). Fluid inclusions in hydrothermal ore deposits. *Lithos*, 55, pp. 229–272. https://doi.org/10.1016/S0024-4937(00)00047-5

Znamensky S.E. (2017). Rare earth elements and yttrium in calcite and pyrite of the Orlovka gold deposit (the Southern Urals). *LITHOSPHERE (Russia)*, 1, pp. 135–146. (In Russ.)

Znamensky S.E., Shafigullina G.T., Znamenskaya N.M., Kosarev A.M. (2019). The Voznesenka porphyry copper deposit (South Urals): structural control of mineralization and geochemistry of intrusive rocks. *Vestnik Akademii nauk Respubliki Bashkortostan*, 2, pp. 25–35 (In Russ.)

## About the Authors

*Sergey E. Znamensky* – Dr. Sci. (Geology and Mineralogy), Chief Researcher, Institute of Geology of the Ufa Federal Research Centre of the Russian Academy of Sciences

16/2 K. Marx st., Ufa, 450077, Russian Federation

*Natalya N. Ankusheva* – Cand. Sci. (Geology and Mineralogy), Researcher, Institute of Mineralogy of the South Urals Federal Research Center of Mineralogy and Geoecology of the Urals Branch of the Russian Academy of Sciences

1 Ilmensky Zapovednik, Miass, 456317, Russian Federation

*Dmitry A. Artemiev* – Cand. Sci. (Geology and Mineralogy), Researcher, Institute of Mineralogy of the South Urals Federal Research Center of Mineralogy and Geoecology of the Urals Branch of the Russian Academy of Sciences

1 Ilmensky Zapovednik, Miass, 456317, Russian Federation

*Manuscript received 9 January 2020;*
*Accepted 11 June 2020; Published 30 September 2020*

ORIGINAL ARTICLE

**DOI**: https://doi.org/10.18599/grs.2020.3.55-61

Russian Original 2020. Vol. 22. Is. 3. Pp. 55–61

# Facies models of the Achimov formation of East-Urengoyskoe license as the basis for optimizing exploration and field development patterns

*A.V. Khramtsova[1*], S.I. Pakhomov[1], N.Yu. Natchuk[1], M.P. Kalashnikova[1], S.V. Romashkin[2], A.D. Musikhin[2], N.G. Semenova[2]*

[1]*LLC «Tyumen Petroleum Research Center», Tyumen, Russian Federation*

[2]*CJSC «Rospan International», New Urengoy, Russian Federation*

**Abstract**. The results of sedimentological core analysis of the Achimov formation (Upper Valanginian, Lower Cretaceous) confirm that it was formed by higher efficiency systems of submarine fans in (relatively) deep marine basin. Lithofacies models of $Ach_{5-6}$ were generated, well correlation was performed based on the comprehensive analysis of core, well logging and seismic data. Distributary channels and proximal parts of depositional lobes are characterized by the best reservoir properties.

**Keywords**: the Achimov formation, facies, turbidities, submarine fan, permeability

**Recommended citation**: Khramtsova A.V., Pakhomov S.I., Natchuk N.Yu., Kalashnikova M.P., Romashkin S.V., Musikhin A.D., Semenova N.G. (2020). Facies models of the Achimov formation of East-Urengoyskoe license as the basis for optimizing exploration and field development patterns. *Georesursy = Georesources*, 22(3), pp. 55–61. DOI: https://doi.org/10.18599/grs.2020.3.55-61

## Introduction

The East-Urengoyskoe license is located in the northern part of Western Siberia in the Nadym-Pur petroleum region, tectonically associated with Urengoy mega-arch. According to the stratigraphic zonation of Nothern Siberian Berriasian-Aptian deposits, the area under study is located in Urengoy-Purpe lithofacies area, Urengoy subarea (Decision of the 6th Interdepartmental Stratigraphic Meeting…, 1991). Achimov formation ($Ach_{5-6}$) of early Valanginian time ($K_1v_1$) conformably overlays the Bazhenov formation and/or the sub Achimov formation and is overlain by Tangalovskaya Series. The Achimov formation occurs at 3500–4070 m (TVDSS) within the area under study.

According to the paleographical scheme of Northern Siberia in Early Valanginian time there was an epicontinental sea basin with maximum depths of 200–400 m (Kontorovich et al., 2014) within the area under study. Larger part of clastic material was transported from the Yenissey Ridge, Siberian platform, Altay-Sayan area and Central-Kazakh massif, and, to a less degree, from the Urals.

Integrated analysis of geological and geophysics data, well logs, 3D seismic data and core was conducted for the purpose of detailed study of $Ach_{5-6}$ geological structure, prediction of reservoir rocks, optimization of exploration and field development patterns. Considering that reservoirs of Achimov formation have low-permeability, the hydrofracturing is used to stimulate oil production. Detailed study of the geological structure is a critical task nowadays, as a number of fields have high watercuts.

## Factual material and research methods

Sedimentological analysis of the Achimov formation was conducted on the cores from 12 wells. The total meterage of the studied core was 567 m with 82% core recovery. Facies were recognized on the basis of diagnostic signatures presented in papers of Russian (Alekseev, 2002; Baraboshkin, 2011; Zhemchugova, 2014, etc.) and foreign authors (Stow, 1976; Normark, 1970, 1990; Mutti, 1992; Lowe, 1982; Walker, 1992; Einsele, 1992; Reading, Richards, 1994, etc.). The results of lithological core research and reservoir properties made in Tyumen Petroleum Research Center were used to characterize lithotypes and facies. For well log correlations theauthors used lithofacies analysis (Alekseev, 2002) and sequence stratigraphy (Catuneanu, 2006). Facies maps of $Ach_{5-6}$ were built on the basis of comprehensive core analysis, well logging, seismic

*Corresponding author: Alena V. Khramtsova
E-mail: khramtsovaav@sibintek.ru

attribute maps (acoustic impedance, coherency, seismic facies, amplitudes), gross thickness and NTG maps. Areas with great potential for drilling were selected on the basis of pressure transient analysis, well logging, seismic materials, and facies models of productive deposits.

## Composition, structure and depositional settings

Reservoir rocks of Achimov formation are mainly presented by very fine-grained and fine-grained, rarely by medium fine-grained sandstones. According to mineralogical composition, sandstones and siltstones are arkoses that are the clastic products of disintegration of granitoids and metamorphic shale feldspar. It has been observed that quartz content predominates over feldspar. The content of rock fragments does not exceed 25% (Figure 1). The content of cement in sandstones and coarse-grained siltstones changes in wide range from 2.5 to 38%. The cement is clayey, carbonated, and regenerative. Chlorite predominates among clay minerals of cement. Calcite prevails among carbonate minerals. Regenerative quartz and feldspar cement which content does not exceed 0.5–1.0% can be encountered. By the X-ray diffraction analysis of the clay fraction an increased content of illite-smectite mixed-layer (up to 30–35%) was detected in the cement of Ach 6 sandstones and siltstones. The content of swelling clay minerals of illite-smectite mixed layer is 1–28% (Figure 1). The rocks are water-wet.

The negative influence of the following secondary processes was established on the reservoir properties of rocks: carbonation, chloritization, pelitization and hydration of biotite, regeneration of quartz and feldspars (only at high intensity). The process of solving feldspars and rock fragments, and kaolinitization exert some positive influence.

Rocks are characterized by very low permeability (mostly <1mD). In some individual wells only the permeability increases up to 30 mD as the content of medium-grained fraction grows in sandstones.

There are two conceptual models of the depositional genesis of the Achimov formation: delta front/avandelta deposits (Alekseev, 2014, etc.) and submarine fans (Nezhdanov et al., 2000; Gurari, 2003; Zverev, 2001; Borodkin et al., 2015; Syngaevsky, Khafizov, Shimansky, 2015, etc.). Structural features of rocks prove the sedimentological model of submarine fans.

According to the diagnostic signatures of facies (structure, texture, fauna, mineral inclusions, contacts and transitions, etc.), it was found that deposits were formed mainly by gravitational flows (grain, debris, and fluid) in the deep water part of the epicontinental sea basin. The rocks lack typical signs of shallow water (wave ripples; large-scale cross-bedding; signatures of subaerial exposure, storm and tidal processes). On the other hand, there are signs of sedimentary material input from the shallow water parts of the basin (carbonaceous

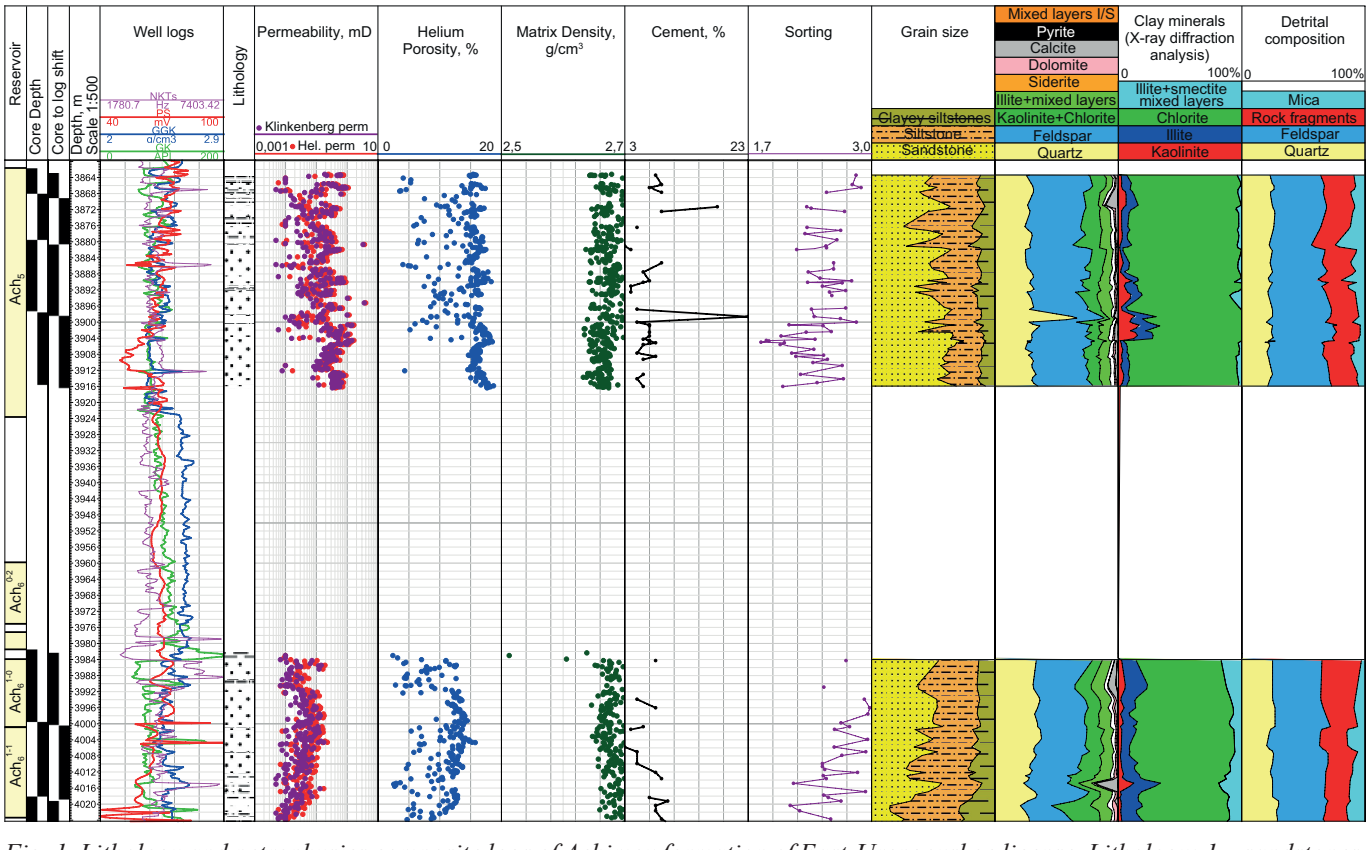


*Fig. 1. Lithology and petrophysics composite logs of Achimov formation of East-Urengoyskoe license. Lithology: 1 – sandstones, 2 – siltstones, 3 – clayey siltstones, claystones.*

detritus, shallow microorganisms and trace fossils). Bottom marks of loading, currents, and fame structures are abundantly developed at the bottom of sand layers (Figure 2a, 2c-d).

The Achimov formation can be characterized by the following: massive structure and graded bedding, texture of plastic deformations (intrusions, convolute, flaming, sand rolls), dish structures, water escape pipes, parallel-laminated, climbing current ripples, bioturbated structures are rare (Figure 2). Trace fossils: *Ophiomorpha, Asterosoma, Thalassinoides, Chondrites* can be found in single wells, in sediments of levees and inter-channel areas. The intensity of bioturbation can be significant.

*Graded bedding* is typical for deposits of turbidite flows. Numerous bibliography on turbidite flows and turbidites is presented in the papers of (Bouma, 2020; Mutti, 1992; Lowe, 1982; Stow, 1976; Prelat, 2009; Nichols, 2012, etc). The turbidite currents can be present in lakes (Dodd, McCarthy et al., 2018), deltas, seas and oceans, but to preserve structural features of turbidites, they should not be reworked by other currents. In fact, this determines the position of turbidites below storm wave base.The probable minimum depths are about 250–300 m (Walker, 1992), which does not contradict the regional data.

As a result of the sedimentological study of the Achimov formation cores, the following facies were identified: submarine feeding and distributary channels, submarine levees, channel edges and interchannel deposits, clay deposits of the slope and shelf, slump scars and depositional lobes. The conceptual structural model of the Achimov formation is presented in Figure 3a.

***The slope channels*** are not studies by core: they are recognized by the seismic data (Figures 3b, 3d). The transition from channels with levees to frontal crevasse splay is well identified on maps and sections in the acoustic impedance cube (Figures 3b, 3c). The main sedimentological sections of facies of the Achimov formation are presented in Figure 4.

***The distributary channels*** are represented by sandstones with massive texture, water escape pipes and dish structures are often found, that indicates an intensive loss of the fluid component during sedimentation period. Massive sandstones graded into typical turbidites from bottom-up. The lower contact of sandy interlayers is usually erosive (Figure 4a), emphasized by mudstones and clayey siltstone intraclasts. The presence of debris indicates the erosion caused by high-density turbidite flows.

*Admixtures:* pyrite compounds, carbonaceous detritus.

*Interpretation:* The formation of submarine channel deposits was a result of high-density and low-density turbidite flows. Both large channels with levees and small channels can be encountered. Quite often the channels are built on each other, as a result the upper fine-grained sequences are eroded by subsequent flows.

Big slope channels are the main sediment transporters from the zone of shallow water shelf to the deep part of the basin. They are well identified on seismic (Figure 3b). Distributary channels can be meandering, braided,

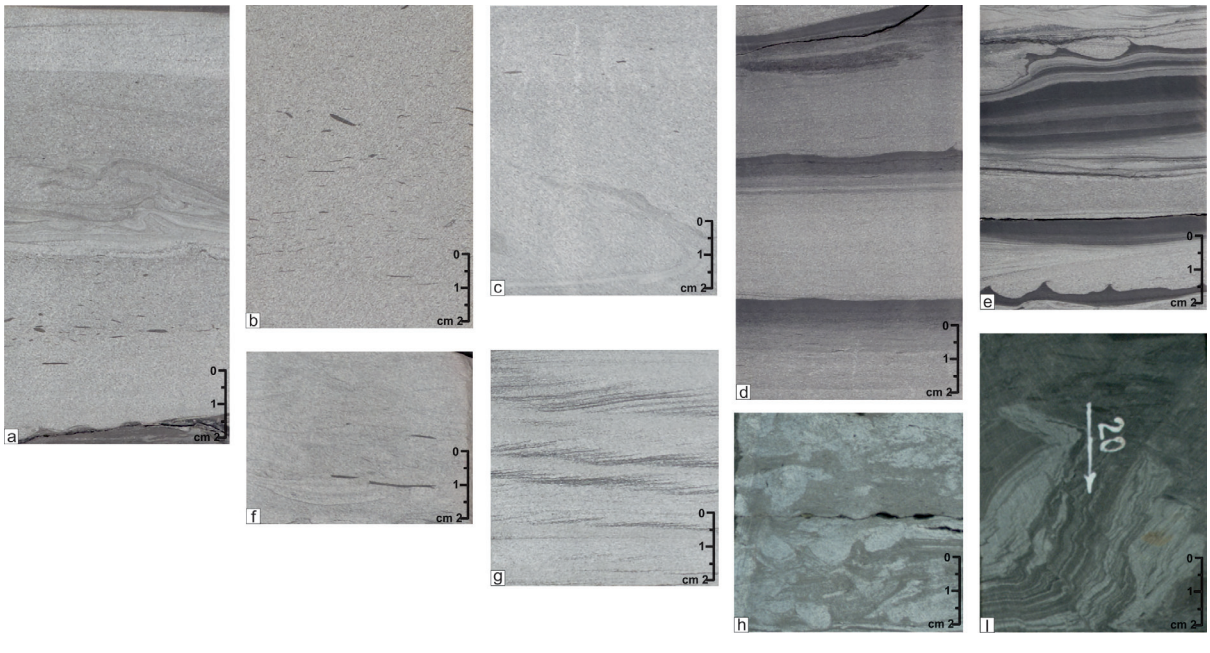


*Fig. 2. Srtuctural features of Achimov formation of East-Urengoyskoe field. a – sandstones with ripped-up clay clasts, convolute lamination and climbing ripples; b – sandstones with debris structure, with small intraclasts of clayey siltstones; c – sandstones with water escape pipes and flames; d – sandstones with gradational bedding; e – interlayering of sandstones and clayey siltstone. There are casts layers on the contact of load; f – dish structures in sandstones, with small clayey siltstone clasts; q – climbing ripples sandstones; h – bioturbation (Thalassinoides);i – fine to coarse siltstones with convolute lamination.*

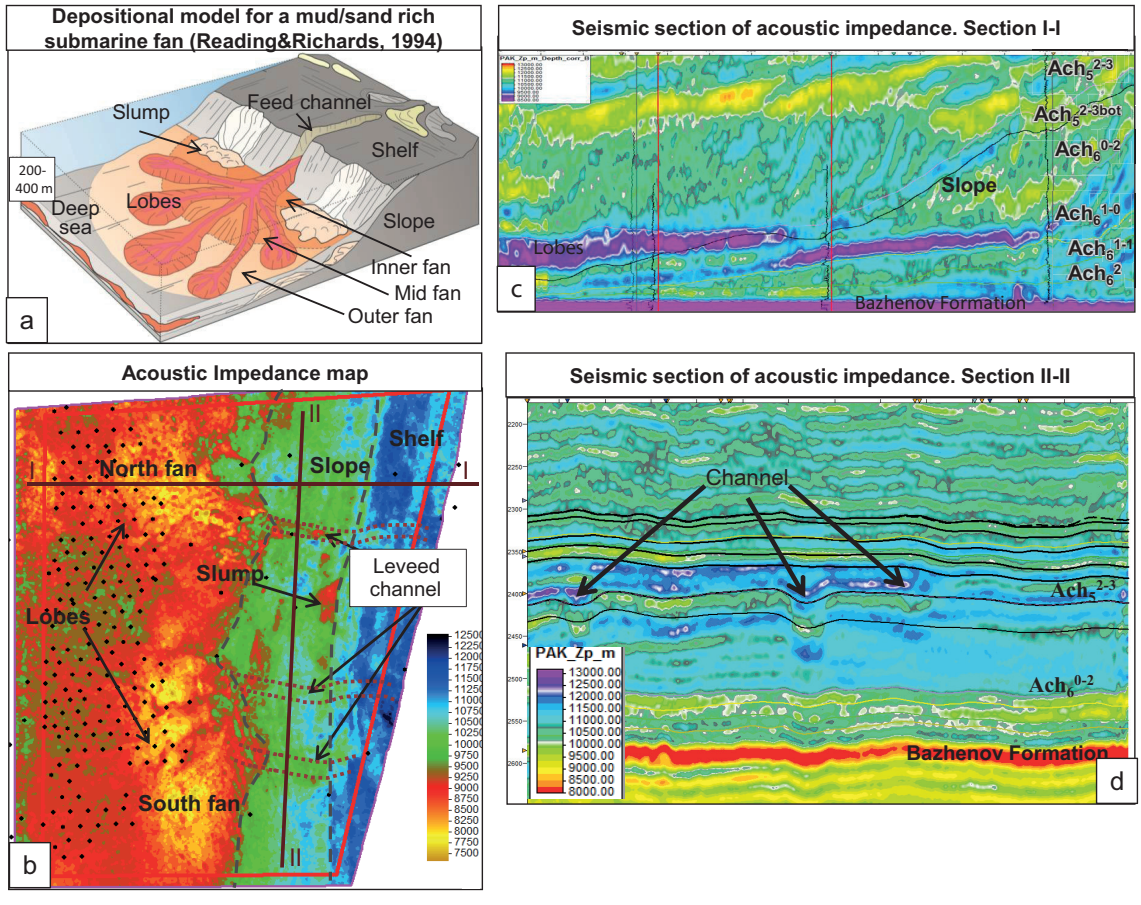


*Fig. 3. Conceptual model of Achimov formation (a) and morphological elements of submarine fan picked by seismic survey results (b-d)*

and straight types. The sand body in section view is U-shaped (Figure 4).

*Thickness*: up to 30 m.

*Well log signature:* blockyshaped, low gamma-ray (5–10$^0$API).

**The turbidite lobe facies** is represented by very fine- to fine-grained sandstones, coarse-grained siltstone with thin interlayers of mudstone and clayey siltstone. The structure in sandstones and siltstones is massive, debris, gradational, with plastic deformations, fluidal, horizontal, partly with climbing ripples (Figure 2g). There are load structures on the contacts of bedding. Turbidite lobes are characterized by layers of sandstones with massive and graded structures without features of channel impact (Figure 4b).

*Admixtures andother features*: carbonaceous detritus, clayey siltstone clasts of elongated and flattened shape.

*Interpretation*: when leaving the channel, the turbidite flows spread to form submarine levees well defined in the landscape. Lobes consist of compensation cycles, each of them represented by turbidites filling the low, located between sediments of older turbidite flows projected out in the landscape. The structure of compensation cycles can feature sandstone tubridite layers thickening and thinning up. Depositional lobes develop during slope gradient change. As the flow meets rapid slope gradient at such knickpoint (transition point) the channels are replaced by frontal splays (Figure 3b, c). The sand body in side view has a shape of flat, elongated lenses (Figure 4).

*Thickness*: up to 15–20 m.

*Well log signature*: medium gamma-ray (7–12$^0$API).

**The submarine levee facies/interdistributary areas** are represented by interlayering of sandstones, siltstones, and mudstones (Fig. 4c). The thickness of sandstones changes from 2 to 50 cm. Clayey siltstones and mudstones are 1–10 cm thick. Moving away from the channel, sand interbeds become thinner.

*Structure:* thin bedding, gradational, with plastic deformations, debris, climbing current ripples, convolute, occasional bioturbation (Figure 2h).

*Trace fossils:* Thalassinoides, Fugichnia, Ophiomorpha and Phycosiphon are in places.

*Admixtures and other features*: plant detritus, small lenses of coal, shell detritus.

*Interpretation:* V-shaped levees are formed on the channel edges and gradually pinch out inward the basin. The height of levees usually decreases down the submarine fan. The channels become less deep. The presence of suspended fines results in growth of the levees. The levees consist of different proportions of laminated sandstones and fine-grained turbidites.

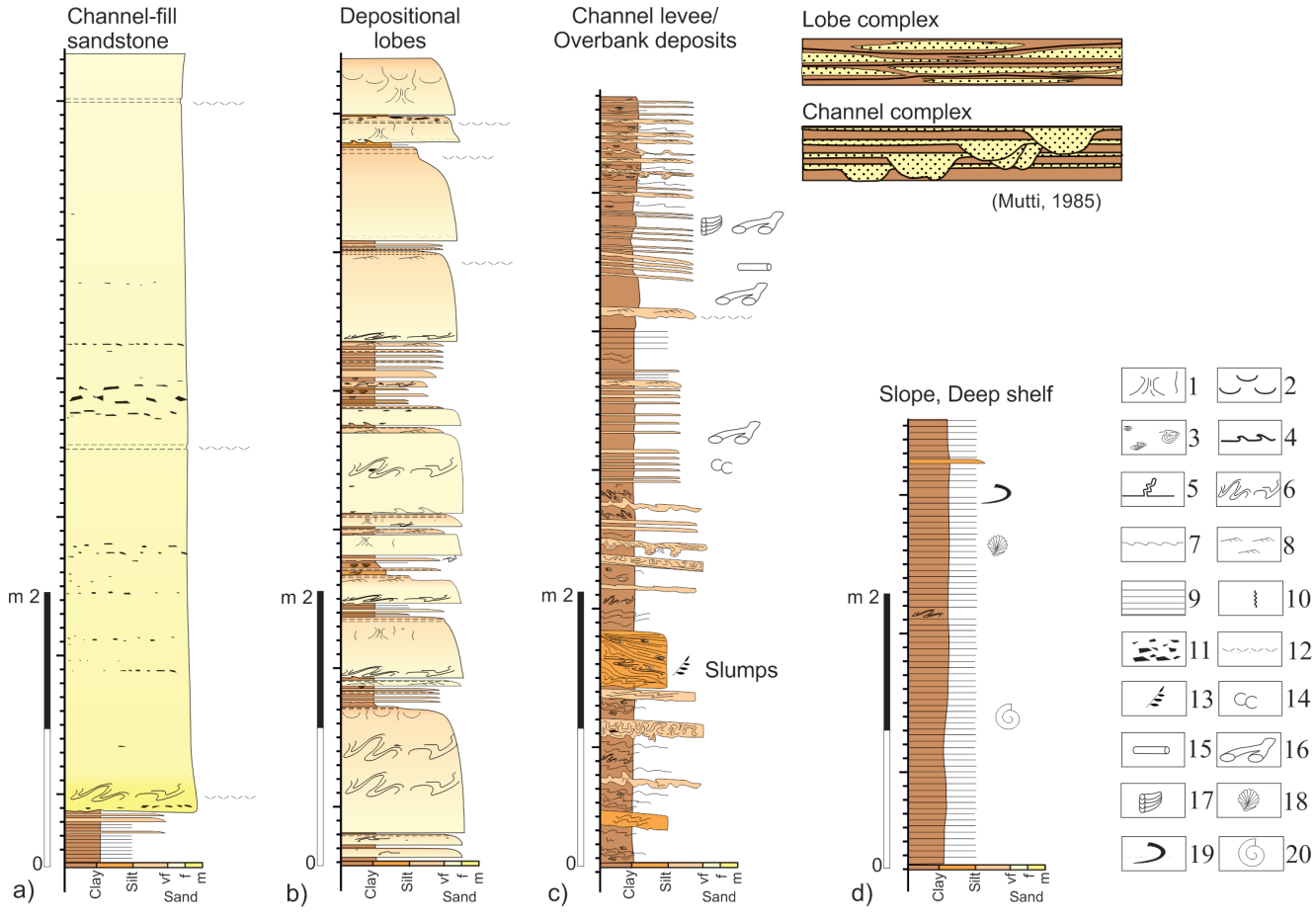


*Fig. 4. Typical sedimentological logs of Achimov formation. Structures: 1 – water escape structures; 2 – dish structures; 3 – sand rolls; 4 – flaming; 5 – injection structure; 6 – convolute; 7 – loadintrusion; 8 – climbing ripple; 9 – horizontal; 10 – bioturbation. Inclusions: 11 – clayey clasts; 12 – thin layers of carbonaceous detritus; 13 – scatteredcarbonaceous detritus; ichnofacies: 14 – Palaeophycus; 15 – Planolites; 16 – Thalassinoides; 17 – Teichichnus. Fauna: 18 – fish scales; 19 – onychitis; 20 – ammonites. On the grain-scale ruler: Svf –very fine sandstone;Sf – fine-grained sandstone; Sm – medium-grainedsandstone*

*Thickness:* 0.10–3.8 m.

*Well log signature:* increased gamma-ray (7–14$^0$API).

**Slump facies** is represented by interlayering of fine-grained clayey siltstones, coarse-grained siltstones, very-fine grained sandstones and silty mudstones. The primary bedding was destroyed by sediment slump.

*Trace fossils:* not common.

*Admixtures and other features:* carbonaceous detritus, shell detritus, small clasts of clayey siltstone.

*Interpretation:* Poorly consolidated sediments slump on the flat slope under the action of gravity.

*Thickness:* 0.45–6.5 m.

*Well log signature:* average and increased gamma-ray (10–12$^0$API) and spontaneous potential (SP).

***Slope*** and **deep shelf facies** are represented by clayey siltstones and silty mudstone (Figure 4d).

*Structure*: microbedding, plastic deformation.

*Fauna:* ammonites, foraminifera, bivalves, onychitis, fish remains.

*Admixtures and other features:* carbonaceous detritus, shell detritus, organic matter, carbonate nodules, pyrite.

*Interpretation:* suspension precipitation, low sedimentation velocity, slumping under gravity.

*Thickness:* up to 10 m.

*Well log signature:* increased gamma-ray (9–14$^0$API).

Facies models of $Ach_{5\text{-}6}$ reservoirs are represented in the Figure 5.

The $Ach_5^{2\text{-}3}$ is characterized be the thickest and most productive sandstones. Two parasequences ($Ach_5^2$ and $Ach_5^3$) are identified in $Ach_5^{2\text{-}3}$ based on integrated analysis of core, well log data and seismic. The thickness of these parating shale break changes from 2 to 26 m. For every parasequence submarine fans were identified: northern and southern fans with lobe systems. Northern fans have increased sandstone thickness, compared to southern and can represent exploration targets for drilling new wells. Submarine fans of $Ach_5^2$, $Ach_5^3$ are of mixed sand-clayey type. Lobes and distributary channels are mainly made of sandstones and coarse-grained siltstones. Their content in the section is >70%.

$Ach_6$ deposits formed on the flat slope by clayey systems. Lobes are elongated. Sand sediments are concentrated next to the channels (Figures 5c, d).

Based on a comprehensive analysis of the core,

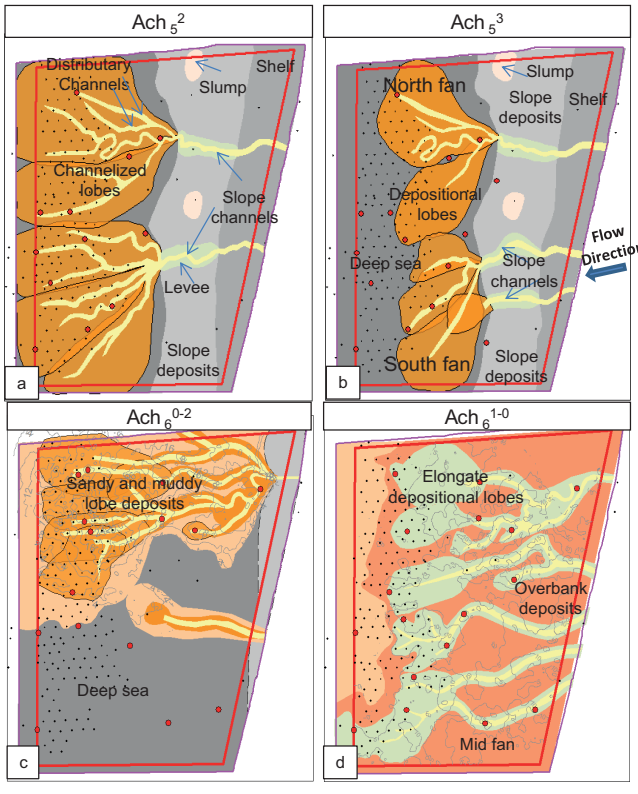


*Fig. 5. Facies models of reservoirs: a – $Ach_5^2$; b – $Ach_5^3$;c – $Ach_6^{0-2}$; d – $Ach_6^{1-0}$. Red spots – wells with the core*

logging, seismic, and well testing data from theAchimov formation, no connectivity of individual lobes was found, which is the reason for varying fluid inflows in the wells. To update the saturation model of the southern submarine fans of $Ach_5^2$ and $Ach_5^3$ reservoirs poorly covered by drilling, interval-by-interval testing as well as wireline formation tests are recommended.

## Summary

The sedimentological analysis of the Achimov formation core showed that the sediments were formed by gravity flows, below the storm wave base, in a relatively deep-water part of the shelf. The material was supplied from east to west. Net-reservoir rocks with the maximum sandstone thicknesses and best reservoir properties (reservoir classes IV and V) are confined to the underwater channels and the proximal parts of turbidite fans of the $Ach_5$ group of reservoirs.

The sediments of the $Ach_6$ group of reservoirs differ from the overlying $Ach_5$ sediments by higher content of mica, carbonate minerals (calcite) and admixture of illite-smectite mixed-layer minerals in the sandstones and siltstones cement and very low permeabilities ($<1*10^{-3}$ μm$^2$).

On the basis of a comprehensive analysis of the core, well logging, and seismic materials, the geological structure of the Achimov stratum was detailed and facies maps of $Ach_5^2$, $Ach_5^3$, $Ach_6^{0-2}$, $Ach_6^{1-0}$ reservoirs were built. Underwater sand lobes and distribution channels are prime targets for exploration and development of the Achimov formation.

Depending on the structure and saturation model of submarine fans, decisions should be made on adjusting the trajectory of horizontal wellbores and optimizing the hydraulic fracturing design.

## Acknowledgments

*The authors are grateful to the Management of CJSC «Rospan International» for the opportunity to study the Lower Cretaceous deposits in detail, for valuable comments and recommendations in the process of research.*

## References

Alekseev V.P. (2002). Lithologic and facies analysis: study guide to practicum and self-guided work on “Lithology”. Ekaterinburg: USMU, 147 p. (In Russ.)

Alekseev V.P. (2014). Atlas of subaqueous facies of the Lower Cretaceous deposits of Western Siberia (Khanty-Mansi Autonomous Okrug-Yugra). Ekaterinburg: UGGU, 284 p. (In Russ.)

Baraboshkin E.Yu. (2011). Practical sedimentology. Terrigenous reservoirs. Core Handbook. Tver: GERS, 153 p. (In Russ.)

Borodkin V.N., Kurchikov A.R. (2015). To the problem of refining the Western and Eastern boundaries of the Achimov clinoform complex (West Siberia). *Russian Geology and Geophysics*, 56(9), pp. 1630–1642.

Bouma A.H. (2000). Coarse-grained and fine-grained turbidite systems as end member models: applicability and dangers. *Marine and Petroleum Geology*, 17, pp. 137–144. https://doi.org/10.1016/S0264-8172(99)00020-3

Catuneanu O. (2006). Principles of sequence stratigraphy. UK: Elsevier. 375 p.

Decision of the 6th Interdepartmental Stratigraphic Meeting on the review and adoption of updated stratigraphic schemes of Mesozoic sediments of Western Siberia. (2004). Novosibirsk, 114 p. (In Russ.)

Dodd T.J.H., McCarthy D.J., Richards P.G. (2018). A depositional model for deep-lacustrine, partially confined, turbidite fans: Early Cretaceous, North Falkland Basin. *Sedimentology*, 66, pp. 53–80. https://doi.org/10.1111/sed.12483

Einsele, G. (1992). Sedimentary Basins Evolution, Facies, and Sediment Budget. Berlin: Springer-Verlag, 628 p. https://doi.org/10.1007/978-3-642-77055-5

Gurari F.G. (2003). Structure and formation conditions of clinoforms of Western Siberian plate (the history of presenting). Novosibirsk: SNIIGGiMS, 141 p. (In Russ.)

Kontorovich A.E., Ershov S.V., Kazanenkov V.A., Karogodin Y.N. et al. (2014). Cretaceous Paleogeography of the West Siberian sedimentary basin. *Russian Geology and Geophysics,* 55(5-6), pp. 582–609.

Lowe D.R. (1982). Sediment gravity flows; II, Depositional models with special reference to the deposits of high-density turbidity currents. *Journal of Sedimentary Petrology*, 52/1, pp. 279–297. https://doi.org/10.1306/212F7F31-2B24-11D7-8648000102C1865D

Mutti E. (1992). Turbidite sandstones: Agip Instituto di Geologia Universita di Parma, Parma, Italy, 275 p.

Nezhdanov A.A., Ponomarev V.A., Turenkov N.A., Gorbunov S.A. (2000). Geology and oil saturation of Achimov sequence of the Northern Siberia. Moscow: Academy of Mining Sciences, 247 p. (In Russ.)

Nichols G.J. (2012). Sedimentology and stratigraphy. 2nd ed. Wiley-Blackwell, Chichester, 419 p.

Normark W.R. (1970). Growth patterns of deep sea fans. *AAPG Bulletin*, 54, pp. 2170–2195. https://doi.org/10.1306/5D25CC79-16C1-11D7-8645000102C1865D

Normark W.R. (1974). Submarine canyons and fan valleys: factors affecting growth patterns of deep-sea fans. In: R.H. Dott, Jr. and R.H. Shaver, eds., *Modern and ancient geosynclinals sedimentation.* SEPM Special Publication, 19, pp. 56–68. https://doi.org/10.2110/pec.74.19.0056

Prelat A., Hodgson D.M., Flint S.S. (2009). Evolution, architecture and hierarchy of distributary deep water deposits: a hight-resolution outcrop investigation from the Permian Karoo Basin, South Africa. *Sedimentology* 56(7), pp. 2132–2154. https://doi.org/10.1111/j.1365-3091.2009.01073.x

Reading H.G., Richards M. (1994). Turbidite Systems in Deep-Water Basin

Margins Classified by Grain Size and Feeder System. *AAPG Bulletin*, 78(5), pp. 792–822. https://doi.org/10.1306/A25FE3BF-171B-11D7-8645000102C1865D

Stow D.A.V. (1976). Deep water sands and silts on the Nova Scotian Continental Margin. *Mar. Sedim.* 12, pp. 81–90. https://doi.org/10.4138/1841

Syngaevsky P.E., Khafizov S.F., Shimansky V.V. (2015). Deepwater alluvial cones and turbidites. Moscow: IKI, 480 p. (In Russ.)

Walker R.G. (1992). Turbidites and submarine fans. In: Walker R.G., James N.P. (Eds.), *Facies Models – response to sea level change*, 2 ed. Geological Association of Canada, St. John's, Newfoundland, Canada, pp. 239–263.

Zhemchugova V.A. (2014). Practical application of reservoir sedimentology in modeling hydrocarbon systems. Moscow: Gubkin Russian State University of Oil and Gas, 344 p. (In Russ.)

Zverev K.V., Kazanenkov V.A. (2001). Sedimentogenesis of deposits of the Achimov strata in the northern Ob region. *Geologiya i geofizika*, 40(8), pp. 12–23. (In Russ.)

## About the Authors

*Alena V. Khramtsova* – Cand. Sci. (Geology and Mineralogy), Expert in lithology and sedimentology of terrigenous reservoirs, LLC «Tyumen Petroleum Research Center».

42 M. Gorkogo st., Tyumen, 625048, Russian Federation

*Sergey I. Pakhomov* – Team leader, LLC «Tyumen Petroleum Research Center».

79/1 Osipenko st., Tyumen, 625000, Russian Federation

*Nikita Y. Natchuk* – Head of Department, LLC «Tyumen Petroleum Research Center».

79/1 Osipenko st., Tyumen, 625000, Russian Federation

*Maria P. Kalashnikova* – Chief Specialist, LLC «Tyumen Petroleum Research Center».

79/1 Osipenko st., Tyumen, 625000, Russian Federation

*Sergey V. Romashkin* – Deputy CEO-Chief geologist, CJSC «Rospan International».

16v Geologorazvedchikov st., New Urengoy, 629300, Russian Federation

*Artem D. Musikhin* – Cand. Sci. (Geology and Mineralogy), Chief Specialist, CJSC «Rospan International».

16v Geologorazvedchikov st., New Urengoy, 629300, Russian Federation

*Nadezhda G. Semenova* – Chief Specialist, CJSC «Rospan International».

16v Geologorazvedchikov st., New Urengoy, 629300, Russian Federation

*Manuscript received 5 November 2020;*
*Accepted 28 May 2020; Published 30 September 2020*

ORIGINAL ARTICLE
**DOI**: https://doi.org/10.18599/grs.2020.3.62-68
Russian Original 2020. Vol. 22. Is. 3. Pp. 62–68

# Petro-elastic modeling deliverables for the Kharyaga Permian carbonate deposits

*S.I. Gusev*
*ZARUBEZHNEFT-Dobycha Kharyaga LLC, Moscow, Russian Federation*
*E-mail: segusev@nestro.ru*

**Abstract**. The purpose of this study is petro-elastic modeling of the Permian deposits occurring in the Kharyaga field, which is located in the Nenets Autonomous District of the Arkhangelsk Region and is confined to the Timan-Pechora Oil and Gas Province. The formations concerned are represented by the Artinskian and Asselian-Sakmarian deposits, which are mainly composed of carbonate sediments admixed with terrigenous material. At the first stage of the petro-elastic modeling, the initial data quality is evaluated, candidate wells are selected, logging curves for the target formation intervals are adjusted and normalized. After that, a comprehensive interpretation of the well logging data is carried out; reservoirs are identified; porosity and oil saturation are evaluated. At the next stage, a petro-elastic model is built, and analysis is carried out in order to understand whether or not reservoirs can be identified and to evaluate a saturation type within the range of elastic parameters. In such case, the elastic model is selected as a function of sedimentation and diagenetic processes, saturating fluid content, etc. As a result of the modeling process, reservoir/non-reservoir zoning was identified based on acoustic and shear impedance; a relationship between the acoustic impedance and porosity was also established. No correlation between the elastic parameters and the saturation type has been established, which may be attributable to hardness of the carbonate matrix and similar elastic properties of oil and water.

**Keywords**: petro-elastic modeling, well logging, porosity, acoustic impedance, shear impedance, oil saturation, carbonate reservoirs

**Recommended citation**: Gusev S.I. (2020). Petro-elastic modeling deliverables for the Kharyaga Permian carbonate deposits. *Georesursy = Georesources*, 22(3), pp. 62–68. DOI: https://doi.org/10.18599/grs.2020.3.62-68

## Introduction

One of the methods to predict structural and reservoir properties is a seismic inversion that helps to evaluate lithological specifics, permeability and porosity, and saturation of the deposits concerned. At the same time, the seismic data inversion can be regarded as a deterministic or stochastic task that provides more opportunities to adapt the deliverables to a priory geological information.

The purpose of the seismic data inversion is to restore the following attributes: acoustic impedance, shear impedance and density. The next link between the elastic characteristics and permeability and porosity of the deposits is a petro-elastic model, which can be derived based on both theoretical and empirical data. For carbonate rock study, inclusion model can be used that approximates a rock as a homogeneous isotropic elastic body, which contains pore inclusions. Since the inclusions (pores) are less hard, as compared to minerals, they significantly impact general elastic rock properties. Such models are referred to as effective carbonate media models. Among the effective models, a differential effective model, self-consistent model, etc, are differentiated (Development of a petro-elastic modeling…, 2018).

The purpose of this study is to provide an assessment in order to understand whether or not the Kharyaga Permian deposits can be disaggregated by reservoirs/non-reservoirs and by saturation types within the elastic parameters range, based on the petro-elastic modeling method.

Given the task set, the following objectives are to be pursued (Sokolova, Popravko, 2012):

- To adjust, normalize and synthesize the logging curves;
- To analyze the main petro-elastic modeling methods and to select the best one;
- To build a petro-elastic model and analyze the effect of the saturation type on the logging curve response;
- To analyze the modeling deliverables and to support recommendations for further seismic inversion.

To pursue each of those objectives, a geoscience data

set was used including lithology and petrophysical study of the core samples, well logging and testing data. The modeling covered 10 wells, which drilled the Permian deposits and had the most representative logs. For the data processing, the Paradigm's Geolog 18 software was used.

## General field information

The Kharyaga oil field is located in the Nenets Autonomous District of the Arkhangelsk Region and is confined to the Timan-Pechora Oil and Gas Province.

The formations concerned include the Artinskian (P1ar) and Asselian-Sakmarian (P1a+s) deposits. The main source minerals of P1ar consist of quartz (49%) and calcite (41%). The grain size distribution analysis carried out for the core samples taken from P1ar shows that the sandstone fraction in the rock matrix is marginal (less than 3%). A share of the siltstone fraction exceeds 30%. Hence, the P1ar reservoirs are represented by argillaceous siltstones. Artinskian calcite serves as cement. Porous-type reservoirs are of primary occurrence in the P1ar deposits.

The mineral analysis of the core samples has shown that calcite is the main source mineral in P1a+s – its average concentration is 93.5%. The carbonate cross-section of P1a+s features the presence of reservoirs that have complex pore geometry (Estimation of geological reserves…, 2017).

## Logging curves normalization

The first stage of the petro-elastic modeling was to evaluate the quality of the logging curves used, to normalize and to restore the curves in the wash-out and log skip intervals. As the method to normalize the curves, a method was selected that enabled comparison of the curves distribution in the pay zone interval, as there was no marker formation, which lithology, petrophysical and stress-strain characteristics had been confirmed. All the studied wells are located within one pad, and, therefore, this rules out variability of the pay zone lithology and petrophysical characteristics that may be driven by the in-fill trend or lateral variability. The bar charts, which were built for all the studied wells, have shown that some of the wells feature a considerable deviation of the median value, as compared to main data selected (Figure 1):

The neutron porosity, bulk density, S and P-wave travel time curves in the wash-out and log skip intervals were adjusted based both on two-dimensional (Figure 2) and multi-dimensional petrophysical relationships with other (neutron and induction log) curves, and on empiric equations, like Gardner-Castagna relationship (equation 1) and Greenberg-Castagna relationship (equation 2) for pure limestones (Gardner, 1974). The curves were normalized, as a rule, through additive correction.

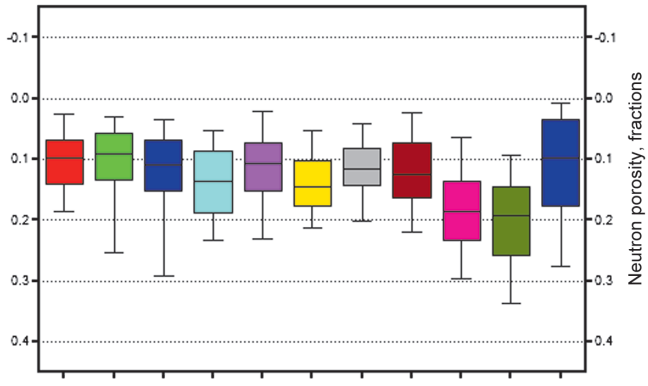


*Fig. 1. Neutron porosity distribution in the pay zones before the logging curves were normalized and adjusted. The color represents different wells.*

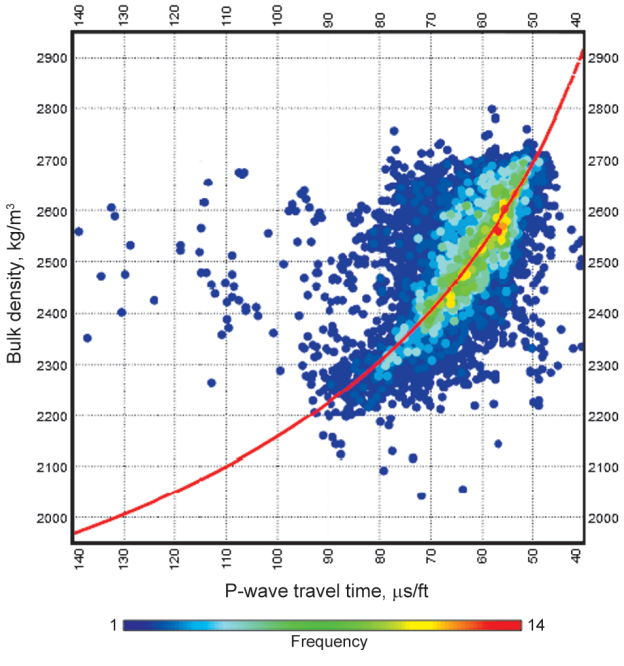


*Fig. 2. Density vs. travel time*

$$\rho = -0.0296 \cdot Vp^2 + 0.461 \cdot Vp + 0.963, \quad (1)$$

$$Vs = a \cdot Vp - b, \quad (2)$$

where $\rho$ – rock density, g/cm$^3$; $V_p$ – P-wave travel time, km/s; and $V_s$ – S-wave travel time, km/s.

An example showing a restored P-wave travel time curve is presented in Figure 3.

An example of normalized bar charts showing neutron porosity distribution is presented in Figure 4.

## Log interpretation

The next stage includes a comprehensive interpretation of the well logging data; reservoirs identification; porosity and oil saturation evaluation. To accomplish this task, a linear and nonlinear equation method was used to trace a relationship between physical properties of the minerals and fluids and the logging curves response. Such approach, for instance, has been implemented in the Multimin module of the Geolog 18 software. Based

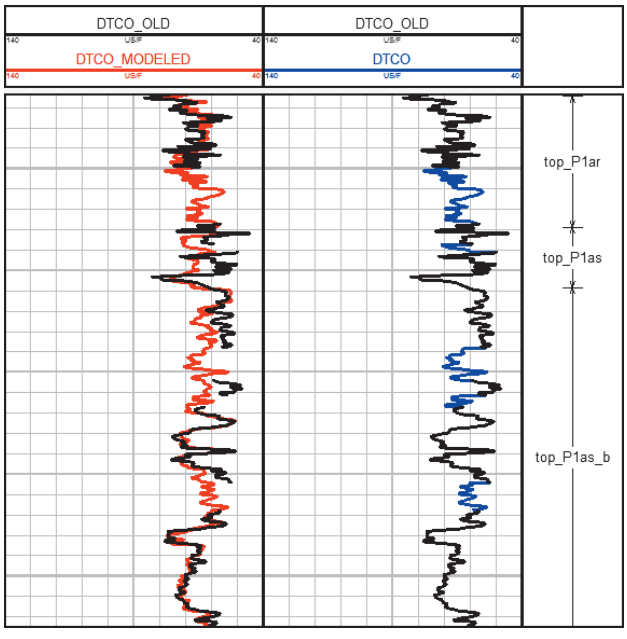


*Fig. 3. An example showing a restored P-wave travel time curve for log skip intervals. The colors represent the following: black indicates a recorded log curve; red indicates a synthetic curve, blue indicates a restored curve for the log skip intervals.*

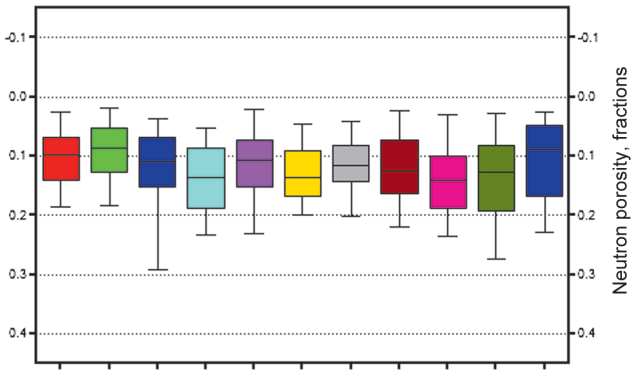


*Fig. 4. Neutron porosity distribution in the pay zones after the logging curves were normalized and adjusted. The color represents different wells.*

on the lithology and petrophysical study of the core and mud logs from the wells drilled, calcite, illite and quartz were selected as minerals to be simulated. Oil and water were selected as the pore fill. The following parameters were selected as arrival curves for the Multimin module: bulk density, neutron porosity calibrated to the limestone matrix, P-wave travel time, photoelectric factor, natural radioactivity, resistance in the washed-out and non-logged zones of the reservoir. To calculate the saturation, the Archie-Dakhnov equation was used, with the m and n factors being derived based on the core study. The produced water resistance was calculated based on salinity of samples taken, considering the reservoir temperature effect (Petersilier, 2003)

As a result, mineral models were derived, and fluids distribution was identified within the studied Artinskian and Asselian-Sakmatian deposits for each of the wells on the pad concerned. The reservoirs were identified based on cut-off porosity for each of the formations. The cut-off porosity was determined based on comprehensive core analysis, WFT, DST and formation testing data. A saturation type was determined based on the water saturation cut-off value, taking into account the accepted OWC (Figure 5).

As validation criteria for the resulting petrophysical model, the core data were used. Unfortunately, no core study data are available for the wells from this pad, which makes the direct comparison difficult. However, a lot of core studies have been run for the Artinskian and Asselian-Sakmarian deposits throughout the field, and given the consistency and regularity of permeability and porosity across the area, the relevant generalized average values can be used for comparison.

To study P1ar permeability and porosity, 682 core samples from 30 wells were used, out of which 171 samples represent reservoirs. P1ar porosity, which was measured on standard samples using the NaCl saturation method, varies from 0.3% to 37%, with the average value being 10.8%. The porosity in P1ar reservoirs varies between 14% and 37%; with the average reservoir porosity for 171 samples being 19.8%.

According to the logs, the average porosity in the Artinskian reservoirs is 20.3% (Figure 6).

To study P1a+sr permeability and porosity, 1336 core samples from 32 wells were used. P1a+s consists of the lower and upper layers. The upper layer has enhanced

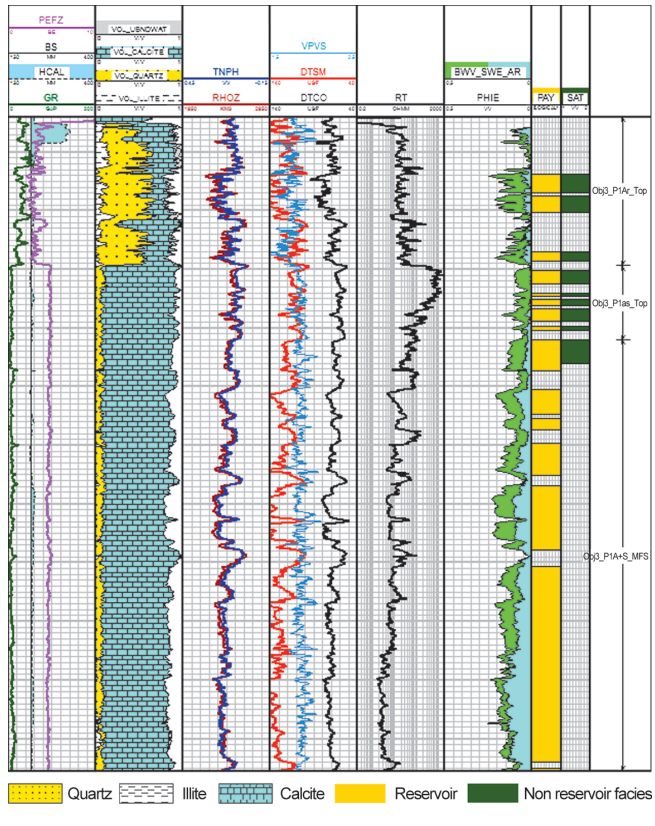


*Fig. 5. An example of a petrophysical model built for one of the wells*

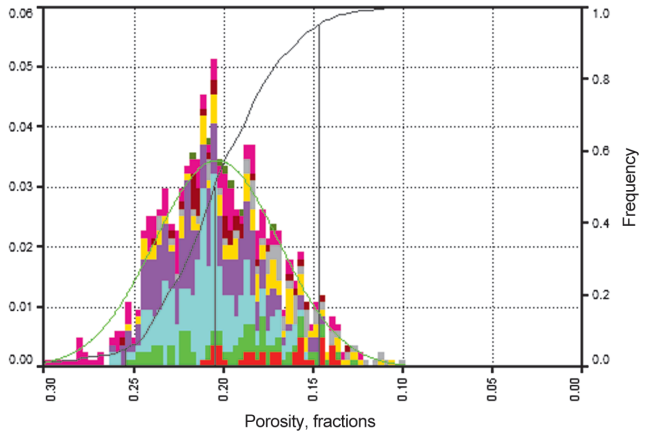


*Fig. 6. Porosity distribution in the Artinskian deposits as per the logs. The color represents different wells.*

reservoir properties. P1a+s permeability and porosity have been considered both as part of one single Object and by separate layers.

P1a+s porosity, which was measured on standard samples using the NaCl saturation method, varies from 0.29% to 26.6%, with the average value being 10.12%. The porosity in the upper layer of P1a+s varies between 8% and 26.6%; with the average reservoir porosity for 246 samples being 13.56%. The porosity in the lower layer of P1a+s varies between 11% and 24.6%; with the average reservoir porosity for 375 samples being 15.7%.

According to the logs, the average reservoir porosity in the upper layer of P1a+s is 11.9%, and that in the lower layer is 16.7%.

Hence, a conclusion can be reached that the resulting petrophysical model is consistent. Apart from that, the reservoir intervals and the estimation of the reservoir saturation were confirmed by the data from repeatable/wireline formation tests run in 4 wells and by the cased hole test data.

## Petro-elastic modeling

At the next stage, a petro-elastic model is built, and analysis is carried out in order to understand whether or not reservoirs can be identified and to evaluate a saturation type within the range of elastic parameters. When selecting a model, the following specific features of the carbonate deposits should be considered (Development of a petro-elastic…, 2018):

Nonlinear relationship between porosity and elastic parameters, which is attributable to the impact of the pore geometry in the carbonate rocks;

Slight impact of the fluid type on the wave speed, which is attributable to the high hardness of the matrix;

The carbonate reservoir quality is not necessarily attributable to high porosity. Reservoir permeability and fluid filtration depend on the presence of fractures.

The multiple use of P- and S-waves velocities is such case is not so efficient, as compared to terrigenous rocks. The Poison's ratio, as a rule, slightly changes.

After the compressibility, density and P-wave travel time moduli for oil and water were determined, those parameters were also calculated for a fluid mixture, taking into account the actual oil saturation of the formations, based on a homogeneous mixing model, where the effective compressibility modulus is estimated based on the Reuss average (equation 3):

$$\frac{1}{K_{fl}} = \frac{S_1}{K_1} + \cdots + \frac{S_i}{K_i}, \quad (3)$$

where $K_{f1}$ – fluid mixture compressibility modulus; $K_i$ – compressibility modulus for the i-th component of the mixture; and $S_i$ – saturation by the i-th component.

Based on the 3D mineral model resulting from the data interpretation, density, P- and S-wave velocities, Poisson's ratio, compressibility and shear moduli, as well as Voight upper bound and Royce low bound for the mineral mixture were calculated.

The resulting parameters were used for simulation of the elastic properties in a saturated rock, based on the effective differential model, with allowance made for various aspect ratios of the pore volume in the Artinskian and Asselian-Sakmarian deposits. The match between the simulated P- and S-wave travel time and density curves and the actual open hole log data was used as a validity criterion for the modeling (Figure 7). The resulting variance between the recorded and simulated logging curves does not normally exceed 5% and may be attributable to the source data quality.

The resulting petro-elastic model can not only simulate the impact of the permeability and porosity change on the elastic parameters, but can also predict the impact of a change in the reservoir saturation type on the elastic parameters, and, as consequence, on the seismic

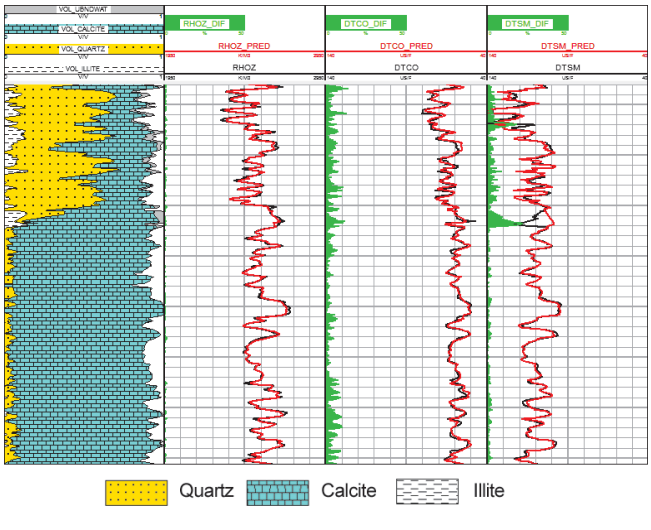


*Fig. 7. Recorded vs simulated values of bulk density, P- and S-wave travel time. The black color represents the recorded logging curves, the red color represents the simulated curves, and the green color displays the percentage variance.*

response, based on the Gassmann theory (equation 4) (Batzle, Wang, 1992).

$$\frac{K_{sat}}{K_0 - K_{sat}} = \frac{K_{dry}}{K_0 - K_{dry}} + \frac{K_{fl}}{phi \cdot (K_0 - K_{fl})} \quad (4)$$

where $K_{dry}$ – dry rock compressibility modulus; $K_{sat}$ – saturated rock compressibility modulus; $K_o$ – composing mineral mixture compressibility modulus; $K_{fl}$ – fluid mixture compressibility modulus; and *phi* — porosity.

To determine elastic characteristics that can be used for disaggregation by reservoirs/non-reservoirs and by saturation types, cross-plots and distribution bar charts were built.

Following the study completed, disaggregation by reservoir/non-reservoir was confirmed based on acoustic and shear impedance at the scale used for petrophysical data (Figures 8–9).

Relationship between acoustic, shear impedances and porosity was identified. This is a linear relationship, which depends on a type of a pore fluid (Figure 10).

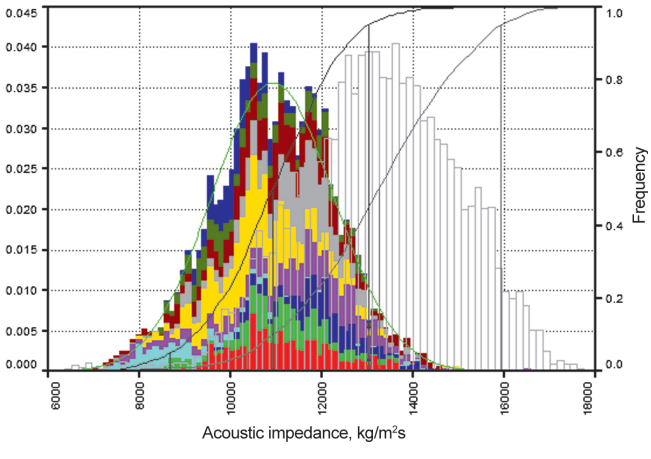


*Fig. 8. Disaggregation by reservoir/non-reservoir based on acoustic impedance. The color fill indicates the reservoir (the color represents different wells), the transparent fill indicates the non-reservoir.*

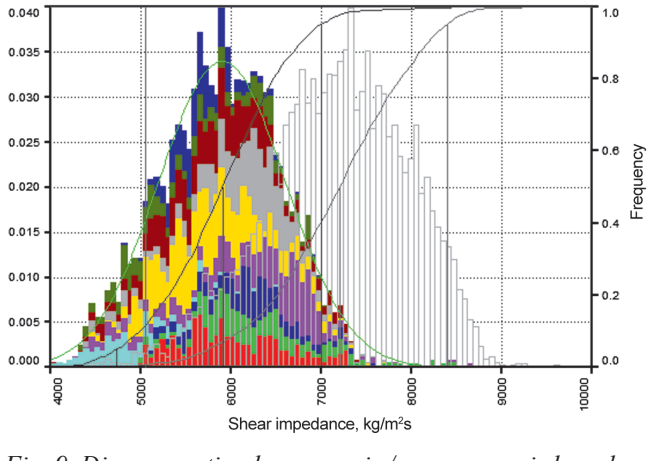


*Fig. 9. Disaggregation by reservoir / non-reservoir based on shear impedance. The color fill indicates the reservoir (the color represents different wells), the transparent fill indicates the non-reservoir.*

The elastic parameters do not differ a lot by a saturation type, and this was confirmed both by the actual data and by the simulation results (Figures 11–12), which makes it impossible to determine cut-off parameters to be able to identify a saturation type, using the seismic data.

As seen from Figure 11, the change in the saturation type from water to oil results in typical decrease in bulk density and P-wave velocity. The P-wave velocity

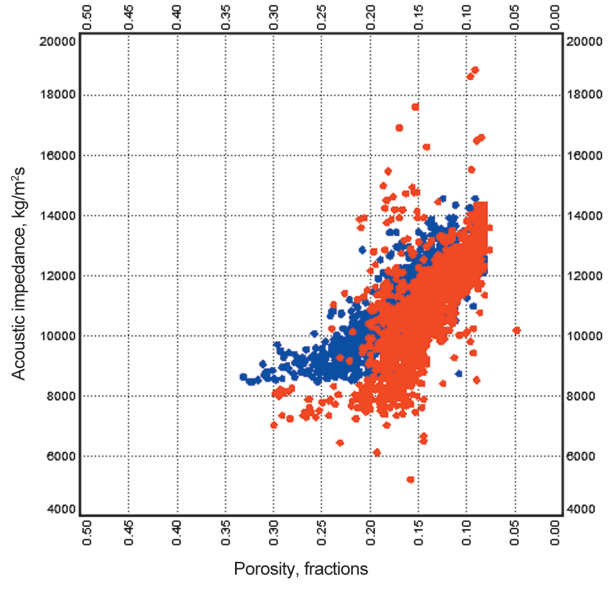


*Fig. 10. Acoustic impedance vs. porosity for oil saturated and water saturated reservoirs. The blue and red colors accordingly represent water saturated and oil saturated reservoirs.*

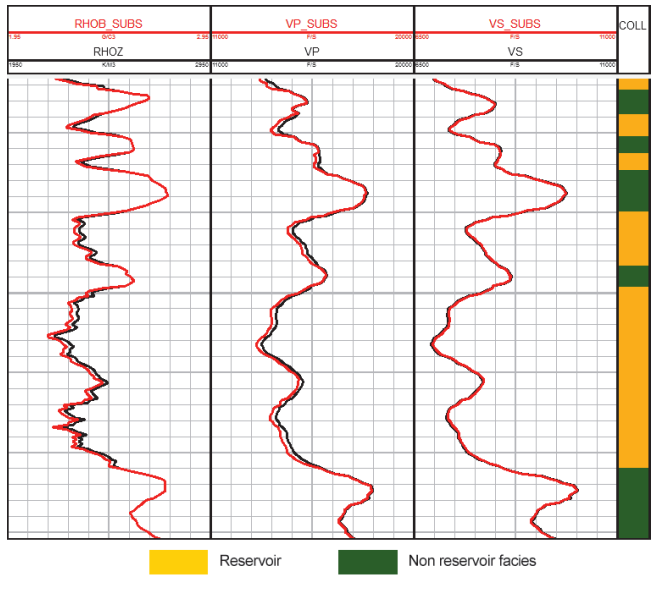


*Fig. 11. An example showing simulation of the reservoir saturation type change from water to oil in one of the wells. The colors represents the following: black displays the logging curves recorded in the water saturated section of the formation; red displays displacement of water with oil after simulation; RHOB – bulk density, VP – P-wave velocity, VS – S-wave velocity, yellow fill displays the reservoir intervals; the green fill shows compact varieties.*

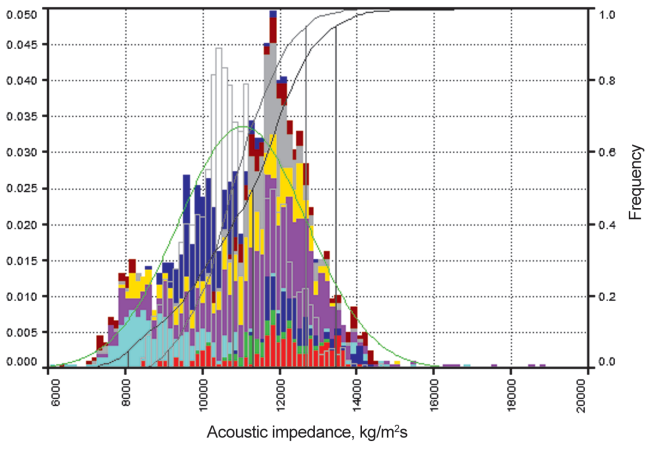


*Fig. 12. Acoustic impedance distribution by saturation type. The color fill indicates water saturated reservoirs (the color represents different wells), the transparent fill indicates oil saturated reservoirs.*

however does not almost change, which is confirmed by the physics of the method.

Apart from that, to study the lithology impact on the elastic characteristics of the deposits, relationship was plotted between the volumetric content of calcite in the rock matrix and density, P- and S-wave travel time.

The actual data confirmed the linear relationship between the volume of calcite, illite and quartz in the rock and the bulk density in the Artinskian and Asselian-Sakmarian deposits.

The relationship between the lithology and P- and S-wave travel time takes different forms for the Artinskian and Asselian-Sakmarian deposits, which can be illustrated in Figure 13.

The modeling of the logging curves response as a function of different calcite and quartz content in

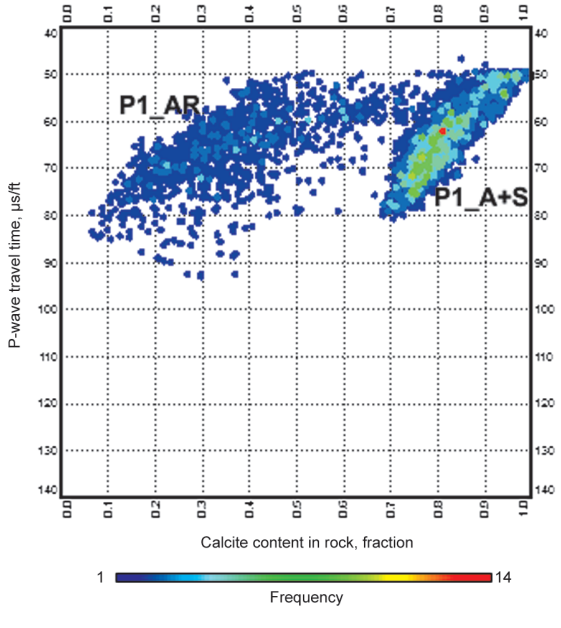


*Fig. 13. Relationship between the P-wave travel time and calcite volume in rock*

rock supports the assumption that variability in the relationships between the S-wave travel time and calcite content in the rock matrix may be explained not only by non-linear petrophysical equation, but also by the impact of Atrinskian shales and calcite cement on the P- and S-wave speed.

Such conclusion confirms the need to use at least 3 different minerals (quartz, illite, and calcite) when building a 3D petrophysical and petro-elastic model, and the need to use different aspect ratios of the pore volume for the Artinskian and Asselian-Sakmarian deposits, given the difference in the pore geometry and in intergranular cement properties.

## Conclusion

Based on the petro-elastic modeling of the Kharyaga Permian deposits, it was established that they can be disaggregated by reservoirs/non-reservoirs using the acoustic and shear impedance; AVO/AVA inversion (Amplitude Versus Angle/Offset) was also found applicable to evaluation of porosity in the space between the wells. It was also established that there was no disaggregation by a saturation type, which may be attributable to the fact that water and oil have similar properties (density, travel time), as well as to the high hardness of the carbonate rock matrix, which alters the effect of the saturating fluid. These results are correlated with the Gubkin Russian Oil and Gas University experts' conclusions that have been made following the study of the Devonian carbonate deposits at the West Khosedayu field (Development of a petro-elastic…, 2018).

Given the fact that the ultimate objective of the petro-elastic modeling procedure is to predict the lithology and reservoir properties of the Kharyaga Permian carbonate deposits, the main efficiency criterion for the petro-elastic modeling will be the match between predicted and actual data. As the actual data, information from both new wells and from wells, which have not been used for the simulation process (reference well), may be used. Apart from that, the resulting volumes and maps showing the lithology and petrophysical properties distribution, shall be compliant with the accepted geological concept. For instance, in case of reef sequences, the lateral distribution of the reef facies shall have a well defined shape, depending on a type of the reef structures genesis.

Hence, a conclusion may be reached that these findings serve as prerequisites for using the seismic data inversion in order to predict the reservoirs distribution throughout the Kharyaga field and to evaluate their porosity. The inversion and evaluation of the findings obtained constitute the next stage of the study to predict lateral distribution of the reservoirs and to evaluate their permeability and porosity.

## References

Batzle M, Wang Z. (1992). Seismic properties of pore fluids. *Geophysics*, 57, pp. 1396-1408. https://doi.org/10.1190/1.1443207

Development of a petro-elastic modeling technique for predicting the lithology and reservoir properties of carbonate deposits of the West Khosedayu deposit. (2018). Moscow: Gubkin Russian State University of oil and gas.

Estimation of geological reserves of oil, dissolved gas and associated components of the Kharyaga oil field. (2017). Moscow: VNIIneft.

Gardner G.H.F. (1974). Formation velocity and density – The diagnostic basics for stratigraphic traps. *Geophysics*, 39, pp. 770-780. https://doi.org/10.1190/1.1440465

Petersilie V.I. (2003). Guidelines for calculating the geological reserves of oil and gas by the volumetric method. Moscow-Tver, 259 p.

Sokolova T.F., Popravko A.A. (2012). Problems of modeling the elastic properties of rocks according to geophysical research of wells for seismic inversion. *Collected papers UkrGRI,* 4, pp. 139-157.

## About the Author

*Sergey I. Gusev* – Head of Well Logging Section, ZARUBEZHNEFT-Dobycha Kharyaga LLC

3 Paveletskaya square, build. 2, Moscow, 115054, Russian Federation

*Manuscript received 12 November 2020;*
*Accepted 2 July 2020; Published 30 September 2020*

ORIGINAL ARTICLE
**DOI**: https://doi.org/10.18599/grs.2020.3.69-78 Russian Original 2020. Vol. 22. Is. 3. Pp. 69–78

# Junction zone stability in coaxial wells of different diameters (on the example of the Khanty-Mansi Autonomous District oil field)

*A.V. Seryakov[1*], M.Yu. Podberezhny[2], O.B. Bocharov[1], M.A. Azamatov[3]*
[1]*Novosibirsk Technology Center, Baker Hughes, Novosibirsk, Russian Federation*
[2]*Gazpromneft-GEO, St. Petersburg, Russian Federation*
[3]*Salym Petroleum Development N.V., Moscow, Russian Federation*

**Abstract**. The paper considers borehole wall stability in a junction zone of coaxial wells where a borehole of bigger diameter connects with a smaller one. To determine the shapes and character of rock destruction, 3D poroelastic modeling of the stressed state of the rock around the coaxial junction with account for mudcake formation was performed. The geomechanical model considers the anisotropy of the medium's deformation properties that are characteristic for the coastal-marine reservoirs of Western Siberia. The rock failure is estimated based on the Mohr-Coulomb criterion with account for tensile destruction condition. The paper considers cases of vertical and inclined junctions of a well drilled at a depth of 2 km in sandstone productive pay with known poroelastic anisotropic properties. The stress and pore pressure analysis has been performed for a mud pressure drop range from 1 to 70 atm and coaxial junctions with different combinations of borehole diameters. The safe mud pressure window has been determined for vertical and inclined junctions. It has been found that the rock failure pattern for junction of bigger diameters is, in general, similar to that for smaller diameters with some insignificant differences in the destruction areas shapes. It has also been demonstrated that in vertical junctions, the bottom holes of smaller diameter are more stable to reduced drilling-mud pressure than the main boreholes, while in the inclined junction it is the main wellbore that is more stable to increased drilling-mud pressure than the bottom hole.

**Keywords**: 3D poroelastic modeling, coaxial junction, vertical and inclined well, anisotropy, rock failure, sandstone reservoir

**Recommended citation**: Seryakov A.V., Podberezhny M.Yu., Bocharov O.B., Azamatov M.A. (2020). Junction zone stability in coaxial wells of different diameters (on the example of the Khanty-Mansi Autonomous District oil field). *Georesursy = Georesources*, 22(3), pp. 69–78. DOI: https://doi.org/10.18599/grs.2020.3.69-78

## Introduction

In prospecting drilling (especially with mobile drilling units) it is a common situation when one has to drill deeper for core sampling and logging, but the unit's capacity does not permit to do it using a bit of the same diameter. This problem is often solved by shifting to a smaller bit diameter to drill in the same hole, but this raises an issue of junction zone stability in such coaxial wells (Figure 1) because intensive bursting of rock chips from a borehole wall leads to their accumulation in the bottom hole.

During sequential core sampling pieces of rock can stick in the core barrel causing its locking that requires additional round-trips to resolve. Moreover, enlarging the bottom hole to match the main wellbore diameter after core sampling and logging are finalized requires the junction zone stability to be assessed.

The stability of different diameters boreholes junction is the relevant problem of core drilling operations at the

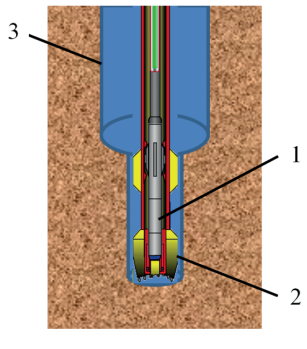


*Fig. 1. Junction zone configuration after core extraction to the sampler barrel (1) in the case when core drilling bit (2) diameter is less than the one of the main borehole (3)*

*Corresponding author: Alexandr V. Seryakov
*E-mail: alexander.seryakov@bakerhughes.com*

oilfields of Khanty-Mansi Autonomous District in Russia (KhMAD). In spite of its urgency the problem statement, description and solution approaches are not presented in the literature sources. It should be noted that there are the similar tasks of tube junction resistance to the inner pressure or external loading increasing (e.g. Grogulenko, 2017) that are solved with the help of the elastoplastic models in commercial computation packages. However such modeling doesn't take into account physical processes in porous rock near the wellbore junction zone at a kilometers depth.

Wellbore stability of the junction should be assessed with the help of the poroelastic modeling that includes non-uniform stress distribution, rock anisotropy, mudcake formation due to the mud filtration into the productive pay.

It should be pointed out that 2D approaches to the stress and pore pressure determination around wellbore (Cui et al., 1997; Liu et al., 2018) have the restricted application in the considered case since the stress distribution close to the junction plane will be essential three dimensional.

Assef Mohamad-Hussein and Julian Heiland (Mohamad-Hussein, Heiland, 2018) successfully performed poro-elasto-plastic modeling and analysis for the multilateral wellbore junction. The hardening porous material model and plastic surface based on the Mohr-Coulomb failure criteria are used in the 3D finite element computations.

We consider the simpler case of wellbore junction configuration and apply the vertical transversely isotropic poroelastic model with mudcake formation taken into account for effective stresses determination and rock failure estimation based on the Mohr-Coulomb criteria.

The modeling goal is the safe mud window determination for the vertical and inclined coaxial wellbore junction.

## Rock characteristics

The modeling was performed for the rocks of the Neocomian age (the Akh Formation productive pays) that belong to the fields of the Surgut Dome and are characterized with the coastal-marine sedimentation conditions. The reservoirs of the formation are aleurolitic sandstones of 13–20% porosity and 10–100 mD permeability (Figure 2) overlaid by argillite-like clays. Cross-dipole acoustic and electromagnetic measurements and core analysis results indicate the anisotropic properties of these rocks (anisotropy coefficient 1–10%). As it was demonstrated in (Seryakov et al., 2018), vertical and inclined wells stability analysis has to be performed considering the anisotropy of rock's poroelastic properties.

## Problem statement

Sandstone productive pay at a fixed depth of 2400 m is considered. At such a depth sandstone's petrophysical properties are anisotropic and experimental data of core deformation tests have the better fit with transversal isotropic poroelastic model.

In the reservoir, we model the junction of vertical and inclined sections of an open well, where a main borehole of bigger diameter $D_1$ meets a bottom hole of smaller diameter $D_2$ (Figure 3). The inclined well is characterized by angle ψ (60°) to the vertical axis and azimuthal angle β (25°) to the direction of the maximum horizontal stress. The model has been considered for two characteristic diameter ratios: I. $D_1$ = 220 mm, $D_2$ = 160 mm; II. $D_1$ = 160 mm, $D_2$ = 120 mm.

It is assumed that both parts of a well in the junction zone experience similar drilling-mud pressure $P_b$ that exceeds reservoir pressure $P_0$ by value dP. The previous studies interpreting electromagnetic measurements from the oilfields of KhMAD have demonstrated that a weakly-permeable mud cake forms on borehole walls while drilling. The laboratory studies such as that of (Podberezhny et al., 2017) determine this layer's permeability to be 0.001 mD. In our modeling, we applied the mudcake growth model presented in (Podberezhny et al., 2017).

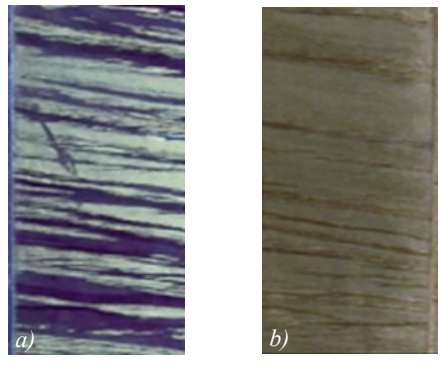


*Fig. 2. Aleurolitic sandstone with lenticular bedding; a) – in ultraviolet light; b) – in daylight*

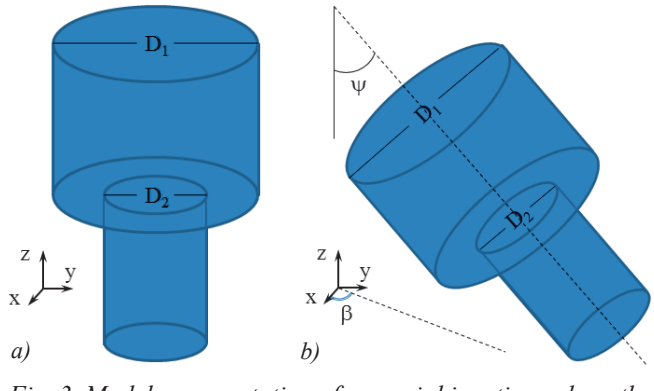


*Fig. 3. Model representation of a coaxial junction, where the main borehole has a bigger diameter than the bottom hole: a) – vertical well, b) – inclined well*

## Poroelastic model

To determine the stress-strain state of the rock surrounding the junction zone, a vertical transversely isotropic poroelastic model was used. Its detailed description can be found in (Cheng, 1997) with the simplifications for poroelastic coefficients presented in (Seryakov et al., 2018). The model is characterized by the homogeneous properties in the plane perpendicular to the symmetry axis Z, which is commonly selected to match rock stratification direction in a geological medium. To describe the deformations of elastic rock matrix one has to set 5 constants that include two Young's modula $E$, $E'$; two Poison's ratios $\nu$, $\nu'$; and one shear module $G'$ (Figure 4). The modeling was performed for a fixed depth and the following constant values: $E' = 12$ *GPa*, $E = 13$ *GPa*, $\nu' = 0.16$, $\nu = 0.17$, $G' = 5.17$ *GPa*.

The medium's permeability was considered equal to 50 mD.

According to geophysics data offered by the operating companies, the Biot-Willis coefficient for the coastal-marine sedimentation reservoirs of KhMAD is $\alpha = 0.95$. The additional poroelastic constants were derived from the main dependencies of the linear poroelastic theory that includes triaxial matrix compression coefficient, fluid compression and porosity coefficients. More details on the constants and their formulas can be found in Bocharov (Bocharov, Seryakov, 2016). Considering that the porosity $\phi = 0.23$, unjacketed bulk compressibility modulus $K'_S = 36$ GPa, fluid compressibility $K_f = 3$ GPa, we obtained the Skempton coefficient B = 0.5 and the Biot module M = 13.38 GPa.

The initial stress state around well was derived from the geophysical data on regional stresses distribution corrected for reservoir microfracturing tests, while the porous pressure was estimated based on logging interpretation results. At the fixed depth, the stresses had the following values: $\sigma_v = \sigma_{zz} = 54$ MPa, $\sigma_{hmax} = \sigma_{xx} = 36$ MPa, $\sigma_{hmin} = \sigma_{yy} = 34$ MPa. The reservoir's porous pressure was $P_0 = 25$ MPa. The ratio of vertical and horizontal stresses indicated the field developed in the normal faulting regime (Zoback, 2010).

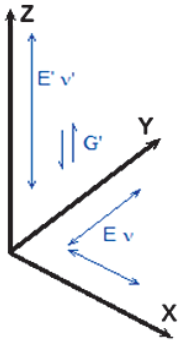


*Fig. 4. Transversal-isotropic modules in a continuum medium*

When modeling the junction's stressed state under pressure, the growing mud cake was taken into account. The considered mudcake properties included mudcake permeability $k_c = 0.001$ mD, porosity $\phi_c = 0.3$, and suspended particle concentration in the drilling mud (6%). Except for the mud cake, we also accounted for colmatation zone assuming the reducing formation permeability $k_d = 5$ mD ( = 0.1k) within 1cm from the well's contour.

The application of a transversely isotropic model to rock deformation description also implies the rock failure criterion in which the strength of the material depends on the angle of inclination of considering plane to the bedding (Ashikhmin, 2018; Geniev, 1993). However due to the lack of experimental data on in-situ rock strength characteristics in different directions, the isotropic Coulomb-Mohr criterion was applied at the first stage of the study:

$$\sigma_1 - \sigma_3 ctg\psi = C_0, \quad (1)$$

where $\sigma_1$, $\sigma_3$ denote the main effective stresses; $ctg\psi = (1+\sin\varphi)/(1-\sin\varphi)$, $\varphi$ is the inner friction angle, $C_0$ is the unconfined compressive strength. Analyzing the rock damage, we considered the equivalent stress function $\sigma_e = \sigma_1 - \sigma_3 ctg\psi$ that is convenient for visualization and comparison against $C_0$. The sandstone's strength properties at the given depth were taken from a laboratory core compression tests and equal to $\varphi = 30°$, $C_0 = 17$ MPa. The critical tensile stress $\sigma_T$ for the sandstone was assigned equal to 1 MPa. The destruction type was determined in relation to the ratio of the main stresses and position relative to the plasticity curve (Fadeev, 1987) determined from (1) and the breaking condition

$$\sigma_1 < -\sigma_T, \quad (2)$$

where we adhered to the statement that tension stresses were negative. Therefore if the medium's stressed state was in the plasticity range, either breakouts or hydrofracturing conditions could be realized in the rock.

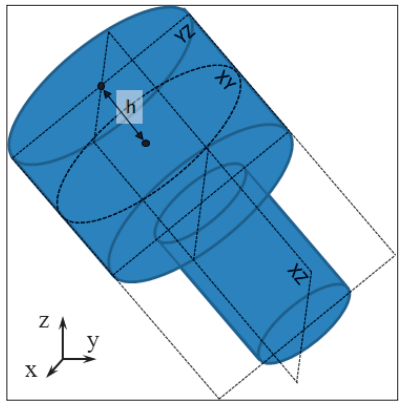


*Fig. 5. Plane sections to visualize rock failure parameters for a 3D model*

The computations were performed using the Geofluid package, whose FEM-based iteration algorithm has been described in particular in (Rudyak et al., 2013).

## Results of modeling

Modeling of the two types of junctions, both vertical and inclined ones, started with a basic case, for which the value of pressure drop on borehole wall was 40 atm and corresponded to the "standard" overpressure while drilling in the hydrocarbon fields of KhMAD. For every other computation that follow, the pressure drop was either increased or reduced by 5–10 atm within a range from 1 to 70 atm.

The destruction area and equivalent stress field visualization in 3D domain was performed along the XY, YZ and XZ plane sections. For the vertical junction, these sections matched the reference planes, while for the inclined one were turned to match the well's angle (Figure 5).

Sections XY were characterized by the distance h from the upper section perpendicular to the well's axis to the studied plane. The distances from the top to the bottom perpendicular sections of the modeled domain was 2 m, and the transition area (from the main hole's diameter to that of the bottom hole) was h = 1.0 m.

## Vertical junction

In the 220/160 mm junction, the standard pressure drop forms a concentric local-depth domain of shear fracturing situated in the main hole next to where the two diameters meet (Figure 6). This figure and the following depict the isolines of the parameter $\sigma_e$. In the figures, the blue digits mark the values of equivalent stresses in MPa and the areas of shear rock failure are filled with red color.

Considering the fact that the destruction is local and that its length along the z-axis is about 5 cm, the junction can be described as conditionally stable.

At the same pressure drop, modeling of a 160/120 mm junction demonstrates a similar character of destruction but with changed equivalent-stress distribution if compared to the previous case (Figure 7).

In fact, redistribution of formation stresses occur at the level of h = 1 m (right at the junction) and the differences

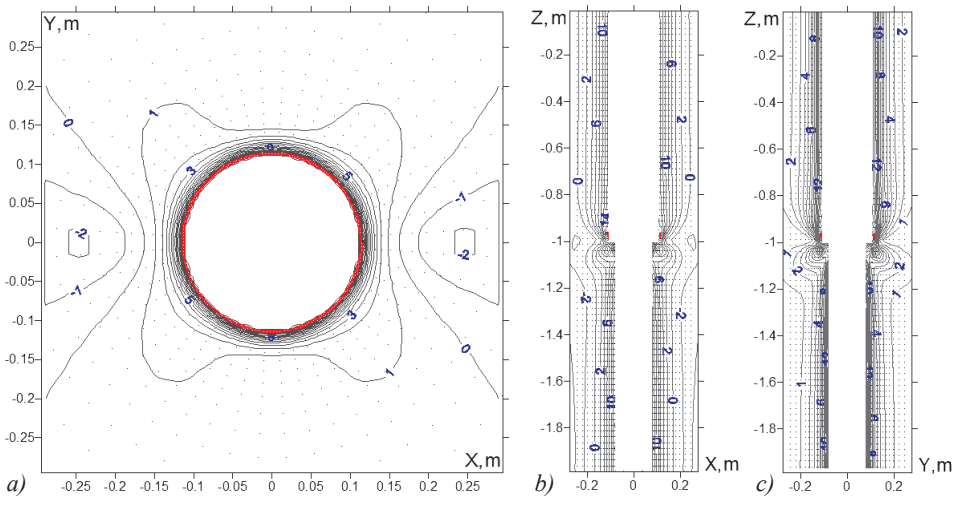


*Fig. 6. Destruction areas in a vertical 220/160 mm junction at dP = 40 atm: the XY (a, h = 0.99 m), XZ (b), YZ (c) planes*

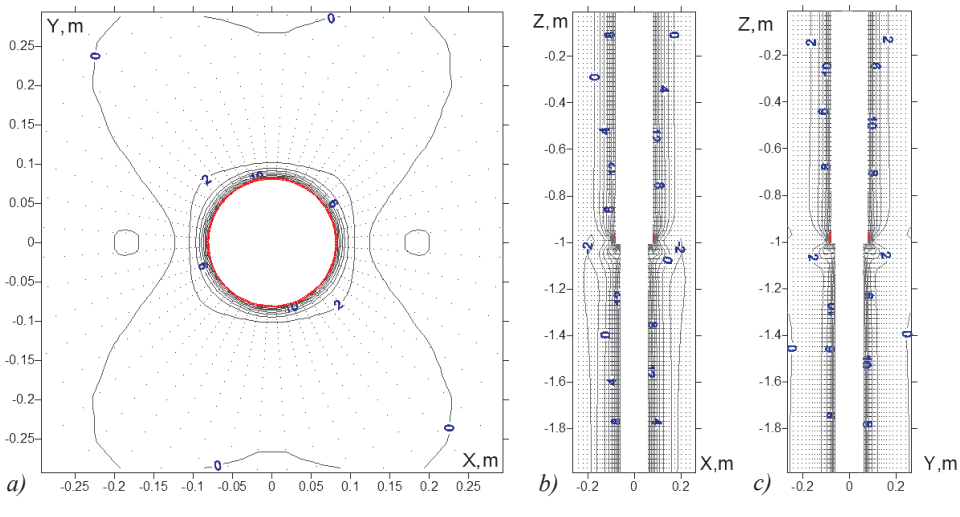


*Fig. 7. Destruction areas in a vertical 160/120 mm junction at dP = 40 atm: the XY (a, h = 0.99 m), XZ (b), YZ (c) sections*

in the stress value $\sigma_в$ between the two junctions may exceed 50%. Moreover, for the 160/120 mm junction the stress gradients increase and the stresses change faster than those of 220/160 mm junction. However, when it comes to the midsections of the wells (h = 0.5 m, h = 1.5 m), $\sigma_в$ behaves much smoother, so the differences between the cases do not exceed 12%.

If the pressure drop decreases to 35 atm, the rock failure area around the main borehole starts to spread downward into the formation forming the semiring depicted in Figure 8.

The formation around the 160/120 mm junction experiences similar changes but the rock failure area forms a closed ring below the main diameter (Figure 9).

Thus, one should expect concentric pieces of rock to split off from the wall and fall down into a borehole of the smaller diameter while drilling an uncased well.

Further decrease in the pressure drop results in the widening of the shear fracturing area that spreads deeper into the formation and propagating along the walls of wellbore both bigger and smaller diameters (Figure 10). In other words, drilling at a pressure drop of below 40 atm makes the junction's walls unstable.

In the opposite scenario, when the pressure drop increases to 55 atm, the rock failure area in the main borehole reduces, breaking the ring of fractured rock as shown in Figure 11. It is noteworthy that in the 160/120 mm junction, the width of the fracturing area also reduces (Figure 11 c).

Further dP increase up to 60 atm leads to complete elimination of the fracturing areas in the vertical junctions. It is noteworthy that even at 70 atm, dP increase does not provoke hydrofracturing.

## Inclined junctions

In an inclined 220/160 mm junction, the standard dP of 40 atm induces breakouts of both main and bottom holes, which can be seen from the XY sections at heights of h = 0.99 m (a) and h = 1.01 m (b) on Figure 12. Moreover, the junction's shoulder contains a

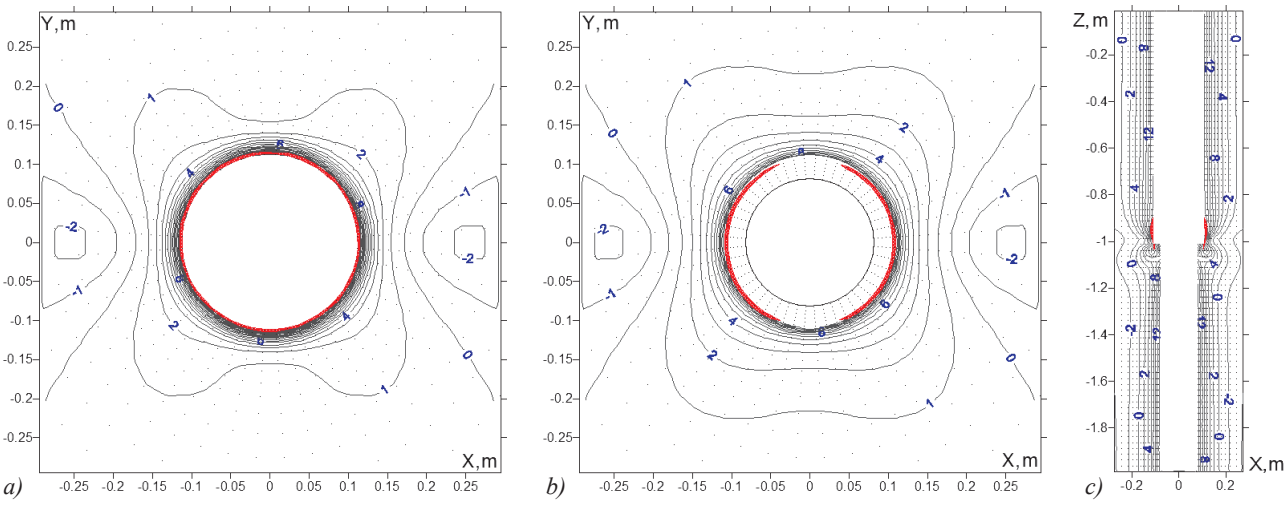


*Fig. 8. Rock failure propagation in a vertical 220/160 mm junction at reduced dP (35 atm). The XY section is shown for h = 0.99 m (a) and h = 1.01 m (b). The vertical extent of the fracturing area is shown in the XZ section (c)*

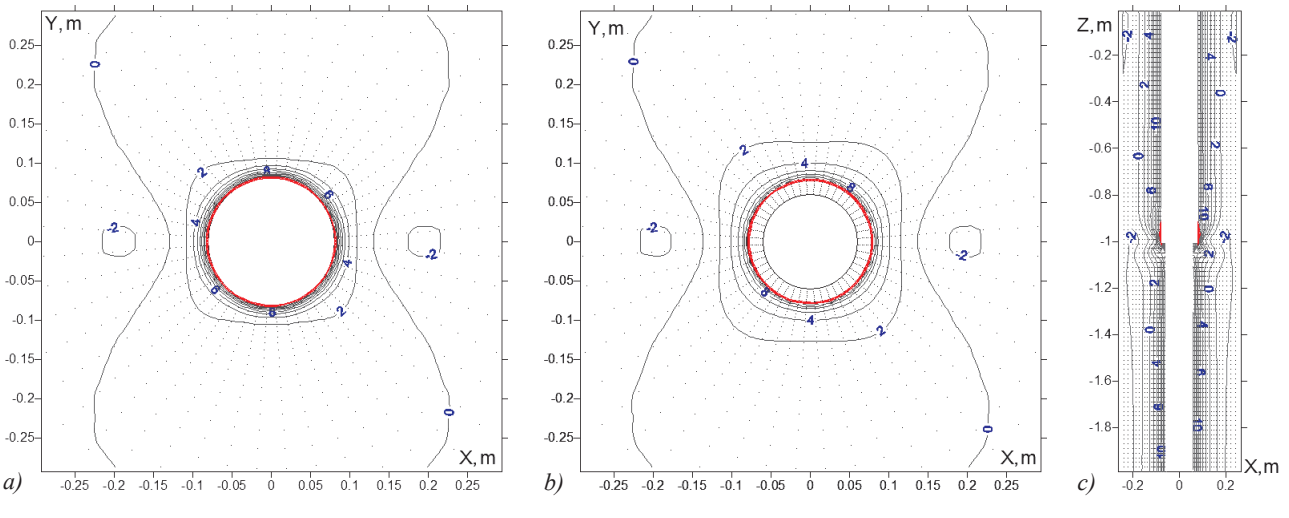


*Fig. 9. Rock failure propagation in a vertical 160/120 mm junction at reduced dP (35 atm). The XY section is shown for h = 0.99 m (a) and h = 1.01 m (b). The vertical extent of the destructed area is shown in the XZ section (c)*

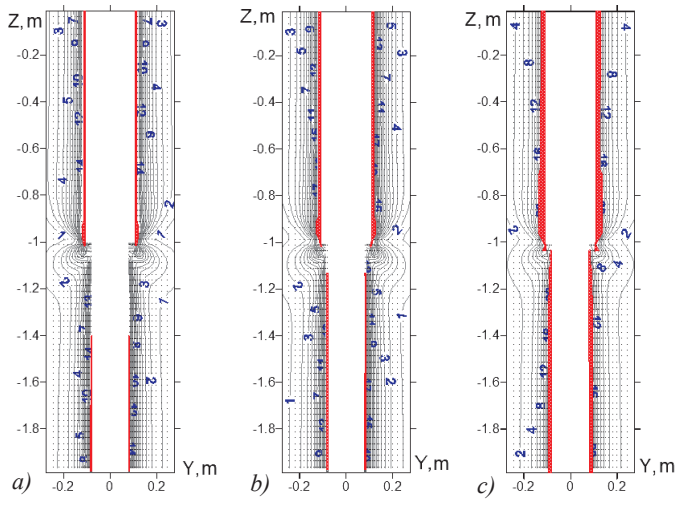


*Fig. 10. Increasing of the breakouts area in the XZ section of a 220/160 mm junction at the pressure drop reduced to 30 atm (a), to 20 atm (b) and to 1 atm (c)*

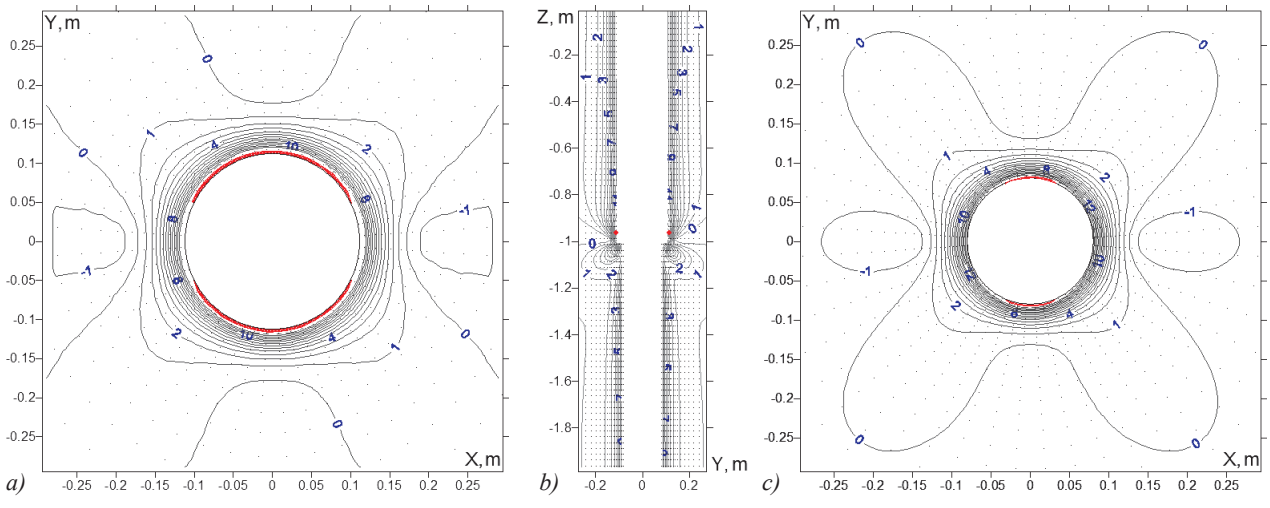


*Fig. 11. Rock failure at increased pressure drop (dP = 55 atm) in the XY (h = 0.97 m) and YZ section of a 220/160 mm junction and the XY (h = 0.97 m) section of a 160/120 mm junction (c)*

hydrofracture marked in yellow (Figure 12, b, d). The breakouts area extension can be traced from the XZ section since the shear failures are mainly directed along the direction of minimum horizontal stress (Figure 12, c). At the same time, the YZ section oriented mainly in the direction of maximum horizontal stress gives a good image of the hydrofracture (Figure 12, d). For its better visualization, the YZ section image has been enlarged.

Considering the fact that the angular size of the shear fracturing exceeds 90° (Figure 12, a), such a junction should be regarded as unstable (Zoback, 2010).

Observing analogous sections for the 160/120 mm juncture, we can see the destruction areas of a similar character and type appeared in sandstone (Figure 13). Since the angular size of the fracturing area still exceeds 90°, it is regarded as unstable as well. Analogous to the case of 220/160 mm diameters ratio, a hydrofracture formed within the juncture's shoulder (Figure 13, b, d)

Let's analyze how the pressure drop decreasing will affect the destruction zones. It should be noted that expected hydrofrac elimination does not happen when reducing dP. There is always at least one damaged cell within the juncture's shoulder and it is so for both for 220/160 mm and 160/120 mm cases. On the other hand, the reduced dP leads to increasing the breakouts area, since the compressing stresses around the holes increase. The way the shapes of destructed areas change can be seen in Figure 14 demonstrating simulation results for the 220/160 mm juncture at dP = 20 atm. In this case, the shear failure area increases both along the well's contour and in the radial direction.

At reduced pressure drop, the inclined 160/120 mm junction demonstrates the behavior similar to the one described for the 220/160 mm and for that reason is omitted.

Further reduction of dP down to 1 atm results in shear failures almost close around the well, in other words, the walls collapse around the juncture.

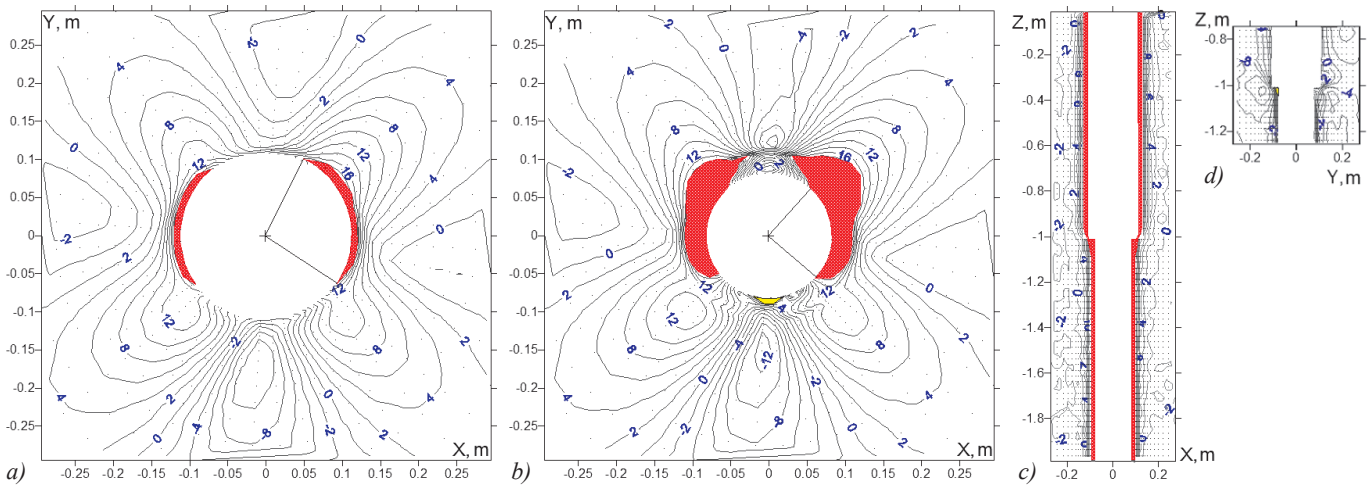


*Fig. 12. Destruction areas in an inclined 220/160 mm junction at dP = 40 atm. The XY section is related to h = 0.99 m (a) and h = 1.01 m (b). Breakouts are marked in red in the XZ section (c). A hydrofracture is marked in yellow in the YZ section (d).*

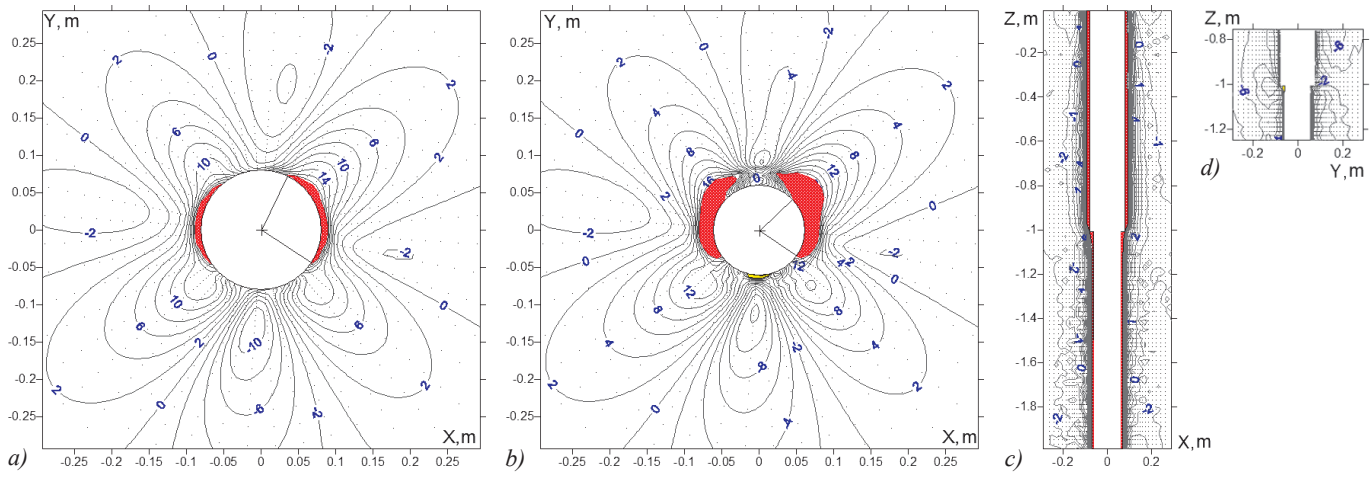


*Fig. 13. Sandstone failure around an inclined 160/120 mm juncture at dP = 40 atm. The XY section is related to h = 0.99 m (a) and h = 1.01 m (b). The XZ and YZ sections can be seen in (c) and (d), respectively.*

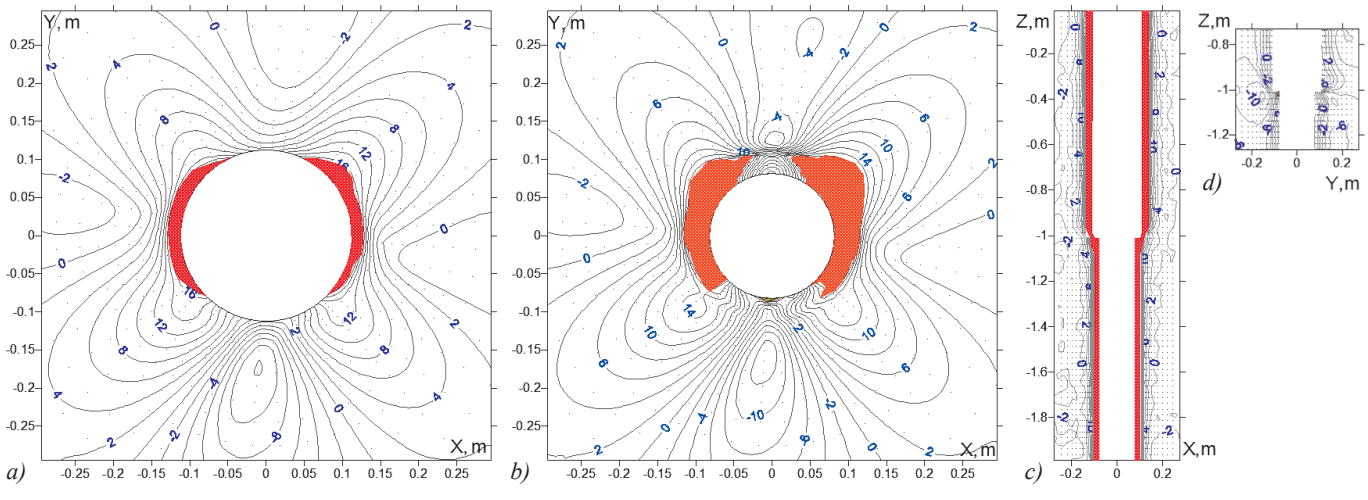


*Fig. 14. Changing the shapes of destructed areas at reduced pressure drop (dP = 20 atm) in a 220/160 mm junction. The section XY is related to h = 0.99 m (a) and h = 1.01 m (b). Increased breakouts can be seen in the XZ section (c). A hydrofracture can be seen in the enlarged YZ section (d).*

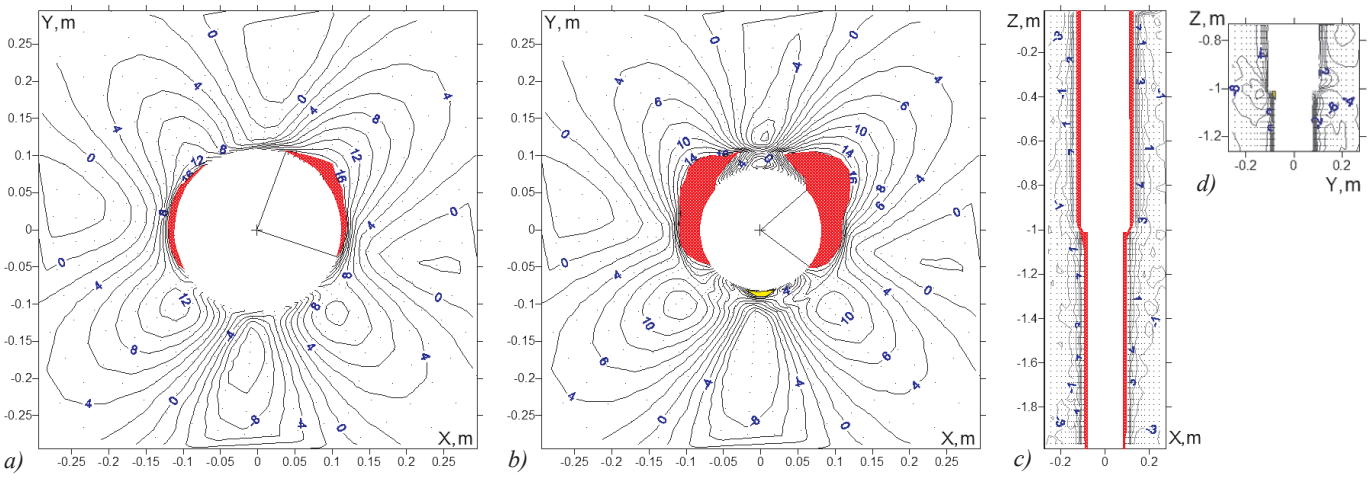


*Fig. 15. Shapes of destructed areas around a 220/160 mm junction at dP = 50 atm. The section XY is related to h = 0.99 m (a) and h = 1.01 m (b). The XZ and enlarged YZ sections can be seen in (c) and (d) respectively.*

Increasing dP up to 50 atm in the 220/160 mm junction causes the angular size of breakouts to reduce, so it becomes smaller than 90° (Figure 15 a, b). Taking into account that the hydrofracture is still localized in the juncture's shoulder (Figure 15, c, d), we can conclude that the junction is stable.

Analogous behavior can be observed in the 160/120 mm juncture, which makes core drilling at dP = 50 atm in such a borehole stable as well.

If in the 220/160 mm juncture, dP increases up to 60 atm, it produces a tensile failure across the juncture's shoulder in the YZ section (Figure 16, a) that elongates downward into the bottom hole. The dispositions of the shear and fracturing areas in a plane perpendicular to the well's axis can be seen in Figure 16 (b).

If in the 160/120 mm junction the pressure drop increases up to 60 atm, it leads to formation of two azimuthal hydrofractures on the opposite walls of the well, and the length of these fractures is bigger than the length of such fractures in the 220/160 mm juncture, which can be seen in Figure 17 (a). The shapes of breakouts as well as the positions of the hydrofractures are demonstrated in Figure 17 (b).

In general, since in the considered junctions the hydrofractures are nonlocal, core drilling at dP = 60 atm should be considered as unstable.

Further increase of the pressure drop in both inclined junctions 220/160 mm and 160/120 mm provokes further hydrofractures propagation downward the bottom hole and upward the main borehole, which is demonstrated in the section YZ presented in Figure 18. It is apparent that core drilling at dP = 70 atm is dangerous.

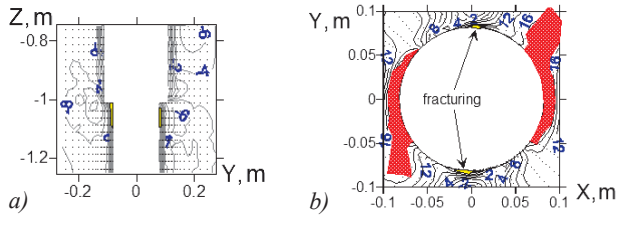


*Fig. 16. Shapes of destructed areas around a 220/160 mm junction at dP = 60 atm. In the YZ section, a hydrofracture propagates from the junction's shoulder downward the bottom hole. Another hydrofracture can be seen on the opposite wall. The XY section is related to h = 1.05 m (b). The shear failure areas keep reducing.*

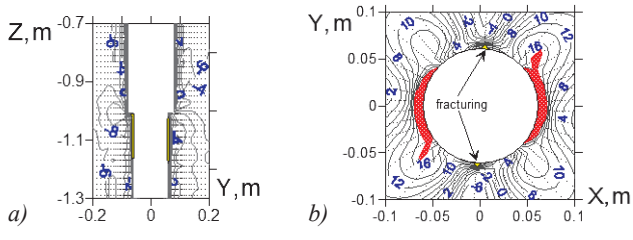


*Fig. 17. Areas of destruction around a 160/120 mm junction at dp = 60 atm. The YZ section (a) shows the extension of the hydrofractures. The disposition of the fractures and breakouts relative to the well's contour can be seen in the XY section (b) at h = 1.1 m.*

## Discussion

The junction stability results were obtained with the help of the vertical transversely isotropic poroelastic model with mudcake buildup taken into account. Due to the slight variation in the elastic parameters reconstructed from the core compression tests the question of the applicability of the isotropic approach to describe the behavior of the formation arises. The modeling of the stress state for isotropic medium was carried out for the vertical and inclined wellbore junction taken into account mudcake growth. Comparison of the results with a vertical transversely isotropic case showed that the difference in the equivalent stress in the area of different diameters wells joining is 6–15%. Due to the fact that experimental data on core deformation are more accurately described by a model with anisotropic properties this system of

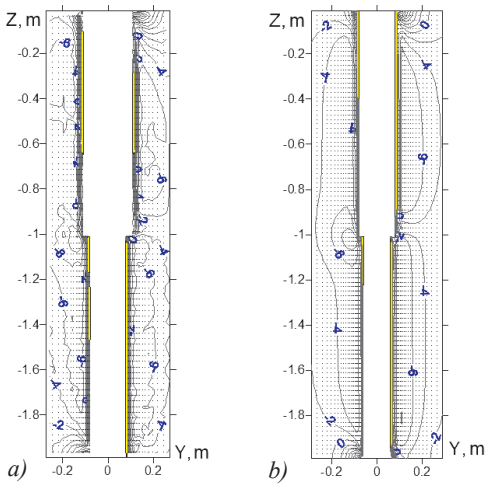


*Fig. 18. Propagation of hydrofractures at dP = 70 atm around 220/160 mm (a) and 160/120 mm (b) junctions in the YZ section*

equations for a poroelastic medium was chosen for numerical calculations.

The important result is that there are no fundamental differences between the 220/160 mm and 160/120 mm junctions when it comes to the type and character of the failure zones that occurs around the joints at changing pressure drop. It other words, the main conclusions concerning stability while core drilling can be generalized for both cases.

Applying the "standard" pressure drop of 40 atm while core drilling with a bit of smaller diameter has proved to be insufficient due to the size of breakouts indicates the juncture's wall instability. The drilling becomes safe if the applied pressure drop increases by 10 atm.

In the anisotropic sandstones of the Surgut Dome, it is better to perform core sampling in either vertical or sub-vertical wells. The modeling has demonstrated that the vertical junction is more stable because it is not prone to hydrofracturing even when the pressure drop reaches 70 atm.

In inclines wells, whose inclination angle is 60° and higher, drilling with a bit of smaller diameter should be performed keeping within quite a narrow window of mud pressure. So, while drilling at pressure drop equals to 50 atm is enough to stabilize an inclined juncture, its decrease by 10 atm leads to critical shear failure while the increase by 10 atm – to hydraulic fracturing of the borehole's walls.

The area most prone to fracturing is the juncture's shoulder where the main and bottom holes diameters meet. It can be assumed that, in reality, rock chipping smooths this area forming a seamless transition area between the holes.

It is also should be noticed that the bottom hole of the vertical junctures is more resistant to a reduced pressure drop because the destructions are initiated in the main wellbore and then spread downward to the bottom one. On the contrary, in the inclined junctures at increased pressure drop, tensile fracture first occur in the bottom hole to spread into the main borehole making the last more stable to an increased dP.

## Conclusions

The performed 3D poroelastic modeling of vertical and inclined 220/160 mm and 160/120 mm well junctions in the anisotropic sandstone of the Akh Formation productive pay for a pressure-drop range from 1 to 70 atm has demonstrated that:

- The shape and character of fracturing around the junctions are qualitatively similar for the diameters ratios in question at equal pressure drops;
- The vertical junctions are more stable if compared to the inclined ones since their formation excludes hydraulic fracturing;
- While core sampling from vertical wells, one should maintain a pressure drop above 55 atm down the hole to guarantee the well's stability;
- In the vertical junctions, the bottom hole is more stable to pressure drop reduction;
- In order to provide stability of the inclined junctions, a pressure drop should be maintained at 50 atm ±10%. Reducing the pressure drop leads to the critical spalling of the walls, and increasing – to propagation of a tensile fracture along the borehole's surface;
- Increasing the pressure drop in the inclined junctions initiates hydraulic fracturing in the bottom hole, while the main borehole preserves its stability.

## References

Ashikhmin S.G., Kashnikov Yu.A., Shustov D.V., Kukhtinskii A.E. (2018). Influence of elastic and strength anisotropy on the stability of inclined borehole. *Neftyanoe khozyaistvo = Oil Industry*, 2, pp. 54–57. https://doi.org/10.24887/0028-2448-2018-2-54-57

Bocharov O.B., Seryakov A.V. (2016). Modeling uncharacteristic destruction of productive sandstone layers during drilling. *Fizicheskaya Mezomekhanika*, 19(6), pp. 86–93.

Cheng A. H.-D. (1997). Material Coefficients of Anisotropic Poroelasticity. *Int. J. Rock Mech. Min. Sci*., 34(2), pp. 199–205. https://doi.org/10.1016/S0148-9062(96)00055-1

Cui L., Cheng A.H-D., and Y. Abousleiman (1997). Poroelastic Solution for an Inclined Borehole. *J. of App. Mechanics ASME*, 64(1), pp. 32–38. https://doi.org/10.1115/1.2787291

Fadeev A.B. (1987). Finite element method in geomechanics. Moscow: Nedra, 221 p.

Geniev G.A., Kurbatov A.S, Samedov F.A. (1993). Issues of strength and ductility of anisotropic materials. Moscow: Interbuk, 187 p.

Grogulenko V.V. (2017). Modeling the application of loads on metal-polymer coiled tubing pipes for the oil and gas industry. *Naukovedenie*, 9(1).

Liu C., and Y. Abousleiman (2018). Multiporosity/Multipermeability Inclined-Wellbore Solutions With Mudcake Effects. *SPE Journal*, 23(5), pp. 1723–1747. https://doi.org/10.2118/191135-PA

Mohamad-Hussein A. and J. Heiland (2018). 3D finite element modelling of multilateral junction wellbore stability. *J. Pet. Sci*., 15, pp. 801–814. https://doi.org/10.1007/s12182-018-0251-0

Podberezhny M., Polushkin S. and Makarov A. (2017). Novel Approach for Evaluation of Petrpphysical Parameters from Time-Lapse Induction Logging-While-Drilling Measurements in Deviated and Horizontal Wells. *Proc. SPE Conf*. Moscow. https://doi.org/10.2118/187911-RU

Rudyak V.Ya., Seryakov A.V., Manakov A.V. (2013). Joint modeling of geomechanics and filtration processes in the near-wellbore zone while drilling. *Proc. Conf.: Geodynamics and the stress state of the Earth's interior.* Novosibirsk: IGD SO RAN, v.1, pp. 383–388.

Seryakov A.V, Podberezhnyi M.Yu., Bocharov O.B. (2018). Formation anisotropy as a key factor in well stability in the West Salym field. *Proceedings of the 8th International Geological and Geophysical Conference EAGE: Innovations in Geoscience – Time for Breakthrough*. St. Petersburg.

Zoback M.D. (2010). Reservoir Geomechanics. Cambridge University Press, 449 p.

## About the Authors

*Alexander V. Seryakov* – Researcher, Cand. Sci. (Engineering)

Novosibirsk Technology Center, Baker Hughes

4A Kutateladze st., Novosibirsk, 630090, Russian Federation

*Maxim Yu. Podberezhny* – Head of Petrophysics Department, Cand. Sci. (Physics and Mathematics)

Gazpromneft-GEO

22A Sinopskaya emb., St. Petersburg, 191167, Russian Federation

*Oleg B. Bocharov* – Deputy Director for HP, , Cand. Sci. (Physics and Mathematics)

Novosibirsk Technology Center, Baker Hughes

4A Kutateladze st., Novosibirsk, 630090, Russian Federation

*Marat A. Azamatov* – Head of Short-Term Development Planning, Master of Physics

Salym Petroleum Development N.V.

31 Novinsky boul., Moscow, 123242, Russian Federation

*Manuscript received 19 December 2019;*
*Accepted 4 June 2020; Published 30 September 2020*

ORIGINAL ARTICLE

**DOI**: https://doi.org/10.18599/grs.2020.3.79-86 Russian Original 2020. Vol. 22. Is. 3. Pp. 79–86

# Development of a comprehensive methodology for the forecast of effectiveness of geological and technical measures based on machine learning algorithms

*A.A. Kochnev[1], N.D. Kozyrev[1,2], O.E. Kochneva[3*], S.V. Galkin[1]*

[1]*Perm National Research Polytechnic University, Perm, Russian Federation*

[2]*Branch of LLC «LUKOIL-Engineering» «PermNIPIneft» in Perm, Perm, Russian Federation*

[3]*Saint-Petersburg Mining University, St. Petersburg, Russian Federation*

**Abstract**. The main part of hydrocarbon production in Russia is represented by old oil and gas producing regions. Such areas are characterized by a significant decrease in well productivity due to high water cut and faster production of the most productive facilities. An important role for such deposits is played by stabilization of production and increase of mobile reserves by improving the development system. This is facilitated by various geological and technical measures.

Today, an urgent problem is to increase the reliability of the forecast of technological and economic efficiency when planning various geological and technical measures. This is due to the difficulty in selecting candidate wells under the conditions of the old stock, the large volume of planned activities, the reduction in the profitability of measures, the lack of a comprehensive methodology for assessing the potential of wells for the short and long term.

Currently, there are several methods to evaluate the effectiveness of geological and technical measures: forecast based on geological and field analysis, statistical forecast, machine learning, hydrodynamic modeling. However, each of them has its own shortcomings and assumptions. The authors propose a methodology for predicting the effectiveness of geological and technical measures, which allows one to combine the main methods at different stages of evaluating the effectiveness and to predict the increase in fluid and oil production rates, additional production, changes in the dynamics of reservoir pressure and the rate of watering of well production.

**Keywords**: geological and technical measures, efficiency forecast, machine learning, mathematical statistics, hydrodynamic modeling, geological and physical parameters

**Recommended citation**: Kochnev A.A., Kozyrev N.D., Kochneva O.E., Galkin S.V. (2020). Development of a comprehensive methodology for the forecast of effectiveness of geological and technical measures based on machine learning algorithms. *Georesursy = Georesources*, 22(3), pp. 79–86. DOI: https://doi.org/10.18599/grs.2020.3.79-86

## Analysis of the effectiveness of the main workover actions in carbonate reservoirs of the Perm Territory fields

The Perm Territory is an old oil-producing region, as a result of which oil fields are characterized by high depletion of reserves, involvement in the development of heterogeneous reservoirs with low fluid storage capacity properties, as well as deposits with high-viscosity oils. Development of fields in difficult geological and technological conditions of operation of carbonate reservoirs, as a rule, is carried out with low annual rates of reserves recovery (no more than 2.5%) and with low oil recovery factor (ORF) (no more than 35%) (Voevodkin et al., 2014).

At the fields of the Perm Territory, starting from the 70s, the methods of production intensification (PI) and enhanced oil recovery (EOR) are being increasingly introduced every year. Even with a high economic effect of a certain technology, it is necessary to use and implement all types of PI and EOR methods in order to maintain facilities at the required level for oil production. Moreover, each technology demonstrates success in certain geological, physical and technological conditions (Putilov et al., 2020).

The most successful methods of oil production intensification and enhanced oil recovery for carbonate objects of the Perm Territory fields are recognized as acid hydraulic fracturing (acid fracturing), acid

[*]*Corresponding author: Olga E. Kochneva*
*E-mail: kochnevaoe@mail.ru*

treatment (AT), radial drilling (RD), drilling perforation (DP), reperforation (RP) and additional reperforation & completion (RPC) (Ilyushin et al., 2015; Kochnev et al., 2018).

Figure 1 shows a comparison of the efficiency of technologies for the analyzed period (2006–2019) for vertical wells in terms of the average additional production per well and the average daily production increase.

Figure 2 shows a comparison of the average duration of the effect from workover actions. The effective period is the time of the well operating with an increase in the oil production rate caused by workover actions, until the oil production rate decreases to the base value.

Analysis of Figures 1–2 shows that the highest additional production and average daily increment are characteristic of acid fracturing, but this technology has significant disadvantages: high cost; the risk of fracture breakthrough into a water-cut reservoir; the use of a large volume of chemical reagents leads to complex work on the disposal of contaminants. In addition, when hydraulic fracturing (hydraulic fracturing), the technical requirements for candidate wells are high, which seriously limits the use of this technology, especially on the old well stock. The rest of the considered technologies are less demanding for the selection of candidate wells and less costly. Radial drilling technology based on the average increment in additional oil production (additional oil production through the well until the oil production rate drops to the base value) from geological and technical measures defers only to acid fracturing, and in terms of time of economic effect is the best one.

Radial drilling technology is one of the main for the Chernushinskaya (25%), Osinskaya (24%) and Nozhovskaya (34%) groups of fields in the Perm Territory. The analysis of the effectiveness of geological and technical measures for various carbonate objects of the Perm Territory fields is described in the works (Ilyushin et al., 2015; Kochnev et al., 2018). Evaluation of the effectiveness of radial drilling technology was carried out in (Galkin et al., 2019).

## Basic methods for forecasting the effectiveness of workover measures

Today, one of the main methods for predicting the effectiveness of workover measures is the mathematical modeling on a hydrodynamic model (Kravchenko et al., 2018; Sayfutdinov et al., 2018; Repina et al., 2018). The advantages of this method include the possibility of a comprehensive assessment of geological and technical measures in conditions of the mutual influence of all wells on the oil production process, as well as taking into account the geological characteristics of the reservoir. Simulation can be performed in a variety of simulators.

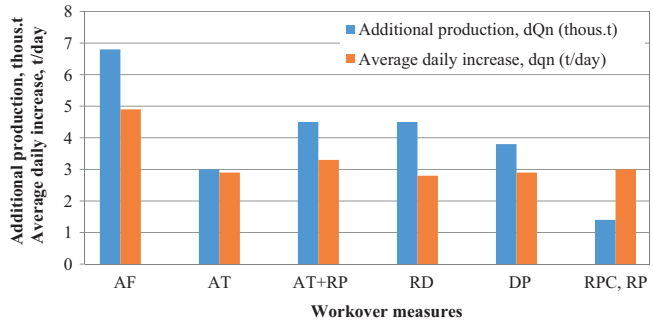


*Fig. 1. Comparison of workover measures in terms of efficiency. Acid fracturing – acid hydraulic fracturing, AT – acid treatment, RP – reperforation, RD – radial drilling, DP – drilling perforation, RPC – reperforation and completion.*

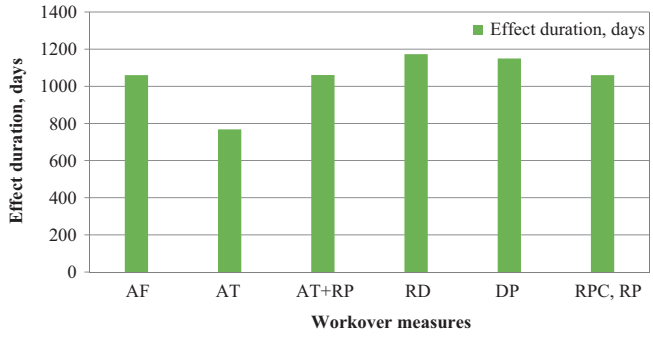


*Fig. 2. Comparison of workover measures in terms of effect duration*

The main software systems for Russian oil and gas companies are Tempest, Eclipse, T-Navigator.

In geological and hydrodynamic modeling, it is important to take into account the subjectivity of the adaptation of the model and the way of the workover actions modeling, which significantly affects the predictive characteristics of the model (Olenchikov, Kruglikova, 2008; Kolbikov et al., 2018; Lyu et al., 2014). The large time and cost of hydrodynamic modeling determines the need for its use mainly for the design of high-cost workover measures (drilling horizontal wells and sidetracks) (Andronov, 2019).

The methodological recommendations (Polukeev et al., 2018) describe a method for predicting the increase in flow rate from geological and technical measures through the specific productivity factor, which is based on a comparison of analogs and fluid flow rate forecast. The calculation of the production rate increase using this method is simple and prompt in the presence of a developed base of measures, but its accuracy is often not great. The calculation does not take into account the complex of geological and technological parameters, but only the specific productivity factor and its components are considered. The approach is currently the main one for the LUKOIL group of companies. Detailed "manual" analysis of wells based on geological field analysis using analytical and statistical methods takes a lot of time and is subjective.

The development of digital technologies provides significant potential for the application of machine learning technologies in the oil and gas industry (Koroteev et al., 2014). These are various methods such as neural networks, decision trees, random forest algorithm, cluster analysis. Among the advantages of machine learning methods for specialists designing geological and technical measures, one can note the possibility of promptly obtaining satisfactory forecasts and the absence of requirements for hydrodynamic modeling skills. In general, the main advantages of using machine learning technologies are: accuracy, automation, speed, customization, scalability (Andronov, 2019).

The main disadvantages are: lack of clear forecasting algorithms, lack of physical justification, low interpretability of the results obtained (Pichugin et al., 2013; Azbuhanov et al., 2019).

Also, various methods of mathematical statistics are used to predict the effectiveness of geological and technical measures. The work (Galkin et al., 2019) notes the successful application of the methods, however, there are drawbacks: the need for manual search and analysis of "outliers", the use of a set of various statistical methods for data preparation.

## Development of a comprehensive methodology for predicting the effectiveness of workover measures

To improve the reliability of forecasting, an approach is proposed for combining methods at different stages of forecasting, which consists of four main stages.

1. Creation of a database on geological and technical measures and the corresponding geological and physical parameters.

For a comprehensive forecast of the effectiveness of geological and technical measures, it is necessary to take into account the influence of both geological and technological parameters. Therefore, at this stage, it is necessary to create a consolidated database, including wells on which geological and technical measures were carried out, as well as the results of geophysical, hydrodynamic and other studies on these wells.

2. Identification of the parameters that have the greatest impact on the potential for additional production for each workover measures by using the methods of mathematical analysis.

To ensure a high-quality forecast, it is necessary to understand what parameters determine the effectiveness of the technology in various geological and physical conditions. To identify these parameters, it is proposed to use one-factor and multivariate mathematical analysis.

3. Construction of regression models based on the identified parameters to predict the increase in liquid/oil production using machine learning methods.

At this stage, machine learning models are built to predict the increase in liquid/oil production rate.

4. Forecasting the potential of additional production by entering the results of machine learning into the hydrodynamic model.

To obtain a long-term forecast, it is necessary to take into account the mutual influence of wells, therefore, it is proposed to integrate mathematical models with a geological and hydrodynamic model (HDM).

In this work, the methodology has been tested using the example of radial drilling technology.

## Identification of parameters affecting the efficiency of radial drilling technology

At the first stage, a consolidated database was created for all wells with measures taken for radial drilling for the period from 2006 to 2019 in the Perm Territory and the corresponding parameters. The database includes the geological and physical characteristics of the reservoir adopted at the fields when calculating reserves; the results of hydrodynamic studies of wells before carrying out measures for RD; the well log interpretation results, oil and liquid production rates before RD, data on perforation intervals, data on previous well interventions. As a result, to assess the effectiveness of radial drilling measures, the analysis took into account data on 590 wells in 40 oil fields and with 36 parameters.

At the second stage, the impact of the geological and physical parameters of the object on the performance indicators of geological and technical measures was assessed. The following parameters were chosen as efficiency indicators: average daily increase in oil production rate (t/day), additional production (thousand tons), maximum flow rate after geological and technical measures (t/day), duration of the effect (days).

Initially, a univariate analysis was performed. The assessment of the influence of parameters on performance indicators was carried out using the Student's t-test. The essence of the method is to test the hypothesis that the mean values are equal (1):

$$t_p = \frac{|X_1 - X_2|}{\sqrt{\frac{1}{n_1} + \frac{1}{n_2}\left(\frac{(n_1-1)S_1^2+(n_2-1)S_2^2}{n_1+n_2-2}\right)}} \quad (1)$$

where $X_1$, $X_2$ – respectively, the average values of the sample indicators; $S_{12}$, $S_{22}$ – variances of sample indicators.

The difference in mean values is considered statistically significant if $t_p > t_t$, where $t_p$ is the calculated value of the criterion, and $t_t$ is the tabular value of the t criterion. The $t_t$ values are determined depending on the amount of compared data and the significance level ($p = 0.05$), if the significance level is less than 5%, then the samples are different with a probability of more than 95%. The results of calculating the Student's test are presented in Table 1. Values with an attainable

| **Additional oil production, t** | **< 2000** | **> 2000** | **t-test** | **p** | **$N_1$** | **$N_2$** |
|---|---|---|---|---|---|---|
| Porosity $K_p$, % | 12,4 | 12,8 | -1,64 | *0,10* | 96 | 93 |
| Oil viscosity μ, mPa*s | 24,9 | 32,0 | -1,76 | *0,08* | 96 | 93 |
| Oil density $\varrho_o$, g/cm$^3$ | 0,87 | 0,89 | -2,06 | **0,04** | 96 | 93 |
| Bottom hole pressure $P_{bot}$, MPa | 5,22 | 6,29 | -2,57 | **0,01** | 56 | 75 |
| Saturation pressure $P_{sat}$, MPa | 10,32 | 10,21 | 0,33 | 0,74 | 56 | 75 |
| Skin factor S, un. | -3,52 | -2,03 | -2,82 | **0,01** | 56 | 75 |
| Oil-saturated thickness $h_{sat}$, m | 8,47 | 9,32 | -1,85 | *0,07* | 96 | 92 |
| **Average daily increase, t/day** | **< 3** | **>3** | **t-test** | **p** | **$N_1$** | **$N_2$** |
| Porosity $K_p$, % | 12,32 | 12,94 | -2,59 | **0,01** | 102 | 87 |
| Oil viscosity μ, mPa*s | 25,38 | 32,04 | -1,65 | *0,10* | 102 | 87 |
| Oil density $\varrho_o$, г/см$^3$ | 0,87 | 0,89 | -1,90 | *0,06* | 102 | 87 |
| Specific interlayer thickness $h_{int}$, m | 2,09 | 1,66 | 2,08 | **0,04** | 97 | 76 |
| Reservoir pressure $P_{res}$, MPa | 11,95 | 13,29 | -2,65 | **0,01** | 71 | 60 |
| Bottom hole pressure $P_{bot}$, MPa | 5,28 | 6,49 | -2,95 | **0,00** | 71 | 60 |
| S, un. | -3,16 | -2,09 | -2,01 | **0,05** | 71 | 60 |
| **Effect duration from RD, day** | **< 900** | **>900** | **t-test** | **p** | **$N_1$** | **$N_2$** |
| Oil flow rate before workover $q_o$, t/day | 3,47 | 2,89 | 2,01 | **0,05** | 98 | 91 |
| Skin factor S, un. | -3,66 | -1,83 | -3,52 | **0,00** | 60 | 71 |
| **Max oil flow rate after RD, t/day** | **< 10** | **> 10** | **t-test** | **p** | **$N_1$** | **$N_2$** |
| Oil flow rate before workover $q_o$, t/day | 2,33 | 4,00 | -6,27 | **0,00** | 92 | 97 |
| Water cut W,% | 21,50 | 16,86 | 2,24 | 0,03 | 87 | 96 |
| **Ad. oil flow rate in 1 year after RD, t/day** | **< 5** | **> 5** | **t-test** | **p** | **$N_1$** | **$N_2$** |
| Total reservoir thickness $H_t$, m | 21,26 | 24,53 | -1,99 | **0,05** | 93 | 96 |
| Porosity $K_p$, % | 12,39 | 12,81 | -1,71 | *0,09* | 93 | 96 |
| Oil density $\varrho_o$, g/cm$^3$ | 0,87 | 0,89 | -2,71 | **0,01** | 93 | 96 |
| Volumetric ratio *b*, un. fr. | 1,09 | 1,06 | 2,65 | **0,01** | 93 | 96 |
| Gas content G, m$^3$/m$^3$ | 41,81 | 31,55 | 2,31 | **0,02** | 93 | 96 |
| Skin factor S, un. | -3,50 | -2,05 | -2,73 | **0,01** | 56 | 75 |
| Total thickness $H_{total}$, m | 22,23 | 25,27 | -1,85 | *0,07* | 93 | 95 |

*Tab. 1. Influence of geological and physical parameters on the efficiency of RD for wells of the Tournaisian facilities of the Perm Territory fields*

significance level p below 0.05 are highlighted in bold type for indicators, at which, with a probability of more than 95%, one can argue about differences in the considered samples. In this case, the studied parameter has a statistically significant (non-random) effect on the differences in indicators in the samples. Values with p in the range from 0.05 to 0.10 are italicized, for which the influence also exists, but somewhat lower.

Greater additional production and average daily growth after RD are characterized by deposits with higher oil viscosity and density, which are more characterized by the formation of stagnant zones in low-permeability zones of the reservoir. It is also more preferable to use RB under conditions of significant energy potential of the reservoir ($P_{res}$, $P_{bh}$) and with a higher porosity of the reservoir. The conditions of large specific interlayer thicknesses, total and oil-saturated thicknesses also generally positively affect the efficiency of the RD. The increase in oil production in the first year after RD is influenced by the effective thickness, reservoir storage capacity, oil density, volumetric ratio and gas saturation.

For a comprehensive assessment of the impact of indicators (multivariate analysis), linear discriminant analysis was used. The most important indicator of efficiency is the increase in the flow rate of oil and liquid after workover measures. In this case, a set of parameters was identified that affects the increase in oil (2) and liquid (3) flow rates after RD. As a result of calculations, the following linear discriminant functions (Z) were obtained, which maximally separate the samples by the average value of the increase in production.

To increase the oil production rate (at R = 0.60):

$$Z = -0.218 \cdot q_o + 10.314 \cdot K_s - 0.061 \cdot K_{calc} - 0.00633 \cdot \mu_o + 0.176 \cdot \varsigma_{ch} + 0.00556 \cdot \chi - 0.762 \cdot h_i + 0.0013 \cdot S - 3.41. \quad (2)$$

To increase the liquid flow rate (at R = 0.79):

$$Z = -0.39 \cdot q_l + 0.27 \cdot P_{res} - 0.102 \cdot h_{oit} + 0.26 \cdot \phi + 0.069 \cdot S - 6.48 \quad (3)$$

where $q_o$ – oil production rate before RD, t/day; $q_l$ – liquid flow rate before RD, $m^3$/day; $h_i$ – oil-saturated thickness, m; $\phi$ – porosity,%; $K_s$ – net-to-gross sand ratio; $K_{calc}$ – coefficient of dissection; $\mu_o$ – oil viscosity in reservoir conditions, mPa*s; $\varrho_o$ – oil density in reservoir conditions, g/$cm^3$; $\chi$ – piezoconductivity, $cm^2$*s; $P_{res}$ – reservoir pressure, MPa; $h_{oit}$ is the average thickness of a single oil-saturated interlayer, m (the average thickness of a single oil-saturated interlayer was calculated as the ratio of $h_i$ to the number of oil-saturated interlayers); S – well skin factor; $\varsigma_{ch}$ – $h_i$, m/number of radial channels.

As a result of multivariate analysis, it was revealed that the increase in oil production rate is affected by the following set of parameters: oil production rate prior to RD, net sand coefficient, compartmentalization, oil viscosity, channel density, piezoconductivity, average thickness of a single oil-saturated interlayer and skin factor.

The increase in fluid flow rate is most influenced by a set of parameters: fluid flow rate to RD, reservoir pressure, oil-saturated thickness, porosity, skin factor.

The identified parameters are used to build computing learning models.

## Forecast of the increase in fluid flow rate after workover measures

At this stage, the forecast of the increase in fluid flow rate was made using machine learning methods. Artificial neural networks are chosen as the first method. Neural networks are a mathematical model built on the principle of biological neural networks and allow solving problems of regression, clustering and data analysis (Voronovsky et al., 1997; Tsaregorodtsev, 2008). As a result, networks with different architectures were built, which quite reliably allow predicting the increase in fluid flow rate (R – from 0.77 to 0.86). For further forecasting, a network with a simpler architecture was chosen – a multilayer perceptron: 17 neurons on the input layer, 1 hidden layer with 5 neurons and 1 neuron on the output layer, the neuron activation function is logistic, the error function is the sum of squares. When training this network, sufficiently high correlation coefficients were achieved, both on the training sample, and on the test and control (Figure 3a).

The second method for calculating the increase in oil production after RD is the support vector machine (SVM). SVM is a class of supervised learning algorithms used for classification and regression analysis problems. As a result of the calculations, several classifying dividing lines are constructed, of which only one corresponds to the optimal dividing (Tsaregorodtsev, 2008). Figure 3b shows the results of model calculations for the training and test samples, respectively.

For comparison, the increase in fluid flow rate was calculated using linear discriminant analysis (LDA). The method solves the problems of classification, not regression, however, in the calculations, a transition to a probabilistic assessment is possible, and through probability it becomes possible to predict an increase in production rate (Figure 4) (Galkin et al., 2019).

The result of training in this case is somewhat worse (R = 0.77–0.72), but the advantage of the method is that in the process of building a model it is possible to verify its physicality. That is, the signs of the linear discriminant function and the parameters should not contradict the physical meaning. When building a neural network or a support vector model, there is no way to track the physicality of the coefficients in the model, which is one of the main disadvantages of the method.

## Forecast of additional oil production from workover measures

In the process of predicting the effectiveness of geological and technical measures, it is important to

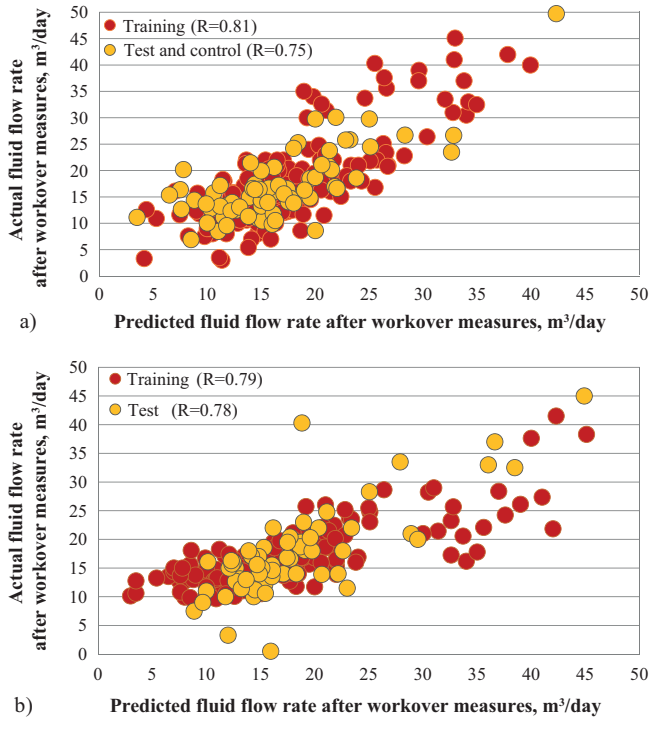


*Fig. 3. Comparison of actual and predicted values of fluid flow rate after workover measures: a) neural networks; b) SVM method.*

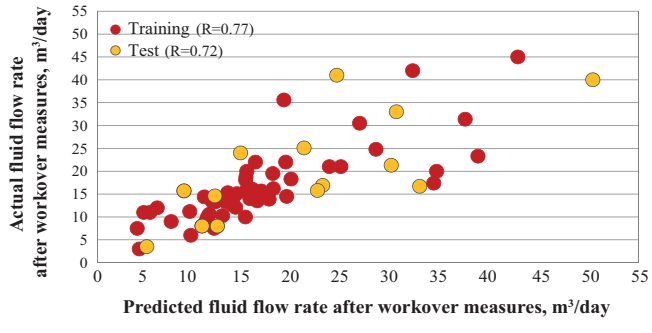


*Fig. 4. Comparison of actual and forecast values. Discriminant analysis.*

assess the potential for additional production. When using only statistical models, changes in the physical and pressure conditions of the reservoir during the forecast period are not taken into account, which does not allow for an assessment of production in the long term. Statistical models are able to predict only for current conditions and for one well, without taking into account mutual influence and interference.

The integration of statistical models and hydrodynamic modeling opens up opportunities for planning workover measures in the long term, that is, taking into account changes in reservoir conditions during development. In addition, the integration approach allows one to take into account the geological structure of the reservoir, namely, the variability of properties in the reservoir volume and the rate of water breakthrough after the event, depending on the hydrodynamic connectivity of the reservoir and the rate of the front of oil displacement by water.

In this work, two algorithms have been developed to predict liquid flow rate and additional oil production after the event: 1) integration of a mathematical model obtained using a neural network and hydrodynamic modeling; 2) integration of a multidimensional model obtained using LDA and hydrodynamic modeling.

The algorithm for calculating additional production using neural networks is as follows:

1. Determination of candidate wells and the date of the event;

2. Calculation of the increase in fluid flow rate using a trained neural network;

3. Entering fluid flow rate values into the hydrodynamic simulator, taking into account the increment from geological and technical measures for the candidate well;

4. Launching the calculation of the HDM;

5. Assessment of the potential for an increase in oil production rate, additional production for the forecast period, the nature of the rate of water cut and the dynamics of reservoir pressure.

To integrate a multidimensional statistical model for calculating the liquid flow rate obtained using linear discriminant analysis, a Python script has been developed that allows taking into account the obtained dependencies in the Roxar Tempest More hydrodynamic simulator.

The developed mathematical models of the increase in fluid flow rate from workover measures are entered into the program code of the script. The variables of the mathematical model refer to the vectors of the values of the simulation model. The script takes into account the static indicators (thickness, compartmentalization, net-to-gross sand ratio, porosity, permeability, fluid properties, etc.) entered in a tabular form in the simulator, and the dynamic performance of the well read by the script at the time of forecasting (reservoir and bottomhole pressure, current flow rate liquid, water cut). As a result, this makes it possible to obtain a forecast of the increase in the liquid flow rate from the event at any time, and then to assess the technological efficiency of the event in the long term.

Thus, when using LDA, the algorithm for predicting additional production can be summarized as follows:

1. Determination of the candidate well and the date of the event;

2. Entering static parameters for the well into the hydrodynamic simulator (net oil pay, porosity, skin factor, etc.) in tabular form;

3. Launching the calculation of the HDM;

4. Determination of the dynamic parameters of the well (current reservoir pressure, current fluid flow rate) on the date of the event in automatic mode using a script;

5. Calculation of the increase in fluid flow rate from geological and technical measures according to the previously obtained LDA dependencies in automatic mode using a script.

According to formula (4), a linear discriminant function is calculated, which maximally separates objects into groups of more and less promising workover measures (the boundary value of the increase in fluid flow rate is 8 $m^3$/day). In this formula, the script reads the parameters of fluid flow rate ($q_l$) and reservoir pressure ($P_{res}$) from the hydrodynamic model at the time of the forecast. The parameters of the oil-saturated thickness ($h_i$), porosity coefficient ($\phi$) and skin factor (S) are entered in a tabular form:

$$Z = -0.39 \cdot q_l + 0.27 \cdot P_{res} - 0.1 \cdot h_i + 0.26 \cdot \phi + 0.07 \cdot S - 6.48. \quad (4)$$

According to the formula (5), the probability of attributing workover measures to a promising class is calculated (an increase in fluid flow rate of more than 8 $m^3$/day):

$$P(Z) = -0.015 \cdot (Z)^3 + 0.021 \cdot (Z)^2 + 0.34 \cdot (Z) + 0.47. \quad (5)$$

According to the formula (6), the value of the increase in fluid flow rate is calculated:

$$\Delta q_l = 12.35 \cdot (P(Z)) + 3.82. \quad (6)$$

6. Calculation of further dynamics of technological parameters of the well in the hydrodynamic model and determination of additional oil production.

As a result, by integrating the LDA model and geological and hydrodynamic modeling, it is possible to calculate the increase in the flow rate of liquid and oil from workover measures in an automatic mode. It should also be noted that geological and hydrodynamic modeling makes it possible to assess additional oil production from geological and technical measures, the dynamics of reservoir pressure and water cut rates after workover, and well interference (Figures 5–6).

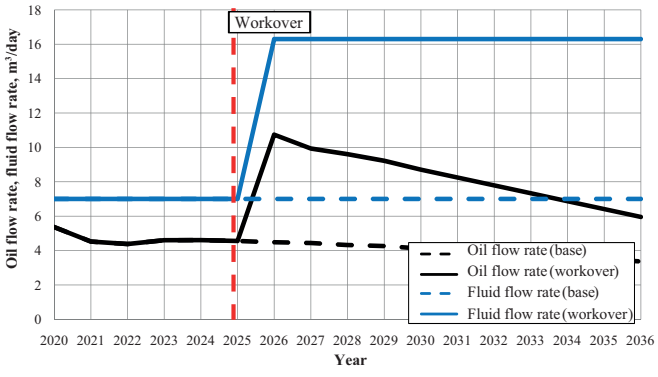


*Fig. 5. Assessment of the effect of workover measures using the proposed method*

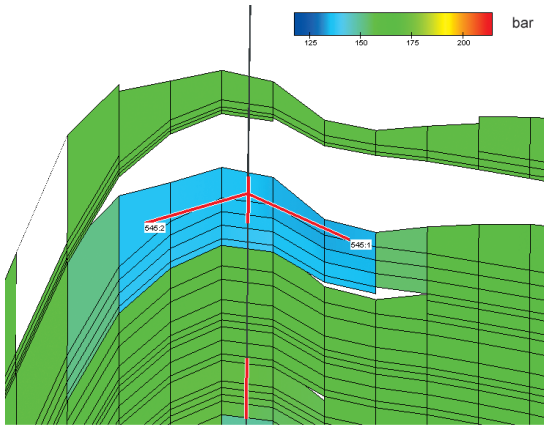


*Fig. 6. Assessment of changes in reservoir pressure after workover measures*

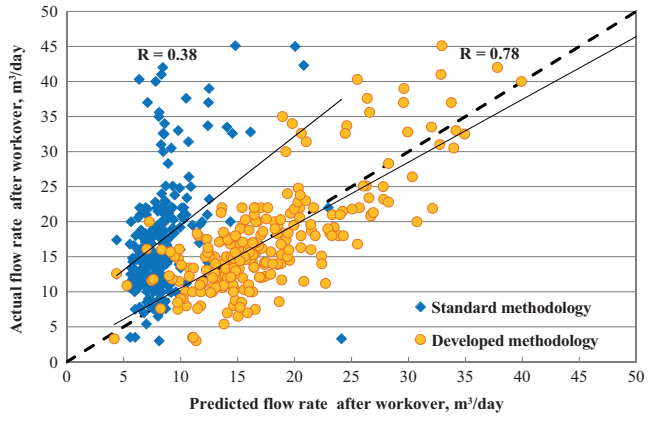


*Fig. 7. Comparison of the forecast accuracy of the standard methodology and the developed methodology for predicting the increase in fluid flow rate after RB*

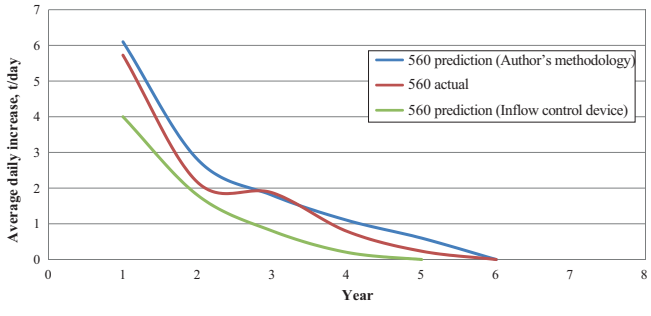


*Fig. 8. Comparison of the forecast of the standard methodology and the developed methodology with the actual data of the average daily increase in oil production by years*

## Results

The developed methodological approach includes a combination of several methods for predicting the increase in the flow rate of liquid, oil and additional production. The combination of statistical and mathematical forecasting methods can significantly increase the predictive reliability of the effects from geological and technical measures. As part of the study, a script has been developed that automatically calculates the effects of radial drilling, which significantly reduces time costs and enables quick assessment of the measure effectiveness.

As a result of the implementation of the methodology, using the example of radial drilling technology, it was possible to increase the predicted reliability of the increase in fluid flow rate, as well as the assessment of additional production (Figures 7–8).

Figure 8 shows a comparison of the results of the forecast of the average daily increase in oil production versus the actual data according to the existing and proprietary methodology. Based on the analysis, it can be seen that the existing methodology significantly underestimates the effect of the workover event relative to the actual effect, both in terms of additional oil production (32%) and in terms of the effect duration. Due to the underestimation of the potential of the candidate well, there is a possibility of abandoning the event and, as a consequence, a decrease in the final oil recovery factor and the efficiency of development in general.

The proprietary methodology repeats with greater accuracy the actual effect of the workover event, although it showed a somewhat overestimated result, while the deviation in additional oil production does not exceed 5%. The combination of statistical and hydrodynamic modeling makes it possible to reduce uncertainties and reduce the shortcomings of existing techniques by combining methods at different stages of forecasting. To refine the machine learning models, the parameters used are physically substantiated using statistical analysis (Student's t-test, linear discriminant analysis). To reduce the time of recording events in the hydrodynamic model and reduce the uncertainties associated with the method of modeling various workover measures on the hydrodynamic model, a developed script is used that allows you to quickly enter data into geological and hydrodynamic models, as well as calculate the increase in fluid flow rate taking into account machine learning models that take physical and technological parameters. The script allows calculation of the effect in automatic mode, thereby reducing the time spent by 2.5 work hour or even more.

## Acknowledgments

*The study was carried out with the financial support of the Russian Foundation for Basic Research within the framework of the scientific project No. 19-35-90029.*

## References

Andronov Yu.V. (2019). Methodology for the operational assessment of the prospectivity of wells for methods of stimulating oil inflow using neural networks and decision trees. *Abstract. cand. sci. diss*. Moscow, 24 p. (In Russ.)

Azbuhanov A.F., Kostrigin I.V., Bondarenko K.A., Semenova M.N., Sereda I.A., Yulmukhametov D.R. (2019). Selection of candidate wells for hydraulic fracturing based on mathematical modeling using machine learning methods. *Neftyanoe khozyaystvo = Oil industry*, 11, pp. 38–42. (In Russ.) https://doi.org/10.24887/0028-2448-2019-11-38-42

Galkin S.V., Kochnev A.A., Zotikov V.I. (2019). Estimate of Radial Drilling Technology Efficiency for the Bashkir Operational Oilfields Objects of Perm Krai. *Zapiski gornogo instituta = Journal of Mining Institute*, 238, pp. 410–414. (In Russ.). https://doi.org/10.31897/pmi.2019.4.410

Ilyushin P.Y., Rakhimzyanov R.M., Solovyov D.Y., Kolychev I.Y. (2015). Analysis of geological and technical measures to increase the productivity of producing wells in the oil fields of the Perm region. *Vestnik Permskogo natsional'nogo issledovatel'skogo politekhnicheskogo universiteta. Geologiya. Neftegazovoe i gornoe delo = Perm Journal of Petroleum and Mining Engineering,* 14(15), pp. 81–89. (In Russ.)

Kochnev A.A., Zotikov V.I., Galkin S.V. (2018). Analysis of the influence of geological and technological parameters on the effectiveness of radial drilling technology on the example of operational objects in perm region. *Izvestiya Tomskogo Politekhnicheskogo Universiteta Inziniring Georesursov = Bulletin of the Tomsk Polytechnic University. Geo Assets Engineering,* 329(12), pp. 20–29. (In Russ.). https://doi.org/10.18799/24131830/2018/12/16

Kolbikov S., Kuznetsova Y., Smirnov A. (2018). Method of anisotropy modeling and its application to hydrodynamic simulation. *SPE Russian Petroleum Technology Conference*. https://doi.org/10.2118/191622-18RPTC-MS

Koroteev D., Dinariev O., Evseev N., Klemin D., Nadeev A., Safonov S., Gurpinar O., Berg S., Kruijsdijk C., Armstrong R., Myers M. T., Hathon L., Jong H. (2014). Direct hydrodynamic simulation of multiphase flow in porous rock. *Petrophysics*, 55(04), pp. 294–303.

Kravchenko M.N., Dieva N.N., Lischuk A.N., Muradov A.V., Vershinin V.E. (2018). Hydrodynamic modeling of thermochemical effects on low-permeability kerogen-containing reservoirs. *Georesursy = Georesources*, 20(3), pp. 178–185. https://doi.org/10.18599/grs.2018.3.178-185

Lyu S., Zhang W., Du J., Gong F. (2014). A Coupled Model for the Hydrodynamics Simulation of the Pearl River Networks and its Estuary. *The Twenty-fourth International Ocean and Polar Engineering Conference*. https://doi.org/10.1155/2014/798579

Olenchikov D., Kruglikova L. (2008). Hydrodynamic Simulation Of Predicted Options Of Field Development. *SPE Russian Oil and Gas Technical Conference and Exhibition*. https://doi.org/10.2118/117408-MS

Pichugin O.N., Prokofieva Yu.Z., Aleksandrov D.M. (2013). Decision trees as an effective method of analysis and forecasting. *Neftepromyslovoe delo*, 11, pp. 69–75. (In Russ.)

Polukeev D.I., Gabdrakhmanova R.R., Lesnoy A.N., Kryukov M.A., Pimenova N.A., Pimenova M.I. (2018). Methodology of technical and economic evaluation of the effectiveness of geological and technical measures. LUKOIL-Engineering LLC. (In Russ.)

Putilov I., Krivoshchekov S., Vyatkin K., Kochnev A., & Ravelev K. (2020). Methods of predicting the effectiveness of hydrochloric acid treatment using hydrodynamic simulation. *Applied Sciences (Switzerland)*, 10(14), 4828. https://doi.org/10.3390/app10144828

Repina, V.A., Galkin, V.I., Galkin, S.V. Complex petrophysical correction in the adaptation of geological hydrodynamic models (On the example of visean pool of Gondyrev oil field). *Zapiski gornogo instituta = Journal of Mining Institute*, 231, pp. 268–274. (In Russ.). https://doi.org/10.25515/pmi.2018.3.268

Sayfutdinov M.A., Khakimzyanov I.N., Petrov V.N., Sheshdirov R.I., Mironova L.M. (2018). Studies on the presence of a hydrodynamic connection between the terrigenous Bobrikovsky and carbonate Tournaisian objects based on the geological and technological model of the field site. *Georesursy = Georesources*, 20(1), pp. 2–8. https://doi.org/10.18599/grs.2018.1.2-8

Tsaregorodtsev V.G. (2008). A constructive algorithm for synthesizing the structure of a multilayer perceptron. *Vychislitelnye tekhnlogii = Computational technologies*, 13, pp. 308–315. (In Russ.)

Voevodkin V.L., Galkin V.I., Krivoshchekov S.N. (2012). Investigation of the influence of oil and gas content criteria and geological and geophysical knowledge on the distribution of hydrocarbon deposits in the Perm Region. *Neftyanoe-Khozyaystvo = Oil industry*, 6, pp. 30-34. (In Russ.)

Voronovsky G.K., Makhotilo K.V., Petrashev S.N., Sergeev S.A. (1997). Genetic algorithms, artificial neural networks, and virtual reality problems. 112 p. (In Russ.)

## About the Authors

*Alexander A. Kochnev* – graduate student, Perm National Research Polytechnic University

29, Komsomolsky av., Perm, 614990, Russian Federation

*Nikita D. Kozyrev* – graduate student, Perm National Research Polytechnic University; Engineer, Branch of LLC «LUKOIL-Engineering» «PermNIPIneft» in Perm

29, Soviet Army st., Perm, 614066, Russian Federation

*Olga E. Kochneva* – Cand. Sci. (Geology and Mineralogy), Department of Oil and Gas Geology, Saint-Petersburg Mining University

2, 21st lines, Vasilyevsky Island, St. Petersburg, 199106, Russian Federation

*Sergey V. Galkin* – Dr. Sci. (Geology and Mineralogy), Professor of the Department of Oil and Gas Technologies, Perm National Research Polytechnic University

29, Komsomolsky av., Perm, 614990, Russian Federation

*Manuscript received 20 July 2020;*
*Accepted 1 September 2020; Published 30 September 2020*

ORIGINAL ARTICLE

**DOI**: https://doi.org/10.18599/grs.2020.3.87-96 Russian Original 2020. Vol. 22. Is. 3. Pp. 87–96

# Application of artificial intelligence methods for identifying and predicting complications in the construction of oil and gas wells: problems and solutions

*A.D. Chernikov[1], N.A. Eremin[1,2*], V.E. Stolyarov[1], A.G. Sboev[3], O.K. Semenova-Chaschina[1], L.K. Fitsner[1]*

[1]*Oil and Gas Research Institute of the Russian Academy of Sciences, Moscow, Russian Federation*
[2]*National University of Oil and Gas «Gubkin University» (Gubkin University), Moscow, Russian Federation*
[3]*National Research Center «Kurchatov Institute», Moscow, Russian Federation*

**Abstract**. This paper poses and solves the problem of using artificial intelligence methods for processing Big volumes of geodata from geological and technological measurement stations in order to identify and predict complications during well drilling. Digital modernization of the life cycle of wells using artificial intelligence methods helps to improve the efficiency of drilling oil and gas wells. In the course of creating and training artificial neural networks, regularities were modeled with a given accuracy, hidden relationships between geological and geophysical, technical and technological parameters were revealed. The clustering of Big data volumes from various sources and types of sensors used to measure parameters while well drilling has been carried out. Artificial intelligence classification models have been developed to predict the operational results of the well construction. The analysis of these issues is carried out, and the main directions for their solution are determined.

**Keywords**: artificial intelligence, machine learning methods, geological and technological research, neural network model, regression model, construction of oil and gas wells, identification and prediction of complications, prevention of emergency situations

**Recommended citation**: Chernikov A.D., Eremin N.A., Stolyarov V.E., Sboev A.G., Semenova-Chashchina O.K., Fitsner L.K. (2020). Application of artificial intelligence methods for identifying and predicting complications in the construction of oil and gas wells: problems and solutions. *Georesursy = Georesources*, 22(3), pp. 87–96. DOI: https://doi.org/10.18599/grs.2020.3.87-96

## Introduction

In a period of increasing competition in the energy market, the task of radically rethinking their activities and approaches to ensuring its efficiency comes to the fore for domestic oil and gas producing and service companies (Abukova et al., 2017; Muslimov, 2017; Dmitrievsky et al., 2019; Dmitrievsky et al., 2020a). Solving this problem requires focusing attention on the key factors affecting the operating activities of companies, the most important of which is the introduction of automation of production processes based on the use of artificial intelligence (AI) systems. Artificial intelligence and machine learning, or computational intelligence, are science and technology aimed at creating intelligent tools, devices, complexes and systems. Its application for solving complex problems in the oil and gas industry is becoming more and more popular and acceptable from an economic point of view (Bobb, 2018; Diakonov et al., 2017; Eremin, 1994; Ivlev et al., 2018; Kabanikhin et al., 2018; Kaznacheev et al., 2016; Djamaluddin et al., 2019).

Artificial intelligence methods are being developed and implemented around the world in an increasing number of applications due to the ability to detect physically hidden processes and phenomena, predictive potential and flexibility. Table 1 shows the application of various artificial intelligence methods in the design and construction of wells based on the analysis of published foreign data (Dmitrievsky et al., 2019; Eremin et al., 2020; Lind et al., 2013; Loermans, 2017; Pichugin et al., 2013; Development of a high-performance automated system..., 2019; Abu-Abed, Khabarov, 2017; Alotaibi et al., 2019; Chen, Guestrin, 2016; Gurina et al., 2019; Kanfar et al., 2020; Kohonen, 1990; Liu et al., 2008; Mayani et al., 2020; Noshi, Schubert, 2018; Rakichinsky, Sledkov, 2014; Singh et al., 2019).

The main advantages of artificial intelligence systems are (Yurchenko, Kryukov, 2018; Kanfar et al., 2020; Li et al., 2019; Gurina et al., 2019; Kohonen, 1990; Liu et

*Corresponding author: Nikolai A. Eremin
*E-mail: ermn@mail.ru*

| Operational Result | Application | Applied AI Methods |
|---|---|---|
| Well design | Bit selection | Artificial neural network (ANN) |
| | Preliminary estimate of the deviation | Generalized regression neural network |
| | Casing failure prediction | Backpropagation neural network |
| | Cement Quality / Performance Assessment | Artificial neural network (ANN) |
| | Offshore drilling platform selection | Hybrid (Backpropagation Neural Network) |
| | Geosteering | Use case-based machine learning (CBR systems) |
| Methodological determination of optimal characteristics | Bottom hole assembly monitoring | Artificial neural network (ANN) |
| | Bit wear control | Artificial neural network (ANN) |
| | Stuck and Load Prediction | Artificial neural network (ANN) |
| | Vibration control | Artificial neural network (ANN) |
| | Cleaning the wellbore from cuttings | Backpropagation neural network / multiple linear regression |
| Wellbore stability | Hydraulic shock monitoring, loss and leak rate | Artificial neural network (ANN) |
| Decision support in problematic situations | Monitoring and troubleshooting | Backpropagation Neural Network / (Artificial Neural Network-GA) hybrid |
| Recognition of troubles, risk assessment | Real time drilling risk assessment | Use case-based machine learning (CBR systems) |
| | Drilling equipment condition | Artificial neural network (ANN) |
| Decision making in critical situations | Determination of permissible operations according to drilling conditions | Use case-based machine learning (CBR systems) |

*Tab. 1. Application of artificial intelligence methods in the design and construction of wells (Dmitrievsky et al., 2019; Eremin et al., 2020; Lind et al., 2013; Loermans, 2017; Pichugin et al., 2013; Development of a high-performance automated system..., 2019; Alotaibi et al., 2019; Chen, Guestrin, 2016; Gurina et al., 2019; Kanfar et al., 2020; Kohonen, 1990; Liu et al., 2008; Mayani et al., 2020; Noshi , Schubert, 2018; Rakichinsky, Sledkov, 2014; Singh et al., 2019).*

al., 2008; Mayani et al., 2020; Noshi, Schubert, 2018; Singh et al., 2019):

1. Ability for self-learning, as well as evolutionary development and self-organization;

2. Great potential for accurate analysis of Big historical and industrial databases in order to reveal hidden correlations and unknown patterns compared to traditional methods;

3. Ability to model complex nonlinear processes without any form of establishing a relationship between input and output variables;

4. High efficiency in forecasting, diagnostics, monitoring, condition control and identification of equipment and production processes;

5. Higher predictive accuracy of results than physical and simulation models using linear or nonlinear multiple regression;

6. Ultra-high performance of the neural network after training due to the use of massive parallelism of information processing;

7. Ability to learn from datasets in real time, without writing a program, which is often more cost-effective and practical, especially when changes become critical;

8. Possibility of rapid development using already existing standard software applications, and the necessary specificity can be incorporated into them in the learning process.

Distinctive characteristics of modern AI systems are not only their ability to learn from experience, but also to improve themselves during operation, which is an integral part of the so-called cognitive computing, which dramatically increases the efficiency of decision-making processes when working with big data.

Wells are the main part of fixed assets in the developed oil and gas fields. During well construction, an average of 20–25% of the construction time is spent on dealing with complications and emergencies. The cost of drilling wells tends to rise, and drilling complications are increasingly undesirable. Reducing the loss of working time to eliminate complications and their consequences

is one of the main opportunities for increasing the productivity factor during well construction.The main types of complications are: sticking of the drill string as a result of debris and collapse of unstable rocks, narrowing of the wellbore by crumbling rocks, losses of drilling mud, and gas, oil, and water inflow (kicks). The share of these complications is up to 85% of their total number recorded during the development of oil and gas fields. The types of major complications under consideration lead to long, costly downtime and significant unproductive costs for their elimination and elimination of consequences. The share of the costs of eliminating complications and the emergencies caused by them can be up to 25% of the cost of well construction. Timely prevention of complications and accidents during drilling is an extremely important and urgent task and requires the creation of a set of methods for their early detection using modern artificial intelligence and machine learning systems.

Taking into account the complexity of operations performed in the development of oil and gas fields, the presence of uncertainties associated with geological and geophysical and external conditions, artificial neural networks (ANN) and machine learning methods can be classified as effective tools in the construction of an automated system for preventing complications and emergencies during construction oil and gas wells (AS POAS) (Yurchenko, Kryukov, 2018) (Figure 1).

The adoption of the necessary measures to prevent accidents is possible with reliable prediction of their occurrence based on the analysis of the results of measurements of the parameters of technological processes of well construction. The automated system must perform software processing of measurement results in real time, predict the occurrence of possible complications and issue warning messages. Moreover, in most cases, the occurrence of complications during well construction is determined by a complex set of geological, geophysical and technological parameters and cannot be detected as a result of visual observations by the operator.

For the effective functioning of the AS POAS, taking into account the specifics of scenarios for the occurrence of various types of complications, it must include an integrated complex of AI technologies, which, as a rule, combines auxiliary machine learning methods and classification neural network models. In this case, the architecture of the system should be open at all levels of the organization: structural, functional, data organization and interface (Bakanov et al., 2009). The decisive factor for the construction of an AS POAS based on modern technologies of artificial intelligence is the collection and organization of information, the formation of an integrated database of technical, technological and geological and geophysical data.

## Organization of storage and preparation of data in an automated system for preventing complications and emergencies during the construction of oil and gas wells

Currently, the international open standard WITSML (Wellsite Information Transfer Standard Markup Language), based on open Internet standards (W3C, SOAP, WSDL, XML), is widely used to exchange data between various services and organizations operating in the oil and gas industryopen interface of application

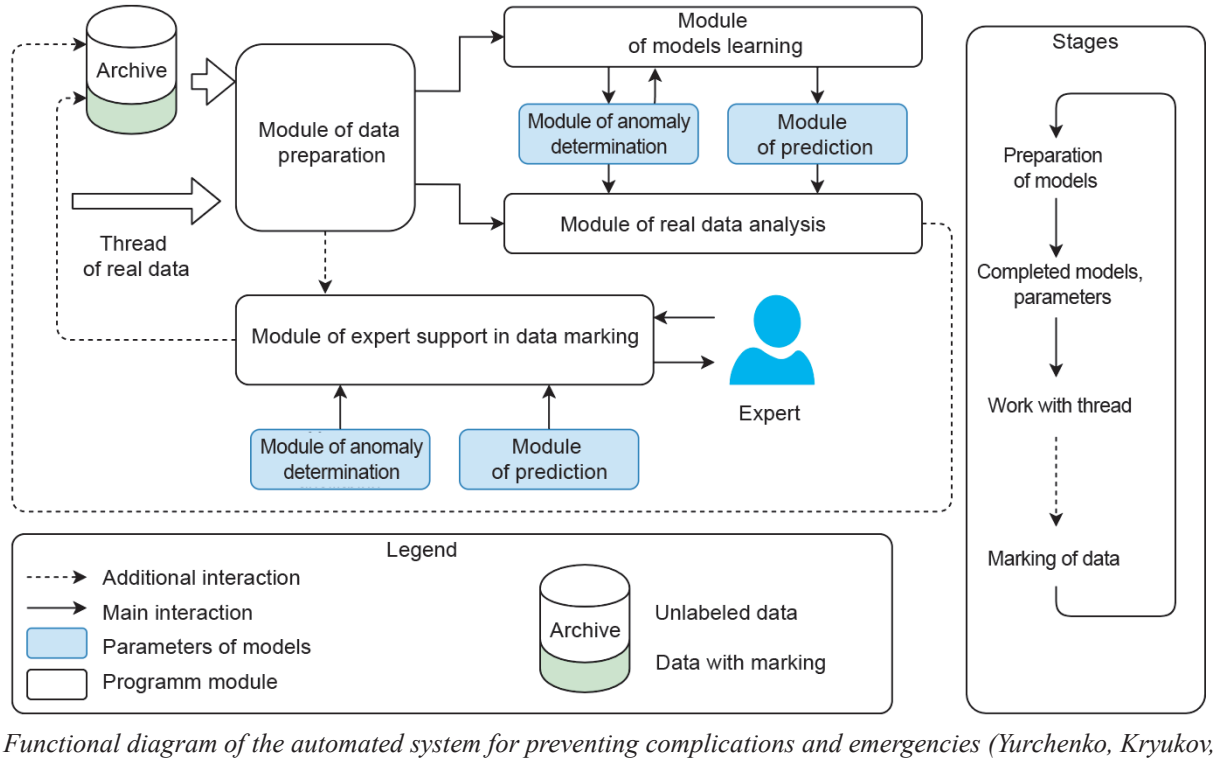


*Fig. 1. Functional diagram of the automated system for preventing complications and emergencies (Yurchenko, Kryukov, 2018)*

programs (Standards Software Development Kit (SDK), Open Subsurface Data Universe). The following data sources were used during the research: the open Dataset of Equinor for the field (https://data.equinor.com/dataset/Volve) – data on the development of 16 wells, archived data of geological and technological studies of domestic companies-developers of West Siberian oil and gas fields basin – 25 wells, and the Central Russian oil and gas basin – 32 wells. As a result of the analysis, data on 38 complications of various types were confirmed and processed.To increase the efficiency of predicting complications during data processing, machine learning methods were used to identify abnormal deviations of parameters from the standard operating modes of drilling equipment.

To expand the area of initial data and its clustering, specially prepared simulation data were used, formed from the results of modeling typical situations of occurrence of complications of specified types on a drilling simulator (Arkhipov et al., 2020; Dmitrievsky et al., 2020).The preparation of initial data for constructing models of neural network calculations consists of the formation and marking of sets of temporary/deep data (WITSLM Realtime drilling data) and data of drilling logs (WITSML Daily drilling reports) in WITSML format (WITSML Data Standards), containing information about complications. Such sets can be generated both using the available information for a specific well, and based on archived data containing information about previously drilled wells with similar geological characteristics.

To work with data in WITSML format and form initial sets for constructing models for detecting and predicting complications, a data preparation software module was developed, consisting of a set of service procedures and a client part (Figure 2).

The data preparation module provides the following procedures:

- viewing and preliminary analysis of WITSML Realtime drilling data for each of the wells and selection of wells for use in further calculations;
- interactive parsing of the data structure of drilling logs Daily Drilling Reports WITSML Data;
- viewing records by lithology for each well;
- selection of records for abnormal and emergency situations according to specified criteria.

When performing procedures, the Energistic object data model is used. The information is stored in the form of linked tables that reflect the XML structure of drillReports objects in accordance with the WITSML 1.4.1 specification. File storage and a database based on the MS SQL Server database management system (DBMS) are used to store data.

For the automated selection of data on complications in accordance with the specified criteria (the presence of specified keywords, characteristic changes in technological parameters, etc.), an operator interface has been developed (Figure 3). For clarity, the records displayed on the screen containing information on various types of complications are highlighted in color: “Sticking” – in red, “Fluid loss” – in purple, “Kick” – in green. For the convenience of the analysis, a procedure for the graphical presentation of parametric information contained in the Realtime Drilling files is implemented (Figure 4).

As a result of automated data collection and preparation, repositories are created for untagged (there is no corresponding contextual information, data of drilling logs, etc.) and marked up according to the results of the examination of geological and technological research data, configuration arrays (files) are formed for the formation and training of models, as well as test arrays for their validation, various types of geological and geophysical, technological and contextual information are structured and stored, forming in their totality an integrated AS POAS database.

**Structural organization of an automated system for preventing complications and emergencies**

The stages of the technological cycle of functioning of the AS POAS are shown on the right side of the diagram (Figure 1), according to which three main stages can be distinguished:

- preparation of data and information support for the work of experts to highlight possible complications in unlabeled data;
- formation, training and validation of neural network models and models of machine learning methods on prepared by experts and on unlabeled data sets;
- processing and analysis of real-time drilling data with predicting the possibility of occurrence of complications of the specified types: “Sticking”, “Fluid loss” and “Kick”, formation and display of the appropriate warning messages and recommendations on the prevention of emergency situations on the driller operator’s screen.

The module for the formation and training of models is implemented in the Python language (Keras: The Python Deep Learning library, LightGBM. Python API) and provides the preparation of models used for predicting and preventing emergency situations in drilling support systems. The module implements the functions of assembling classification neural network models.

The generated topology of the neural network of the AS POAS consists of three main layers:

- the first layer is a Multilayered perceptron (MLP);
- then there is a recurrent layer, consisting of 4 neurons of a controlled recurrent unit (Gated Recurrent Units, GRU);

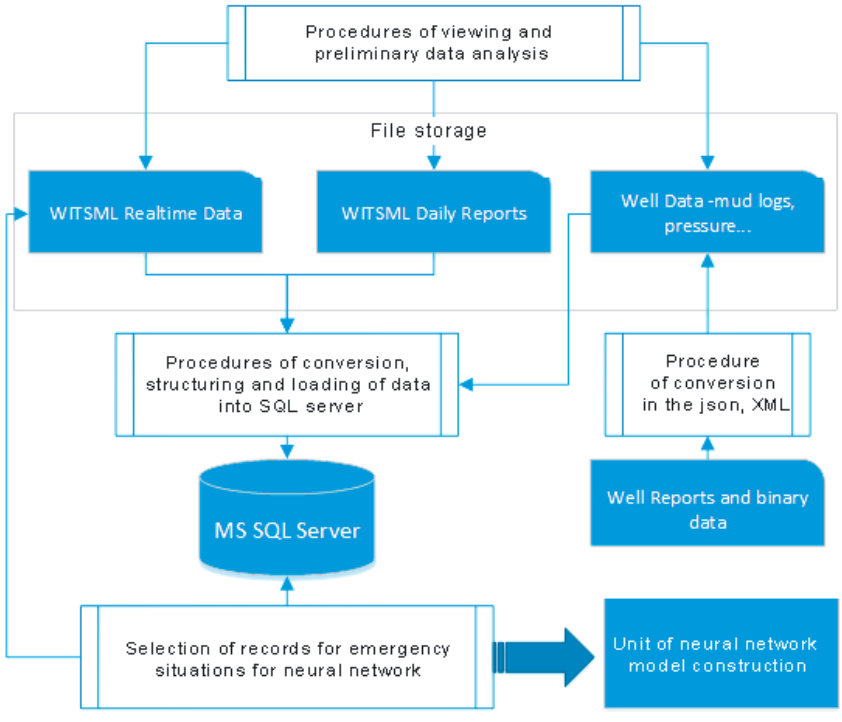


*Fig. 2. Block diagram of the data preparation module*

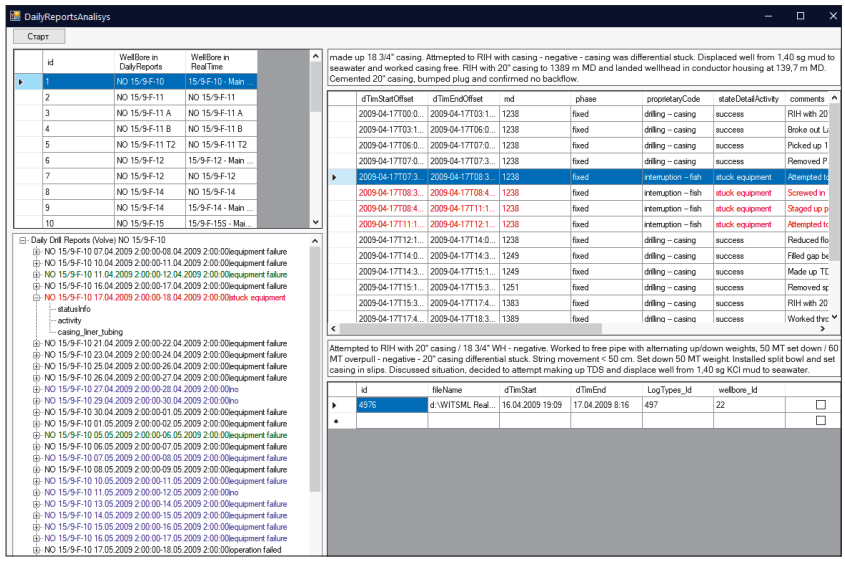


*Fig. 3. Interface of the block for selecting information related to complications*

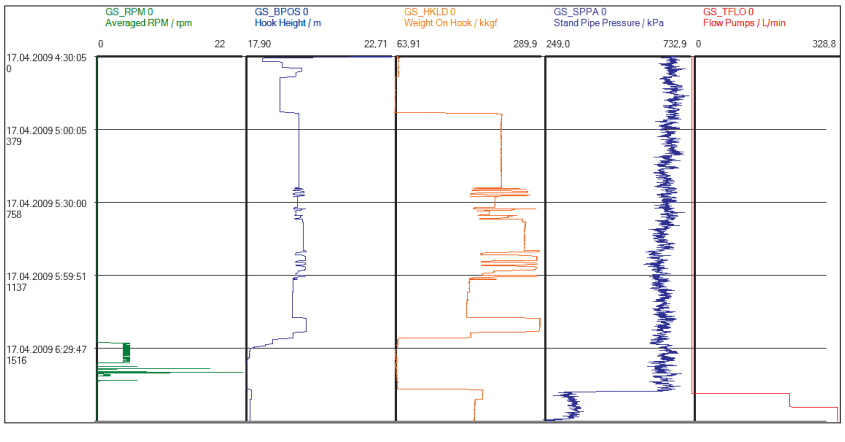


*Fig. 4. An example of a graphical presentation of parametric information on selected drilling problems*

- the output layer for solving the classification problem consists of two neurons with the softmax activation function.

The structural diagram of the classification neural network model for identifying and predicting complications of the AS POAS is shown in Figure 5.

Models are formed and trained in accordance with the specified configuration files, which allows you to change the hyperparameters of the models without making changes to the module code. The trained models are used as output data, which are saved as separate files with their own name in the hdf5 format and include the following structure:

- the topology of the model, which allows you to reproduce the trained model;
- customized model weights;
- the state of the optimizer.

The real-time data processing module ensures the integration of models into the AS POAS and performs the following functions:

- loading of trained models of prediction of emergency situations and preprocessing parameters in accordance with configuration files;
- transfer of the obtained vectors of parameters to the module for processing real data and obtaining the predicted values of the models from the accumulated window of parameters;
- logging (recording system information) of the models.

The operator interface of the AS POAS for a detailed parametric analysis of the causes of complications of the "Fluid loss" type during the drilling operation is shown in Figure 6.

On the left side of the screen, the timeline and the technological operations and modes being performed are displayed, and on the right, a graphical representation of the change in time parameters to identify the specified types of complications.

A simplified interface has been developed for the driller operator with automatic determination of the predicted probabilities of complications and displaying warning messages and alarms on the screen in case of exceeding a predetermined threshold (Figure 7).

On the left side of the screen, the values of technological parameters are displayed in real time, with the possibility of selection by the operator, and on the right, the values of the probabilities of complications, calculated according to the predicted and actual parameters of geological and technological studies (GTI). Warnings about the possibility of complications are displayed on the operator's screen in the form of arrow indicators, as well as time scales for the probability of occurrence of complications of specified types with color alarms: green when there is no threat and red when the threat probability is greater than 0.5.

Accuracy and f1 score metrics were used to calculate the accuracy. The Accuracy score was calculated as the ratio of the number of moments in which the reference and predicted marks coincided to the total number of moments. To calculate the f1 score, the number of points correctly assigned (TP) to it, incorrectly assigned (FP) and incorrectly unassigned (FN) was first calculated for each class. After that, the total value of accuracy was calculated, equal to TP/(TP + FP), and completeness – TP/(TP + FN). Moreover, each example was taken with a weight depending on the representativeness of the class. The choice of quality metrics was based on the composition of the data used and the methods used for their processing.

Based on the results of testing the classification neural network model, the following predictive accuracy of

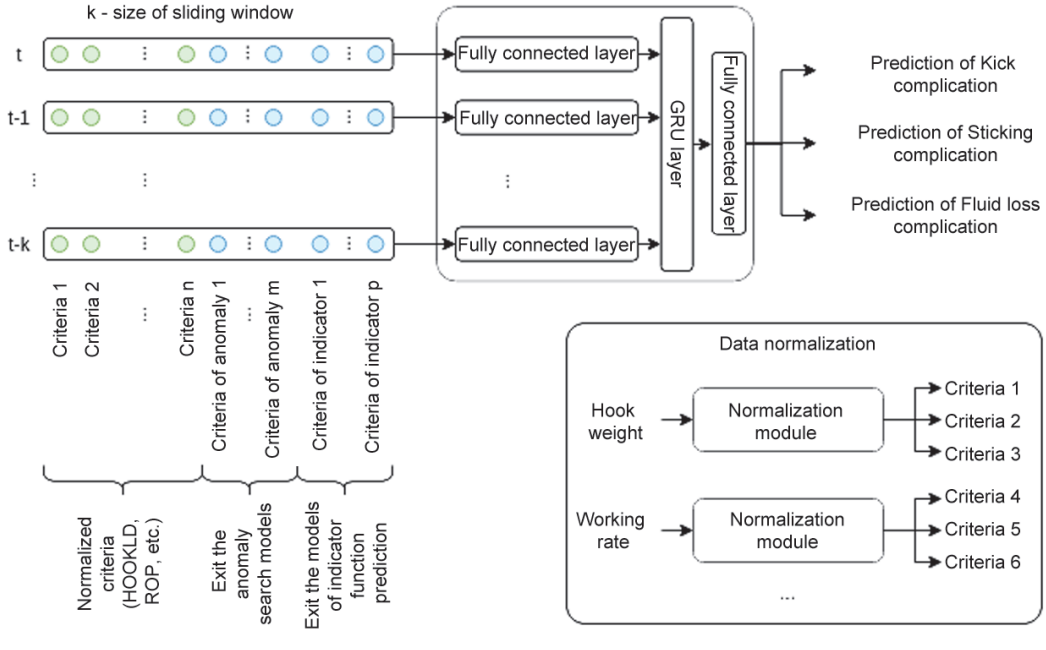


*Fig. 5. Block diagram of the classification neural network model for predicting drilling problems*

various types of complications was obtained: “Kick” – 96%; “Fluid loss” – 79%; “Sticking” – 87%.

**Problems and main directions of their solution**

One of the main problems in the development and implementation of AI systems in the domestic oil and gas industry is the problem of data availability, organization of their collection, structuring, storage and distribution to consumers. The main obstacles in solving this problem are departmental barriers and the protectionism of such oil and gas companies -operatorsof the fields.

Currently, the oil and gas industry has made significant strides in improving drilling performance by adding high-tech downhole tools and sensors, redefining classic drilling procedures, and utilizing state-of-the-art surface rig systems. Progress in optimizing the construction of oil and gas wells based on the use of constantly available historical and operatively obtained geological, geophysical and technological data turned out to be insignificant. Equipping drillers and engineers with specific and fastsolutions based on the implementation of artificial intelligence technologies for modeling and processing field data in real time is now the key to increasing operational efficiency and reducing costs in the construction of oil and gas wells, ensuring operational and environmental safety.

The main development vectors in this direction are the following:

- creation of modern interactive environments to ensure the collection, systematization and analysis of

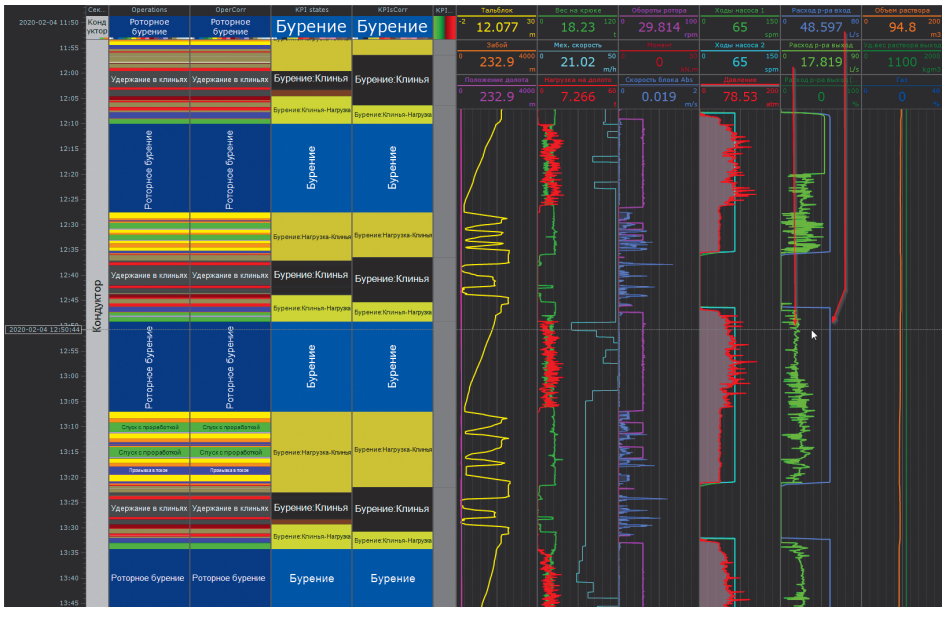


*Fig. 6. Identification of drilling problems such as “Fluid Loss” during well drilling*

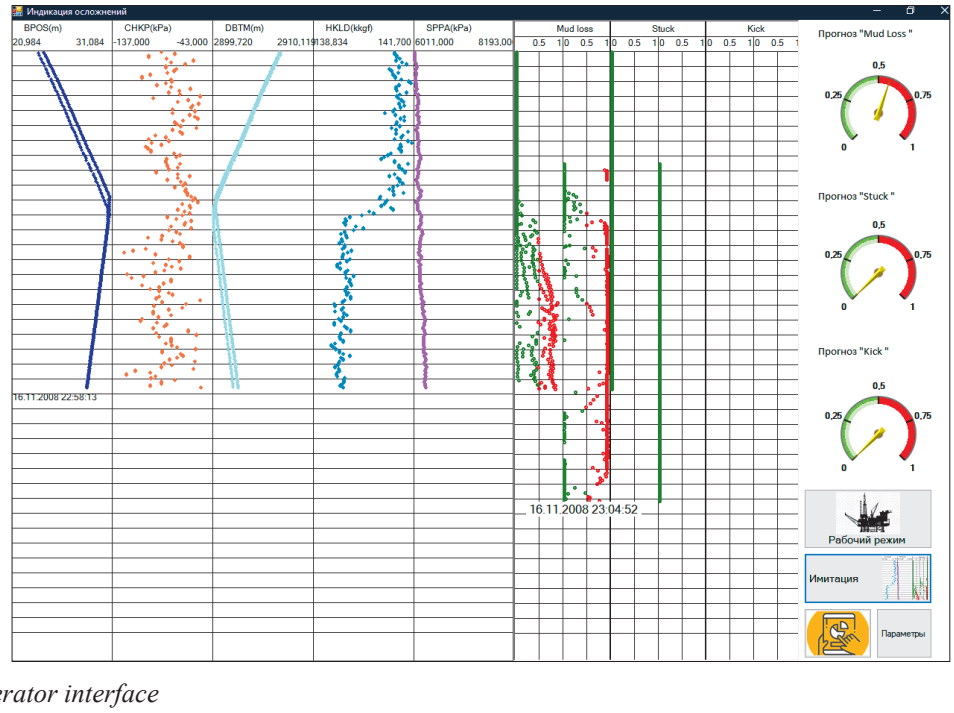


*Fig. 7. Drilling operator interface*

all operational information in real time and providing on this basis proactive management of the process of construction of wells (fields);

- automation of production processes based on the introduction of artificial intelligence systems;

- creation and implementation of new AI tools for remote monitoring and management of operational activities;

- use of integrated cross-functional performance indicators for AI systems and the company's overall performance, which allow optimizing all stages of their operational activities.

The main vectors of development in this direction are the following:

- creation of modern interactive environments to ensure the collection, systematization and analysis of all operational information in real time and providing on this basis proactive management of the process of construction of wells (fields);

- automation of production processes based on the introduction of artificial intelligence systems;

- creation and implementation of new AI tools for remote monitoring and management of operational activities;

- use of integrated cross-functional performance indicators for AI systems and the company's overall performance, which allow optimizing all stages of their operational activities.

Due to the scale and complexity of this task, it cannot be solved without the introduction of modern methods of artificial intelligence and innovative information technologies with direct participation in projects of it and service companies, as well as specialized scientific organizations.

An example is the activity of Equinor, which became one of the founders of the OSDU (Open Subsurface Data Universe™) initiative, a global collaboration between most of the world's largest operators and service companies in defining standards for the open data architecture for subsurface resources, creating open data banks of geological and technological information generated from the design and construction of wells to their support at all stages of the life cycle. When designing new wells and fields, accumulated data integrated on the basis of cloud technologies is used.

The increasing use of artificial intelligence methods to improve the efficiency of oil and gas well construction leads to an exponentially growing number and greater specialization of artificial neural network models that are configured to solve various target objectives: development planning, optimization of technological modes, forecasting various types of drilling complications (drilling column sticking, lost circulation, kicks of reservoir fluid, bit wear, etc.) of oil and gas wells.

Currently, in the field of application of information technologies in the oil and gas industry, the image of universal information systems has developed – a single digital platform with the ability to create an API programming interface for interconnection with the combined resources of the developer company and consumers of different levels. In contrast, in the field of AI, there are no unified approaches for combining specialized systems, methods and solutions (ANN, machine learning methods, decision support systems, expert systems), based on a single digital AI platform, which allows working with Big amounts of unstructured data.

At the same time, the main problematic issue is the integration of specialized models of artificial neural networks and machine learning methods into a single system that provides an effective solution to a given set of problems under conditions of a priori uncertainty associated with specific geological and geophysical, technical and technological conditions and factors. With regard to the problem of implementing a systematic approach when introducing AI methods to solve problems of increasing the efficiency of construction of oil and gas wells, the question arises: on what basis is it possible to combine such heterogeneous models as forecasting complications that differ in nature: sticking, lost circulation, gas, oil andwater kicks, etc.

Therefore, the main direction for solving this problem in the oil and gas industry is the aggregation of heterogeneous software algorithmic complexes (SAC) for AI into a single system. The aggregation of heterogeneous SAC AI is understood as their integration into a self-learning system based on unified AI self-organization algorithms that form a single Smart environment (platform) in the information and control space of the oil and gas industry technological processes.

This paradigm of a self-organizing AI-System, as the latest concept of dynamic adaptation to the conditions of a specific oil and gas production, will allow to ensure the integration of promising oil and gas technologies based on the implementation of a Smart platform for aggregating heterogeneous SAC for AI. The development of new Smart AI technologies for the oil and gas industry is planned to be implemented as part of the creation of an Integrated Center for Oil and Gas Technologies based on an aggregated artificial intelligence system, the creation of which will allow moving to a qualitatively new technological level of solving the entire complex of problems in the oil and gas industry.

## Conclusion

In the course of the research, the structure and parameters of the optimal configuration of models of neural networks and machine learning methods were

determined, an experimental sample of a software complex was developed, designed to ensure the functioning of an automated system for preventing complications and emergencies during the construction of oil and gas wells.

The research made it possible to identify a number of common problematic issues in the implementation of artificial intelligence technologies in the oil and gas industry and to determine the main directions for their solution within the framework of the development and implementation of a single integrated digital AI platform and improvement of methods for streaming processing of Big volumes of geological-geophysical and real-time technological data.

## Acknowledgments

*The article was prepared as part of the work of the Federal Target Program «Research and Development in Priority Areas of Development of the Scientific and Technological Complex of Russia for 2014–2020» on the topic: «Development of a high-performance automated system for preventing complications and emergencies during the construction of oil and gas wells based on permanent geological and technological models of fields using artificial intelligence technologies and industrial blockchain to reduce the risks of geological exploration, incl. on offshore projects» under the Agreement with the Ministry of Science and Higher Education of the Russian Federation on the allocation of a subsidy in the form of a grant dated November 22, 2019 No. 075-15-2019-1688.*

## References

Abu-Abed F, Khabarov A. (2017). Classification of pre-emergency situations in the process of industrial drilling of oilfield well systems. *J. Fundam. Appl. Sci.*, 9(2S), pp. 1171–1181.

Abukova L.A., Dmitrievsky A.N., Eremin N.A. (2017). Digital modernization of Russian oil and gas complex. *Neftyanoe Khozyaystvo = Oil Industry*, 11, pp. 54–58. (In Russ.). DOI: 10.24887/0028-2448-2017-10-54-58

Alotaibi B., Aman B., & Nefai M. (2019, March 15). Real-Time Drilling Models Monitoring Using Artificial Intelligence. *Society of Petroleum Engineers*. https://doi.org/10.2118/194807-MS

Arkhipov A.I., Dmitrievsky A.N., Eremin N.A., Chernikov A.D., Borozdin S.O., Safarova E.A., Seinaroev M.R. (2020). Data quality analysis of the station of geological and technological researches in recognizing losses and kicks to improve the prediction accuracy of neural network algorithms. *Neftyanoe Khozyaystvo = Oil Industry*, 8(1162), pp. 63–67. (In Russ.)

Bakanov A.B., Drozhdin V.V., Zinchenko R.E., Kuznetsov R.N. (2009). Methods of adaptation and generation of software development. *Izvestiya PGPU im. V.G. Belinskogo*, 13(17), pp. 66–69. (In Russ.)

Bobb I.F. (2018). International experience of E&P software solutions development. *Georesursy = Georesources*, 20(3), pp. 193-196. DOI: https://doi.org/10.18599/grs.2018.3.103-196

Chen T., Guestrin C. (2016). Xgboost: A scalable tree boosting system. *Proc. 22nd ASM SIGKDD Int. Conf on Knowledge Discovery and Data Mining*, pp. 785–794.

Development of a high-performance automated system for preventing troubles and emergencies during the construction of oil and gas wells based on constantly operating geological and technological models of fields using artificial intelligence technologies and industrial block chain to reduce the risks of geological exploration, including on offshore projects. (2019). Report. Oil and Gas Research Institute of the Russian Academy of Sciences. (In Russ.)

Diakonov A.G., Golovina A.M. (2017). Detection of anomalies in the work of mechanisms by machine learning methods. Analytics and data management in areas with intensive data use: *Proc. XIX Int. Conf. DAMDID/RCDL*, pp. 469–476.

Djamaluddin B., Prabhakar P., James, B., Muzakir A., & AlMayad H. (2019). Real-Time Drilling Operation Activity Analysis Data Modelling with Multidimensional Approach and Column-Oriented Storage. Society of Petroleum Engineers. https://doi.org/10.2118/194701-MS

Dmitrievsky A.N., Eremin N.A., Stolyarov V.E. (2020). The role of information in the application of artificial intelligence technologies in the construction of wells for oil and gas fields. *Nauchnyi zhurnal Rossiiskogo gazovogo ob-shchestva*, 3(26), pp. 22–37. (In Russ.)

Dmitrievsky A.N., Eremin N.A., Filippova D.S., Safarova E.A. (2020a). Digital oil and gas complex of Russia. *Georesursy = Georesources*, Special issue, pp. 32–35. (In Russ.). DOI: https://doi.org/10.18599/grs.2020.SI.32-35

Dmitrievsky A.N., Eremin N.A., Stolyarov V.E. (2019). Digital transformation of gas production. *IOP Conference Series: Materials Science and Engineering*. https://doi.org/10.1088/1757-899X/700/1/012052

Eremin N.A. (1994). Hydrocarbon field simulation by fuzzy logic methods. Moscow: Nauka, 462 p. (In Russ.)

Eremin N.A., Chernikov A.D., Sardanashvili O.N., Stolyarov V.E., Arkhipov A.I. (2020). Digital well-building technologies. Creation of a high-performance automated system to prevent complications and emergencies in the process of construction of oil and gas wells. *Business magazine «Neftegaz.RU»*, 4(100), pp. 38–50. (In Russ.)

Gurina E., Klyuchnikov N., Zaytsev A., Romanenkova E., Antipova K., Simon I., Makarov V., Koroteev D. (2020). Application of machine learning to accidents detection at directional drilling. J*ournal of Petroleum Science and Engineering*, 184, 106519. https://doi.org/10.1016/j.petrol.2019.106519

Ivlev A., Eremin N. (2018). Petrobotics: robotic drilling systems. *Burenie i neft*, 2, pp. 8–13. (In Russ.)

Kabanikhin S.I., Shishlenin M.A. (2018). Digital field. *Georesursy = Georesources*, 20(3), pp. 139–141. https://doi.org/10.18599/grs.2018.3.139-141

Kanfar R., Shaikh O., Yousefzadeh M., Mukerji T. (2020). Real-Time Well Log Prediction From Drilling Data Using Deep Learning. arXiv: 2001.10156. DOI: 10.2523/IPTC-19693-MS

Kaznacheev P.F., Samoilova R.V., Kjurchisky N.V. (2016). Improving Efficiency of the Oil and Gas Sector and Other Extractive Industries by Applying Methods of Artificial Intelligence. *Ekonomicheskaya Politika = Economic Policy*, 11(5), pp. 188–197. DOI: 10.18288/1994-5124-2016-5-09

Kohonen T. (1990). The self-organizing map. *Proceedings of the IEEE*, 78(9), pp. 1464–1480.

Li Y., Sun R., Horne R. (2019). Deep learning for well data history analysis. *SPE Annual Technical Conference and Exhibition*. Society of Petroleum Engineers. https://doi.org/10.2118/196011-MS

Lind Yu.B., Mulyukov R.A., Kabirova A.R., Murzagalin A.R. Online prediction of troubles in drilling process. *Neftyanoe Khozyaystvo = Oil Industry*, 2, pp. 55–57. (In Russ.)

Liu F.T., Tony T.K.M., Zhou Z.H. (2008). Isolation forest. *Proc. Eighth IEEE Int. Conf. on Data Mining*, pp. 413–422.

Loermans T. (2017). AML (Advanced Mud Logging): First Among Equals. *Georesursy = Georesources*, 19(3), pp. 216–221. https://doi.org/10.18599/grs.19.3.11

Mayani M.G., Baybolov T., Rommetveit R., Ødegaard S. I., Koryabkin V. & Lakhtionov S. (2020). Optimizing Drilling Wells and Increasing the Operation Efficiency Using Digital Twin Technology. Society of Petroleum Engineers. https://doi.org/10.2118/199566-MS

Muslimov R.Kh. (2017). Solving the Fundamental Problems of the Russian Oil Industry is the Basis for a Large-Scale Transition to Innovative Development. *Georesursy = Georesources*, 19(3), pp. 151–158. https://doi.org/10.18599/grs.19.3.1

Noshi C.I., & Schubert J.J. (2018). The Role of Machine Learning in Drilling Operations. A Review. Society of Petroleum Engineers. https://doi.org/10.2118/191823-18ERM-MS

Pichugin O.N., Prokofiev, Y.Z., Alexandrov D.M. (2013). Decision Trees as an effective method for analysis and forecasting. *Nefteprom yslovoe delo*, 11, pp. 69–75. (In Russ.)

Rakichinsky V.N., Sledkov V.V. (2014). Risk Management for Well Construction Technology Implementation at Lukoil. *Rogtec*. 10.09, pp. 62–72. (In Russ.)

Singh K., Yalamarty S.S., Kamyab M., & Cheatham C. (2019). Cloud-Based ROP Prediction and Optimization in Real Time Using Supervised Machine Learning. *Unconventional Resources Technology Conference*. https://doi.org/10.15530/urtec-2019-343.

Yurchenko I.G., Kryukov A.O. (2018). Advantages and disadvantages of introducing self-learning neural networks at oil and gas industry. *Problems of geology and development of mineral resources: Proc. XXII Int. Symp.* Tomsk, vol. 2, pp. 835–836. (In Russ.)

**About the Authors**

*Alexander D. Chernikov* – Leading Researcher, Cand. Sci. (Engineering), Oil and Gas Research Institute of the Russian Academy of Sciences

3, Gubkin st., Moscow, 119333, Russian Federation

*Nikolai A. Eremin* – Dr. Sci. (Engineering), Chief Researcher, Deputy Director, Oil and Gas Research Institute of the Russian Academy of Sciences; Professor, National University of Oil and Gas «Gubkin University» (Gubkin University)

3, Gubkin st., Moscow, 119333, Russian Federation

E-mail: ermn@mail.ru

*Vladimir E. Stolyarov* – Deputy Head of the Analytical Center for Technology Forecasting in the Oil and Gas Industry, Institute of Oil and Gas Problems of the Russian Academy of Sciences

3, Gubkin st., Moscow, 119333, Russian Federation

*Alexander G. Sboev* – Leading Researcher, Cand. Sci. (Engineering), National Research Center «Kurchatov Institute»

1, Ak. Kurchatov pl., Moscow, 123098, Russian Federation

*Olga K. Semenova-Chashchina* – Leading Engineer, Cand. Sci. (Engineering), Oil and Gas Research Institute of the Russian Academy of Sciences

3, Gubkin st., Moscow, 119333, Russian Federation

*Leonid K. Fitsner* – Leading Engineer, Cand. Sci. (Engineering)

Oil and Gas Research Institute of the Russian Academy of Sciences

3, Gubkin st., Moscow, 119333, Russian Federation

*Manuscript received 21 July 2020;*
*Accepted 10 September 2020;*
*Published 30 September 2020*

ISSN 1608-5043 (Print)
ISSN 1608-5078 (Online)

Key title: «Georesursy»
Parallel title: «Georesources»

# GEORESURSY

A peer-reviewed scientific and technical journal published since 1999


The journal is included/indexed in:

| | |
|---|---|
| Clarivate Web of Science™ | Web of Science Core Collection<br>Emerging Sources Citation Index (ESCI) |
| Scopus | Scopus |
| CAS A DIVISION OF THE AMERICAN CHEMICAL SOCIETY | CAS (Chemical Abstracts Service) databases |
| GeoRef | GeoRef database |
| EBSCOhost | EBSCOhost™ databases |
| DOAJ DIRECTORY OF OPEN ACCESS JOURNALS | Directory of Open Access Journals (DOAJ) |

The full-text electronic versions of the articles are freely available to the public on journal's website: **www.geors.ru**



Contacts:
Deputy Chief Editor - Daria Khristoforova
E-mail: mail@geors.ru
Tel: +7 (843) 239-05-30